The Influence of Cracks on the Durability and Service Life of Reinforced Concrete Structures in relation to Chloride-Induced Corrosion

A Look from a Different Perspective

Proefschrift

ter verkrijging van de graad van doctor

aan de Technische Universiteit Delft,

op gezag van de Rector Magnificus prof. ir. K.C.A.M. Luyben,

voorzitter van het College voor Promoties,

in het openbaar te verdedigen op woensdag 27 januari 2016 om 12:30 uur

door

Andrija BLAGOJEVIĆ

Civiel Ingenieur aan de Universiteit van Niš, Servië
geboren te Niš, Servië

The Influence of Cracks on the Durability and Service Life of Reinforced Concrete Structures in relation to Chloride-Induced Corrosion

A Look from a Different Perspective

Andrija Blagojević

TUDelft Delft University of Technology

Faculty of Civil Engineering & Geosciences,
Department of Structural Engineering,
Concrete Structures

Delft, the Netherlands

Посвећено Мами и Тати

Summary

The service life of concrete structures can be significantly shortened when corrosion of steel reinforcement occurs, especially in a marine environment and in structures exposed to de-icing salts. The influence of load- or deformation-induced cracks on corrosion progress is an important issue which was studied in this research in relation to the durability and service life of reinforced concrete structures. An experimental set-up was designed in order to generate knowledge and contribute to existing codes and practice. 32 reinforced concrete beams ($1500 \times 100 \times 150$ mm^3) were exposed to alternately wetting and drying cycles in order to simulate an aggressive chloride environment. The interrelated influence of surface crack width, crack frequency (distance), concrete cover thickness and loading conditions on the corrosion development of steel reinforcement has been monitored during two years. After two years of exposure all concrete beams were split into two parts in order to visualize the achieved chloride penetration and the development of steel corrosion.

In order to limit the influence of load- or deformation-induced cracks on the potential reduction of service life, this research showed that maximum steel stress in cracked reinforced concrete members/structures plays an important role in corrosion behaviour, rather than the maximum surface crack width, since the stress level determines directly the damage of the concrete at the steel reinforcement level. Two different types of corrosion processes can be distinguished in concrete structures, localized and uniform corrosion. The localized depassivation of steel reinforcement is not necessarily the theoretical end of service life of a concrete member where a negligible localized reduction of the steel cross-section should be allowed in the SLS. Uniform corrosion along a certain bar length occurs mainly by chloride transport through the uncracked part of the concrete surface, between the main cracks.

The maximum steel stress affects both, localized and uniform corrosion along a certain bar length by the damage of the concrete around the main crack at the bar level and the reduction of the effective undamaged concrete cover in the uncracked part at the concrete surface (between the main cracks), respectively.

In order to take a step forward towards direct incorporation of the influence of load- or deformation-induced cracks in a more reliable assessment of the structure's service life, an explanatory model for cracked reinforced concrete members/structures in an aggressive environment is proposed. It is highlighted that the maximum service load level governs the development of the steel corrosion, rather than the frequent or the quasi-permanent service load level, as is prescribed at present by codes. Furthermore, the influence of load- and deformation-induced cracks in future codes and regulations, should be limited by defining the maximum allowable steel stress in conjunction with bar diameter and concrete cover at a certain concrete strength under the maximum service load, in order to assure the desired service life of a concrete structure exposed to an aggressive environment.

Samenvatting

De levensduur van betonconstructies kan aanzienlijk worden verkort door het optreden van corrosie, speciaal in een mariene omgeving en in constructies die blootgesteld zijn aan dooizouten. Hierbij spelen scheuren, ontstaan door belasting of opgelegde vervorming, een belangrijke rol. De relevantie van deze scheuren voor de levensduur van betonconstructies is het hoofdthema van het hier gepresenteerde onderzoek. Een experimenteel programma werd ontwikkeld met het doel nieuwe kennis te ontwikkelen voor het verbeteren van bouwvoorschriften en de ontwerppraktijk. 32 gewapende balken ($1500 \times 100 \times 150$ mm^3) werden in het kader van het onderzoek blootgesteld aan een natrium chloride oplossing in nat-droog cycli, om een agressief milieu te simuleren. De invloed van oppervlakte scheurwijdte, scheurafstand, betondekking en belastingcondities op de corrosie van de wapening werd gedurende twee jaar gemonitord. Na twee jaar blootstelling aan de genoemde condities werd elke balk in twee delen gespleten om de chlorideindringing en de ontwikkeling van wapeningscorrosie vast te stellen.

Het onderzoek toonde aan dat voor het beperken van de invloed van de scheuren op de duurzaamheid de maximale staalspanning in de scheur een meer geschikte parameter is dan de oppervlakte-scheurwijdte, omdat de staalspanning direct gerelateerd is aan de beschadiging van het beton rondom de wapening.

Twee verschillende typen corrosie worden onderscheiden, en wel uniforme corrosie en lokale corrosie. Een lokale depassivering van de betonstaalwapening betekent echter niet automatisch het eind van de levensduur van een betonconstructie of -element, waar een beperkte reductie van de staaldoorsnede in de bruikbaarheidsgrenstoestand kan worden toegestaan. De uniforme corrosie

over een deel van de staaflengte treedt vooral op door chloridetransport door het ongescheurde deel van het beton tussen de hoofdscheuren.

De maximale staalspanning beïnvloedt beide corrosieprocessen. Bij de lokale corrosie gebeurt dit door de beschadiging van het beton ter weerzijden van de hoofdscheur op het niveau van de wapening, en bij uniforme corrosie door de reductie van de effectieve betondekking door scheuren die zich ontwikkelen vanuit de ribben van het betonstaal.

Om te komen tot een meer betrouwbare bepaling van de levensduur van de constructie wordt een verklarend model voorgesteld voor het gedrag van gescheurde betonconstructies in een agressieve omgeving. Er wordt op gewezen dat de maximaal tijdens de levensduur optredende belasting op de constructie bepalend is voor de mate van corrosie, en niet de frequente of de quasi-permanente belasting, zoals bijvoorbeeld in EN 1922-1-1 is opgenomen. In toekomstige voorschriften kan beter een bovengrens worden gesteld aan de maximaal optredende staalspanning, in samenhang met wapeningsdiameter en betonsterkte, dan aan de oppervlakte-scheurwijdte.

Table of Contents

Chapter 1

Introduction

1.1.   General background

Reinforced concrete is a versatile composite structural material. Even decades after the first applications of reinforced concrete engineers and contractors were not fully aware of the aspect of service life, implicitly assuming that the physical service life exceeds the functional service life. However, meanwhile it has become clear that deterioration of structures should be a major design criterion. According to modern structural design codes, like the Model Code for Concrete Structures 2010 (fib, 2013), therefore structures have to be designed for safety and serviceability for a specified service life: during this period no, or only limited, maintenance should be necessary.

A durable performance of a concrete structure is only possible if the material properties are taken into account in combination with other essential aspects like execution, structural design, curing and maintenance (CEB, 1992). These requirements have to be fulfilled to a certain minimum level in order to assure sufficient durability of concrete structures. It is of vital importance that the engineers who are in charge of structural design, have a good understanding of the most dominant deterioration mechanisms which can occur during service life of the structure. Deterioration mechanisms are a function of time and may gradually change the bearing resistance of a structure and its serviceability (Fig. 1-1). A specified margin of safety has to be assured between the bearing resistance R of a structure and the maximum load S. Due to deterioration this

margin will reduce in time until an unacceptable level is reached. It should be ensured that this level will not be reached before the end of the specified service life of the structure.

In daily practice often a deemed-to-satisfy approach is used, with requirements for minimum cover thickness and appropriate concrete composition in order to limit permeability for aggressive substances. A distinction is made for different exposure classes. In code recommendations mostly limits for crack width are specified as well. However, these limits have never been convincingly confirmed by practice. Since they may considerably influence the amount of reinforcing steel, this aspect should be much better investigated. This study will focus on the role of cracks and their width on the service life of concrete structures with respect to chloride-induced reinforcement corrosion.
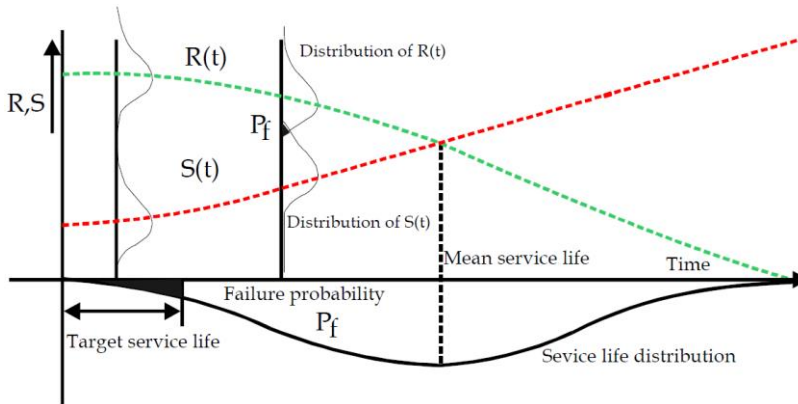
Figure 1-1: Probabilistic determination of service life (Rostam, 2003)

1.2.   Chloride-induced corrosion in reinforced concrete structures

Chloride-induced corrosion is a mechanism which has led to premature deterioration of many concrete structures worldwide. Nowadays, huge amounts of money have to be spent to deal with this deterioration mechanism. The corrosion process is an electrochemical process, which is generally caused by large chloride ion concentrations close to the embedded steel. Permeable concrete allows moisture and chloride ion ingress which will result after some time in corrosion of the reinforcement. Initially a thin protective layer on the surface of reinforcing steel, which inhibits the corrosion of the steel in the

beginning, was formed during the cement hydration process. The passive film is stable by virtue of the high alkalinity of the pore solution, which usually has a pH-value >13. However, the passive layer can be destroyed by the action of chloride ions or when the alkalinity of the environment with regard to the pH value due to carbonation of the cement paste sinks below a pH-value of 9. Beside chloride ions and moisture, the presence of oxygen is necessary to cause corrosion of the steel reinforcement. The most severe conditions in practice are to alternately wetting and drying cycles exposure of concrete members. Therefore, the tidal and splash zones in a marine environment are the areas with the highest risk for chloride-induced corrosion (Fig. 1-2). Other sources of chlorides can be de-icing salts, which can generate chloride-induced corrosion on huge concrete surfaces. The process of chloride-induced corrosion is explained in Chapter 2 in more detail.

Figure 1-2: Chloride-induced corrosion in a marine environment

1.3.   Prediction of service life

Service life prediction models have been developed by many authors aiming at determining the time that reinforced concrete structures are able to meet the design demands with regard to functionality (DuraCrete, 2000; fib, 2006). Among the many proposed models the most general is the one proposed by Tuutti (1982). According to this conceptual model, the service life can be divided into two subsequent phases: the initiation period and the propagation period. During the initiation period chloride ions, water and oxygen penetrate through the concrete cover as a consequence of the exposure of the structure to an aggressive environment. The initiation period is finished when aggressive

substances in a certain concentration reach the reinforcing steel destroying the passive layer. Thereupon, the propagation phase starts. In this phase voluminous corrosion products induce concrete cracking which will further facilitate penetration of aggressive substances through cracks. Furthermore, corrosion can lead to spalling of the concrete cover or eventually to collapse of the structure. Corrosion-induced damages are regarded as appropriate limit states depending on the level of damage as is shown in Fig. 1-3. Many efforts have been undertaken to model chloride penetration until a critical chloride content is reached at the steel surface. Most models take into account only the initiation phase, which is at the safe side with respect to service life design. However, part of the propagation phase can also be taken into account based on two important reasons (Raupach, 2006). At first, for new structures the time between depassivation of steel reinforcement (limit state 1) and corrosion-induced cracking (limit state 2) can be in the order of at least several years and even several decades. Furthermore, the length of the propagation phase should be estimated to quantify the residual service life of existing structures in order to apply well-planned maintenance and repair measures. However, the estimation of the propagation phase is difficult because many parameters (binder type, concrete quality, concrete cover, loading, relative humidity, electrical concrete resistivity, cracks, temperature, exposure conditions, aging effects, chloride binding, self-healing etc.) will affect the corrosion process. Especially, service life models for cracked concrete structures have still not been sufficiently investigated. Consequently, better prediction models for the service life of cracked concrete structures are needed and represent an aim for further research.
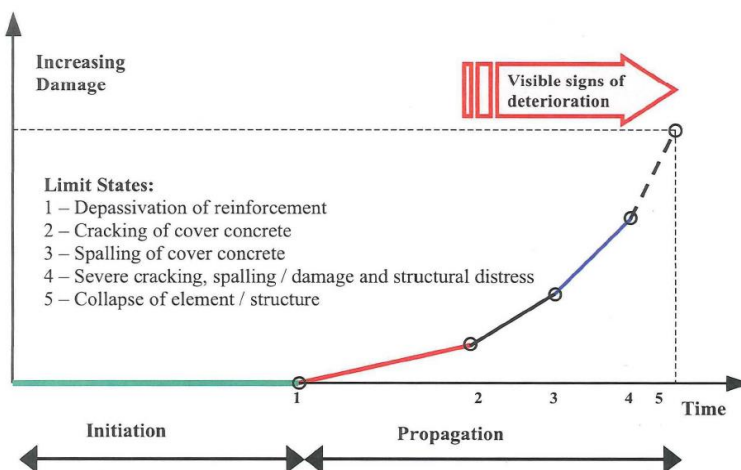
Figure 1-3: Corrosion process in reinforced concrete structures (fib, 2006)

1.4.   The role of crack width in relation to durability

1.4.1.   *Crack width limits in codes*

In current codes for structural concrete the maximum crack width under a defined load level is regarded to be a major criterion for durability. In Eurocode 2 (2005) the maximum crack width for reinforced concrete structures is determined under the quasi-permanent load combination, while for prestressed concrete structures - the frequent load combination applies. EN 1992-1-1 (2005) is flexible with regard to the choice of authorities in each country to determine the loading level and the maximum allowable crack width with respect to the relevant environmental class. No indication is given for the most appropriate choice. The crack width criteria in the various codes show substantial differences. For example, Eurocode 2 (2005) recommends a value of 0.3 mm for the maximum allowable crack width in reinforced concrete members exposed to an aggressive environment under the quasi-permanent load combination, whereas the Dutch code NEN 6720 (1995) prescribes 0.2 mm under the frequent load combination and ACI Committee 224 (1994) prescribes 0.15 mm under the design service load. Based on that, the question can be raised:

"If crack width is an important factor in relation to durability, which loading level is the most appropriate for the determination of the critical maximum crack width?"

1.4.2.   *Surface crack width versus crack width at reinforcement level*

An aspect that should be considered as well is that the crack width is measured at the surface of the structure, whereas it decreases into the direction of the reinforcement. This is not logical since the crack width at the reinforcement bar should be the governing parameter, although this width cannot easily be measured. The present guidelines can even lead to conflicting conclusions, since if the concrete cover is increased to account for increased durability, the surface crack width will also increase, which erroneously suggests that durability is decreased. In other words, increasing the concrete covers will require more reinforcement in order to limit the surface crack width to its allowable value. Only in a small number of codes this anomaly is avoided by defining the maximum allowable surface crack width as a function of the concrete cover, like

the former Dutch code NEN 6720 (1995) and the fib Model Code for Concrete Structures 2010 (2013).

1.4.3. *The influence of crack width on the corrosion process*

An extremely important and logic question is whether the crack width matters at all for durability. Already in 1987, acknowledging fundamentals, CEB Bulletin 182 states that for the corrosion process to occur and proceed, a separation in anodic and cathodic areas is necessary. In a simplified way, the reinforcing steel in the cracked region would generally act as the anodic area, whereas the cathodic process will mostly occur at the steel surface within the uncracked areas or "between the cracks". In the case of crack widths up to 0.4 mm, "self-healing", resulting from calcium-bearing compounds, dirt- and rust deposits within the cracks is frequently observed. Hence, further penetration of aggressive substances, water and oxygen through these cracks is suppressed and consequently the rate of the corrosion process decreases. On the other hand, chloride-induced corrosion is an autocatalytic process with the following sequence: once chloride ions have reached the steel surface in a sufficient amount, localised corrosion starts and propagates; corrosion products form above and in the vicinity of the area of corrosion initiation; this limits further chloride ions penetration in the same area. However, chloride ions remain trapped within the "pits" and the corrosion process proceeds in depth of the reinforcement. Within this process, Fe^{2+}, Cl^- and H^+ ions are present in the pits and the pH can locally drop to a value below 5, resulting in fast corrosion propagation. The presence of a depolarizer in the medium (e.g. OH^-) is necessary for the released electrons (within oxidation) to be discharged (within reduction). Since oxygen and water are always present in concrete, the reduction (or cathodic process) is hard to be controlled. Therefore, the mechanism of chloride-induced corrosion, especially in an alkaline environment, is mainly dependent on the continuous ingress of aggressive substances, propagation in existing pits (through the porous "pit" membranes) and initiation of new ones. Although both anodic (steel oxidation) and cathodic (reduction) processes can be generally controlled, the anodic process plays the major role and depends on aggressive ions penetration. Therefore, the existence of cracks, their width, frequency and type are considered significantly contributing factors to corrosion-induced degradation of concrete structures.

1.4.4. *Conflicting opinions with regard to significance of crack width*

In the Model Code for Service Life Design (fib, 2006) the role of crack width is even ignored, suggesting that cracks are not relevant. Nevertheless, even in the most recent codes like EC2 (2005), tables with crack width limits are given, indicating that obviously doubts about the role of crack width for structural performance still exist. These uncertainties mainly refer to:

- Can we confidently state that steel corrosion is significantly minimised due to self-healing, dirt of rust deposits in various cracks? Concrete structures are often subjected to variable loads, which hampers self-healing. Hence, the presence and development of cracks cannot be ignored, especially if self-healing cannot be relied upon.

- If the crack width is large, this means that at the reinforcement level, considerable micro-cracking has occured, enabling additional access of oxygen, water and chloride ions to areas away from the main crack. In the case of close-by positioned principal cracks, the result will be the formation of a scaffold of micro-cracks, extending along substantial areas between the principal cracks. Logically, these microstructural changes may contribute to a significant spreading of ions and water penetration, i.e. these changes will determine the electrochemical phenomena occuring at the steel surface. Therefore, their development cannot be ignored.

Aiming at gaining more insight to answer the above-raised questions, an experimental program was developed in order to generate more knowledge and contribute to the improvement of codes and engineering practice.

Chapter 2

Corrosion of steel reinforcement in concrete

2.1.   General background

Concrete structures can be damaged by different types of deterioration processes (chloride-induced corrosion, carbonation-induced corrosion, alkali-silica reaction, freeze-thaw attack, sulphate attack). Corrosion of steel reinforcement in concrete structures is one of the major threats to durability. Among different degradation mechanisms which can lead to corrosion of embedded steel in concrete two of them can be especially emphasized: chloride penetration and carbonation. Many investigations have been undertaken in recent years for better understanding of the aforementioned degradation mechanisms and corrosion of reinforcing steel (Alonso, 1998; Andrade, 1993 and 2001; Arya and Ofori-Darko, 1996; Castel et al., 2003; Francois, 2006; Granju, 2005; Jaffer, 2009; Otieno et al., 2008; Otieno, 2010; Pacheco 2014; Schießl, 1997; Scott and Alexander, 2007; Šavija, 2014; Walraven, 2015).

Initially the embedded steel in concrete is protected by the passive layer on its surface formed as a result of the high alkalinity of the cement matrix (pH >13) and through an appropriate cover depth. This passive layer is formed during the process of cement hydration and it is very thin (1-10 nm) preventing direct contact between steel and chloride ions, moisture, oxygen and carbon dioxide. It consists of a passive ferric oxide film γ- Fe_2O_3 and can resist corrosion. However, this passive layer can be destroyed by chloride ingress even at a high pH level or by carbonation.

Carbonation occurs when atmospheric carbon dioxide (CO_2) reacts with water (H_2O) in concrete pores forming carbonic acid (H_2CO_3) which further reacts with calcium hydroxide ($Ca(OH)_2$) to form calcium carbonate (C_aCO_3) as shown in equations (2-1) and (2-2).

$$CO_2 + H_2O \rightarrow H_2CO_3 \qquad\qquad (2\text{-}1)$$

$$H_2CO_3 + Ca(OH)_2 \rightarrow CaCO_3 + 2H_2O \qquad\qquad (2\text{-}2)$$

Carbonation is a neutralizing reaction which is results into a lowering of the pH from above 12.5 to a value below 9 indicating that no more stable passive layer is present. The passive film is destroyed when it is in contact with the carbonated zone and steel corrosion can occur. As can be seen from equation (2-2) water is released in the carbonation process, which leads to a sustained process of carbonation. A simplified model for carbonation was proposed (Eq. 2-3):

$$x = K_{CO_2} \cdot t^{\frac{1}{n}} \qquad\qquad (2\text{-}3)$$

where:

x - carbonation depth at time t

K_{CO_2} - carbonation factor which depends on concrete and environmental conditions

n - exponent which is around 2

Measuring carbonation depth by spraying freshly broken concrete with a phenolphthalein solution, is a fast and economic method. After spraying the concrete will become purple for pH > 9, pink for 8 < pH < 9 or remain colorless for pH < 8. Although carbonation can induce corrosion of reinforcing steel in reinforced concrete structures, a more important cause of degradation worldwide is chloride attack.

2.2. Chloride-induced corrosion

2.2.1. The electrochemical process of corrosion

Corrosion of reinforcing steel is an electrochemical process which occurs when metal is exposed to a reactive environment. Along the reinforcing steel two sites are formed: a cathode and an anode. That part of the steel which has more locally a negative potential acts as the anode, while the other part of the steel which remains passive acts as a cathode. Corrosion occurs at the anodic side from which a current flows to the cathodic site where occurrence of corrosion does not apply. The anode and cathode site are connected by the electrolyte (concrete pore solution) which conducts a current. The current comes back through the steel and the electric circuit is completed. The corrosion process is shown in Fig. 2-1.

In a study by Neville (1995) it was shown that positively charged ions Fe^{2+} dissolve in water and electrons are set free (Eq. 2-4). Thereupon, these free electrons e^- flow to the cathodic side where they are combined with constituents of the electrolyte, oxygen and water forming hydroxyl ions OH^- (Eq. 2-5).
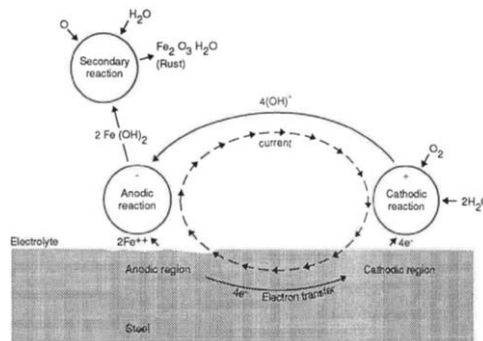
Figure 2-1: Corrosion process in concrete (Arya, 1995)

Anodic reaction:

$$Fe \rightarrow Fe^{2+} + 2e^- \qquad (2\text{-}4)$$

Cathodic reaction:

$$2H_2O + O_2 + 4e^- \rightarrow 4OH^- \qquad (2\text{-}5)$$

Further, OH^- ions which flow through the pore solution react with moving Fe^{2+} ions forming ferrous hydroxide $Fe(OH)_2$ (Eq. 2-6). After that ferric hydroxide is converted to rust by the process of oxidation (Eq. 2-7).

$$Fe^{2+} + 4OH^- \rightarrow Fe(OH)_2 \qquad (2\text{-}6)$$

$$4Fe(OH)_2 + 2H_2O + O_2 \rightarrow 4Fe(OH)_3 \qquad (2\text{-}7)$$

A permanent supply of oxygen and water at the cathodic sites as well as concrete conductivity, are required for a continuous process of corrosion. Therefore, the influence of RH is an important factor affecting the kinetics of the corrosion process. There is progress at a RH value of 70-80%. In the case of dry concrete, a high level of electrical resistivity leads to the absence of significant steel corrosion. However, in conditions of partly saturated concrete, a high corrosion rate occurs in time due to the high conductivity of concrete. If concrete is fully water saturated, for instance in immersed concrete members, the corrosion process stops in time due to the lack of oxygen being unable to diffuse into the concrete.

As far as cracked concrete is concerned, two mechanisms of corrosion can occur in the cracked zone or in the nearby area: microcell corrosion and macrocell corrosion (Schießl, 1997) (Fig. 2-2). Two different corrosion mechanisms can be seen in Fig. 2-2 which are theoretically possible for steel corrosion in the region of cracks.
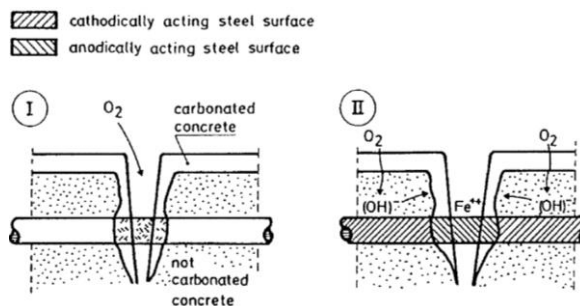
Figure 2-2: Schematic presentation of microcell and macrocell corrosion (Schießl, 1997)

Mechanism I shown in Fig. 2-2 is characterised by microcell corrosion in the crack zone, in which both cathodic and anodic processes occur on a small space, side by side, where the oxygen can easily penetrate from outside. However, according to mechanism II the reinforcement in the crack-zone acts as an anode

while the passive steel between the cracks acts as a cathode. Mechanism II (macrocell corrosion) leads to a much higher rate of steel corrosion caused by the cathodic site than in the case of mechanism I (microcell corrosion).

Corrosion of reinforcing steel in concrete can be induced by various influencing factors, but the most important one is chloride penetration. When the passive layer is broken down and reinforcing steel starts corroding actively, corrosion initiation can be detected even at initially low corrosion rates. An appropriate concentration of chlorides at the reinforcing steel is required, the so-called chloride threshold level which is discussed later in Section 2.2.3, in order to locally destroy the protective layer (ferric oxide film γ- Fe_2O_3) and allowing the process of corrosion to go faster. In this process, chloride ions act as a catalyst to corrosion when the concentration of chlorides at the steel surface is high enough. One of the most common chloride-induced types of steel corrosion is localized pitting corrosion. The morphology of the attack by pitting corrosion is shown in Fig. 2-3. It can be seen that once corrosion has been initiated, a very aggressive environment will be produced inside the pits. Chloride-induced corrosion is highly localized at a small anode with pitting corrosion of steel occurring. With high concentrations of chloride ions at the steel surface, the attack can involve larger areas but the mechanism remains the same. The following reactions are involved:

$$Fe^{2+} + 2Cl^- \rightarrow FeCl_2 \tag{2-8}$$

$$FeCl_2 + 2H_2O \rightarrow Fe(OH)_2 + 2HCl \tag{2-9}$$

$$FeOCl + H_2O \rightarrow Fe(OH)_2 + Cl^- \tag{2-10}$$
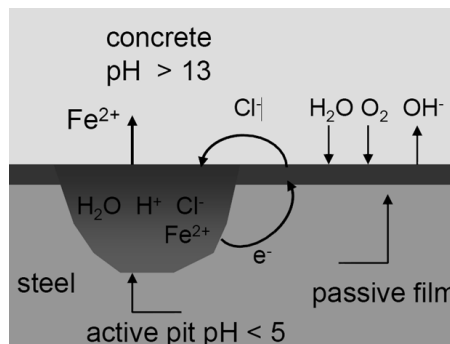
Figure 2-3: Schematic representation of pitting corrosion of steel in concrete (Bertolini, 2004)

In the reaction between chloride ions Cl^- and Fe^{2+} ferric chloride $FeCl_2$ is formed which increases the pit area by lowering the pH value. In the same reaction oxychloride, $FeOCl$, can also be formed. The increased acidity of the anodic area is leading to further oxidation of iron. As can be seen from equations 2-9 and 2-10, chlorides are not contained in the rust formed and by hydrolysis they are set free. After that, this process becomes self-propagating.

Various hypotheses have been reported on the process of destroying the passive layer at the steel surface, but until now none of them is generally adopted. However, it is not vital for understanding the impact of chloride ions on depassivation and subsequent corrosion of reinforcing steel in concrete. The most simple explanation is that steel corrosion can be initiated at a certain concentration value of chloride ions, which destroys the protective film present at the steel surface.

Various corrosion products can be formed, with volumes that can be many times larger than the original steel volume. Depending on the environmental conditions, high amounts of oxides and hydroxides can be formed. In Fig. 2-4 the most common corrosion products of iron are presented.
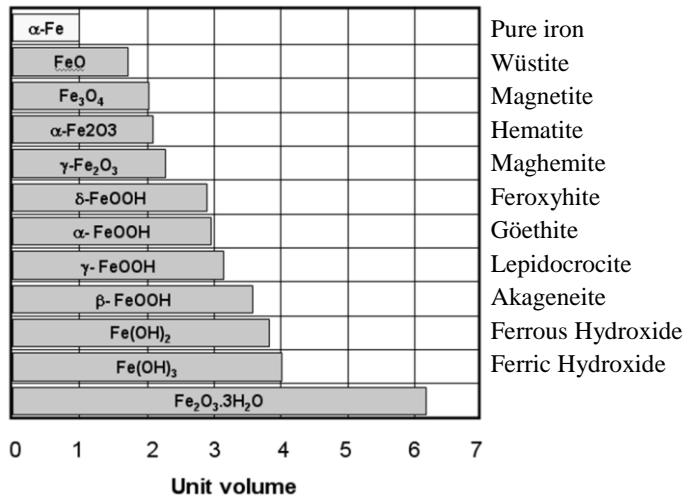
Figure 2-4: Iron corrosion products (Jaffer, 2009)

2.2.2. *Transport mechanisms of chloride ions in concrete*

As is already mentioned, durability of concrete structures is influenced by various deterioration mechanisms like, reinforcement corrosion and other physical or chemical processes in concrete structures. Many gases, liquids and ions have the ability to penetrate into concrete by several more or less dominant transport mechanisms: diffusion, migration, permeation, capillary suction, convection, wick action etc. or by any combination of these (Fig. 2-5). Since this research studies chloride ingress in cracked concrete and chloride-induced corrosion, therefore attention will be given mainly to moisture transport, chloride penetration, oxygen availability etc. which have a major impact on these phenomena. The governing mechanisms of transport in concrete structures depend on the exposure conditions, actually, on the degree of saturation of pores in concrete. The most important and often governing transport process in fully water saturated concrete is diffusion. A typical exposure condition for this transport mechanism is the submerged area. If, however, alternately wetting and drying cycles occur, unsaturated pores are present causing capillary suction as the most important transport process. The properties of the concrete composition are also of vital importance to the transport mechanisms, like cement paste permeability and aggregate size. Initially many models were used to predict chloride ingress in uncracked concrete, and since the last decade of the previous century a lot of efforts have been undertaken to apply those versions of models in practice, taking into account the main transport processes.
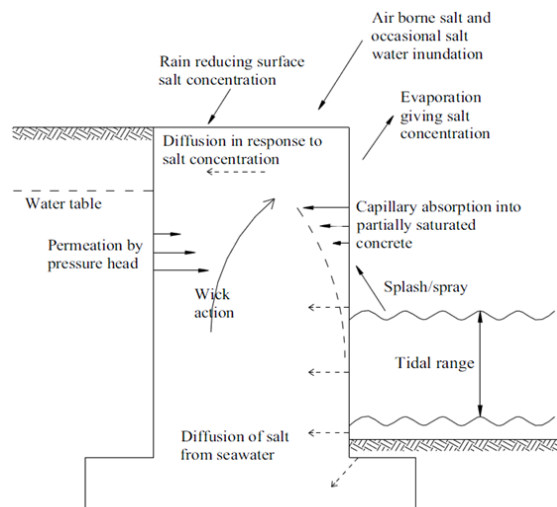
Figure 2-5: Transport mechanisms of chloride ions into concrete (Adiyastuti, 2005)

2.2.2.1   Diffusion

Diffusion is a process of ion movement from an area of high concentration to an area with a low concentration. This concentration difference allows ingress of chloride ions from the environment into the concrete, to be more specific, into the concrete pore solution. Furthermore, the presence of pore water is necessary for chloride ion ingress in concrete. The process of diffusion will be faster if concrete pores are completely saturated but it also occurs in partially saturated concrete in combination with some other transport mechanisms. Diffusion is considered to be the most important transport mechanism and many models have been developed on the basis of that assumption. Only in some studies concrete specimens have been cracked and specimens continuously immersed in chambers with artificial sea water, water with 3-10% NaCl solution, (Adiyastuti, 2005; Garces Rodriguez, 2003; Gowripalan, 2000; Ismail, 2008; Ismail, 2004; Win, 2004). The concrete specimens exposed to these conditions represent saturated concrete where diffusion is the governing transport mechanism.

Fick was the first to develop an expression based on diffusion processes. The first Fick's law (Eq. 2-11) presents differential equation for a diffusion process with respect to a concentration gradient where molecules diffuse from zones with a high concentration to zones with a low concentration. The steady state diffusion is synonym for Fick's first law, according to which the diffusion through materials with uniform diffusivity can be estimated.

$$J = -D \cdot \frac{\partial C}{\partial x} \tag{2-11}$$

where:

J - mass transport rate [mol/m^{2}s]

D - diffusion coefficient [m^2/s]

C - chloride concentration [mol/m^3]

x - distance [m]

Fick's first law is not time-dependent; therefore, concentration of chlorides must be achieved at one constant level to apply this model in reality. Therefore, Fick developed a new model for non-steady state conditions based on the previously

mentioned model. One more parameter was involved, being the time dependence, which was implemented in Fick's second law (Eq. 2-12).

$$\frac{\partial C}{\partial t} = D \cdot \frac{\partial^2 C}{\partial x^2}$$

(2-12)

In this equation the assumption was made that the diffusion coefficient, D, is independent of the concentration and position. However, the concentration depends on position and time of exposure to aggressive substances. The following boundary conditions were used for concrete:

- initial condition - C=0 at x>0 at time t=0

- boundary condition - C=C$_s$ at x=0 and t>0

where C$_s$ is the constant surface chloride content.

Furthermore, chloride concentration with regard to x and t can be determined if the complimentary error function, Crank's solution, is applied to cementitious materials (Crank, 1983) as is shown in equation (2-13).

$$C(x,t) = C_s \left[1 - erf \left(\frac{x}{2 \cdot \sqrt{D_a \cdot t}} \right) \right]$$

(2-13)

where:

C(x,t) – concentration of chloride as a function of depth and time [wt. % of binder content]

C$_s$ – surface chloride concentration [wt. % of binder content]

x – depth [mm]

t – time of exposure [years]

D$_a$ – apparent chloride diffusion coefficient [m^2/s]

$$\frac{x}{2 \cdot \sqrt{D_a \cdot t}} = z$$

erf(z) – error function (Eq. 2-14)

$$erf(z) = \frac{2}{\sqrt{\pi}} \int_0^z e^{-t^2} dt \tag{2-14}$$

The error function can be calculated or taken from tables. However, in the convection zone the development of the chloride content in depth can deviate from Fick's second law. Therefore, the expression for the chloride profile has been modified by DuraCrete (2000) as follows:

$$C(x,t) = \left[C_0 + (C_{s,\Delta x} - C_0) \cdot \left[1 - erf\left(\frac{x - \Delta x}{2 \cdot \sqrt{D_a \cdot t}} \right) \right] \right] \tag{2-15}$$

where:

$C(x,t)$ – chloride content [% by mass of cement]

C_0 – initial chloride concentration [% by mass of cement]

$C_{s,\Delta x}$ – chloride concentration at a depth of Δx [% by mass of cement]

x – depth [m]

Δx – depth of the convection zone [m]

t – concrete age [years]

D_a – apparent chloride diffusion coefficient in concrete [m^2/s]

Many assumptions were made to deal with the diffusion process in concrete materials. Therefore, many models have a lack of accuracy caused by factors such as the degree of hydration, maturity, relative humidity, water-binder ratio, temperature, chloride binding, chemical admixtures, etc. Equation (2-12) was developed only for a one dimensional diffusion process but in practice two or even three dimensional diffusion processes often occur requiring modified equations.

An apparent chloride diffusion coefficient (D_a) was used by some authors where the diffusion process has to be regarded as penetration of ions in concrete as an unity. Diffusivity of chloride ions is not the same in solid zones as in porous parts of the concrete. Due to many assumptions which were made in the models to simulate certain conditions, the application of these models has its limitations.

2.2.2.2 *Capillary suction*

Capillary suction is caused by pore pressure in dry or partly saturated porous concrete materials. Capillary suction occurs when chloride contaminated liquid comes into porous concrete due to surface tension which occurs in capillaries. The level of absorption depends on alternating wetting and drying cycles which have a vital influence on this type of chloride transport mechanism into concrete structures. Namely, during a drying period water evaporates from the pores but chloride ions remain in the pores of a near surface zone. The next wetting cycle brings more chlorides into the pores and unlike the previous cycle a higher concentration of salts develops in the pore system. It can be reasoned that after many consecutive wetting and drying cycles the water in the capillary pores will be saturated with chlorides. Moreover, after a certain number of cycles the concentration in the concrete can be even higher than the chloride surface concentration (Neville, 1995). Young-Laplace presented an equation under the assumption of one round pore (Eq. 2-16).

$$P = -\frac{2\gamma\cos\theta}{r} \qquad (2\text{-}16)$$

where:

P - pressure pulling water and chlorides [Pa]

γ - liquid-vapor surface tension of fluid [N/m]

θ - the contact angle between liquid and solid phases [^{0}]

r - the pore radius [m]

For one dimensional penetration capillary suction in a porous material can be estimated by equation (2-17).

$$\frac{W}{A} = S\sqrt{t} \qquad (2\text{-}17)$$

where:

W - volume of absorbed water [m^3]

A - exposed surface area [m^2]

S - sorptivity [$m\,s^{-1/2}$]

t - time [s]

2.2.2.3   Migration

Migration is the movement of (chloride) ions in a solution caused by an electric field. According to the accelerated method in the laboratory chloride ions move in opposite direction from the current due to the negative charge of Cl^- ions. The movement, under the action of the electric field with regard to diffusion, is determined by the concentration and is described in equation (2-18):

$$D_i = \frac{RTu_i}{z_i F}$$
(2-18)

where:

D_i – migration coefficient [m^2/s]

z_i – electrical charge of ion I , for chloride z=1

F – Faraday's constant [96548 C/mol]

T – absolute temperature [K]

R – the gas constant [8.314 J/molK]

u_i – potential difference in the sample [V]

Chloride ions penetrate through the concrete sample by water filled, tortuous and interconnected capillary pores. The resistivity of concrete to chloride ingress is determined by the velocity of migration, which depends on concrete porosity and the aforementioned pore's features.

In a lot of research methods non-steady-state migration experiments are applied, e.g. the test described in Build NT492 (1999) or its modified version, to determine the chloride migration coefficient in concrete, mortar or cement-based materials (Audenaert, 2009; Marsavina, 2009; Yoon, 2007; Spiesz and Brouwers, 2013). The difference between the chloride migration coefficient determined according to the mentioned Nordic method and the diffusion coefficient obtained from a non-steady-state immersion test or a steady-state migration test has to be emphasized. While the diffusion coefficient represents the movement of chloride

ions from a high concentration zone to a low concentration zone, migration is actually influenced by an external electrical field. Hardened cylindrical specimens which are cast under laboratory conditions or drilled from structures in practice are necessary to determine the chloride migration coefficient. Mostly drilled cores are used with a minimum diameter of 100 mm and a thickness of 50 mm. The test is carried out by using an electrical potential difference, forcing chloride ions to migrate into the specimen. 10% NaCl (100 g NaCl in 900 g water) solution is a catholyte. The anolyte solution is 12 g NaOH in 1 l water. Both solutions are stored at 20-25 °C (Fig. 2-6).

Deliberately induced migration can be achieved by turning on the power with appropriate voltage after some time stops. The initial and the final current as well as temperature in the solution are recorded. Furthermore, after the test voltage is finished, the specimen has to be axially split into two parts. On one of the split parts a silver nitrate solution is sprayed and as a consequence white silver chloride precipitation will be visible after a short period of time.
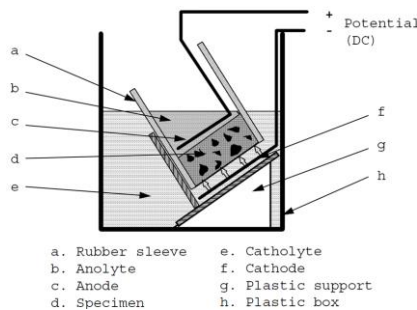
Figure 2-6: One arrangement of the migration set-up (Build NT492, 1999)

Thereupon, the depth of chloride penetration has to be measured at 10 mm intervals from centre to edge where seven measurements are made in total (Fig. 2-7).
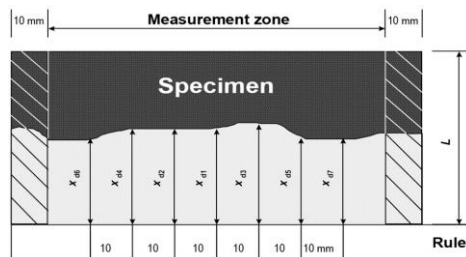
Figure 2-7: Illustration of measurement of chloride penetration depths (Build NT492, 1999)

The calculation of the non-steady-state migration coefficient follows from the following equation:

$$D_{nssm} = \frac{0.0239(273+T)L}{(U-2)t}\left(x_d - 0.0238\sqrt{\frac{(273+T)Lx_d}{U-2}}\right)$$

(2-19)

D_{nssm} - non-steady-state migration coefficient [10^{-12} m^2/s]

U - absolute value of the applied voltage [V]

T - average value of the initial and final temperatures in the anolyte solution [°C]

L - thickness of the specimen [mm]

x_d - average value of the penetration depths [mm]

t - test duration [hours]

In addition, the chloride content in the specimen may be determined by a method prescribed in Nordtest (1996).

2.2.2.4 Permeation

Although permeation is not one of the governing transport processes of chloride ions in concrete, it sometimes has to be taken into account, for example, in the case of submerged members of concrete structures which are exposed to a marine environment. Permeation is a process in which chloride ions are flowing through porous concrete under a hydrostatic head. Permeation can be described by Darcy's law (Eq. 2-20) as follows:

$$\upsilon = \frac{k}{\mu}\frac{\Delta P}{\Delta x}$$

(2-20)

where:

Δx – distance [m]
ΔP – applied pressure difference [Pa]
μ – dynamic viscosity of the fluid [Pa·s]
k – coefficient of permeability [m^2]
υ – fluid flow velocity [m/s]

2.2.3. <u>Chloride threshold level</u>

A certain minimum amount of chlorides is required at the reinforcing steel surface to destroy the protective layer. The chloride content which is necessary for destroying the passive film is generally known as the chloride threshold level or critical chloride content. The value of the chloride threshold level is important for recording the beginning of corrosion initiation. A unique value does not exist, because it depends on various factors. The most common influencing parameters are: concrete quality, binder type, water-binder ratio, relative humidity, temperature, concrete-steel interface, Cl^-/OH^- ratio, total chlorides to free chlorides ratio, steel potential, environmental conditions (submerged zone, splash and tidal zone or atmospheric zone) under which structures are exposed to chloride penetration. Since most of these factors are time dependent, the chloride threshold will vary with time. In a study by Bertolini (2004) it was stated that the most important factors which affect the chloride threshold level are the quality of concrete-steel interface, OH^- concentration in the pore solution (pH), steel potential and the properties of concrete. Furthermore, the presence of voids at the concrete-steel interface can be considered as one of the most important factors which results into a decreased chloride threshold level (Glass, 2000). The chloride threshold level is often expressed by the following parameters: Cl^-/OH^- ratio, free chloride threshold level and total chloride content. The Cl^-/OH^- ratio represents the chloride threshold but it is not clear enough. First of all, it does not include the amount of bound chlorides. It is assumed that above a certain value of the Cl^-/OH^- ratio, the risk of steel corrosion increases as shown in Fig. 2-8.
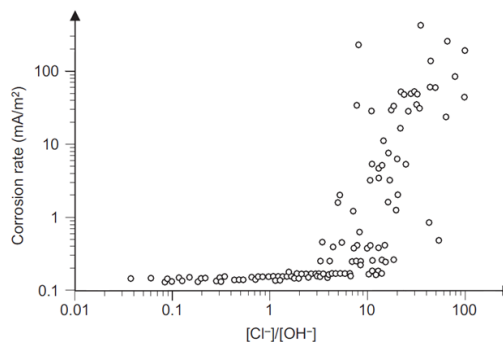
Figure 2-8: Relationship between Cl^-/OH^- ratio and corrosion rate of steel (Bertolini, 2004)

Metal hydroxides (NaOH, KOH) lead to a highly alkaline pore solution in concrete (increased pH) acting as inhibitor to the corrosion process. However, increasing the pH leads to a decrease of the bound chlorides. Consequently, it was found that at a certain level of the total chloride an increased pH is followed by an increased Cl^-/OH^- ratio and thus an increased corrosion risk. Taking into account that hydroxides act as inhibitors and lead to higher pH alkalinity, it is contradictory that a higher pH is accompanied by a higher level of corrosion risk. It can be concluded that this approach to determine the chloride threshold level is not appropriate.

The free chloride threshold, which includes only water soluble chlorides, like the previous approach, does not take into consideration bound chlorides as a factor which influences steel corrosion. As was pointed out already earlier that bound chlorides also have an impact on the corrosion process, this method is also not generally adopted.

The most common approach which has been used by various codes to represent the chloride threshold level is based on the total chloride content. As mentioned, due to different influencing factors various minimum total chloride contents have been proposed in the literature (from less than 0.1 to more than 3 per cent of chloride content by cement mass). In Fig. 2-9 the different values, required for corrosion initiation, are shown (Adiyastuti, 2005) depending on the critical chloride content by mass of binder, Cl^-/OH^- ratio and exposure type.

However, the most common value which is applicable nowadays lies between 0.2 and 0.4 per cent of chloride content by cement mass for reinforced concrete and between 0.1 and 0.2 for prestressed concrete. The higher value can be expected in a moderate climate while the lower value is determined for more aggressive environmental conditions. The relationship between chloride content at the steel surface and half-cell potential measurements can be used to predict corrosion risk of steel reinforcement. Furthermore, low corrosion risk can be expected if the potential is > -250 mV versus copper/copper sulphate (CSE) reference electrode at chloride levels < 0.4% by weight of cement (Bentur, 1997).

Total Chloride wt % cem.	[Cl⁻]:[OH⁻]	Exposure Type	Researcher
0.17 – 1.4		Field	R.F. Stratful, W.Jurkovich and D.L Spellman
0.2 – 1.5		Field	P.Vassie
0.25		Field	R.E.West and W.G.Hime
0.25 – 0.5		Laboratory	B.Elsener and H.Böhni
0.3 – 0.7		Field	C.F.Henriksen
0.4		Outdoors	P.B.Bamforth and J.F.Chapman-Andrews
0.4 – 1.6		Laboratory	C.M.Hanson and B.Sorensen
0.5 – 2		Laboratory	P.Schiessl and M.Raupach
0.5		Outdoors	M.D.A.Thomas, J.Matthews and C.A.Haynes
0.5 – 1.4		Laboratory	K.Tuuti
0.6		Laboratory	C.E.Locke and A.Siman
1.6 – 2.5		Laboratory	P.Lambert, C.L.Page and P.R.W.Vassie
1.8 – 2.2		Field	W.Lukas
	2.5 – 6	Laboratory	K.Pettersson
	0.26 – 0.8	Laboratory	S.Goni and C.Andrade
	0.3	Laboratory	S.Diamond
	0.6	Laboratory	D.A.Hausmann
	1 – 40	Laboratory	T.Yozenawa, V.Ashworth and R.P.M.Procter

Figure 2-9: Critical chloride content required to initiate reinforcement corrosion (Adiyastuti, 2005)

2.2.4. *Parameters affecting chloride-induced corrosion in cracked concrete*

Many factors can have a significant influence on chloride penetration and chloride-induced corrosion in concrete. A literature review shows that the concrete composition is the most important influencing parameter on the processes mentioned. The concrete transport properties depend on the binder type, water-binder ratio, supplementary cementitious materials, curing, execution, porosity, aggregate size etc. Besides the concrete composition, the exposure conditions are also important to take into consideration. These include factors such as exposure time, chloride content, temperature and relative humidity. Most of the time reinforced concrete structures are under some degree of loading during their service life. According to the loading-state (static, dynamic, compressive, tensile or unloaded-state) a different behaviour of chloride ingress and chloride-induced corrosion can be noted.

Many studies were conducted to examine the impact of the aforementioned factors on chloride penetration and chloride-induced corrosion in sound concrete.

Some efforts have been undertaken in the last 20 years to compare those results with obtained data on cracked concrete specimens exposed to chlorides. While some factors have a more or less similar impact on cracked concrete compared to sound concrete with respect to the ingress of chlorides and corrosion, other factors are, typically, used only to examine their influence on cracked specimens.

2.2.4.1 Exposure conditions

As far as exposure conditions are concerned, two types can be emphasized: alternately wetting and drying cycles and immersion (non-steady diffusion state in both cases). Pre-cracked concrete beams were exposed to periodic wetting and drying cycles which represents the most severe condition in an aggressive environment. This environmental condition was simulated by several authors (Francois, 1998; Francois, 2006; Konin, 1998) who made a confined chamber where specimens were exposed to periodic cycles by spraying salt fog (Fig. 2-10a).

Some researchers (Adiyastuti, 2005; Garces Rodriguez, 2003; Gowripalan, 2000; Ismail, 2008; Ismail, 2004; Win, 2004; Yoon, 2010), have applied a steady state of exposure, more commonly known as immersion test, to examine the impact of cracks on chloride ingress. Artificial salt water was used to simulate exposure conditions in which the cracked concrete specimens were immersed for some period of time. In some cases the beam sides were epoxy-sealed except the cracked side which was exposed to chloride ingress (Adiyastuti, 2005; Gowripalan, 2000). After that period cracked concrete specimens were taken out and chloride profiles were measured. In a study by Gowripalan (2000) cracked concrete prisms were immersed in a 3% NaCl solution for 300 days in a temperature and moisture-controlled room at $23\pm2°C$ and $50\pm5\%$ RH. Immersed beams, up to two years, were also used by Adiyastuti (2005) in a standard laboratory environment $26\pm4°C$ and $80\pm15\%$ RH (Fig. 2-10b). Win (2004) used a different NaCl solution (3-7%) in which cracked concrete specimens were immersed for one week and one month, respectively, after 3 months of curing in a controlled environment of 20°C and 60% RH.

The fastest method to determine chloride penetration in concrete is an electrical migration test, the rapid chloride migration test, which was described in more detail (Build NT492, 1999) in Section 2.2.2.3. Although the execution of this method requires only a short period of time, the reliability of data has to be regarded with a considerable amount of limitations with respect to applicability

on real reinforced concrete structures. Anyway, during a study by Yoon (2007 and 2010) a comparison between the immersed method and the migration test was done. The border between the chloride-contaminated zone and the healthy zone was clear in the concrete in the short-term experiment, while it was ambiguous in the long term experiment.

In a marine environment the splash and tidal zones are considered as the areas which cause the highest corrosion risk of reinforcing steel due to alternating wetting and drying cycles. For structures exposed to de-icing salts, such as bridge decks, car parks, concrete pavements and reinforced concrete roads, the corrosion risk is mainly caused by the very high concentrations of chloride ions in the water after ice melting. When the steel reinforcement starts to corrode, due to these high concentrations of chloride, structures eventually might lose integrity and service life can be influenced negatively.
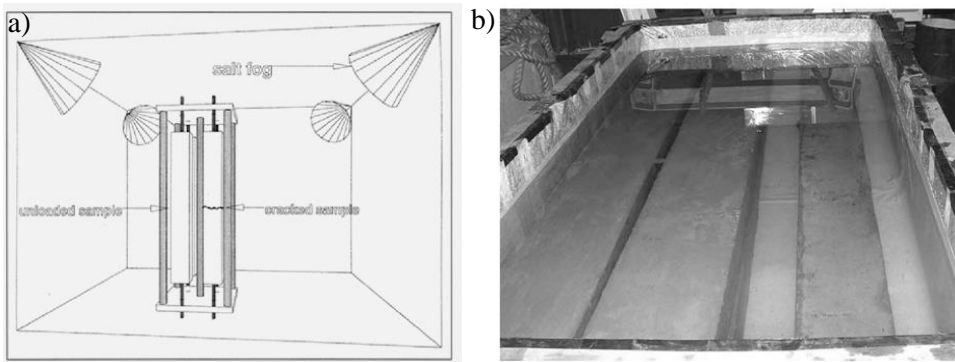
Figure 2-10: Exposure conditions: a) Simulated aggressive environment (Konin, 1998); b) Immersed beams in salt solution (Adiyastuti, 2005)

2.2.4.2 Binder type

Many researchers have investigated the influence of binder type on chloride ingress and chloride-induced corrosion in concrete. Besides ordinary Portland cement, blends of Portland cement with fly ash, silica fume, ground granulated blast furnace slag have been tested. These blends are supplementary cementitious materials. From these experiments it is generally accepted that supplementary cementitious materials have a higher resistance to chloride penetration than samples with OPC (ordinary Portland cement). This is due to chemical and physical reasons. Concrete mixtures made with supplementary cementitious materials are more resistant to chloride penetration than those made with OPC

alone as a result of the ability of chloride binding. Furthermore, the pore structure of OPC is more prone to chloride penetration in comparison with the pore structure of SCM-s. In a study by Konin (1998) the chloride ingress was decreased in presence of silica fume in cracked concrete specimens and a similar observation was made by Jang (2011) but in presence of fly ash and Garces Rodriguez (2003) who used blast furnace slag. In a study by Audenaert (2009) and Marsavina (2009) the cement content was varied to investigate the impact of this factor on chloride ingress in cracked concrete. It turned out that chloride penetration was decreased by increasing the cement content at a permanent water-to-cement ratio.

In a study by Scott and Alexander (2007) the impact of binder type on the corrosion rate was investigated using seven different concrete mixtures comprising ordinary Portland cement and blends of Portland cement with ground granulated blast furnace slag, silica fume and fly ash. Corrosion rates were measured for two concrete covers (20 mm and 40 mm) and two crack widths (0.2 mm and 0.7 mm) (Fig. 2-11).
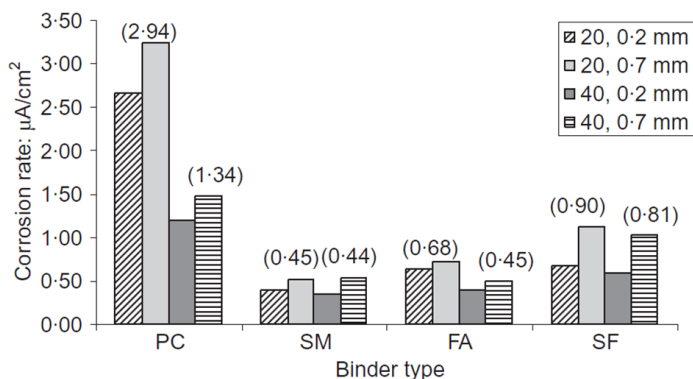
Figure 2-11: Impact of binder type on corrosion rate depending on concrete cover and crack width (Scott and Alexander, 2007)

It can be seen that the use of any supplementary cementitious material leads to a significant reduction of the corrosion rate compared to ordinary Portland cement. It is important to note that the samples with Portland cement showed a significant reduction in corrosion rate caused by a larger cover depth of 40 mm compared to 20 mm. However, only a negligible reduction was obtained in the case of samples with supplementary cementitious materials due to the increased cover depth. The samples which were cast with supplementary cementitious materials

have a higher resistivity and a lower permeability than those made with ordinary Portland cement. This means that the corrosion rate of samples cast with supplementary cementitious materials is controlled by the resistivity and that the limitation of oxygen availability by an increased concrete cover has negligible impact. However, in the case of samples with ordinary Portland cement which have a low resistivity, an increase of the cover depth leads to a significant reduction in corrosion rate due to limiting the availability of oxygen. On the other hand, all samples with supplementary cementitious materials have a lower corrosion risk with a cover depth of 20 mm and 0.7 mm crack width than ordinary Portland cement with 40 mm cover depth and 0.2 mm crack width. However, these results were obtained on samples with one single crack and the results might be different in the case of many cracks with approximately the same width under a variable load (most common case in practice). Further research is needed for a better determination of the interrelated influence of binder type, concrete cover and surface crack width on the corrosion of steel reinforcement. The resistivity of supplementary cementitious materials leads engineers to utilize this binder in severe environmental conditions because of a lower risk of deterioration.

2.2.4.3   *Water-binder ratio*

The water-binder ratio is an important factor with regard to chloride penetration in cracked concrete. It was found by many authors (Djerbi, 2008; Konin, 1998; Win, 2004) that the higher is the water-binder ratio, the higher is the chloride ingress in cracked concrete. A higher water-binder ratio leads to a more permeable concrete cover and a higher corrosion rate. In a study by Win (2004) different values of the water-cement ratio (0.25, 0.45, 0.65) were used to investigate its influence on chloride concentration in cracked concrete beams from the exposed surface and around the crack. The binder was ordinary Portland cement. It was found that cracked concrete specimens with a lower water-cement ratio led to lower chloride concentrations in the concrete from the exposed surface (Fig. 2-12).
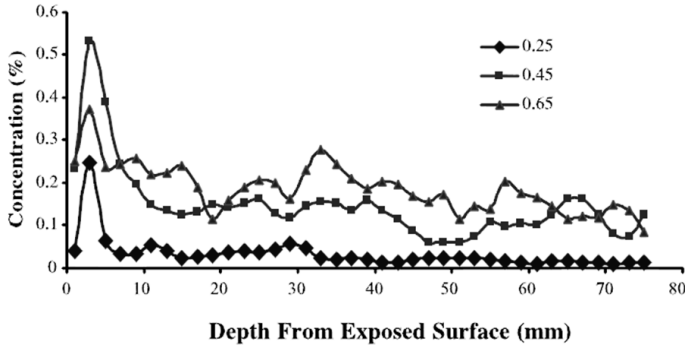
Figure 2-12: Chloride concentration profile after one month of exposure for concretes with a different w/c ratio (Win, 2004)

In a study by Mohammed (2001) the influence of crack width and water-binder ratio on the corrosion rate was investigated on 28 days old concrete prisms. It was concluded that the relationship between water-cement ratio and corrosion rate of steel reinforcement in cracked concrete is more relevant than the relationship between crack width and corrosion rate. In a study by Otieno (2010) the influence of two types of binder, OPC and 50/50 OPC/GGCS (ground granulated Corex slag) blend, on the corrosion rate in cracked concrete was investigated. It was found that the corrosion rate is decreased when the water-binder ratio is decreased, but OPC specimens are much more sensitive to changes in water-binder ratio than Corex slag specimens.

2.2.4.4   Loading

A wide variety of test methods have been employed to produce cracked specimens by loading as described in Section 3.6. However, after cracking many of the specimens have been exposed to chloride ingress in an unloaded state to obtain relevant data in connection with chloride penetration despite of the fact that an unloaded state is not common in reality. Consequently, these results cannot be accepted with a high level of reliability. However, the important influence of loading has been taken into account by applying a sustained static load by some authors (Antoni, 2005; Gowripalan, 2000; Lim, 2000). In a study by Gowripalan (2000) a flexural sustained load was applied during chloride exposure which was executed in the form of an immersion test. It was found that under flexural loading, the tensile face had a higher chloride ingress than the compressive face.

In a study by Antoni (2005) sustained compressive load as well as cyclic loading was applied on plain and fibre reinforced concrete specimens. Under a low level of static loading the results showed a slight reduction of chloride ingress but under higher stresses an increased ingress has been found. The chloride ingress increased even more under cyclic loading conditions, showing a difference between the behavior of fibre reinforced concrete and plain concrete at a different number of cycles and load level. The impact of cyclic loading on chloride penetration was also studied by authors (Küter, 2005; Wang, 2011) who found a significant difference between static and cyclic loading. It can be seen in a study by Küter (2005) that the difference in chloride ingress is obvious under cyclic opening and closing of concrete cracks compared to cracks with a constant width under static loading. Obviously crack opening and closing under dynamic load leads to increased chloride ingress, especially towards the crack tip. It was concluded that the increased chloride penetration in dynamic cracks is rather controlled by the frequency and rate of load application than by the surface crack width. Wang (2011) drew similar conclusions but the impact of temperature and water-binder ratio were combined with dynamic loading which also increased the chloride ingress into concrete. In a study by Otieno (2010) the impact of surface crack width on chloride-induced corrosion has been investigated under a constant load which has been increased to a higher level just twice during 31 weeks of chloride exposure. However, in reality the process of reloading occurs every day, going along with re-opening of the crack all the time.

2.2.4.5   Type of bar

As far as chloride-induced reinforcement corrosion is concerned, the impact of bar type should not be neglected. In a study by Mohammed (2001) an electrochemical investigation was carried out on cracked prismatic reinforced concrete beams with plain and deformed bars. It was observed that cracked samples with deformed bars have a higher oxygen permeability, lower concrete resistance, higher chloride concentration, more surface and internal cracks compared to samples with plain bars. Moreover, the cathodic reaction in the samples with plain bars is slower than that in the samples with deformed bars. It can be concluded that deformed bars tend to corrode more than plain bars in cracked reinforced concrete samples. This might be caused by larger internal microcracking introduced by the ribs when the bar slips in the concrete.

2.2.4.6   Self-healing

In recent years the phenomenon of auto (self) healing has been studied (Aldea et
al., 2000; Edvardsen, 1999; Ramm, 1998). It was, generally, known that crack
width would be narrower in concrete after some time of exposure to (different)
environmental conditions. Consequently, during the process of autogenous
healing water flow is decreased with time and in some case cracks can be
completely closed. Several mechanisms influence self-healing of cracks:
chemical processes, physical processes and mechanical processes. As far as
chemical processes are concerned, the formation of calcium carbonate and the
growth of crystals on the crack walls are considered to be the most important
factors which affect self-healing of cracks. In particular, calcium ions from the
concrete pore solution react with carbonate ions in the water and form calcium
carbonate ($CaCO_3$) which precipitates in the crack. In the study by Edvardsen
(1999) it was stated that the precipitation of calcium carbonate crystals ($CaCO_3$)
in the crack is almost the sole cause for autogenous healing of the cracks and
growth rate of the $CaCO_3$ crystals depends on crack width and water pressure. It
was also stated that the formation of $CaCO_3$ responds to two different crystal
growth processes. In the initial phase of water exposure the kinetics of crystal
growth is surface controlled, but in time it is a diffusion controlled crystal
growth. The other chemical process is the hydration of cement particles which
have not hydrated due to an insufficient amount of water. Self-healing can be
taken into account when crack widths are smaller than 0.1 mm and the concrete
is in an early age. Physical processes have almost no impact on self-healing.
Only swelling of hydrated cement paste (HCP) near the crack walls represents a
noteworthy physical contribution. Mechanical processes represent also minor
mechanisms in self-healing of cracks. Clogging of the cracks by fine particles
originally present in water or by particles broken off from a fractured surface are
some of the mechanical processes. It can be seen that the presence of water is
necessary for the process of self-healing. The impact of self-healing on chloride
penetration into concrete is different depending on environmental conditions.
Although a few authors have used stiffness recovery to quantify self-healing, the
most common method is to measure water leakage through cracked concrete.
Even though self-healing was not measured in investigations by some authors
(Francois, 2006; Otieno, 2010), they concluded that decreased chloride
penetration was a consequence of self-healing. However, it should be emphasized
that the impact of self-healing as corrosion arresting mechanism is questionable
under a variable load.

Chapter 3

The influence of cracks on chloride penetration and chloride-induced corrosion in concrete: State-of-the-Art

The influence of cracks on chloride penetration and chloride-induced corrosion in concrete has been investigated in a wide range during recent years. Cracks facilitate the ingress of chloride ions, moisture and oxygen through the concrete cover, especially if cracks are interconnected, because then concrete is more permeable. Cracks can appear in concrete due to various reasons which can be seen in Fig. 3-1: a distinction is made in two different groups of cracks, occurring before hardening and after hardening.
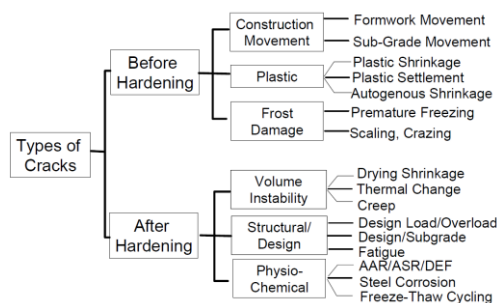

Figure 3-1: Causes of cracking (CEB, 1992)

The influence of cracks on chloride penetration and chloride-induced corrosion depends on crack width, crack frequency, crack geometry, crack orientation with respect to embedded steel reinforcement, steel-concrete interface and crack depth.

3.1.   Crack width

As far as the influence of cracks on chloride penetration in cracked concrete is concerned, the surface crack width is considered to be the most important parameter by many authors. In several research projects an effort has been made to determine the critical crack width which represents its maximum allowable limit value. In the case of limited crack width the transport properties of concrete are regarded by a number of authors similar to those in sound concrete (Ismail, 2004; Jang, 2011; Yoon, 2010). However, different values are presented by these authors. While a value of 0.053 mm was reported by Ismail (2004), Jang (2011) found a value of 0.08 mm. Furthermore, different critical values were determined by Yoon (2010) for a short period of exposure (RCM) 0.012 mm and 0.05 mm for a long period of exposure, by immersion of specimens in artificial sea water. In a study by Garces Rodriguez (2003) the influence of artificially created crack widths in the range of 0.08 to 0.68 mm on chloride penetration was investigated. It was concluded that chloride transport in concrete containing parallel-wall cracks is independent of crack width or crack wall roughness. The impact of crack width on chloride penetration in concrete cubes was also examined by Audenaert (2009) and Marsavina (2009). The range of crack widths was 0.2-0.5 mm in this study, but at the end of the investigation the results have not shown any clear relation between crack width and chloride ingress into concrete. In a study by Djerbi (2008) a critical crack width of 0.08 mm was found. Furthermore, it was concluded that the diffusion coefficient is higher if the crack width is larger, as long as the width is less than 0.08 mm. Otherwise, if the crack width is higher than 0.08 mm, the diffusion coefficient is constant and does not depend on crack width.

The impact of crack width on the corrosion rate of steel reinforcement has been investigated by many authors (Arya, 1995; Francois, 1998; Francois, 2006; Jaffer, 2009; Mohammed, 2001; Otieno et al., 2008; Otieno, 2010; Otsuki, 2000; Sahmaran, 2008; Schießl, 1997; Scott and Alexander, 2007; Pacheco, 2015). While it is generally accepted that the presence of cracks accelerate corrosion initiation, there is still a debate about the impact of cracks on corrosion propagation. On the one hand some authors state that cracks do not have an influence on the behavior in the propagation period (Francois, 1998; Schießl, 1997), while on the other hand there is a thought (Otieno, 2010; Otsuki, 2000) that cracks affect the behavior both in the initiation period and in the propagation period. In a long term corrosion observation program by Francois and Arliguie

(1999) and Francois (2006) the corrosion process in relation to mechanical cracks and the mechanical behavior in relation to corrosion intensity was investigated. It was found that the corrosion development has no correlation with the crack width (for widths smaller than 0.5 mm) or even with the presence of cracks. It was stated that the type of load applied to a reinforced concrete beam is more important than the crack width if this is below 0.5 mm with respect to chloride ingress and chloride-induced corrosion of reinforcing steel. In a study by Otsuki (2000) the influence of bending crack and water-cement ratio on chloride-induced corrosion of reinforcing bars and stirrups was investigated. A significant impact of bending cracks and water-cement ratio on the corrosion rate of reinforcing bars was observed. Furthermore, macrocell corrosion occurred and an increased corrosion rate was observed in the vicinity of a bending crack. The impact of crack widths (0.1 mm, 0.3 mm and 0.7 mm) on the corrosion of steel reinforcement was investigated by Mohammed (2001). In Fig. 3-2 the macrocell current densities in function of the exposure period are shown for different crack widths. The figure shows, that the relation between crack width and corrosion rate is obvious until the second week of exposure, where the wider crack is related to the higher current density i.e. the corrosion rate. However, the relation changes after four weeks of exposure. Taking into consideration the design service life of a concrete structure which is based on the initiation period, the presence of cracks is more important than their widths with respect to corrosion of steel reinforcement. It should also be mentioned that the current density of uncracked specimens was negligible even after 13 weeks of exposure.
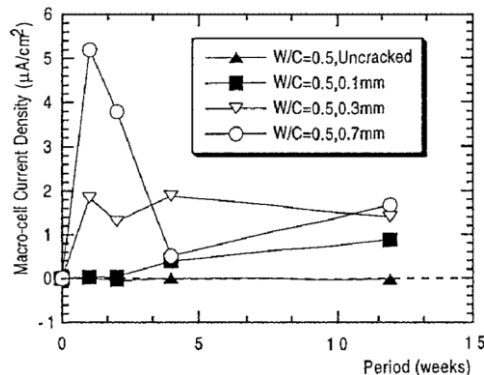

Figure 3-2: Macrocell current density of steel elements at crack (different exposure periods and crack widths) (Mohammed, 2001)

In a study by Schießl (1997) the impact of the crack width on the process of corrosion was investigated. It was found that although wider cracks lead to increased corrosion of steel reinforcement, the concrete cover and the concrete composition have a larger influence on the corrosion process than crack width. A significant relationship between crack width and corrosion rate was not observed. It was concluded that the corrosion rate in the cracked zone depends on the conditions between cracks and the problem of reinforcement corrosion in the cracked zone cannot be solved by crack width limitation in a range from 0.3 mm to 0.5 mm only.

In a study by Scott and Alexander (2007) the impact of crack width on the corrosion rate for a different binder types and concrete covers was investigated. It was concluded that an increased crack width leads to an increased corrosion rate. Furthermore, wider cracks prevent self-healing by corrosion products which can block the crack and limit chloride penetration through the crack to the steel reinforcement. It was concluded that the impact of crack width on the change of corrosion rate over time is most pronounced in the case of silica fume (SF). Furthermore, for a concrete cover of 20 mm, the change in corrosion rate for crack widths from 0.2 mm to 0.7 mm is 67%, but for a concrete cover of 40 mm it is even more than 75%. It should also be emphasized that the lowest value of the corrosion rate is noted for blast-furnace slag which is the most suitable supplementary cementitious material with respect to chloride-induced corrosion of steel reinforcement in cracked concrete.

In a study by Otieno (2010) the influence of crack width (incipient crack, 0.4 mm and 0.7 mm) on the corrosion rate of steel reinforcement for different types of binder and water-binder ratio, but for a constant concrete cover has been investigated for 31 weeks. Two times re-loading was applied (between weeks 9-10 and 18-19) where the crack widths have been maintained for 24 hours (0.2 mm, 0.6 mm and 1.0 mm) under a higher load before being reduced to the previous widths. In Fig. 3-3 the average corrosion rates (weeks 26-31) for different crack widths and concrete compositions are shown.
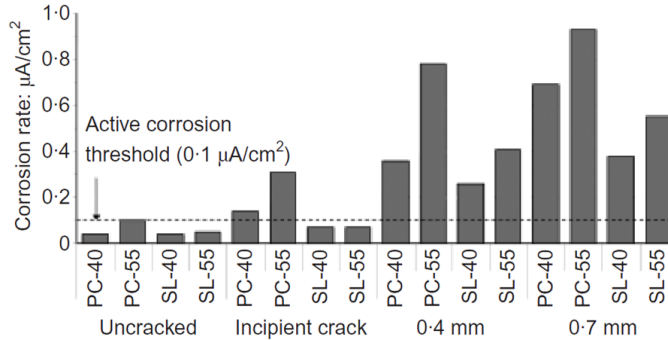
Figure 3-3: Average corrosion rates (weeks 26-31) for different crack widths and concrete compositions (Otieno, 2010)

It can be seen that for the same water-binder ratio, the influence of crack widths on the corrosion rate is higher in the case of OPC than in the case of slag. 0.1 $\mu A/cm^2$ is the active corrosion threshold value. The influence of crack width on the corrosion rate is less for widths between 0.4 mm and 0.7 mm than between the uncracked and incipient cracked samples. It is obvious that the adoption of a unique threshold crack width can lead to overestimation or underestimation of the rate of the corrosion process. Consequently, a threshold crack width can be determined for a specific combination of concrete cover, binder type and water-binder ratio. The statement that 0.4 mm is the general threshold crack width is shown not to be valid due to the fact that incipient cracks, in the case of OPC, lead to a significant impact on the corrosion rate during both phases, initiation and propagation. The process of self-healing was stopped by re-loading, but re-loading was applied just twice during 31 weeks of exposure. However, in reality the process of re-loading is actual every day, which leads to reopening of crack widths all the time. There is a peak hour in the traffic over many bridges twice a day. It means that variable loading should be experimentally applied to observe the impact of a variable crack width on chloride ingress and chloride-induced corrosion for a specific binder type, water-binder ratio and concrete cover. It can be concluded that in general there is no correlation between crack width and corrosion, but the initiation period is shorter if the crack is wider. Furthermore, cracks have impact on the corrosion rate and, therefore, should not be neglected in service life models. However, the impact of crack width on corrosion initiation and propagation has still not been sufficiently explored, especially with regard to the propagation period, and there is a clear need for further research.

3.2.   Crack frequency

Chloride penetration and chloride-induced corrosion in cracked concrete are not dependent only on surface crack width. Also the number of cracks per specific length (crack frequency) is reported to play a significant role. In a study reported by Arya and Ofori-Darko (1996) the impact of crack frequency on corrosion of reinforcing steel was investigated using reinforced concrete beams containing 0, 1, 4, 8, 12, 16 and 20 parallel sided cracks per meter length. However, in each case the crack depth was constant at 40 mm and the sum of the total width was kept constant at 2.4 mm. The water-binder ratio and the concrete cover were constant, being 0.65 and 42 mm, respectively. The impact of the crack frequency on the cumulative weight loss due to corrosion, as a function of time, is shown in Fig. 3-4.

It can be seen that an increased crack frequency leads to a higher corrosion rate except in the case of 20 cracks where the process of self-healing is obviously interfering. It was concluded that limiting the crack frequency is more important than limiting the surface crack width to control corrosion of steel reinforcement. However, those conclusions are not applicable in practice. First of all, flexural cracks do not have the same depth along the beam in reality which is opposite to this experiment. Furthermore, in reality cracks are V-shaped and not rectangular-shaped. Self-healing was present due to the unloaded state of the beam. Otherwise, in practice self-healing would be impaired under the action of the variable load and corrosion products, blocking the crack, will be eliminated. This means that the relations shown in Fig. 3-4 would be significantly different under conditions which are common in practice.
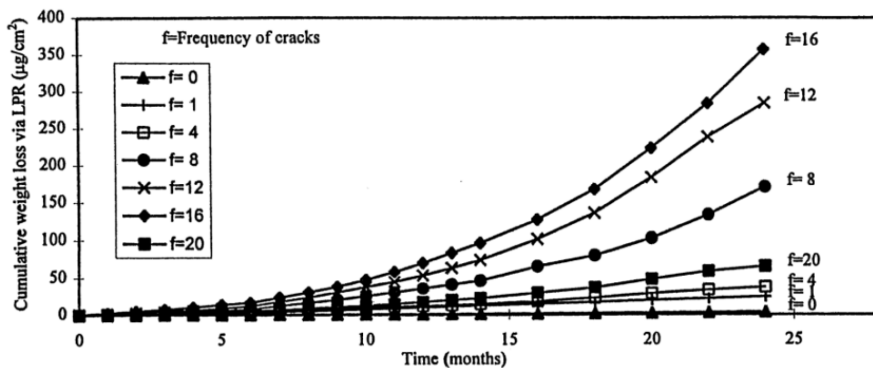

Figure 3-4: Effect of crack frequency on cumulative weight loss due to corrosion (Arya and Ofori-Darko, 1996)

An appropriate experimental set-up is still required to involve in a right way the interrelated impact of crack width and crack frequency on chloride-induced corrosion under simulated realistic conditions by future research.

3.3. Crack orientation and geometry

As far as crack orientation is concerned, two groups can be distinguished: longitudinal (coincident) cracks and transverse (intersecting) cracks relative to steel rebar orientation. While coincident cracks are parallel to the reinforcement, intersecting cracks are across the reinforcement. Coincident cracks can be extremely dangerous with regard to corrosion of steel reinforcement due to easy access of chlorides, moisture and oxygen to a large area of the steel reinforcement. The corrosion process will become even faster in time. Therefore, coincident cracks can significantly shorten the service life of the structure. However, this is not the case with respect to intersecting cracks. Even though intersecting cracks can shorten the initiation period, they do not significantly affect the propagation phase. Furthermore, the cathodic site is situated between cracks where oxygen and moisture have to reach the embedded steel through sound concrete in order to enable the corrosion process. However, there is still an open question on to which extent intersecting cracks affect the corrosion rate during the propagation phase.

In a study by Arya (1995) it was stated that the corrosion rate in the propagation phase depends on crack, concrete and steel properties. In the case of crack properties, the crack propagation status and crack geometry should not be neglected with respect to the impact of cracks on the corrosion of the steel reinforcement. While some crack widths do not vary in time (dormant cracks), others may vary (live cracks). Cracks can also be distinguished with respect to their propagation status due to the self-healing process and crack blocking by corrosion products. Particularly, dormant cracks can be blocked or self-healed. On the other hand, live cracks cannot be blocked due to loading, shrinkage, thermal effects and other expansion reactions. The crack geometry should also be taken into consideration with respect to the crack properties. While it is simple to measure the surface crack width, the crack width at the bar surface cannot be observed and quantified in practice. Furthermore, the crack width at the bar surface is not directly related to the surface crack width. It depends on the origin of the crack, the cover depth, the steel stresses, the distance between the bars, the

bar diameters and the depth of the tensile zone (Arya, 1995). An example of the variation of crack width with depth is shown in Fig. 3-5a. It should be emphasized that crack width at the bar surface is more important than surface crack width with respect to corrosion of the steel reinforcement. Although there is no clear relationship between surface crack width and corrosion rate, there seems to be an effect of the crack width on the corroded length as shown in Fig. 3-5b. The wider crack leads to a longer corroded area at the steel surface.
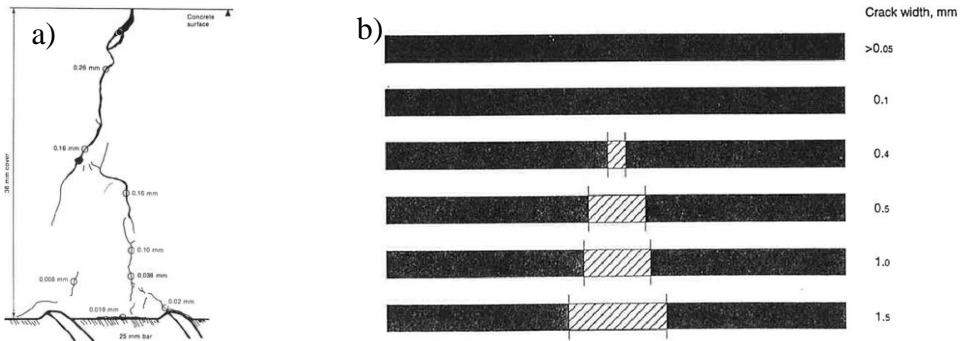

Figure 3-5: a) Variation of crack width with depth; b) Effect of crack width on corroded length of bar (Arya, 1995)

3.4.   Steel-concrete interface

The condition of the steel-concrete interface is related to the fracture properties of the concrete. In a study by Goto (1970) light was shed on the development of cracks in concrete around the rebar. That research work is appreciated as a basis for many other works related to the steel-concrete interface later on. It was stated that not only main ("primary") cracks are formed when a deformed bar is under tension in concrete, internal ("secondary") cracks are developed as well close to the main crack. When the steel stress is increased or the load is repeated, shortly after the formation of the main cracks, internal cracks will be formed even between the main cracks as depicted in Fig. 3-6. Furthermore, for high steel stresses in the vicinity of the main cracks the internal cracks might reach the inner part of the main crack, where sometimes the internal cracks are becoming visible at the concrete surface even, denoted as secondary cracks which are adjacent to the main crack. Once the internal crack is formed, "recovery" will never occur even when the load is reduced to a very low level. According to the aforementioned facts, the presence of internal cracks must not be neglected and

should be at least indirectly quantified in relation to potential chloride-induced corrosion.
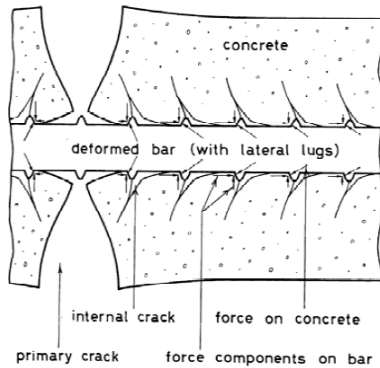

Figure 3-6: Steel-concrete interface after formation of the internal cracks (Goto, 1970)

In a study by Šavija (2014), focus was on the influence of the damage of the steel-concrete interface on chloride ingress in cracks and around the reinforcement as is depicted in Fig. 3-7. It was found that the larger the surface crack width, the longer the de-bonded region, which then becomes easily accessible to chloride ion penetration. This could potentially have an important impact on reinforcement corrosion, and has to be taken into consideration in the future quantifications of cracks on chloride-induced corrosion in concrete. Furthermore, a numerical model was proposed for chloride ingress in cracked concrete (Šavija et al. 2013). Although the model is simplified for saturated conditions (i.e. diffusion is considered as the only transport mechanism), they were able to simulate chloride ingress in cracks of different widths.
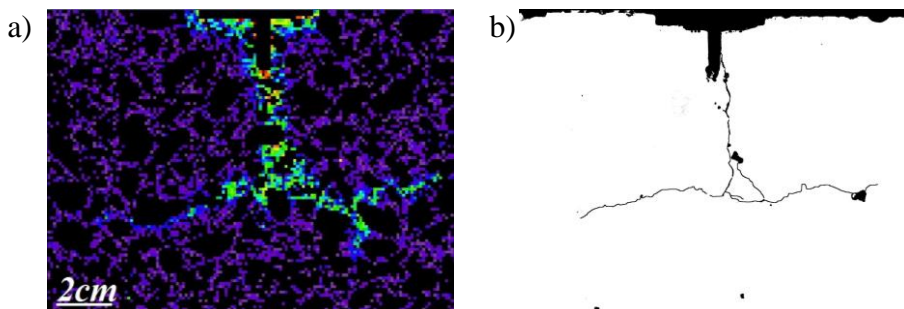

Figure 3-7: a) Chloride distribution, obtained by LIBS (Laser Induced Breakdown Spectroscopy), along the steel-concrete interface of a cracked specimen exposed to Cl wetting/drying cycles for 36 weeks; b) Cracks inside the specimen (impregnated with fluorescent epoxy resin, photographed under UV light) (Šavija, 2014)

In a study by Pease (2010) a detailed description of crack development under a flexural load in reinforced concrete is given. Different crack widths have been induced by flexural loading in order to investigate their effect on chloride ingress and development of reinforcement corrosion. As a tool for the assessment of flexure induced cracking of reinforced concrete beams under service load three-dimensional photogrammetry was used. Additionally, this experimental technique allows detailed inspection with respect to the crack geometry and cracking schemes. After casting, the beam was loaded. Subsequently it was cut and sprayed in order to observe the steel-concrete interface and cracking patterns (Fig. 3-8 and 3-9).
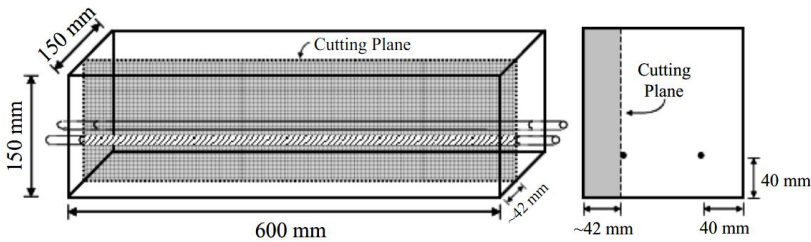

Figure 3-8: Specimen geometry with location of saw cutting indicated (Pease, 2010)

It is seen in Fig. 3-9 that the 8 mm aggregate specimens have more tortuous cracks than the 16 mm aggregate specimens under single load applications. Furthermore, under cyclic loading the cracks are interconnected nearly as a straight-line as opposed to the highly tortuous cracking caused by single load at the steel-concrete interface.
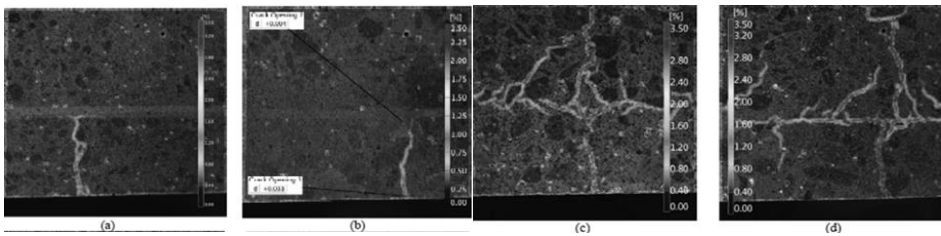
Figure 3-9: Computed Strain Overlay on Specimen with (a) 8 mm Maximum Aggregate Size under Estimated Cracking Load (14.0 kN) and with 16 mm Maximum Aggregate Size under (b) Estimated Cracking Load (13.0 kN), (c) 35.0 kN (single load), and (d) 35.0 kN (increasing cyclic load) (Pease, 2010)

At transverse crack, caused by loading, is initiated at the tensile side and in the same time slip and separation at the steel-concrete interface start to develop. The higher level of loading leads to an increase of the slip and separation. Slip and

separation along the bar can extend from 10 mm to 50 mm from the transverse crack and their maximal displacements in this research are 0.06 mm and 0.11 mm, respectively. It depends on the load level and the number of load cycles.

In a study by Tammo (2009) the impact of different parameters (concrete cover, bar diameter and concrete quality), affecting the crack width at the reinforcement level, was investigated. Specimens with a central reinforcing bar were axially loaded during the test procedure. It was concluded that a change of the concrete cover and the bar diameter affect the width of the crack near the bar less than the crack width at the concrete surface. Furthermore, the weak correlation between corrosion and surface crack width was confirmed. It was recommended that the use of the steel stress in the crack is more relevant as a measure of the potential level of exposure of the reinforcement through the cracks than the concrete cover and reinforcing bar diameter. However, further investigation of specimens in bending are required to assess the role of the parameters.

3.5. Crack depth

The impact of crack depth on chloride penetration in concrete was emphasized in a study by Audenaert (2009) and Marsavina (2009). It was reported that the influence of crack depth is of major importance compared to crack width, and this influence is more emphasized if the duration of the exposure is longer. However, the cracks are artificially induced with a parallel-wall. So, the testing conditions deviate from practice, where the cracks are V-shaped and the crack width and depth are different from the conditions in the experiment, where a constant crack width and a variable crack depth are created.

3.6. Methods used to induce cracks in concrete specimens

In the past twenty years various methods have been developed to induce cracks in specimens after some standard procedure of preparation. Stimulated by the remarkable differences between the international codes with respect to allowable cracks in concrete members (such as between Eurocode 2 and NEN 6720), many types of simulations on cracked concrete members were carried out during the last ten years. The purpose of most of these experiments was to control the crack width and to relate this to the other significant parameters with regard to chloride

ingress (concrete cover, water-binder ratio, concrete quality etc.). Different crack widths, ranging from 0.1 mm to 0.7 mm, have been induced to compare their influence on chloride penetration and corrosion of steel reinforcement in cracked concrete and to give recommendations for future codes. Two types of cracks, realistic and artificial, have been induced in laboratory tests by researchers. Both natural and artificial cracks can be produced by applying destructive and non-destructive techniques, which are described in the sequel.

3.6.1.   *Wedge splitting test method*

This method was used by a number of authors (Pease, 2010; Yi, 2011; Yoon, 2010; Šavija 2014). Actually, the wedge splitting method was created and improved by Brühwiler (1990), Linsbauer and Tschegg (1986). Using this method, the fracture properties of the concrete or some other materials can be provided. Cylindrical specimens are used and executing this method is simple. A wedge which is placed in a vertical groove induces compression which is further transferred in two horizontal tension forces creating the appropriate crack width (Fig. 3-10).
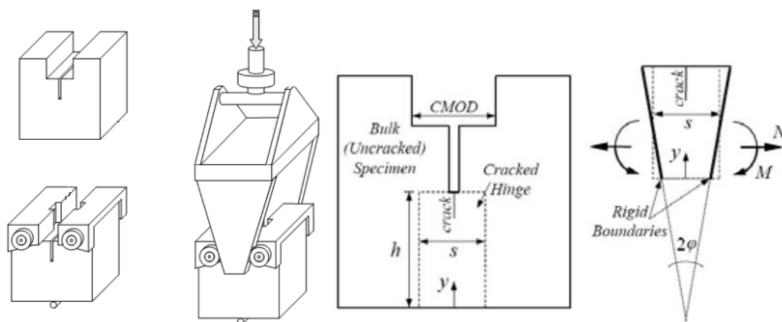

Figure 3-10: Wedge splitting method (Pease, 2010)

Crack width control is possible utilizing LVDT (linear variable displacement transducer) measurements and the CMO (crack mouth opening) can be recorded. It should be emphasized that cracks, which are induced in this way, are V-shaped and can be considered as realistic. The specimens can be exposed to chloride penetration after preparation but only in the unloaded state. Reinforcing steel is mostly not applied in this type of specimen, therefore, the influence of corrosion of steel reinforcement is not possible. However, the rapid chloride migration test (RCM) is conducted on these cracked specimens to determine the migration coefficient. In a study by Pease (2010) different material compositions were used

to determine their influence on fracture mechanics. Furthermore, an inverse analysis was applied. An increase of the aggregate size turned out to lead to increased fracture energy and a larger critical crack width, while varying the water-cement ratio only shows a slight influence on that. Furthermore, an increase of the fracture energy causes a less tortuous crack geometry.

3.6.2.   *Brazilian splitting method*

The Brazilian splitting method has been used by many authors (Aldea, 1999a; Aldea, 1999b; Aldea et al., 2000; Djerbi, 2008; Garces Rodriguez, 2003; Jang, 2011; Wang, 1997). The specimens do not contain any steel reinforcement. Therefore, it is not possible to measure the corrosion rate or potential. Similar as in the WST method specimens are exposed to chlorides only in the unloaded state. The execution of the Brazilian splitting test is simple. The test was slightly changed and adopted with some modifications by some authors during their experiments. The test is executed by a machine which induces compressive loading on specimens (Fig. 3-11).
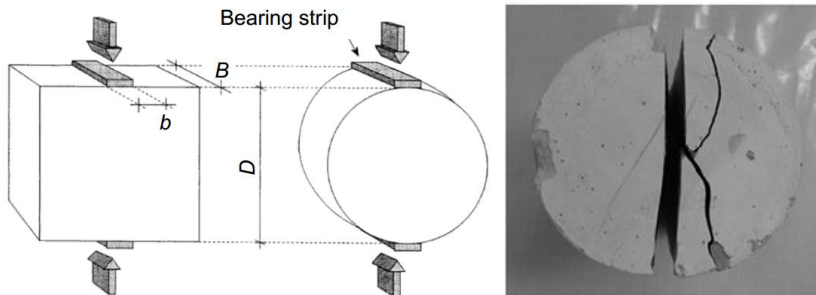

Figure 3-11: Brazilian splitting method

Two plywood ribbons are used to prevent crushing of the specimens at the contact points and, therefore, they are situated between the specimens and the loading machine transferring a compressive load to cylindrical specimens. As a consequence tension will be applied in the specimen orthogonally to the load direction and cracks will appear in the direction of loading. To control the crack width, LVDT measurements are made, orthogonally to the load direction. Furthermore, CMOD (Crack Mode Opening Displacement) is measured as the mean value of the displacements recorded by the sensors. In this way, the crack width can be measured and the required compressive loading can be controlled. It has to be emphasized that the crack width should be measured also after

unloading, because it will not be the same width as in the loaded state. A disadvantage of this method is that the induced cracks do not fully agree with the cracks in a structure (V-shaped). They have approximately the same width over their length, from the surface to the inside of the specimen.

3.6.3. *Expansive core method*

The expansive core method was used by Ismail (2004 and 2008). The cracks were induced in inert mortar materials. Disk shaped specimens with an external diameter of 100 mm and an internal diameter of 50 mm were used (Fig. 3-12).
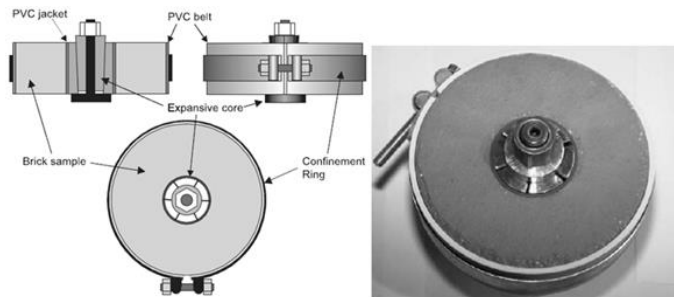

Figure 3-12: Schematic view of the sample, expansive core and brick disk (Ismail, 2004)

The height of the disc is 50 mm. Furthermore, the ring and mechanical expansive core were used forming together the mechanism of loading. After compressive load application cracks are produced at the internal part of the specimens with a required width. If these sort of cracks are compared with cracks obtained with some other methods, the cracks have a similar geometry as achieved with the Brazilian splitting test. It can be concluded that the cracks are not V-shaped having almost parallel walls which are not as in practice. While in the aforementioned methods, which were used to produce cracked specimens, the exposure to chlorides was limited to the unloaded state, in this method exposure is applied in the loaded state. Furthermore, like in the previous methods, reinforcing steel is not applied in the specimens.

3.6.4.   *Artificially induced cracks*

This method was used by many authors (Arya and Ofori-Darko, 1996; Audenaert, 2009; de Schutter, 1999; Garces Rodriguez, 2003; Marsavina, 2009). According to a generally applied method artificial cracks are produced by putting plastic shims or copper sheets in the concrete specimen before casting. A couple of hours after casting, the plastic shims are removed from the concrete specimen. As a consequence, the cracked concrete samples are obtained with the required crack width, crack depth, crack frequency or even crack spacing (Fig. 3-13).
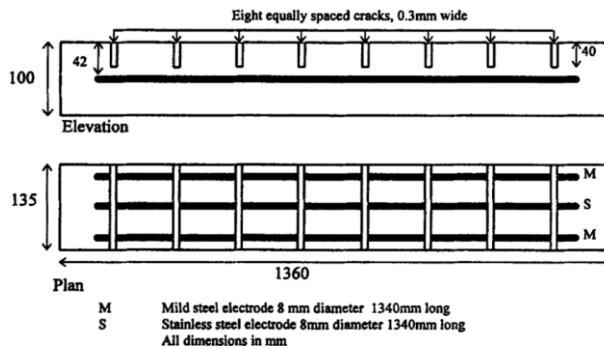

Figure 3-13: Reinforced concrete beam with artificial cracks (Arya and Ofori-Darko, 1996)

In the study of Garces Rodriguez (2003) saw-cutting and clamping were applied to produce artificial cracks. It can be seen that execution of this method is simple achieving parallel-sided cracks. Although these smooth cracks can be easily controlled, the disadvantage of this method is that the cracks obtained are not fully realistic. For instance, crack roughness, crack tortuosity and crack shape are only a few important parameters with regard to the difference between realistically-induced and artificially-induced cracks.

Although modeling of chloride penetration in this kind of specimen is the easiest, realistic chloride ingress will not be obtained because of differences in crack shape and absence of self-healing. The specimens can be reinforced concrete beams but also small concrete cubes without steel reinforcement depending on the purpose of the research project (corrosion of steel reinforcement or just chloride penetration, respectively (Garces Rodriguez, 2003) and (Audenaert, 2009; Marsavina, 2009)).

3.6.5.   *Bending method*

The bending method was used by more authors than all other aforementioned methods (Adiyastuti, 2005; Francois, 1998; Francois, 2006; Gowripalan, 2000; Granju, 2005; Jaffer, 2009; Küter, 2005; Lorentz and French, 1995; Marcotte, 2003; Maruyama, 2006; Miyazato and Hiraishi, 2005; Mohammed, 2001; Otieno et al., 2008; Otieno, 2012; Otsuki, 2000; Pease, 2010; Sahmaran, 2007a; Sahmaran, 2007b; Schießl, 1997; Scott, 2004; Tottori et al., 1999; Win, 2004). Two types of bending methods have been applied to create one or several flexural cracks: three point bending and four point bending (Fig. 3-14). Consequently, in the case of three point bending the force was applied in the middle of the span while, as far as four point bending is concerned, loading was applied at the thirds of the beam span. The method can be applied to prismatic specimens of different cross-section and span. The required crack width can be measured and controlled by a digital microscope, LVDT (linear variable displacement transducer) and CMOD (crack mouth opening displacement) when appropriate loading was applied on the specimens. Three and four point bending can be applied to one single beam or as back-to-back in the loaded state. After the cracks have been induced, the specimen can be exposed to a chloride solution in the loaded state. Alternatively, after inducing cracks by three and four point bending, the samples can be exposed to chlorides in the unloaded state. However, during chloride exposure specimens can be re-loaded and unloaded to the previous loading level after for example 24 hours (Otieno, 2010). The embedded bolts through the ends of the beams are used to control the crack width. If the bolts are tightened, a wider crack can be produced. When this method is used steel reinforcement can be applied, which allows for measuring and monitoring the corrosion potential and the corrosion rate of steel reinforcement.
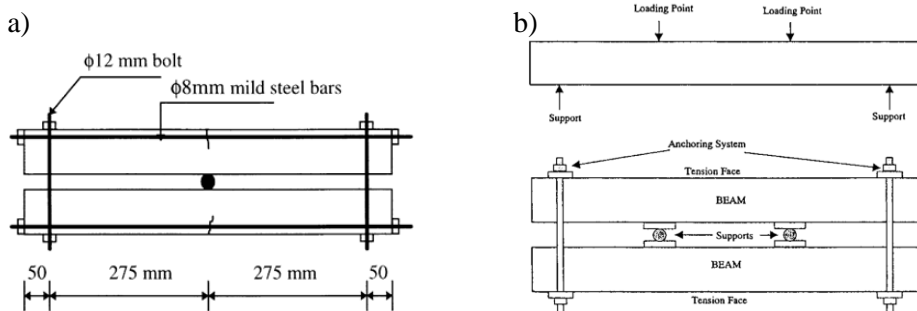

Figure 3-14: Back-to-back loading: a) Three-point bending (Gowripalan, 2000);   b) Four-point bending (Mohammed, 2001)

Chapter 4

Development of experimental set-up and program

4.1. Corrosion monitoring – considerations and launch

In a good quality concrete, in the absence of a detrimental external influence, the steel reinforcement is in a passive state. Passivity is maintained as long as the concrete bulk matrix maintains high alkalinity and performs as a sound physical barrier against penetration of aggressive substances (i.e. as a buffer to corrosion initiation). However, concrete is a porous material and depending on the pore network permeability and pore inter-connectivity, corrosion-accelerators as chloride ions, can penetrate the concrete bulk matrix, reach the steel-cement paste interface and initiate steel corrosion, even at high pH (12.9 – 13.5) of the surrounding medium. Logically, the process of chloride-induced corrosion would have a faster onset and will be further more pronounced when except porosity, concrete cracking occurs. Cracks are common in civil structures, ranging from micro to macro level. Therefore, standards define permissible crack widths for engineering applications (e.g. by Eurocode 2).

The application of general electrochemical techniques, e.g. open circuit potential (OCP) and linear polarization resistance (LPR) method, or more sophisticated ones as electrochemical impedance spectroscopy (EIS), cyclic voltammetry (CVA), etc. is well accepted for measuring corrosion rates of steel in reinforced concrete. The general approach within performing these techniques is based on fundamental electrochemical principles. Monitoring and data interpretation for steel corrosion in reinforced concrete structures, however, can be challenging in

many ways when lab techniques, suitable for a controlled environment, are to be employed in practical applications. Next to that, various purely structural parameters as concrete cover thickness, crack frequency, crack width, loads, etc., logically exert additional impact, which needs to be considered in case the electrochemical behaviour of the steel reinforcement has to be assessed. To this end, an experimental program was developed for monitoring steel corrosion in comparatively large (>1000 mm in length) reinforced concrete beams, considering the effect of the aforementioned structural parameters on the steel corrosion rate in time. Preliminary tests (Section 4.3) were first performed, followed by the subsequent large-scale tests (Section 4.4). The tests execution, data reproducibility, reliability and interpretation, as derived from the preliminary tests, served for defining the optimum test-schedule in the large-scale series of a representative number of 32 beams of $1500 \times 100 \times 150$ mm^3. In the large-scale series of experiments the following parameters were varied: crack width, crack frequency (distance between cracks), concrete cover and type of loading. The development of the experimental set-up, the concrete composition and parameters' variation are specified in detail in Section 4.4.

In order to account for the effect of the abovementioned structural variables and mainly, to determine the most suitable and reliable approach for monitoring steel corrosion in relatively large specimens, a preliminary investigation on the applicability of the chosen experimental set-up and the application of electrochemical methods was performed and discussed in the sequel.

4.2.   Suitability of electrochemical methods and techniques for corrosion monitoring in reinforced concrete beams

As previously mentioned, various electrochemical methods and techniques can be employed for reinforced concrete in order to derive the corrosion state of the steel reinforcement. However, the execution of most of these techniques in lab conditions is not always directly applicable for field tests and large specimens. Therefore, in order to find the optimum solution for the large-scale set-up of reinforced concrete beams (Section 4.4), mainly aiming at optimal efficiency in corrosion assessment of a large number of specimens of varying structural parameters and loading conditions, preliminary tests were performed. The electrochemical methods involved in these preliminary tests were open circuit potential (OCP) monitoring, electrochemical impedance spectroscopy (EIS),

linear polarization resistance (LPR) and potentio-dynamic polarization (PDP). For the large-scale tests mainly OCP and LPR were involved. Section 4.3 will summarise the results from the preliminary test series, whereas extensive presentation of recorded electrochemical parameters for the large-scale series, recorded through OCP and LPR will be presented and discussed later on in the Chapters 5, 6 and 7.

In what follows, OCP and LPR will be introduced, being the techniques mostly employed in this thesis. The additionally used methods as EIS and PDP will be discussed and some results will be briefly presented with relevance to the preliminary tests only (Section 4.3). The equipment used was Autolab PGSTAT101 and a high performance Autolab PGSTAT302N, combined with FRA2 module, using GPES, FRA and NOVA interface.

4.2.1. *Open circuit potential (OCP)*

The open circuit potential (OCP) measurement is the most widely used standard and non-destructive technique for assessing the active or passive state of steel in concrete. The OCP (or half-cell potential) measurements, in a simplified way, provide an electrode potential reading for the embedded steel (voltage difference between the steel reinforcement and a reference electrode). Following standards, requirements and experience, the probability of corrosion initiation and further propagation is judged, based on the recorded (steel) potential values. Different reference electrodes (reference cells) can be used, including external and embedded ones. For the preliminary tests (Section 4.3.), an external reference electrode was used, whereas for the large-scale tests, both external and internal (embedded) reference electrodes were used. Silver-silver chloride (Ag/AgCl) was used as an external reference electrode. The OCP measurements were conducted using an electrical connection to the reinforcement and the external reference electrode, placed on the concrete surface – denoted as "point (spot)" or localized measurement (Fig. 4-1a). The average potential value (for the whole rebar active surface) was recorded at the end of every wetting cycle by placing the electrode in the solution, above the concrete cover (Fig. 4-1b).

In general, the OCP values are also used to estimate the time to corrosion initiation. In a chloride-containing environment, corrosion initiation is due to a breakdown of the passive layer on the steel surface, resulting in localized corrosion. For reinforced concrete, the steel surface is considered passive if the OCP is equal to or more anodic than -270 mV (SCE) (ASTM, 1991). In lab-

conditions a well-defined geometry of the electrochemical cells applies, where the reference electrode (embedded or external) is positioned in the cell itself, accounting for minimal influence of IR drops and other factors i.e. a three-electrode cell arrangement is used. For field conditions, the OCP monitoring (or the so called half-cell potential mapping) is similarly performed through embedded pseudo-reference cells (e.g. Mn/MnO_2, Pt/Ti) or externally via $Cu/CuSO_4$ or $Ag/AgCl_2$ electrodes. In the former case an average OCP (for the total exposed steel surface) is recorded. In the latter case, localized measurements could be also recorded. For external measurements, the tip of the electrode is pressed on a wet sponge on the concrete cover in order to minimize the contact resistance i.e. the "spot" method applies (Fig. 4-1a). Logically, the RH in the time of measurement influences these measurements.
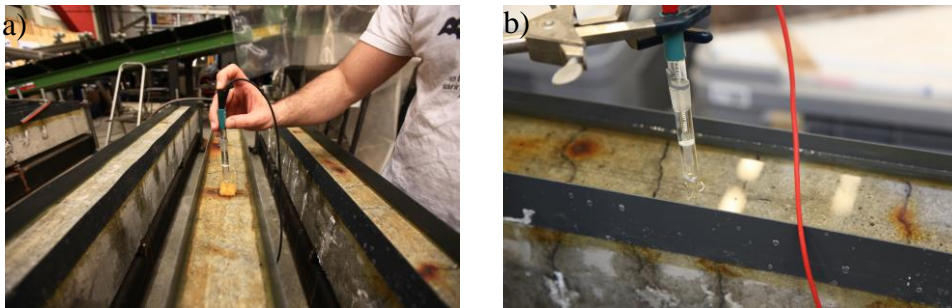

Figure 4-1: OCP measurements: **a)** *Point (spot);* **b)** *Average over exposed surface area*

In this study, two methods were employed:

1) "spot" measurement, executed immediately after the "wetting" cycles (with still saturated concrete cover), and during the drying cycles with equally handled "wet sponge" application; the "spot" measurement was performed above sound (uncracked) concrete cover, between cracks and above cracks in both situations.

2) "average" record for the total exposed steel surface: the OCP measurements were performed during the wet-cycles by simply positioning the reference cell in the solution above the reinforced concrete cover, where average OCP readings for the total exposed steel surface were recorded (Fig. 4-1b). The motivation behind these two monitoring techniques was to possibly distinguish "active" surface underneath the various cracks and differentiate between levels of activity, and further to compare these results to all other records.

The OCP readings within the preliminary tests are discussed in Section 4.3. The OCP evolution for the large-scale test results are presented and discussed in Chapter 5. The OCP measurements for the preliminary and for the large-scale tests were conducted as point ("spot") measurements twice a week, at the end of wetting and drying cycles, aiming at assessing the probability of steel corrosion (Table 4-1). For the large-scale tests, the OCP readings were additionally recorded through an embedded Pt/Ti pseudo-reference cell (Section 5.1), which gives the average value for the whole rebar. Since information on steel corrosion rates cannot be obtained through OCP measurements, the linear polarization resistance (LPR) technique was applied for a quantitative assessment of the corrosion state of the steel reinforcement.

Table 4-1: Probability of steel corrosion in concrete (C876-91, 1991)

Ag/AgCl electrode	Probability of corrosion
> - 106 mV	Low (10% corrosion risk)
- 106 to - 256 mV	Intermediate corrosion risk
< - 256 mV	High (90% corrosion risk)
< - 406 mV	Severe corrosion

4.2.2. *Linear polarization resistance (LPR)*

The linear polarization resistance (LPR) technique can be considered as a non-destructive, mostly a straight-forward rather than a complex technique for corrosion current (and corrosion rate respectively) measurements in concrete structures. The principle of LPR, as fundamentally known and applied, (Broomfield, 1996), is applicable to reinforced concrete by steel polarization in a range of at least ±10 mV around the OCP and record of the corrosion current response within polarization.

For both preliminary and large-scale tests, the steel reinforcement was the working electrode where external (Ag/AgCl) and/or embedded internal (Pt/Ti) electrodes were used as reference electrodes. The counter electrode in the preliminary set-up (Section 4.3.) was an embedded stainless steel rebar, whereas embedded Ti mesh served as a counter electrode for the large-scale set-up (Section 4.4).

A polarization window from -20 mV to +20 mV with a scan rate of 0.1 mV/s and a step of 0.5 mV were applied (Fig. 4-2a). Well known fundamental considerations (Stern-Geary, 1957) apply with LPR tests and were followed for all measurements. For example, the steel electrochemical response in the anodic and cathodic regions of immediate proximity to the corrosion potential (Fig. 4-2b) are considered to be linear, therefore a window of ±10 mV versus corrosion potential is the region considered for polarisation resistance (R_p) calculation through linear regression (Eq. 4-1). The Stern-Geary equation (Eq. 4-2) was employed to calculate corrosion current, where the constant B can be either experimentally derived e.g. through PDP tests and Tafel plot analysis, or employed as generally accepted theoretical values of 0.026 V/dec for corroding cases and 0.052 V/dec for passive cases (Andrade, 1996).
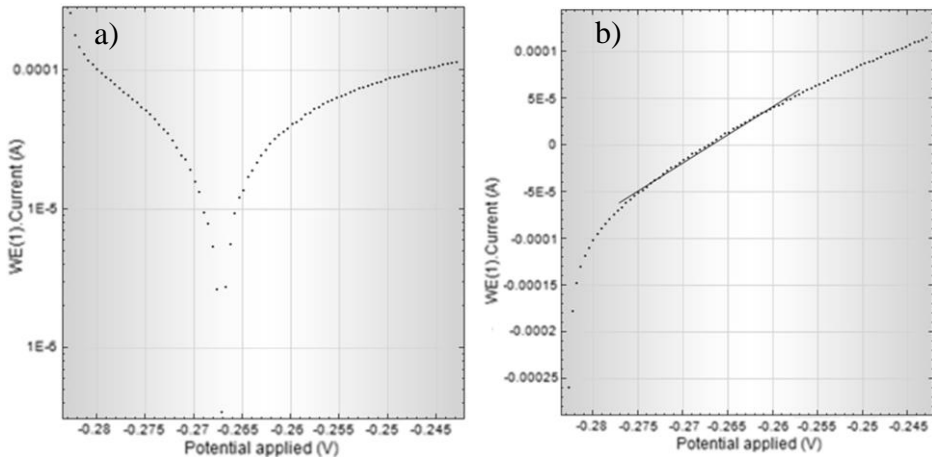

Figure 4-2: LPR measurement: **a)** *Polarization curve; **b)** Linear regression*

$$R_p = \frac{\Delta E}{\Delta I} \tag{4-1}$$

$$I_{corr} = \frac{B}{R_p} \tag{4-2}$$

$$B = \frac{b_a \cdot b_c}{2.303 \cdot (b_a + b_c)} \tag{4-3}$$

$$i_{corr} = \frac{I_{corr}}{A} \tag{4-4}$$

$$A = \pi Dl \tag{4-5}$$

Normalization to corrosion current densities was performed through considerations of IR drop correction (electrical properties of surrounding medium were derived through an AC 2-pin method and via EIS for the preliminary tests) and geometrical constants (Equations 4-4 and 4-5), where D is the diameter and l is the length of the exposed steel rebar. Automated calculation is also possible and was additionally employed.

4.3. Results of preliminary tests

4.3.1. *Preliminary test set-up*

Two reinforced concrete beams $1000 \times 125 \times 125$ mm^3 were cast with one ribbed bar and one stainless steel bar which were embedded at the desired position (Fig. 4-3). High yield, ribbed, cold-rolled reinforcing bars B500A were used, with a diameter of 16 mm and length of 960 mm.
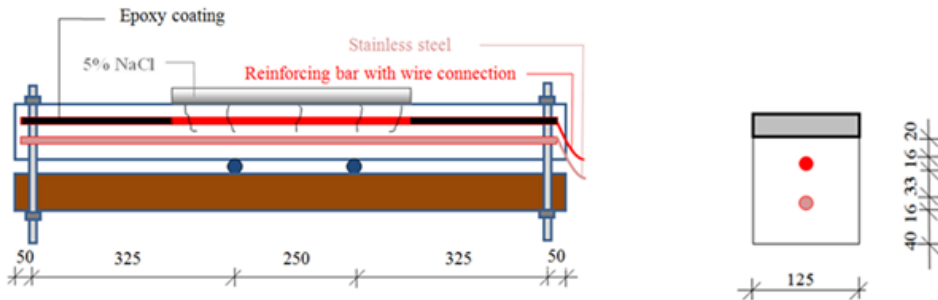

Figure 4-3: Preliminary set-up

Before casting, the reinforcing bar was degreased and sealed by epoxy at both ends in order to obtain a desired exposed surface area of 200 cm^2 (middle section of the beam). The stainless steel bar was embedded at the opposite side with a distance of 40 mm from the concrete cover (Fig. 4-3) in order to act as a counter electrode for the corrosion measurements. The side of the beam, situated at the bottom of the mould, was later on exposed to wetting and drying cycles (chloride solution or tap water during the wetting cycles). Ordinary Portland cement CEM I 42.5 N was used as a binder in the concrete mixture. The concrete was vibrated in three layers. Concrete cubes from the same batch were cast to monitor the compressive strength. After casting, the beam specimens and the cubes were

covered with plastic sheets for 72 hours under laboratory conditions. Subsequently, all specimens were cured in a climate-controlled (fog) room (20±2°C and 95±5% RH) until the age of 28 days. Three cubes were tested to evaluate the compressive strength which was around 45 MPa at 28 days of concrete age, while the reinforced concrete beams, designated A and B, were maintained under laboratory conditions (20°C, 50% RH) for additional 10 days (beam A) and 160 days (beam B), respectively. After that, 4-point bending was applied to beams A and B to induce cracks. In these experiments, exposure to NaCl was applied to simulate an aggressive environment, whereas tap water was used for control cases. Beam B was exposed to alternating wetting and drying cycles once a week for a 2 days ponding (5% NaCl solution) and a 5 days drying period. Beam A was a control beam, exposed to the same regime, but using tap water instead of NaCl solution.

4.3.2.   *Results from corrosion monitoring for the preliminary set-up*

All electrochemical tests were performed after open circuit potential (OCP) stabilization. EIS and LPR were performed at frequent time intervals throughout the investigation period, whereas PDP was performed at the end of these preliminary tests. For LPR a polarization window of ± 20 mV versus OCP at a scan rate of 0.1 mV/s was used. PDP was performed in the range of -150 mV to + 150 mV versus OCP at a scan rate of 0.5 mV/s. The EIS measurements were carried out in a frequency range of 1 MHz to 10 mHz by superimposing an AC excitation perturbation amplitude of 10 mV (rms), recording ten points per decade. The execution and data interpretation of all electrochemical measurements was as previously reported for steel in reinforced concrete systems (Koleva, 2007, 2009 and 2011). All potential values were recorded versus the Ag/AgCl reference electrode. However, for an easier comparison with standards (criteria), some figures present these values re-calculated versus a saturated calomel electrode (SCE).

4.3.2.1. *OCP records*

The open circuit potentials (OCP) for the steel reinforcement were recorded in both corroding and control beams through "spot" measurements, where a wet sponge was used for ensuring concrete conductivity. The measurements were conducted above and between cracks (cracked and non-cracked regions) or when the concrete was in a "wetting cycle" (average OCP for the whole active rebar

surface) . Figures 4-4a and 4-4b present the OCP readings for the "control" beam A and "corroding" beam B, recorded via local "spot" measurements.

The values indicate passive behaviour, as expected, for beam A, irrelevant of "spot" measurement location i.e. irrespective of crack width or sound concrete. Furthermore, the OCP values were not exceeding -50 mV also within the wetting cycles. Alteration of values within drying and wetting was as expected, OCP-s ennoblement was recorded at later stages, reflecting stabilization of the passive layer on the steel surface with time.
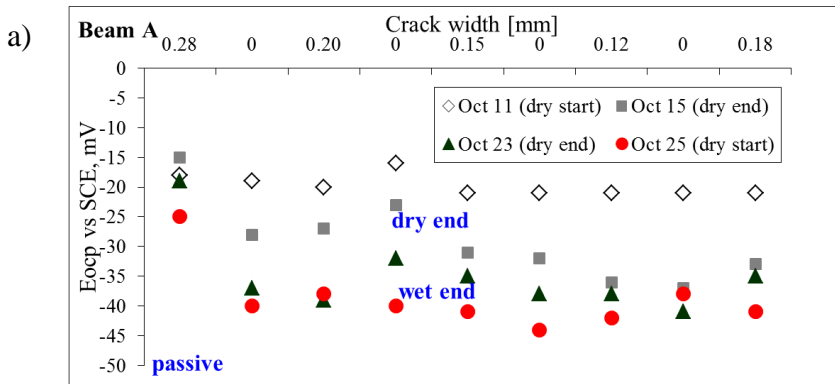
Figure 4-4a: OCP "spot" measurements for control beam A
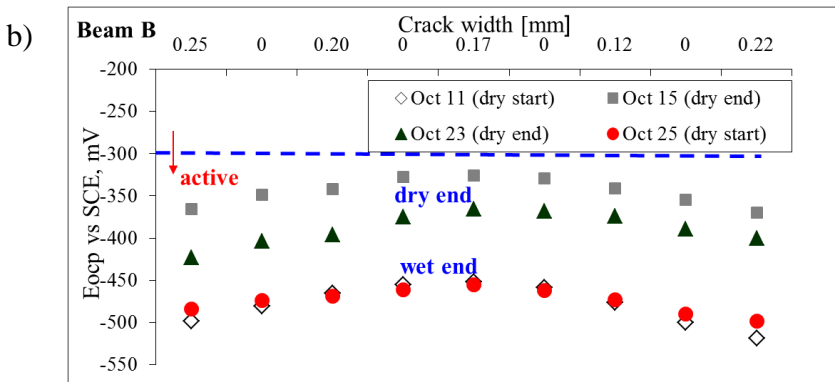

Figure 4-4b: OCP "spot" measurements for corroding beam B

In contrast, the OCP values for beam B vary more significantly with wetting and drying, presenting more cathodic values in the former and more noble values in the latter case (all values, despite fluctuations were in the activity region). This was also as expected, denoted to chloride ions penetration and steel active behaviour i.e. increased corrosion activity within the wetting cycles. A general trend of more cathodic potentials, recorded for the locations of larger crack widths (0.22 – 0.25 mm) was expected, but not really observed for all crack locations in this test: e.g. for the middle of the beam B – at crack width of 0.17 mm, more anodic values were recorded, possibly due to the adjacent wider sound concrete areas i.e. presumably less damaged concrete-steel interface at both sides of this crack. This is in addition to the effect of macrocell corrosion, where more active adjacent areas, acting predominantly as active anodes would result in a more pronounced cathodic behaviour for adjacent areas where a smaller crack width or a sound concrete cover is relevant.

Figure 4-5 presents the average OCP values recorded during wet cycles only for both beams A and B. The average values for beam A indicated passive behaviour during three weeks of exposure. However, in the case of beam B depassivation of the steel reinforcement was relevant at all times. The average OCP values (i.e. total steel surface) were recorded at the beginning, in the middle and at the end of the ponding cycles. As can be observed, the recorded OCP for beam B is more negative at the end of a ponding cycle than in the beginning, which is due to the contribution of both moisture and chloride ingress. The average OCP readings are dominated by the active areas on the steel reinforcement, therefore the values depicted in Fig. 4-5 for beam B coincide with the readings, recorded for the most active "spots" where the largest cracks in Fig. 4-4b were located.
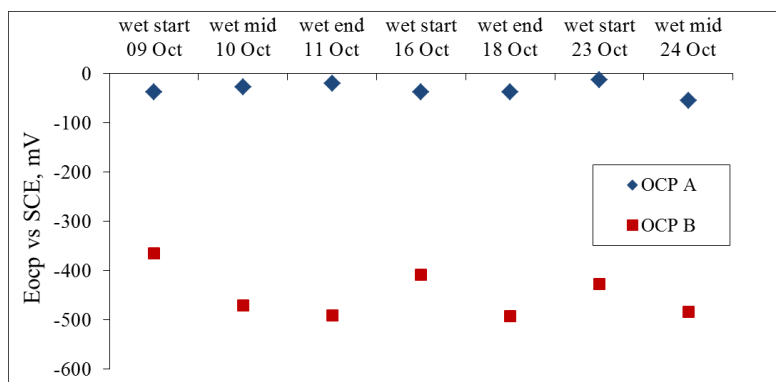

Figure 4-5: Average OCP for beam A and B during wetting cycles

Clearly, the OCP readings provide valuable information on active/passive state for the steel reinforcement if both control and corroding conditions are to be compared. However, OCP readings can only give an indication for the corrosion state of the steel reinforcement and are significantly affected by electrical properties of the bulk matrix, RH, structural variations (e.g. crack width and number of cracks), relevant interfaces, etc.

4.3.2.2. *Electrochemical Impedance Spectroscopy (EIS)*

Within the preliminary tests series, a more in-depth investigation was performed in order to clarify possibilities versus ease of application of electrochemical tests in large reinforced concrete specimens. Additionally, reliability and efficiency in recording corrosion state was sought, considering the significant number of specimens in the large-scale test series.

EIS was performed for the preliminary test set-up only. The motivation was in view of demonstrating the well-known capabilities of this technique to non-destructively distinguish the electrochemical state (active or passive) of the steel reinforcement, together with the properties of the bulk matrix. EIS was employed in a manner, similar to previously reported such for an otherwise in-depth characterization of steel-concrete systems (Sagüés, 1995; Feliú, 2004; Koleva, 2007). The presented results and discussion in this thesis, however, are restricted to a limited amount of EIS-related information only, illustrating the applicability and considering the limitations thereof, of this technique to the discussed specimens.

4.3.2.2.1. *General considerations EIS tests and response*

The EIS response was recorded in the frequency range of 1 MHz to 10 mHz (full response), in order to evaluate both bulk matrix properties and steel electrochemical response. Additionally, a series of measurements in the frequency range of 50 kHz to 10 mHz were performed, aiming to reveal mainly the steel electrochemical state. As generally accepted, the high frequency (HF) region is related to frequencies higher than several tens of Hz, the medium frequency (MF) region is in the range of several Hz, and the low frequency (LF) region corresponds to response at frequencies lower than the MF region towards mHz domain (Keddam, 1997). The HF domain of the full response would more accurately present variation in bulk matrix properties (e.g. resistance of solid phases, resistance and capacitance of disconnected and/or connected pore

network etc.), whereas the 50 kHz to 10 mHz response accounts for contribution only of bulk matrix, together with the steel electrochemical response. Fig. 4-6 displays an overlay of the 1 MHz to 10 mHz response for both beam A (control) and beam B (corroding) during wet-to-dry regime of conditioning. Fig. 4-7 depicts the response for beam A as an overlay of full response (1 MHz to 10 mHz) and 50 kHz to 10 mHz response. As can be observed, a complete overlap in the relevant frequency range of both records is relevant, which demonstrates the possibility to derive the contribution of the connected pore network (i.e. partial bulk matrix properties) in the 50 kHz to 10 mHz range, together with the steel electrochemical response.
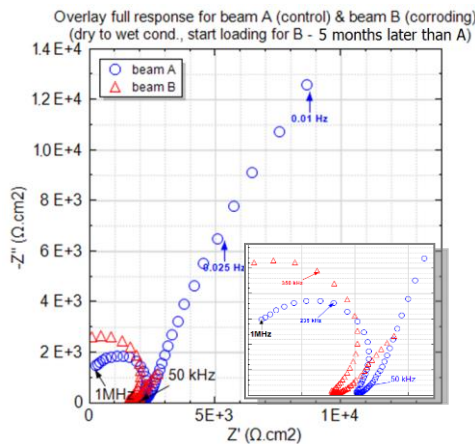

Figure 4-6: Overlay of the 1 MHz to 10 mHz EIS response for beam A and beam B in wet-to-dry conditions
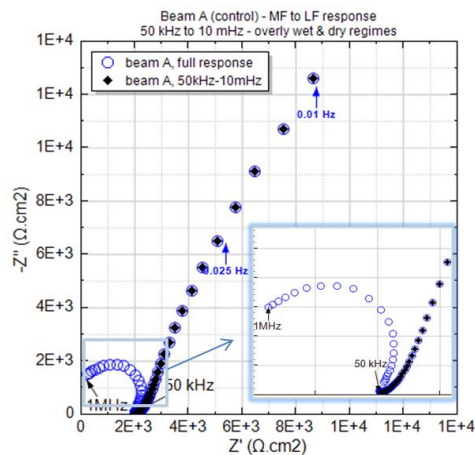

Figure 4-7: Overlay of the 1 MHz to 10 mHz and 50 kHz to 10 mHz EIS response for beam A

Usually, absolute values for concrete (or cement-based materials in general) bulk properties can be derived at high frequency range above the 1 MHz region e.g. starting at 10 MHz (Keddam, 1997). However, due to equipment limitations, 1 MHz was the highest frequency employed. This is another reason why the EIS tests were used within the preliminary series of experiments for illustrative purposes only. Although quantification of the full response was performed and concrete bulk matrix electrical properties were derived, due to the complexity of data interpretation, namely the equivalent electrical circuits employed and relevant considerations thereof, these results are not hereby presented and discussed. Qualitative approach towards evaluation of specimens' response is also possible and generally accepted, and this is what is discussed further in short. As far as the steel corrosion state (active or passive) is concerned, both qualitative and quantitative results are briefly presented. All derived parameters and discussed results are for comparative purposes only, rather than claiming absolute values.

4.3.2.2.2.   *Brief reflection on EIS results evaluation*

Qualification EIS results: if a qualitative assessment only of EIS data is to be performed, both HF and MF-to-LF response can provide valuable information, for example the difference in electrical properties of the bulk matrix (HF to MF domain) and active or passive state of the steel reinforcement (LF domain). A distinction between active and passive steel is possible, based on the shape of the curves in the MF to LF domain. As seen from Fig. 4-6, the response for beam A (control) shows a significantly larger magnitude of impedance |Z| compared to that for beam B. For passive steel, a general feature would be an inclination in the MF-LF domain to the imaginary (Z") axis of the complex plot, denoted to the close to capacitive-like behavior in such condition (Koleva, 2007). This is reflected by the initial response for beam A as depicted in Fig. 4-6. In contrast, the MF to LF domain for beam B clearly shows active behavior, with a response strongly inclined to the real axis, already indicating chloride ions presence at the steel surface (Koleva, 2007) in this case, and a significantly lower magnitude of impedance.

Interpretation of EIS results towards quantification: for a quantitative interpretation of EIS results, an equivalent electrical circuit is to be employed for data fitting. The complexity of employing EIS tests in a large frequency window, as for the hereby discussed specimens (e.g. from MHz to mHz domain), arises from the necessity to use more complex equivalent circuits for fitting of the

obtained response. Next to that, the contribution of the bulk concrete matrix and interfaces (interfacial transition zones of aggregates/cement paste and steel/cement paste interface) result in additional distortion from ideal behavior and response, respectively. To that end, the generally employed elements of equivalent circuits e.g. pure capacitance (C, F/cm^2) or pure resistance (R, $Ohm \cdot cm^2$) need to be altered within data fitting to represent heterogeneities in the system at various levels and/or additional phenomena. This is generally done by substituting pure capacitance with constant phase elements (CPE) and/or additional elements to account for diffusion or mass transport phenomena (e.g. Warburg impedance). An equivalent circuit, comprising of one to several time constants (linked capacitive and resistive components in parallel or in series) is further designed to represent the total response of the system. All these considerations are well known and reported in the field and are not subject to discussion in this Chapter. Only a brief discussion on considerations with respect to the equivalent circuits used for the preliminary series is presented in what follows.

Equivalent circuits and fitting: for the full EIS response, an equivalent circuit, comprising of four time constants was employed, whereas for the 50 kHz to 10 mHz response an equivalent circuit of two time constants was used. All employed circuits resulted in good fitting results with acceptable errors (full fit error χ^2 in the range of $2.1e^{-4}$ to $8.2e^{-4}$ and error per element < than 7%). For the full response (1 MHz to 10 mHz) the HF was presented by two time constants in series with the electrolyte resistance, the latter being negligible if compared to the concrete bulk resistance. Next, pure capacitance C for the solid phase (recorded in the expected range of nF) was employed in the first time constant. All other time constants used pseudo-capacitance (Q), or constant phase element (CPE) - a common approach to account for structural heterogeneity (bulk matrix and pore network) as well as to reflect heterogeneity of the product layer on the steel surface (Sagüés, 1993; Feliú, 2004). The second part of the four-time constants circuit reflected the middle (MF) to low frequency (LF) domain, denoted to the electrochemical reaction on the steel surface, including the contribution of redox processes and product layer transformation and/or contribution of the steel/cement paste interface. For deriving polarization resistance (R_p) from EIS measurements in reinforced concrete, the medium-low and LF limits of the impedance spectra are generally considered, as reported (Fedrizzi, 2005; Suryavanshi, 1995), as previously discussed and reported for reinforced mortar and concrete (Andrade, 1996; Koleva, 2007 and 2011). As well

known, a circuit containing more time constants would generally result in a better fit of the EIS response. Yet, the most accurate circuit will be the one with the lowest possible number of time constants, representing a clear physical meaning. More discussion on employing various equivalent circuits and this relatively complex approach is, however, not subject to this chapter. The HF domain, accounting for bulk matrix properties is only qualitatively discussed later on. The qualitative approach and brief quantification, using equivalent circuits of two time constants with relevance to the response in the frequency range of 50 kHz to 10 mHz, are discussed in Section 4.3.2.2.3.

4.3.2.2.3. <u>*Qualification high frequency (HF) response*</u>

As far as the HF response and bulk matrix properties are concerned, qualitative interpretation clearly differentiates the bulk matrix characteristics in both beams A and B. The HF domain (magnified as inlet in Fig. 4-6) depicts the semi-circular capacitive arcs, attributed to the properties of the concrete bulk matrix. As seen from the plot, the contribution of the solid phase within the bulk matrix resistance for beam A is actually lower than that for beam B. The result is attributed to the fact that although A and B were at an equal cement hydration (concrete) age, load was applied and crack patterns induced (Fig. 4-3) for beam A five months earlier than for beam B. Therefore, the concrete bulk in beam A was already significantly altered, whereas the crack patterns in beam B were induced just before the hereby employed electrochemical tests. Additionally, well known is the effect of chloride binding on cement-based microstructural properties e.g. pore network refinement, which generally results in modified global properties (Suryavanshi, 1995; Koleva, 2007). The result would be a higher bulk matrix resistance in terms of solid phase/disconnected pore network and lower overall bulk matrix resistance for beam B, compared to beam A in wet-to-dry conditions (Fig. 4-6). Next to these, except the contribution of internal structural changes, the bulk matrix resistance properties are determined by both the relative humidity of the matrix, the composition of the external environment (ponding solution) and the crack width. Since only a qualitative interpretation is relevant for the HF response, further in-depth discussion on bulk matrix-related properties is not subject to this chapter. However, the following can be summarized, based on generally accepted considerations, the observed behavior as well as some indicative calculations as previously outlined for the full response.

The connected pore network resistivity contributes to the recorded global behavior. This is also determined by the ionic strength of the pore solution, which is lower in case of A and higher for B (due to the presence of chloride ions). A larger connectivity in A (enhanced structural damage), but higher pore solution resistance would determine similar to beam B pore network capacitance values during wet regimes, whereas the values for beam B would maintain higher values irrelevant of the wetting-drying cycles, consistent with the on-going chloride penetration in wet regimes and physical and chemical chloride binding in transition and drying regimes. In other words, high resistivity of the connected pore network in beam A during wet regimes (derived in the range of 470 to 690 ohm·cm^2) would balance the lower solid phase resistance, while lower connected pore network resistance in B (280 to 360 ohm·cm^2), would counteract the higher otherwise solid phase resistance. Therefore the HF response accounts for similar global bulk matrix resistance in both beams during the wetting regime, ending-up with slightly higher global resistance for the overall bulk matrix for beam A (global bulk matrix resistance values of 2800 to 3500 ohm·cm^2 for beam A and 2200 to 2600 ohm·cm^2 for beam B were derived). To this end, EIS is a very useful technique to determine bulk matrix properties and the effect of the latter on the electrochemical response. Next to that, destructive microstructural analysis, coupled to EIS response in the HF domain would result in a detailed quali- and quantification of bulk matrix alterations, an approach already performed and reported (Koleva, 2007). This correlation of experimental techniques and further investigation, however, was not subject to this research in view of the large scale of the main test series (Section 4.4) and the previously discussed objective for optimized monitoring efficiency.

4.3.2.2.4.   *EIS response in the middle to low frequency domains*

The global electrochemical response for the steel reinforcement is to be discussed in this Section, however, for completeness and to account for contribution of bulk matrix in terms of connected pore network within fitting, the response for beams A and B is presented as recorded in the frequency range of 50 kHz to 10 mHz. The experiment-fit overlay for this frequency window, including the employed equivalent circuit and best-fit parameters are depicted in Fig. 4-8 for beam A.
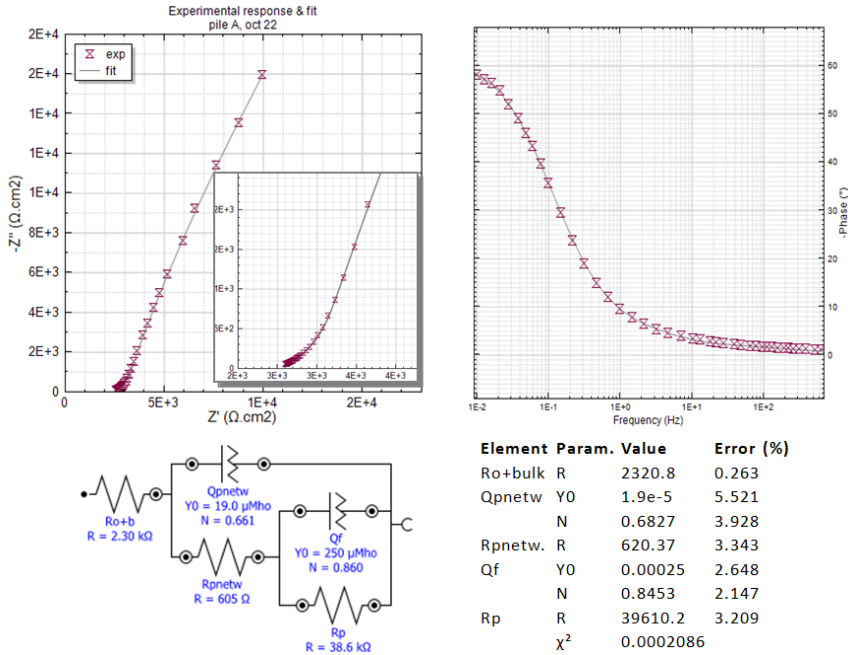
Element	Param.	Value	Error (%)
Ro+bulk	R	2320.8	0.263
Qpnetw	Y0	1.9e-5	5.521
	N	0.6827	3.928
Rpnetw.	R	620.37	3.343
Qf	Y0	0.00025	2.648
	N	0.8453	2.147
Rp	R	39610.2	3.209
	χ^2	0.0002086	

Figure 4-8: Experimental response and fit for beam A (50 kHz -10 mHz), equivalent circuit and best-fit parameters

The circuit presents a "nested" sequence of two time constants in series with the "solution" resistance – in this case, plus contribution of bulk matrix resistance (R_{0+b}). The first time constant ($R_{pnetw}Q_{pnetw}$) reflects the contribution of connected pore network (bulk matrix); the second time constant (R_pQ_f) deals with the electrochemical reaction on the steel surface, including the contribution of possible oxi-/redox transformations in the product layer on the steel surface. Should be noted that although a separation of charge transfer resistance/double layer capacitance and capacitance/resistance attributed to oxi-/redox process within the product layer on the steel surface is possible, presentation and discussion on these is considered to be too detailed for the purpose of this research and overall aim, respectively. Therefore, two time constants were employed in this frequency domain and only global polarization resistance (R_p) and interfacial pseudo-capacitance (Q_f) are quantified and summarized in Fig. 4-10. An overlay of the MF to LF response (including partial HF response) is presented for beams A and B in Fig. 4-9.

a)

b)
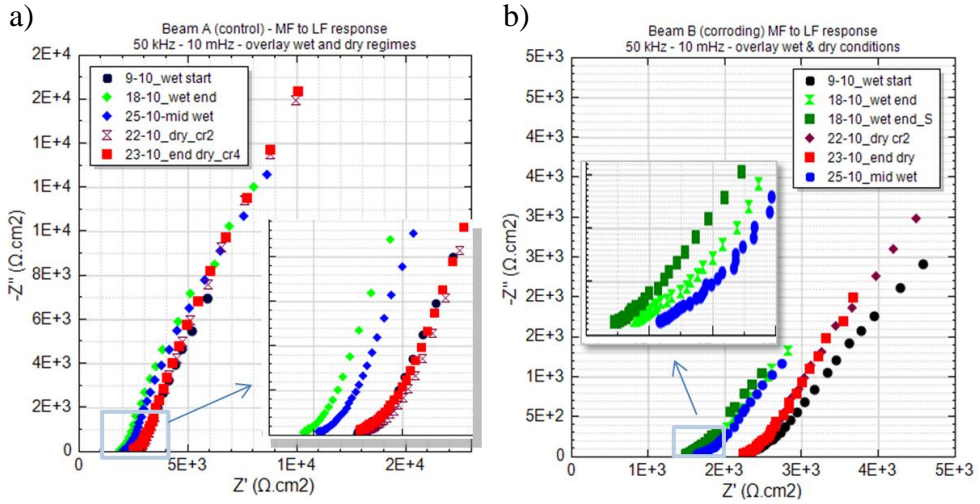
Figure 4-9: EIS response for: a) beam A (50 kHz - 10 mHz);   b) beam B (50 kHz - 10 mHz)

As seen in Fig. 4-9a, the wetting and drying cycles do not exert a significant influence on the steel/cement paste interface and the electrochemical behavior of the steel reinforcement in control (beam A) conditions, which was as observed via the OCP readings (Fig. 4-4a). The steel reinforcement in beam A is in a passive state throughout the experiment, reflected by the higher magnitude of impedance |Z|, compared to this for beam B (Fig. 4-9b).
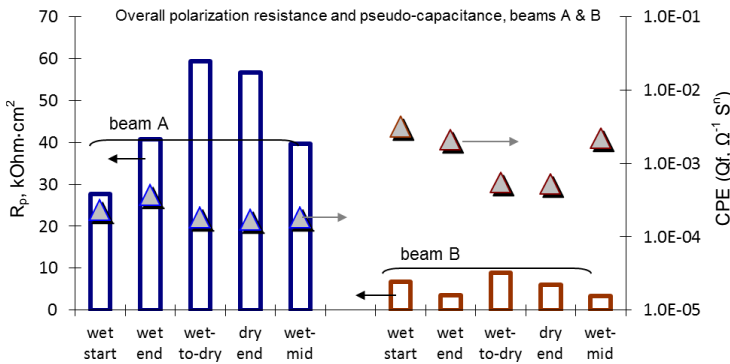
Figure 4-10: Summarized electrochemical parameters for beams A and B in all tested regimes

The influence of the wetting regimes is mainly in terms of pore network properties, partially seen in this response (inlet in Fig. 4-9a), where a shift towards lower real |Z| values was observed with wetting, which does not have a significant effect on the passive state, although lower global polarization resistance was recorded in wetting regimes and higher in drying regimes (Fig. 4-10). These are attributed to hydration-dehydration mechanisms at the steel-cement paste interface and changed mass transport-diffusion processes within wetting or drying. The passive state in beam A is reflected by the derived polarization resistance, which maintains higher values if compared to that for beam B, irrespective of the conditioning regime (Fig. 4-10). In contrast, for beam B, a larger significance of altered environmental conditions was observed with regard to the electrochemical state of the steel reinforcement. As seen from Fig. 4-9b, the MF-LF response presents a more pronounced inclination to the real axis when wetting regime occurs. This is attributed to both chloride ions penetration and activation of the steel surface. This active state of the steel reinforcement is in line with the previously discussed OCP readings (Fig. 4-4b).

The sequence of wetting and drying exerts alternating changes in the values for pseudo-capacitance for beam B, whereas these are relatively stable and maintain lower values for beam A, as expected (Fig. 4-10). Higher capacitance and lower resistance were recorded during or at the end of the wetting regime for beam B, attributed to both re-structuring of the product layer on the steel surface and corrosion propagation within chloride ions penetration. The polarization resistance values are significantly lower for beam B, compared to beam A, which accounts for the active corrosion state in beam B.

In conclusion, the above discussed EIS tests, responses and relevant considerations are just on the surface of what could be derived, discussed and presented as outcome form such tests. A more comprehensive type of presentation and discussion is far beyond the objectives of this thesis. Coupled with the relatively higher complexity with this set-up, fitting of the recorded full response and data interpretation would have been a challenging task for the full (large-scale) test. Therefore EIS, although a very useful and non-destructive technique, was not further used, keeping in mind the objective of this thesis for global evaluation of corrosion state and ease of monitoring and results' interpretation.

4.3.2.3. *DC electrochemical tests (LPR and PDP)*

As previously introduced, this work aimed at clarifying the suitability of electrochemical tests to corrosion monitoring in large reinforced concrete beams. Except the OCP records which are not sufficient with respect to quantitative results, but just indicative, the commonly accepted LPR technique was applied. LPR was supported by PDP measurements, performed at the end of this test. Both LPR and PDP were performed for the wetting and drying regimes. The measurement in the wetting regime corresponds to a response for the average steel surface (total exposed steel surface). The measurements in the transition and drying regimes were performed following the "spot" method as specified above and refer to "local" response of the steel surface, corresponding to the relevant crack position and width.

Fig. 4-11 depicts the recorded LPR curves for beam A (left) and B (right) in consecutive wetting regimes with drying cycles in between. In other words, the first response (curves 1) refer to measurements in the middle of the first wetting cycle (one cycle being of 2 days duration). The second response (curves 2) refer to measurements, taken at the end of wetting cycle N^o2, which was preceded by a dry cycle of 5 days. The third response refers to measurements taken in the middle of a third wetting cycle (already preceded by two wetting and 2 drying cycles) i.e. response after 2 weeks of conditioning.

For both A and B beams a slight cathodic shift of corrosion potential was observed within wetting, which for both beams is related to limited oxygen access to the steel surface, but accompanied by chloride penetration (increased rate of chloride-induced corrosion) for beam B. As expected the relevant corrosion current densities stabilize over time for beam A and are at least one order of magnitude lower (reflecting passive state, Fig. 4-11), compared to the values for beam B, which increase in time and alterations from more to less active behaviour is observed. The result is consistent with the EIS tests, supporting the previously discussed observations for limited or none effects on wetting-drying regimes on steel electrochemical behaviour for beam A (Fig. 4-9a, 4-10) and larger effect of the environmental conditions on the steel response in beam B (Fig. 4-9b, 4-10), where mainly chloride ions penetration and subsequent chloride binding occur.
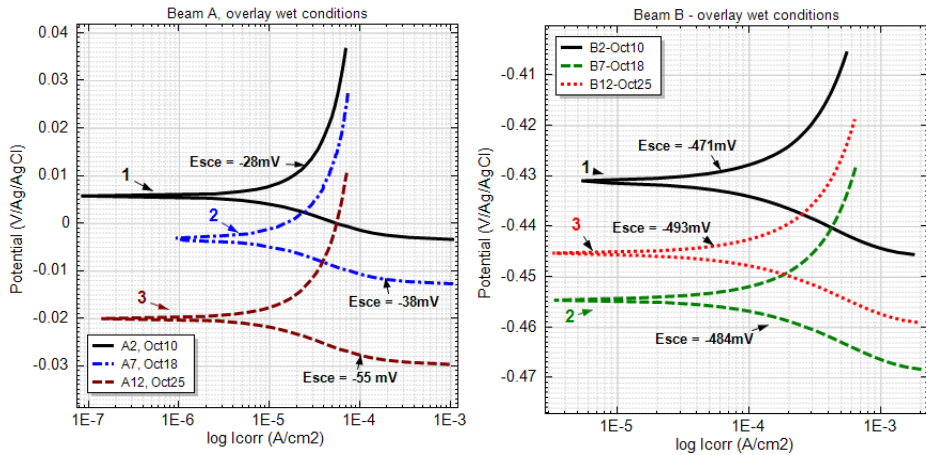
Figure 4-11: LPR curves for beam A (left) and B (right) in wetting cycles (average response)

Similar observations hold within the "spot" measurements – e.g. above cracks N^o2 (0.20 mm) and N^o4 (0.12 mm), Fig. 4-12. Within the LPR measurement in beam A (i.e. within polarization) the cathodic shift in consecutive measurements is less pronounced for the location of crack 4 (smaller crack width), compared to crack 2 (larger crack width), the range of corrosion currents remaining as previously recorded for the average response. This is a logic observation, reflecting the influence of crack width on the response and the measurement itself, where a different crack width corresponds to varying oxygen availability and ease of external solution (water in this case) penetration, bulk matrix level of RH respectively. The result is a restructuring of the passive layer, which would be more pronounced for the location of crack N^o2.

For the case of beam B, the corrosion state of the steel surface and cathodic shift of corrosion potentials is also determined by both RH and oxygen availability, which depend on the crack width, but a major factor here is chloride ions penetration (5% NaCl used as external solution). As a result, more "active" corrosion potentials within the "wet spot" analysis are recorded for the locations of wider crack widths - for crack position N^o2 (0.2 mm) (Fig. 4-12c), accompanied by a significantly larger potential shift between the first and third measurement, whereas for crack 4 (0.12 mm) a small ennoblement is even recorded. The corrosion current densities maintain higher (active) values, similar to the recorded average (Fig. 4-11) values.
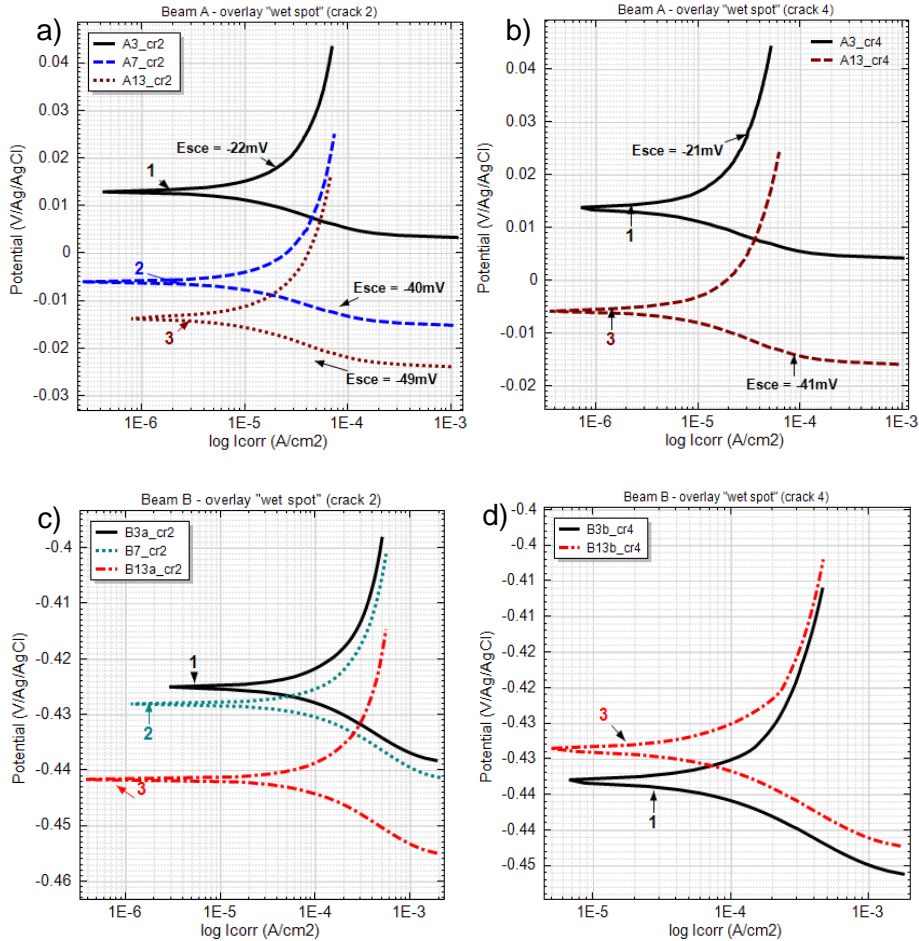
Figure 4-12: LPR response with "spot" analysis for beam A (a,b) and beam B (c,d) at relevant crack locations

As aforementioned, PDP curves were recorded for both beams in wetting and drying regimes (the former presents an average response, the latter was recorded also as an average for the total exposed surface via a "spot" measurement over a sound (uncracked) location in the middle of the beam). As seen from Fig. 4-13, the wetting cycles increase corrosion and anodic currents for both beams A and B. However, only a very small variation of these is relevant for the control beam A (due to already discussed phenomena), where environmental changes do not significantly affect the electrochemical response, as already discussed and supported from EIS results. In contrast, larger variation and enhanced corrosion activity within changing the external environment is relevant for beam B, where chloride penetration in the wetting cycles is the effect governing corrosion

behaviour. As expected, the corrosion current densities recorded for beam A are at least one order of magnitude lower than those for beam B.
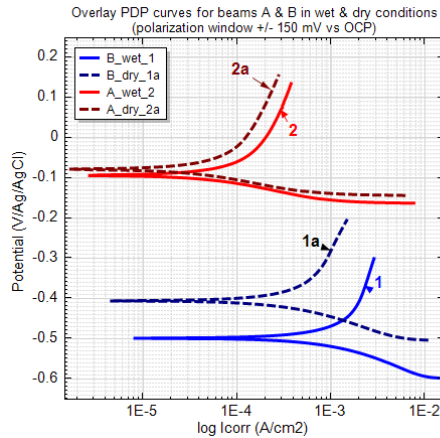
Figure 4-13: PDP curves for the steel reinforcement in beams A and B during wetting and drying regimes

The PDP also served for performing an indicative Tafel slope analysis in a polarization window of -50 mV to +50 mV around the corrosion potential. The aim was to experimentally derive B constants for the tested specimens at the relevant age and environmental conditions, having in mind possible large deviations with respect to the steel response in concrete. Therefore, the analysis followed reported for reinforced concrete procedures and considerations (Sagüés 1995, Hu and Koleva 2012). The derived B values were between 23 and 42 mV/dec for corroding and control cases, which is in the range of well-known and accepted B values for steel in concrete (Andrade, 1996) i.e. 26 mV/dec for active and 52 mV/dec for passive state. Therefore, for more accuracy and comparative purposes, the calculation of corrosion current densities for all investigated time intervals was performed by employing the Stern-Geary equation, using the R_p values derived from LPR measurements and already reported B values (Andrade, 1996). The calculated corrosion current density values are summarized in Fig. 4-14, including the relevant OCP potentials before the LPR tests. The corrosion current densities for beam A are around the range of passivity (0.1 μA/cm^2 accepted as a threshold value), whereas the derived current densities for beam B determine active corrosion.
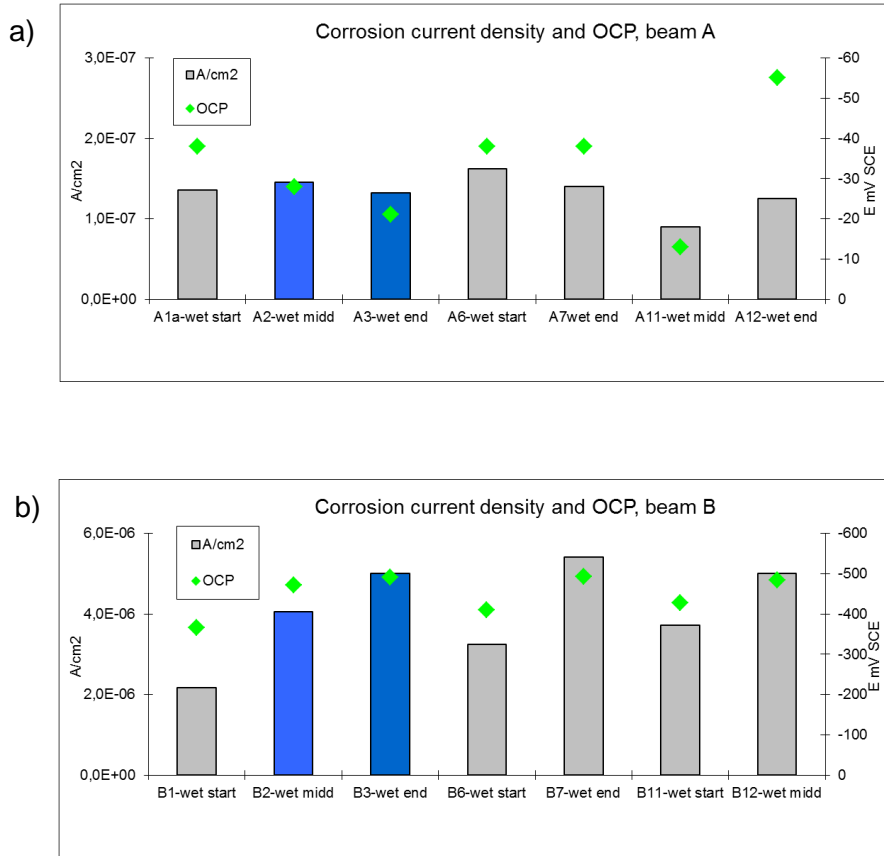
Figure 4-14: Corrosion current density and average OCP for a) beam A; b) beam B

4.4.   Design of the final, large-scale experimental set-up

Taking into consideration durability provisions for chloride-induced corrosion of reinforced concrete structures, the following issues are prescribed by codes:

- Exposure class (X0, XC, XD, XS, XF, XA)

- Concrete mixture (w/c ratio, cement content, binder type)

- Maximum allowable crack width and minimum concrete cover

As far as variables are concerned, in general experiments have been carried out, in which the following parameters were varied to obtain a better understanding of the influence of cracks on chloride-induced corrosion:

- Crack width

- Crack frequency

- Concrete cover

- Type of loading

4.4.1.   *Exposure class*

The exposure classes for concrete structures are defined in EN 206-1.

Table 4-2: Exposure classes

Exposure class	Description
XO	No risk of corrosion or attack
XC	Carbonation-induced corrosion of reinforcement
XD	Chloride-induced corrosion of reinforcement by chlorides other than from seawater
XS	Chloride-induced corrosion of reinforcement by chlorides from seawater
XF	Freeze-thaw attack on concrete
XA	Chemical attack on concrete

In experiments the most severe conditions will be applied by alternating wetting and drying cycles to simulate environmental class XD3 and/or XS3. Examples of these exposure classes are car park slabs, pavements, parts of bridges exposed to spray containing chlorides, splash and tidal zones in a marine environment. Several researchers used a different chloride ponding-drying ratio to simulate corresponding exposure conditions. For example, in a study by Otieno (2010), 3 days ponding by 5% NaCl and 4 days drying weekly cycles were applied to accelerate corrosion of steel reinforcement. Furthermore, 24 hours ponding and 60 hours drying cycles were applied twice a week in research by Mohammed (2001) and Otsuki (2000), using 3.5% and 3.1% of NaCl, respectively. However, the most realistic conditions were applied in a study by Schießl (1997), where 1 day of ponding using 1% NaCl and a 6 days drying period were applied twelve times, followed by two wetting periods without chlorides in solution. After that, the specimens were exposed to 80% RH in a climatic chamber without further wetting cycles for one year. After one year, the same procedure was conducted once again to simulate exposure conditions as closely as possible in the splash zone of a motorway near Düsseldorf during the harsh winters of 1986 and 1987. Most commonly research is carried out during limited time, but it is not desirable to exaggerate with acceleration of steel corrosion in comparison with real exposure conditions. Based on that, the cracked reinforced beams were exposed to alternately wetting and drying cycles once a week for 2 days ponding using a 3.5% NaCl solution and a 5 days drying phase to simulate an aggressive environment.

4.4.2.   *Concrete mixture*

In order to reduce the number of parameter combinations, and taking into account that the role of the concrete composition is not the subject of this research, only one concrete mixture was used for all experiments. The research project aims at investigating the influence of cracks on chloride-induced corrosion during a limited period of time. Consequently, a relatively low value of the concrete strength class was aimed at for the concrete mixture, C20/25 (w/c ratio 0.60 and cement content 260 kg/m^3). The concrete mix design is shown in Table 4-3 for 1000 litres where the air content was around 15 litres. A maximum aggregate size of 16 mm was used in the concrete.

Table 4-3: Concrete mix design

Component *	Dry Weight [kg/m³]	Litres [l]
CEM I 42.5 N	260	82.28
Sand 0.125-0.250 mm	78.830	29.86
Sand 0.250-0.500 mm	256.199	97.05
Sand 0.500-1 mm	256.199	97.05
Sand 1-2 mm	157.661	59.72
Sand 2-4 mm	98.538	37.33
Gravel 4-8 mm	394.152	149.30
Gravel 8-16 mm	729.181	276.21
Water	156	156
Super plasticizer	0.26	0.22
Air content		15
Total litres		1000

4.4.3. <u>Method used to induce cracks</u>

Methods used to induce cracks in concrete specimens have been thoroughly described in Chapter 3. In relation to this research project focusing on the influence of cracks on the durability and service life of reinforced concrete structures in relation to chloride-induced corrosion, the most appropriate method used to induce cracks in concrete specimens should be determined. The WST (wedge splitting test) method induces V-shaped and realistic cracks, however steel reinforcement was mostly not applied so far. Therefore, chloride profiles can be measured, but there is limited possibility to measure corrosion of steel reinforcement. Cracks created by the Brazilian splitting test on cylindrically-shaped specimens are cracks with parallel-side cracks which are not common in practice. Other disadvantages are that no reinforcing steel can be applied for corrosion measurements and cracks cannot be controlled in the loaded state. Although cracks induced by the expansive core method can be held open during chloride exposure, their shapes are similar to the parallel-sided cracks as obtained with the Brazilian splitting method. Steel reinforcement is not applied so far limiting the use of this method to the purpose of investigating chloride profiles only. Artificially induced cracks e.g. by plastic shims, represent the easiest way to create and control crack width, depth and frequency. However, in that case the shape of the crack (parallel walls), crack's roughness, tortuosity, connectivity and process of self-healing cannot be taken into account. Reinforcing steel can be applied for corrosion measurements, but for this research project the option of

artificially induced cracks was not selected because of crucial differences in crack geometry of this method compared to cracks in real structures.

The difference between the bending method and the aforementioned methods is that the induced cracks resemble realistic V-shaped cracks the best. Corrosion of steel reinforcement in concrete can be monitored. As far as four point bending is concerned, loading can be applied over the desired span. The specimen can be exposed to a chloride solution in the loaded state. Furthermore, specimens can be re-loaded and unloaded to the previous loading level during chloride exposure. It can be concluded that cracks induced by 4-point bending are reliable enough to carry out experiments. The results obtained from tests conducted on this type of cracks, can be used further to propose a step forward towards improved models for service life prediction of reinforced concrete structures. Based on the bending method, some recommendations and limitations can be proposed with the intention to be accepted by official codes with regard to cracked reinforced concrete structures exposed to aggressive environmental conditions.

4.4.4. *Steel reinforcement*

High yield-stress ribbed cold-rolled reinforcing bars B500A were used, diameter 12 mm and length 1460 mm. A wire was connected at the end of the bar for measurements in a later stage. An ultimate tensile strength test was carried out in order to check the maximum stress that a reinforcing bar can withstand while being pulled before breaking (Fig. 4-15a). One piece of bar, length 42 cm, was stretched until failure with a speed of 0.1 mm/s. The stress-strain relation was recorded during the test (Fig. 4-15b). The reinforcing bar was tested to check the following properties: limit tensile stress in the region of linear-elastic behaviour (1), yielding strength (2) and ultimate tensile strength of the bar (3). The values were 529 MPa, 561 MPa and 601 MPa, respectively. Furthermore, the modulus of elasticity (E_s) was determined in the region of linear-elastic behaviour as stress-strain ratio, giving a value around 200000MPa.
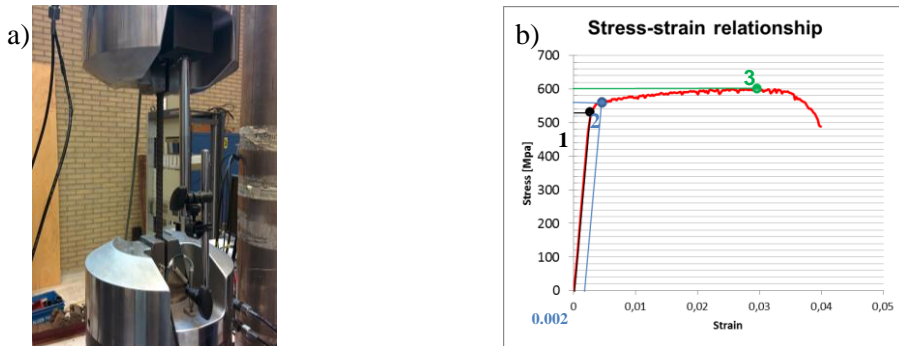
Figure 4-15: Determination of stress-strain relation of the reinforcing steel

4.4.5.   *Casting and curing*

The reinforced concrete beams $1500 \times 100 \times 150$ mm^3 were cast with one ribbed bar which was embedded at the desired position. Before casting, all reinforcing bars were thoroughly cleaned and degreased. The internal reference electrode (Pt/Ti - platinized titanium) was fixed next to the reinforcing bar using plastic strips. The side of the beam, which was later exposed to a chloride solution, is situated at the bottom in the mould (Fig. 4-16a). The concrete was vibrated in three layers. Titanium mesh (MMO Ti) was embedded at the opposite side at 15 mm from the concrete surface in order to act as a counter electrode for corrosion measurements as can be seen in Fig. 4-16b.
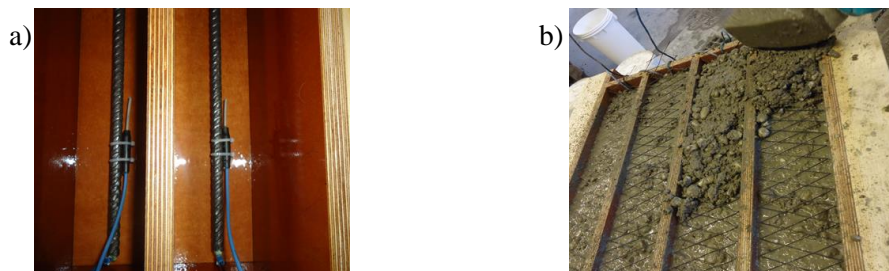
Figure 4-16: a) Reinforcing bar and internal reference electrode; b) Titanium mesh – counter electrode

Four beams and nine cubes were cast per batch. Eight batches have been cast, in total delivering 32 beams. Several cubes were cast for each batch to check the compressive strength. Three cubes per batch were cast in order to be exposed to a chloride solution under the same conditions as the beams for the purpose of finding chloride profiles in uncracked concrete. After casting, beam specimens

and cubes were covered with plastic sheets for 72 hours under laboratory conditions (Fig. 4-17).
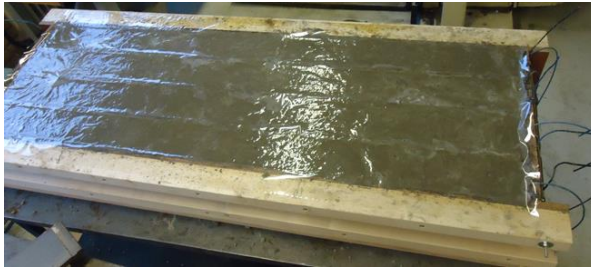
Figure 4-17: Casting of reinforced concrete beams in laboratory

After that, the concrete specimens were stored in a climate-controlled room (20±2°C and 95±5% RH) until the age of 28 days. Then, six cubes were tested to check the compressive and tensile strength, while the reinforced concrete beams were exposed to air drying under laboratory conditions (20°C, 50% RH) for an additional 7 days. After that, the test set-up has taken place. The cube compressive strength after 28 days was 31±2 MPa. Cube tensile splitting tests were carried out as well, resulting in tensile strength values of 2.8±0.2 MPa.

4.4.6. *The role of crack width and crack frequency*

Up to recently, several research programs have been carried out on reinforced concrete specimens with only one single flexural crack in order to obtain a clear understanding of the corrosion mechanism (Schießl, 1997) and the effect of a single crack width on the corrosion rate of steel reinforcement (Otieno, 2010), as described in Chapter 3. On the other hand, in a study by Arya and Ofori-Darko (1996), it was concluded that limiting the crack frequency is more important than limiting surface crack width to control the corrosion of steel reinforcement as described in Section 3.2. However, taking into consideration the disadvantages of that experimental set-up (artificial cracks) which does not reflect reality, real flexural cracks would represent a much better solution than artificial cracks in order to investigate the interrelated influence of crack width and crack frequency on chloride-induced corrosion under simulated real conditions. For instance, crack roughness, crack tortuosity and crack shape are a few important factors which might have an influence on the corrosion process and these factors should therefore be regarded in order to generate practical rules.

In a study by Mohammed (2001) two similar reinforced concrete beams were cracked under the same load with different types of steel reinforcement, plain and deformed. The specimen with the plain bar had a higher maximum crack width and total (summed) crack widths than the specimen with the deformed bar (Table 4-4). The specimen with the deformed bar showed finer cracks but the number of cracks and corroded area were higher than in the specimen with the plain bar.

Table 4-4:   Cracks characteristics and corrosion of specimen with plain and deformed bar (Mohammed, 2001)

Crack characteristics	Specimen with plain bar	Specimen with deformed bar
Maximum crack width (mm)	0.4	0.2
Sum of total crack widths (mm)	1.85	1.60
Number of cracks	6	10
Corroded area (cm^2)	30	90

The deformed bars appeared to be much more prone to corrosion than plain bars in cracked concrete specimens. As explanation it was stated that concrete specimens with plain bars have a smaller number of surface cracks and, therefore, less internal cracks which lead to smaller oxygen permeability compared to specimens with deformed bars. Taking into account that oxygen is necessary for a cathodic reaction during the corrosion process of steel reinforcement, concrete specimens with deformed bars appeared to corrode faster than specimens with plain bars due to faster ingress of oxygen through the concrete cover. However, no investigation was carried out into the influence of cracks (different combinations of crack widths and number of cracks) on chloride-induced corrosion in multicracked specimens with the same type of bar, which would allow a better comparison.

According to the aforementioned research programs it can be concluded that the hypothesis about the influence of crack frequency on chloride-induced corrosion should not be neglected in order to incorporate the influence of flexural cracks on service life design of reinforced concrete structures. An appropriate experimental set-up was required to involve in a right way the interrelated influence of crack width, crack frequency and concrete cover on chloride-induced corrosion under simulated severe exposure conditions.

4.4.7. *Concrete cover and loading procedure*

Three different concrete covers were applied: 20 mm, 30 mm and 40 mm. The larger is the concrete cover, the longer is the distance from the surface to the steel reinforcement for aggressive substances. Consequently, a larger concrete cover should provide better corrosion protection of the steel reinforcement. On the other hand, a larger concrete cover leads to a higher surface crack width. Based on that, the surface crack width-concrete cover ratio is a parameter which should be taken into consideration. Steel beams were required for the purpose of accommodating supports (steel rods) on them and to use a downer bracket in interaction with threaded rods, bolts and an upper bracket to apply the force on the concrete beam as is shown in Fig. 4-18.
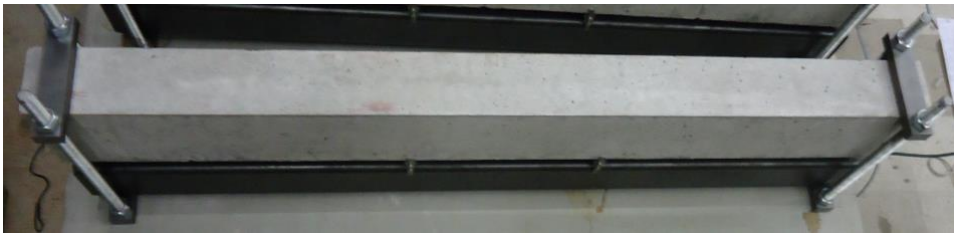
Figure 4-18: Concrete beam in set-up before loading was applied

Four-point bending was applied in order to induce predefined crack widths in the reinforced concrete specimens. The experimental set-up is shown in Fig. 4-19.

The series of different mean crack widths, maximum crack widths, number of cracks, total crack widths were tested in combination with various concrete covers and types of loading during experiments. The experimental schedule is presented in Table 4-5. Crack widths were measured by a digital microscope and the average value was compared with the target value (Fig. 4-20a). In order to control the number of cracks in some series undesired surface cracks had to be sealed by epoxy (Fig. 4-20b). It was simple to seal the surface crack, but pre-testing had to be carried out in order to check the effectiveness of crack sealing in terms of crack depth. One concrete beam was cut by a diamond saw in order to see whether crack depth was sealed completely (Fig. 4-21a). A few pieces were cut at the concrete-steel interface where crack depth intersects the reinforcing bar as well (Fig. 4-21b). Taking into consideration that the crack width in function of the depth is decreasing, it was confirmed that even crack widths less than 0.05 mm were sealed completely. It can be concluded that an undesirable crack can be de-activated completely by epoxy.
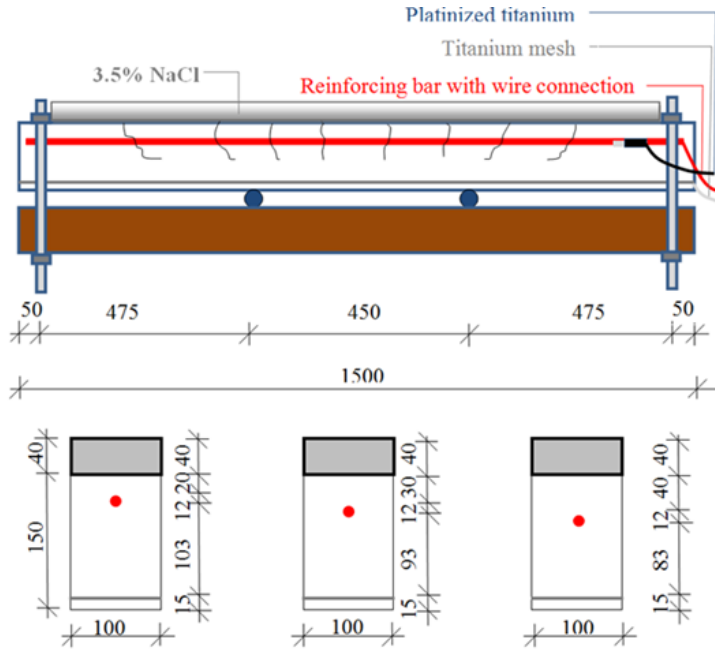
Figure 4-19: Experimental set-up
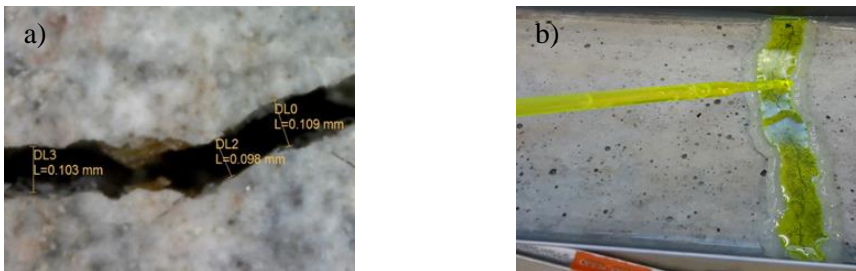
Figure 4-20: a) Crack width 0.1 mm – digital microscope; b) Surface crack is sealed by epoxy
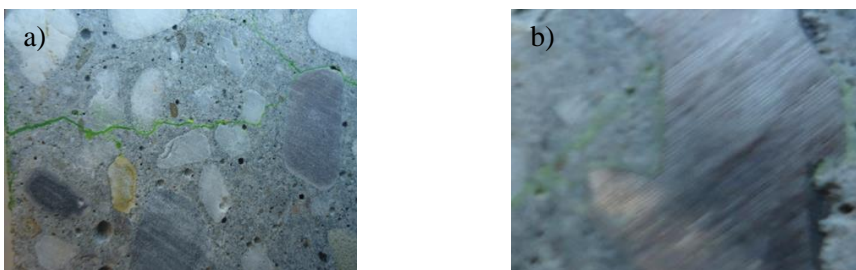
Figure 4-21: a) Crack depth is sealed by epoxy; b) Microcracks around bar are sealed by epoxy

Table 4-5: Series of variable combinations

Beam	Concrete cover (mm)	Mean crack width (mm)	Number of cracks	Type of loading
1A	C=20	0	0	Unloaded
1B	C=20	0	0	Unloaded
2A	C=20	0.15+long.	9	Sustained
2B	C=20	0.15+long.	9	Sustained
3A	C=20	0.15	9	Sustained
3B	C=20	0.15	9	Sustained
4A	C=20	0.15	6	Sustained
4B	C=20	0.15	6	Sustained
5A	C=30	0	0	Unloaded
5B	C=30	0	0	Unloaded
6A	C=30	0.15	8	Sustained
6B	C=30	0.15	8	Sustained
7A	C=30	0.10-0.20	8	Variable
7B	C=30	0.10-0.20	8	Variable
8A	C=30	0.15	6	Sustained
8B	C=30	0.15	6	Sustained
9A	C=30	0.2	6	Sustained
9B	C=30	0.2	6	Sustained
10A	C=30	0.3	4	Sustained
10B	C=30	0.3	4	Sustained
11A	C=40	0	0	Unloaded
11B	C=40	0	0	Unloaded
12A	C=40	0.35	3	Sustained
12B	C=40	0.35	3	Sustained
13A	C=40	0.4	5	Sustained
13B	C=40	0.3	5	Sustained
14A	C=40	0.15-0.25	6	Variable
14B	C=40	0.15-0.25	6	Variable
15A	C=40	0.15	6	Sustained
15B	C=40	0.25	6	Sustained
16A	C=40	0.20	6	Sustained
16B	C=40	0.45	2	Sustained

The containers for the NaCl solution were made of PVC. They were placed on top of the beam and the cracks were sealed by silicone at both sides in order to prevent leakage of solution through cracks as is shown in Fig. 4-22. An impression of the test series is shown in Fig. 4-23.

The reinforced concrete beams were tested under sustained, variable and unloaded conditions as is shown in Table 4-5. However, based on the test set-up where the reinforced concrete beams were under sustained load at constant deflection in time, a reduction of the load was expected to occur during the prolonged exposure period due to the effects of creep and shrinkage (analysed and discussed in Chapter 6). In relation to that, it can be noted that the concrete beams were actually under a declining sustained load. On the other hand, a few concrete beams were exposed to a chloride solution under a variable (alternating) load where re-loading was applied once a week for 18 hours. However, after 18 hours of re-loaded period, the concrete beams were relaxed to be at the previous loading level for the rest of the week. One re-loaded period consisted of 6 hours of drying and 12 hours of wetting. In addition, for the rest of the week (150 hours) the beams were relaxed to be at the previous loading level which consisted of 114 hours of drying and 36 hours of wetting. The unloaded concrete beams were denoted as uncracked.
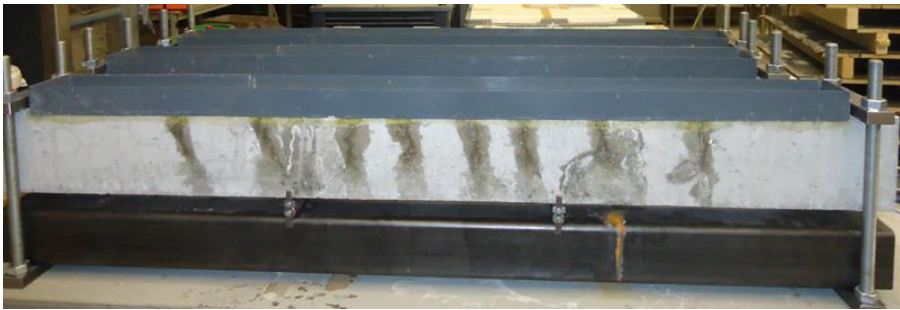
Figure 4-22: Four-point bending is applied and cracks are sealed by silicone on both sides

Figure 4-23: Overview of test series in Stevin Lab II

4.5. Conclusions

This chapter reported on the electrochemical measurements and results recorded for the preliminary tests and development of the final, large-scale experimental set-up. The main objective of the preliminary tests was to evaluate the applicability of electrochemical measuring methods as EIS, LPR and PDP to monitor corrosion of steel in large reinforced concrete beams. The tests and data interpretation took into consideration variable structural parameters as crack widths, crack frequency and load. The generally employed (both lab and field tests) OCP monitoring can only serve as an indication of corrosion initiation and propagation and even in this case, the contribution of cracks, oxygen and humidity levels respectively, need to be taken into account to avoid misinterpretation. Next to that, a meaningful and reliable electrochemical measurement can be only obtained when equal environmental conditions apply, especially for the "spot" method. Even then, knowledge on bulk matrix properties is very important in order to account for observed fluctuations or discrepancies in response. To that end, EIS is a very useful technique, providing information for the whole system and at different (desired) levels. As a more sophisticated approach, continuous EIS measurements are possibly not appropriate in terms of time efficiency for large test series.

LPR tests provide meaningful results, however additional measurements as PDP would increase the level of reliability of the LPR tests. Taking into consideration that 32 concrete beams are analysed, OCP and LPR were applied for the final large scale series due to time efficiency in relation to the number of specimens. It is important to emphasize that trends in observed behaviour are more appropriate to be discussed, rather than absolute values, especially when only the OCP and LPR techniques are employed for corrosion monitoring. The final experimental program was developed with emphasis on a better understanding of the influence of cracks on chloride-induced corrosion. For that purpose, a series of different mean crack widths, maximum crack widths and number of cracks, were tested in combination with various concrete covers and types of loading.

Chapter 5

Corrosion monitoring of steel reinforcement in concrete beams: Description of test results linked to variation of structural parameters

5.1. Half-cell potential (HCP) measurements

As already introduced in Chapter 4, open circuit potential (OCP) or HCP (half-cell potential) measurements were performed in order to assess the active or passive state of the steel reinforcement i.e. the probability of steel corrosion. Whether the steel reinforcement is in the active or passive state with regard to corrosion, can be approximately determined from the HCP readings, following the series of variable combinations given in Table 4-5, Chapter 4. The HCP was recorded through both embedded i.e. internal platinized titanium (Pt/Ti) and external silver-silver chloride (Ag/AgCl) reference electrodes. The HCP records with the embedded Pt/Ti electrode (casting and positioning at the end of a rebar as depicted in Fig. 4-16a) were performed in "wet" and "dry" conditions throughout the experiment, providing average HCP values for the embedded steel rebar.

When an external Ag/AgCl reference electrode was used, the HCP measurements were carried out using the "point (spot)" measurement, through placing the electrode on the concrete surface at the end of wetting and drying cycles, thus recording "local" HCP values above and between cracks (Section 5.3). The average HCP values for the whole rebar were recorded through the external

Ag/AgCl electrode as well, by placing the electrode in the solution at the end of the wetting cycles. Average HCP readings, recorded at that moment, are actually "mixed potential" for the total exposed steel surface. More details on the execution of HCP measurements and considerations with regard to this were specified in Chapter 4.

The average HCP values at the end of the wetting phases, recorded with external Ag/AgCl and internal embedded Pt/Ti reference electrodes for 2 years of exposure are shown for three different concrete covers of 20 mm, 30 mm and 40 mm in Fig. 5-1, 5-2 and 5-3, respectively. The figures present the HCP values as recorded with both electrodes. The values, recorded with the embedded Pt/Ti electrode, could be converted to Ag/AgCl for clarity and accurate comparison. In the cement extract of pH 12.9 i.e. concrete pore water, the Ag/AgCl reads around +20mV vs Saturated Calomel electrode (SCE), whereas the Ag/AgCl versus the Pt/Ti reads around +25mV.

As already discussed in Chapter 4, the HCP record is a qualitative measurement, only providing an indication of the corrosion state. However, a sustained and stable trend of change of the HCP values, especially if recorded over a prolonged time interval, serves as a direct evidence of altered electrochemical behavior i.e. an active or passive state of the steel reinforcement.
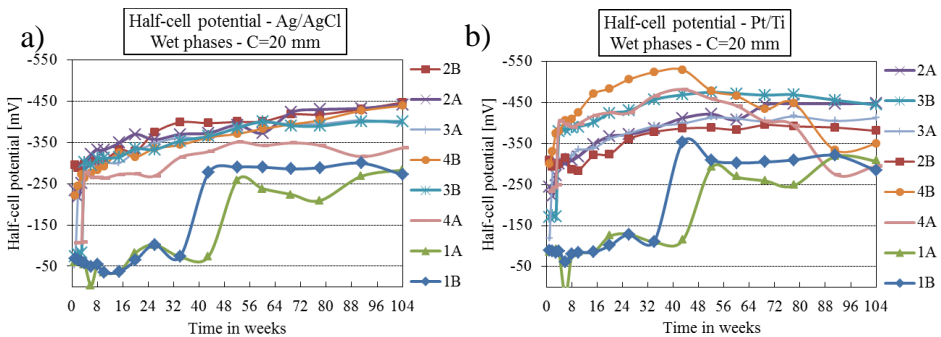
Figure 5-1: Average HCP using Ag/AgCl and Pt/Ti at the end of wet phases for beams with a concrete cover of 20 mm
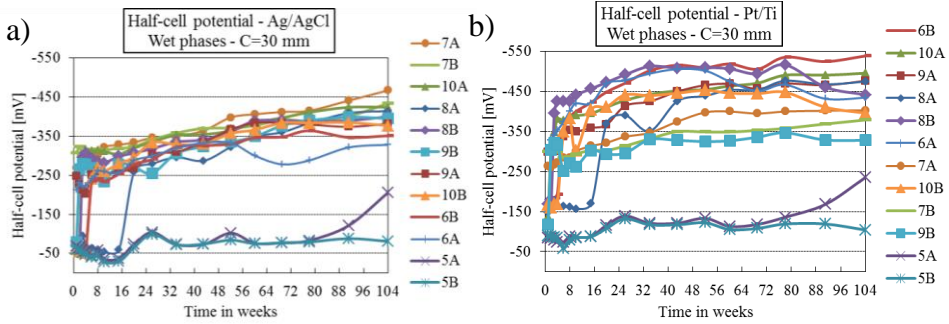
Figure 5-2: Average HCP using Ag/AgCl and Pt/Ti at the end of wet phases for beams with a concrete cover of 30 mm
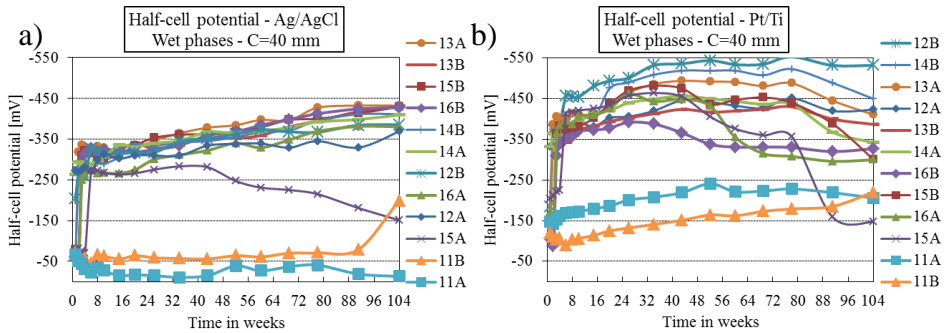
Figure 5-3: Average HCP using Ag/AgCl and Pt/Ti at the end of wet phases for beams with a concrete cover of 40 mm

5.1.1. *HCP average values during wetting cycles with a concrete cover of 20 mm*

Fig. 5-1 depicts the evolution of HCP over the time of exposure of the reinforced concrete beams with a 20 mm concrete cover, recorded with external (5-1a) and embedded (5-1b) electrodes, allowing a direct comparison of the HCP values in view of geometrical position of the reference cell and manner of HCP measurements execution. The potential difference and variation of the derived values can be attributed to ohmic drops (concrete resistivity) i.e. readings with an external electrode would reflect the contribution of the concrete cover resistivity. In contrast, readings with an embedded electrode are affected only by the geometrical position of the reference cell, which was in direct proximity to the rebar, hence arranged in a manner towards minimal bulk matrix resistance contribution. As can be observed in Fig.5-1 both external (5-1a) and internal (5-

1b) electrode arrangements provide generally similar values i.e. a good agreement of the HCP values, recorded with the two electrodes, was observed. This is especially the case for the unloaded (uncracked) beams 1A and 1B, where the recorded HCP values are the most noble ones from the start of the tests until 32 to 40 weeks of exposure. After 40 weeks, a cathodic shift towards more negative values was observed for both beams 1A and 1B, denoted to corrosion initiation of the steel reinforcement as a result of gradual NaCl penetration through the porous concrete matrix (20 mm cover) during the wetting phases. After week 40 the HCP values for 1A and 1B approached, invaded and further stabilized around the threshold value for the active/passive state (~ -250 mV versus Ag/AgCl which can be converted to ~ -270 mV vs SCE based on ASTM C876-91, 1999).

For all other beams with 20 mm concrete cover, a cathodic shift of HCP values was recorded almost immediately after exposure to the external NaCl solution. This is attributed to a faster chloride penetration through the already existing cracks, under load conditions, and consequently immediate corrosion initiation occurred on the rebar's steel surface. In contrast to beams 1A and 1B, a larger variation in HCP was observed for the cracked beams, recorded with external and internal electrodes. This occurs due to the contribution of the concrete cover in the case of an external electrode and minimized ohmic drop in the case of an internal reference electrode. For example, for beam 4B the HCP recorded with Ag/AgCl (Fig. 5-1a) depicts a gradual cathodic shift over time, whereas the HCP recorded with Pt/Ti shows a relatively more active state in the beginning, with values approaching -530 mV vs. Pt/Ti (or converted, -505 mV vs Ag/AgCl). After 48 weeks the HCP recorded with Pt/Ti for beam 4B gradually stabilizes around -450 mV versus Pt/Ti (or converted, -425 mV versus Ag/AgCl), a value similar to the one recorded with an external Ag/AgCl. A slight anodic shift was observed later on, starting at 72 weeks of exposure. A slight anodic shift can also be observed for all other beams under sustained load. It occurs due to autonomous "self-healing" and closure of cracks over time (precipitates filling-in cracks, carbonation, declined sustained load etc.) and, therefore, NaCl penetration towards the steel surface is impeded in case of sustained load. These microstructural alterations, though, are barely reflected through the measurements with an external Ag/AgCl electrode, where the overall concrete resistance is the dominating factor, rather than the contribution of micromechanical changes in the bulk matrix and concrete cover (cracked or uncracked). The result is a more stable HCP reading over time, which although

reflecting an active state similar to the Pt/Ti electrode, is obviously less sensitive to bulk matrix alterations and microstructural changes at the concrete-steel interface.

For the 20 mm concrete cover beams, the measurements with both external and internal electrode show the most active state to be in beams 2A, 2B, 3A and 3B, followed by beams 4A and 4B. The more active state for beams 2A and 2B is as expected, resulting from the additional longitudinal cracks (Table 4.4, Chapter 4), which contribute to enhanced chloride transport in the vicinity of the steel reinforcement. Further, beams 3A and 3B demonstrate a presumably (HCP records are just an indication of corrosion state) higher corrosion activity than beams 1A, 1B, 4A and 4B due to the larger number of cracks, reflected by more cathodic HCP values. It can be noted that for all beams with a concrete cover of 20 mm, Fig. 5-1, both external and internal electrodes provide similar accuracy in determining the corroding state of the steel reinforcement, reflected by similar HCP values over time, with only slight fluctuations, recorded with the embedded electrode for the case of cracked specimens.

5.1.2. *HCP average values during wetting cycles with concrete covers of 30 mm and 40 mm*

Similar observations during wetting cycles hold for the specimens with a concrete cover of 30 mm and a concrete cover of 40 mm (Figs. 5-2 and 5-3). However, a larger variation of HCP values was observed with the embedded electrode (Figs. 5-2b and 5-3b), whereas a more stable trend of HCP changes was recorded with an external Ag/AgCl electrode (Figs. 5-2a and 5-3a). Although HCP values, recorded with both internal and external electrodes for all loaded specimens show an active state of the steel reinforcement, some differences can be observed.

If Fig. 5-1 is compared to Figs. 5-2 and 5-3 with respect to the role of concrete cover thickness, one well distinguished effect of concrete cover is pronounced and reflected by both electrodes. The unloaded (uncracked) beams for both 30 mm and 40 mm cover (beams 5A, 5B, 11A and 11B) show the most anodic potentials and, therefore, passive state until the end of the hereby reported monitoring period of 2 years. In contrast, a transition from the passive to the active state was observed after 32 to 40 weeks of exposure for the unloaded beams 1A and 1B with 20 mm cover (Fig. 5-1). It is obvious that 20 mm cover provides a reduced "barrier" effect towards penetration of chloride which needs

less time to reach the steel surface in case of a thinner concrete cover. By increasing the concrete cover for uncracked concrete, a longer period of time is expected for chlorides to reach the steel surface and break the passive layer. It is observed that HCP values for the unloaded beams with 30 mm and 40 mm cover remain more anodic than -250 mV versus Ag/AgCl and Pt/Ti electrodes. Only a slight cathodic shift was observed towards 104 weeks, however, according to the HCP readings all these cases i.e. beams 5A, 5B of 30 mm and beams 11A and 11B of 40 mm cover remain in passive state.

The second well distinguishable effect of concrete cover on the HCP records, observed by comparing readings for 20 mm cover (Fig. 5-1) and readings for 30 mm and 40 mm cover (Figs. 5-2 and 5-3), is the more stable trend of the HCP evolution for 30 mm and 40 mm cover when values are recorded with an external electrode (Figs. 5-2a and 5-3a) and larger variation when HCP was recorded with an internal electrode (Figs. 5-2b and 5-3b). In case of external electrodes, increasing the concrete cover from 20 mm to 40 mm clearly results in a reduced sensitivity of the measurement. As can be observed in Figs. 5-2a and 5-3a, all beams show an increasingly active state towards 104 weeks of exposure, with a variation of maximum 50 to 100 mV between the HCP values for the various beams. In contrast, the HCP values for the same beams measured with an internal electrode (Figs. 5-2b and 5-3b) clearly show a larger variation (50 mV to 200 mV), especially pronounced at the end of the reported period. These differences are attributed to the pronounced contribution of the concrete cover (bulk matrix) resistivity on HCP measurements performed with an external electrode and reduced or minimum effects of these alterations with an internal embedded electrode. In other words, monitoring HCP values with an embedded electrode reflects more accurately the influence of crack width and number of cracks on probable corrosion activity. This is concluded from the observed larger variation of HCP values over time for specimens with different crack width and number of cracks in the experiments. However, a more sophisticated trend for a less or more active state as a dependence of crack width, number of cracks and type of load is hard to make for the 30 mm and 40 mm cover.

It is noted that concrete bulk matrix and microstructural alterations are dominant factors, which increase with increased concrete cover thickness. In other words, an uncracked concrete cover of increased thickness is able to delay corrosion initiation, whereas a cracked concrete cover, irrespective of concrete cover magnitude, simply allows faster chloride penetration and the rate of the corrosion process varies following the relevant microstructural alterations. For example,

whereas the specimens with a larger number of cracks and additional longitudinal cracks for the 20 mm cover (Fig. 5-1) show the most active state, specimens with a larger number of cracks and a variable crack width in the case of 30 mm and 40 mm cover (beams 7A and 7B, Fig. 5-2 and beams 14A and 14B, Fig. 5-3) are not necessarily the ones where the most cathodic potentials were observed. This is in addition to the larger discrepancy, observed between readings with external and internal electrodes for the 30 mm and 40 mm cover. In the case of 30 mm cover, beams 7A and 7B (variable crack width, larger number of cracks) are expected to be most active. The HCP records with the external electrode confirm this expectation. A different observation holds for the HCP records with the embedded electrode (Fig. 5-2b) where the most active state was recorded for beam 6B and an additional variation with the replicate beam 6A (100 mV – 120 mV). Obviously, the HCP records with an external electrode provide a more average potential reading, reflecting the overall and more global state of the steel reinforcement. It also includes the influence and contribution of the concrete cover, including presence or absence of load and cracks.

In contrast, the HCP records with an internal electrode are more sensitive towards microstructural changes and reflect the corrosion state with higher precision. In other words, the embedded electrode reflects the electrochemical state of the steel reinforcement, affected overall from the higher or lower chloride permeability that varies with crack width, number of cracks etc. A direct link to changes in bulk matrix microstructure or micromechanics, however, is not always clearly reflected by the measurement. Therefore, even a closer look at the HCP readings, recorded with an internal electrode for each concrete cover, mean crack width, crack frequency or type of load cannot provide a clear trend for the influence of these crack-related variations on corrosion initiation and propagation. For example, for a concrete cover of 30 mm (Fig. 5-2) beams 6A and 6B, which are replicate cases, present very different values. Although, reflecting the active state, beam 6B being the most active from this group, whereas beam 6A is the specimen closest to the beams in the passive state. Similarly, beams 9A and 10A present cathodic values (active behavior), which holds for beams with higher crack width and number of cracks, however, a more active state is to be expected in beams 7A and 7B which are under a variable load. On the other hand, the external reference cell shows a more active state for beams 7A and 7B.

For a concrete cover of 40 mm (Fig. 5-3) the HCP values recorded with the external electrode are very similar, the most active ones being for beams of

highest mean crack width, which is as expected. This is not necessarily the case when values are measured versus the embedded electrode, where the most active state observed was for beam 12B which is a specimen with a lower crack width and frequency, randomly followed by the other cases. In other words, here again, a clear trend towards linking the HCP records with crack width, frequency and loading conditions is not recognized.

It can be concluded that the HCP values recorded during the wetting phases for the reinforced concrete beams for varying concrete cover, mean crack width, number of cracks and type of load are accurately determined by both external and internal (embedded) reference cells. It leads to a good indication of the passive or active state of the steel reinforcement and in terms of the sustained values over time of exposure. For a smaller concrete cover (20 mm) the discrepancy between values recorded with external and embedded reference cells is smaller and reflects well the microstructural alterations in terms of cracks evolution and micromechanical changes over time. Additionally, the variation of potential readings between different specimens of similar structural parameters is smaller. For larger concrete covers (30 mm and 40 mm) the discrepancy between values measured versus external and embedded reference cells increases, although both measurements accurately present the corrosion state of the steel reinforcement. Measured values with an external electrode show a reduced variation with increased concrete cover thickness where all passive or all active specimens show similar values. On the other hand, the HCP record with embedded electrodes reflect microstructural and micromechanical alterations. The HCP records with the embedded electrode show a large variation with increasing concrete cover, however, no clear trend and direct link to the microstructure can be made. Obviously, the ohmic drop, induced by concrete bulk matrix resistivity, plays a role within measurements with an external electrode. Larger fluctuations are recorded with the embedded cell, resulting from the higher sensitivity of the measurements and reduced or minimal bulk matrix contribution. Hence, the measurements reflect variations in water and chloride ion transport which affect alterations in the corrosion state.

5.1.3. *HCP average values at the end of wet and dry cycles*

When an embedded internal reference electrode (Pt/Ti) was used, HCP measurements were carried out at the end of wet and dry cycles during two years

of exposure. Results are shown for three different concrete covers of 20 mm, 30 mm and 40 mm in Fig. 5-4, 5-5 and 5-6, respectively.
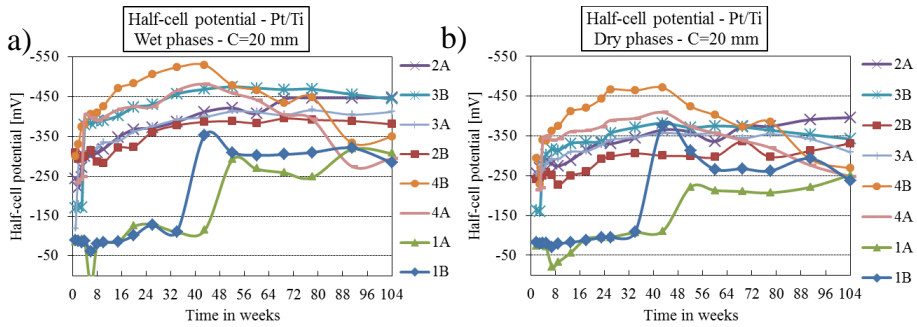
Figure 5-4: *Average HCP using Pt/Ti at the end of wet and dry phases for beams with concrete cover of 20 mm*
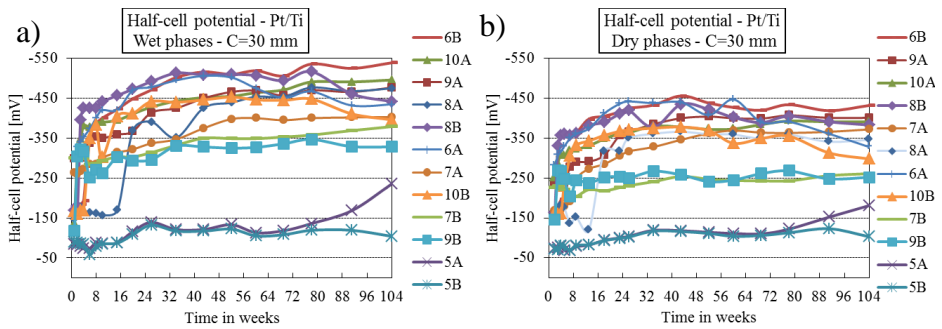
Figure 5-5: *Average HCP using Pt/Ti at the end of wet and dry phases for beams with concrete cover of 30 mm*
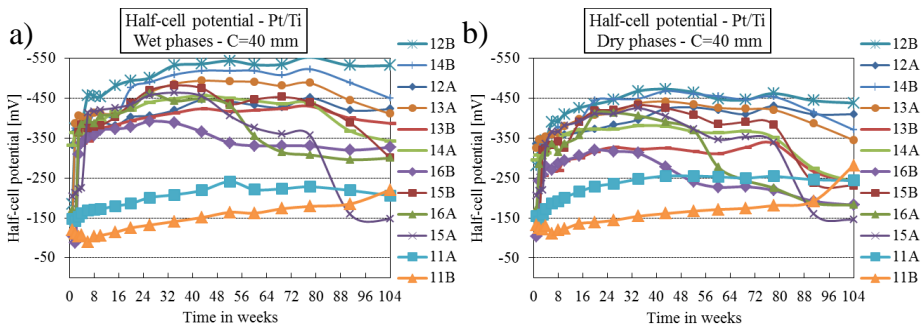
Figure 5-6: *Average HCP using Pt/Ti at the end of wet and dry phases for beams with concrete cover of 40 mm*

The main difference in HCP values is determined by the concrete resistivity which is lower during the wetting phases and higher during the drying phases. A cathodic shift was observed for the steel reinforcement with higher relative humidity (oxygen diffusion limitations) and enhanced chloride ions penetration. Consequently, the HCP values during the wetting phase end up more cathodic than the HCP values for the drying phases. This holds true for all groups of concrete specimens, irrespective of the concrete cover thickness.

A larger variation of HCP values between specimens with equal concrete cover is observed for the larger concrete cover. It occurs due to higher concrete bulk matrix resistivity for the larger concrete cover, as previously commented for the wetting phases. It should be noted that the variation between HCP values in one and the same group for the corroding specimens of larger concrete cover is smaller in dry conditions, compared to wetting phases (Figs. 5-5 and 5-6). This is attributed to the fact that within the drying phases, chloride ion and water transport in the bulk (sound) matrix and through cracks is limited. Consequently, the corrosion state is determined by the chemistry and availability of the pore solution in the vicinity of the steel reinforcement, which is similar for all corroding cases. As seen from the plots, the HCP values for passive steel are almost identical for the wetting and drying phases which can be seen in Fig. 5-4, specimens 1A and 1B until 48 weeks and Figs. 5-5 and 5-6, specimens 5A, 5B, 11A and 11B. This is determined by the stability of the passive film on the steel reinforcement and there are no changes relevant to the chemistry of the pore solution, in terms of chloride ions concentration, in the vicinity of the steel reinforcement during wetting and drying cycles.

Information on the corrosion rate is not available via HCP, only the probability of steel corrosion is obtained. After steel depassivation, a linear polarization resistance technique was applied in order to quantitatively assess the corrosion state of the steel reinforcement in the concrete beams.

5.2.   Linear polarization resistance

After the high probability of depassivation using external Ag/AgCl electrode (average OCP < -256 mV), LPR was applied in order to calculate the corrosion current density at the end of wetting cycles. On the other hand, LPR measurements were also conducted using an internal reference electrode (Pt/Ti)

to verify the reliability of corrosion current density results. In case of Pt/Ti, corrosion current densities were derived at the end of both wet and dry phases.

The corrosion current densities are considered to be in the range of passivity where the value of 0.1 $\mu A/cm^2$ is assumed as a threshold value. If the derived corrosion current densities are higher than 0.1 $\mu A/cm^2$, active corrosion is occurring. In this research only active corrosion was taken into account due to the negligible influence of passive corrosion current densities.

The instantaneous corrosion rate has been derived for a period of two years. It should be emphasized that the instantaneous corrosion rate is the corrosion current density at a certain moment and the development of steel corrosion can be monitored in time. The instantaneous corrosion rate, derived from the measurements with internal reference electrode Pt/Ti and external reference electrode Ag/AgCl at the end of the wet phases for the different concrete cover of 20 mm, 30 mm and 40 mm, is shown in Fig. 5-7, 5-8 and 5-9, respectively.
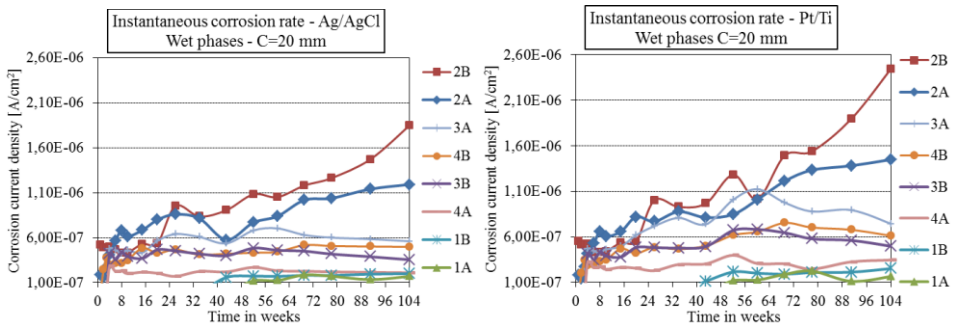
Figure 5-7: Instantaneous corrosion rate using Ag/AgCl and Pt/Ti at the end of the wet phases for beams with a concrete cover of 20 mm
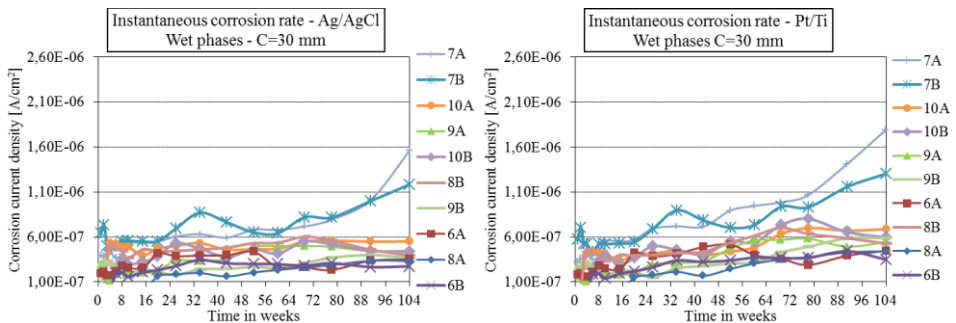
Figure 5-8: Instantaneous corrosion rate using Ag/AgCl and Pt/Ti at the end of the wet phases for beams with a concrete cover of 30 mm
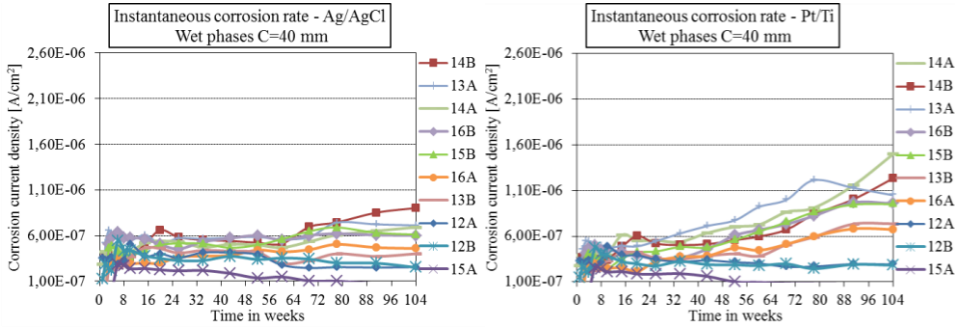
Figure 5-9: Instantaneous corrosion rate using Ag/AgCl and Pt/Ti at the end of the wet phases for beams with a concrete cover of 40 mm

The instantaneous corrosion rate, derived for measurements with internal reference electrode Pt/Ti at the end of wet and dry phases for the different concrete covers of 20 mm, 30 mm and 40 mm, is shown in Fig. 5-10, 5-11 and 5-12, respectively.
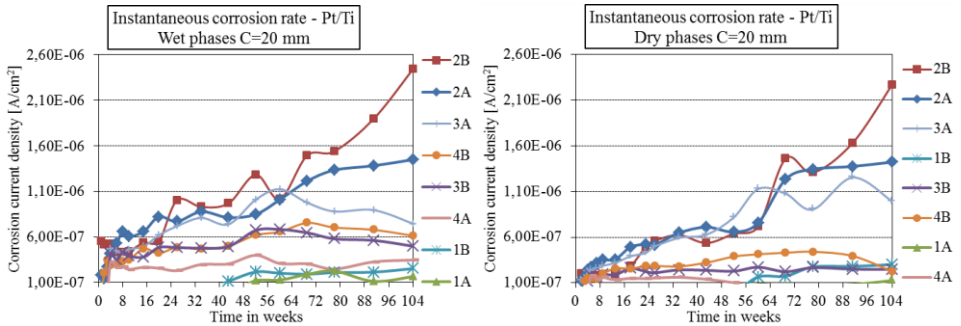
Figure 5-10: Instantaneous corrosion rate using Pt/Ti at the end of wet and the dry phases for beams with a concrete cover of 20 mm
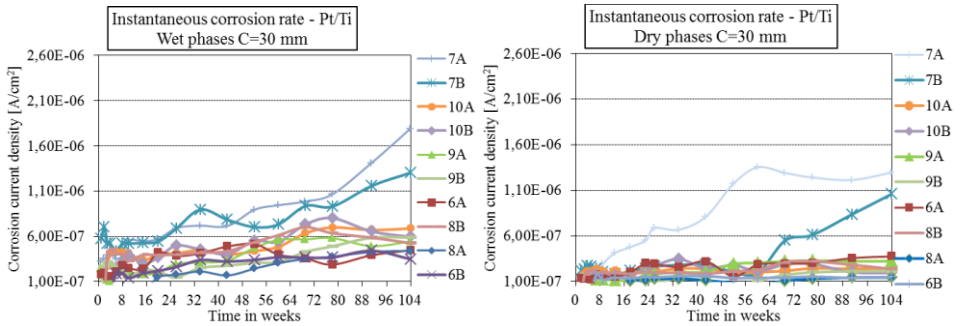
Figure 5-11: Instantaneous corrosion rate using Pt/Ti at the end of wet and the dry phases for beams with a concrete cover of 30 mm
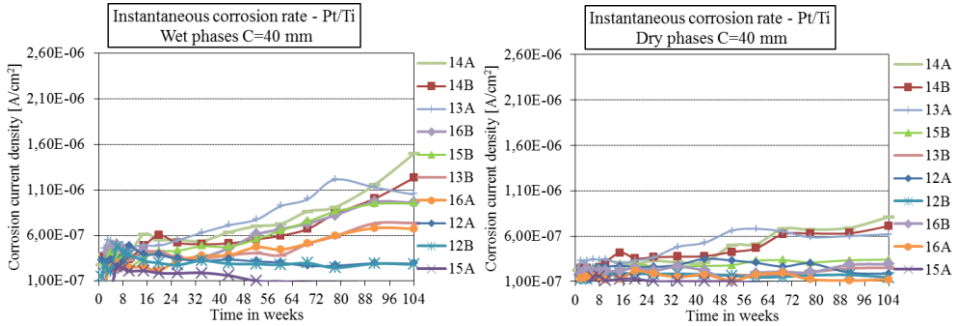
Figure 5-12: Instantaneous corrosion rate using Pt/Ti at the end of wet and the dry phases for beams with a concrete cover of 40 mm

5.2.1. *Steel corrosion in beams with a concrete cover of 20 mm*

In order to discuss corrosion currents for beams with a cover of 20 mm, a description of each beam is explained. Beams 1A and 1B were not loaded and they were uncracked. Beams 2A and 2B were loaded until the intended maximum crack width was reached. Flexural cracks were created but a few longitudinal as well. After that, the load was decreased in order to reach a mean flexural crack width of 0.15 mm. The cracks in beams 3A and 3B were created by applying the load until the mean crack width was 0.15 mm. Nine flexural cracks were created in beams 3A and 3B as well as in beams 2A and 2B. However, longitudinal cracks have not been created in beams 3A and 3B. In beams 4A and 4B after loading a few cracks have been deactivated by epoxy so that only 6 active cracks were left. The reinforcement in the uncracked beams 1A and 1B started slightly to corrode after one year of exposure. However, the corrosion current density was very low. The highest corrosion current densities were recorded in beams 2A and 2B. Corrosion products were visible at the top of the cover even after 26 weeks of exposure. Depassivation of the reinforcing bar occurred very fast in all aforementioned cracked beams with 20 mm concrete cover during the first ponding cycle (i.e. within 2 days). Corrosion of steel reinforcement occurred, but after a short progress it slowed down in beams 4A and 4B. The higher number of cracks in beam 3A leads to a slightly higher corrosion current than in beams 4A and 4B. The corrosion current densities are still increasing in beams 2A and 2B due to easy access of chlorides, moisture and oxygen to a large area of the steel reinforcement as a result of the longitudinal cracks. So, longitudinal cracks can be even more dangerous than flexural cracks with regard to corrosion of steel reinforcement.

5.2.2.   *Steel corrosion in beams with a concrete cover of 30 mm*

Beams 5A and 5B were not loaded and they remained uncracked. Corrosion of steel has not occurred yet after two years of exposure. Beams 6A, 6B, 7A and 7B contain an equal number of 8 cracks. Beams 6A and 6B were under a sustained load where the mean crack width was 0.15 mm. The mean crack width in beams 7A and 7B was 0.10 mm. However, beams 7A and 7B were reloaded once a week in order to reach a mean crack width of 0.20 mm for 18 hours, 6 hours during the wetting phase and 12 hours during the drying phase. After reloading, the beams were relaxed to the previous loading where the mean crack width is again 0.10 mm for the rest of the week (150 hours). Taking into account the duration of the loaded and the reloaded state of the beams 7A and 7B, it can be concluded that the mean crack width is 0.10 mm during 88% of the exposure time and 0.20 mm only during 12% of the exposure time. Consequently, the mean crack width under the quasi-permanent load combination in this case would be slightly higher than 0.10 mm, but certainly lower than 0.15 mm. However, higher corrosion currents were recorded in the case of beams 7A and 7B, than in beams 6A and 6B. Although the mean crack width is lower in beams 7A and 7B than in beams 6A and 6B, under the quasi-permanent load combination the corrosion activity is higher due to the variable load. A possible explanation is that additional microcracks were formed under the maximum variable load. Those additional microcracks do not close completely after reducing the load level. In beams 8A, 8B, 9A and 9B after loading a few cracks have been deactivated by epoxy so that 6 active cracks were left under sustained load, where the mean crack width was 0.15 mm and 0.20 mm, respectively. In the case of beams 10A and 10B epoxy was used in order to have only 4 active cracks under sustained load, where the mean crack width was 0.30 mm. However, in those beams which were under sustained load, corrosion of steel started very fast, but stabilization was reached within a few months.

It can be noted that the influence of the maximum variable load obviously largely determines the corrosion rate of the steel reinforcement. This means that with regard to the role of crack width in durability aspects, if any, the maximum service load should be accounted for and not the quasi-permanent or the frequent load. It should be noted that in the case of the variable load (Beams 7A and 7B) no stabilization of the corrosion current density was reached, even after 2 years, in contrast to all other beams under sustained load where stabilization was reached within a few months.

5.2.3.   *Steel corrosion in beams with a concrete cover of 40 mm*

Beams 11A and 11B were not loaded and thus they were uncracked. Corrosion of steel has not occurred for two years of exposure yet. In beams 12A, 12B, 13B, 15B and 16B after loading at the beginning of the test, a few cracks have been deactivated by epoxy and remained under sustained load, where the mean crack width was 0.35 mm (12A and 12B), 0.30 mm, 0.25 mm and 0.45 mm, respectively. Beams 13A and 16A contain 5 and 6 cracks, respectively, without any crack sealing by epoxy, where the mean crack width was 0.4 mm and 0.2 mm, respectively, under sustained load. Beams 14A and 14B were subjected to an alternating load and the same duration of reloading applied which was previously mentioned for beams 7A and 7B. However, the mean crack widths in these beams were 0.15 mm and under reloading 0.25 mm.

The corrosion activity in time for the four beams with the same concrete cover (40 mm) and number of cracks (6), but different crack widths is compared. Beams 15A, 16A and 15B were subjected to a sustained load where the mean crack widths were 0.15 mm, 0.20 mm and 0.25 mm, respectively. It can be seen that a wider mean crack width leads to higher corrosion currents under a sustained load for a constant concrete cover and constant number of cracks. However, beams 14A and 14B were subjected to an alternating load and it can be seen that the corrosion activity (higher corrosion current density), in these beams was much higher than the corrosion of steel reinforcement in beam 15A, where self-healing probably was occurring after a few months of exposure. Furthermore, the reinforcement in beams 14A and 14B corroded even slightly more than in beam 15B, which was subjected to a sustained load where the mean crack width was 0.25 mm at the beginning of test. It can be concluded that the difference in corrosion rate is obviously influenced by alternating opening and closing of cracks, compared to cracks under a sustained load. Obviously crack opening and closing under an alternating load leads to increased chloride ingress and a higher corrosion rate. This occurs due to the fact that a lot of internal microcracks form and the width of the bending cracks varies, preventing the previously discussed self-healing and crack blocking.

5.2.4.   *The influence of crack frequency and steel stress on corrosion*

In order to induce a mean crack width of 0.15 mm in beams 3A, 6A and 15A for example the number of cracks without any crack sealing was 9, 8 and 6, respectively. Beam 15A (concrete cover 40 mm, 6 cracks) has the same mean

surface crack width of 0.15 mm as beam 3A (concrete cover 20 mm, 9 cracks). The corrosion current density of beam 3A is significantly higher than that of 15A. It can be seen that corrosion rate of beam 6A is in between, which is logically taking into account the concrete cover and the number of cracks. In this case according to the theory of crack formation a larger concrete cover leads to a smaller number of cracks and as such a lower corrosion current density. In beams 15A (6 cracks) and 6A (8 cracks) the corrosion current density seems to stabilize after about one and three months, respectively. In beam 3A, with 9 cracks, stabilization has been reached after about one year. However, a higher load was required in order to reach the mean surface crack width of 0.15 mm in the beam with 20 mm concrete cover than in the beam with a cover of 40 mm. A higher load leads to a higher steel stress, which leads on its turn to a higher crack width at the level of the bar.

It can be concluded that crack frequency depends on the concrete cover for the same steel cross-section. Crack frequency is decreased by increasing the concrete cover which leads to decreasing steel corrosion in concrete. It should be noted that crack frequency is a secondary parameter in relation to steel corrosion while the dominating parameter is most probably the steel stress which determines implicitly the damage at the steel-concrete interface. The experimental crack patterns according to the tests and the prediction of the relation between crack width and steel stress are analyzed in Chapter 6.

5.2.5. *Corrosion rate - Reduction of steel diameter*

In the beginning of Section 5.2 the instantaneous corrosion rate for different samples was presented in function of time. The corrosion current density (instantaneous corrosion rate) for a specific period of time can be transferred into the average corrosion rate (reduction of steel diameter). Engineers in practice use the average corrosion rate rather than the instantaneous corrosion rate due to the need to estimate the residual service life of existing structures. In other words, based on measurements in function of time, it is of vital importance to assess what is the average reduction of the steel diameter per year. Instantaneous corrosion current density in time was interpolated in order to obtain the average value of the corrosion rate during a specific period of time. The average corrosion rate is presented as the loss of steel diameter in µm per year. The longer the measurements are conducted, the more reliable is the average corrosion rate during the service life of the structure. The average corrosion rate

was estimated by interpolation of the instantaneous corrosion rate for concrete beams in the experiments after any six months (6, 12, 18 and 24) from the beginning of the test. The average corrosion rate, derived from the measurements with the internal reference electrode Pt/Ti at the end of wet and dry phases after any six months for all concrete beams in the experimental set-up, is shown in Figs. 5-13, 5-14, 5-15 and 5-16.
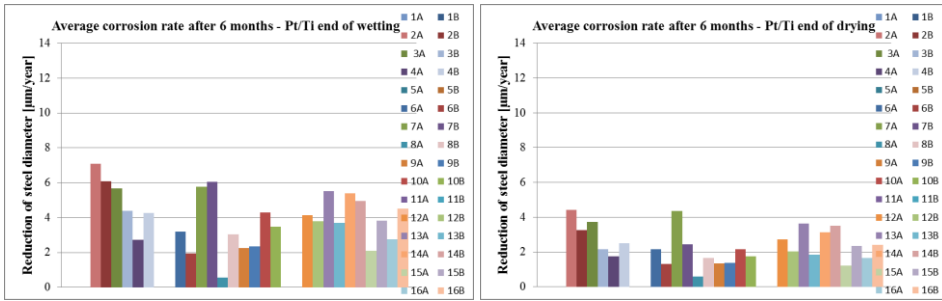
Figure 5-13: Average corrosion rate with internal reference electrode Pt/Ti at the end of wet and dry phases after six months of exposure
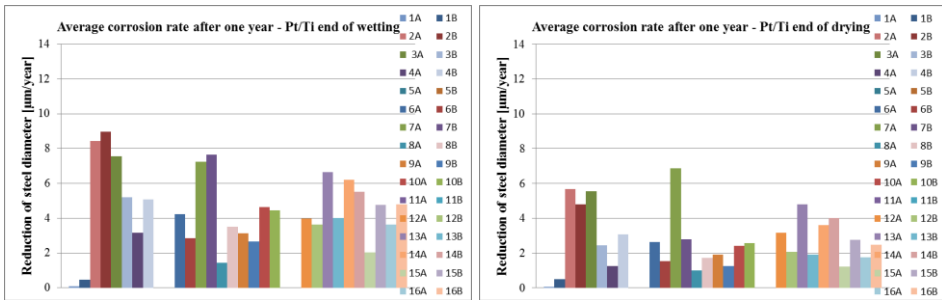
Figure 5-14: Average corrosion rate with internal reference electrode Pt/Ti at the end of wet and dry phases after one year of exposure
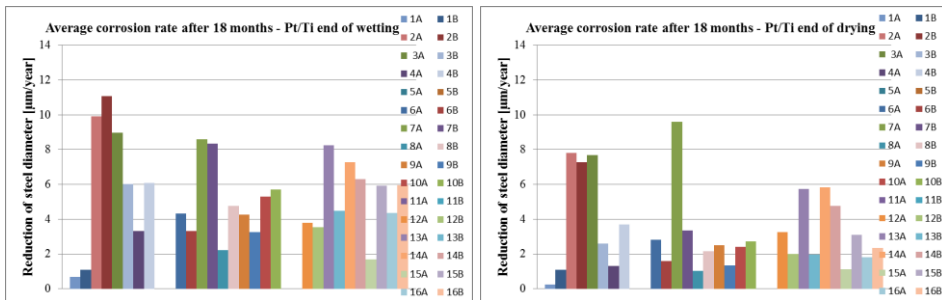
Figure 5-15: Average corrosion rate with internal reference electrode Pt/Ti at the end of wet and dry phases after 18 months of exposure
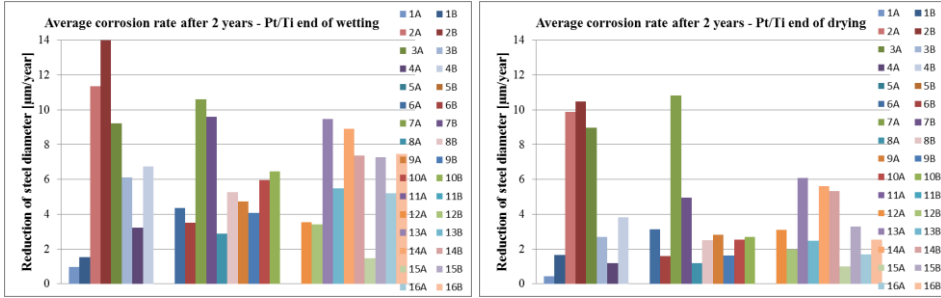
Figure 5-16: Average corrosion rate with internal reference electrode Pt/Ti at the end of wet and dry phases after 2 years of exposure

The average reduction of the steel diameter was estimated for measurements performed with an external reference electrode Ag/Cl at the end of the wet phases after any six months for all concrete beams in the experimental set-up. A comparison of the average reduction of steel diameter at the end of the wet phases with external and internal electrode, is shown in Figs. 5-17, 5-18, 5-19 and 5-20.
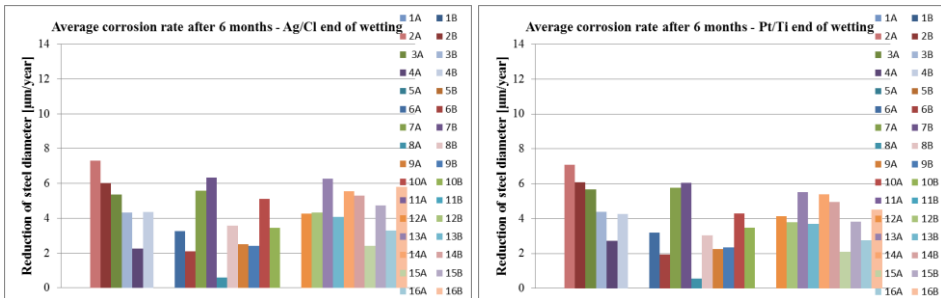
Figure 5-17: Average corrosion rate at the end of wet phases with external and internal electrode after six months of exposure
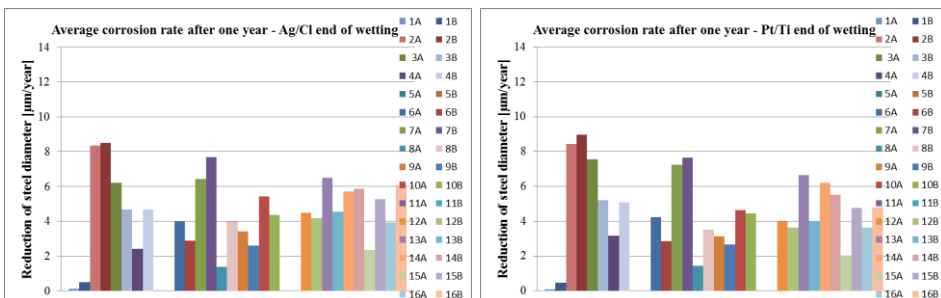
Figure 5-18: Average corrosion rate at the end of wet phases with external and internal electrode after one year of exposure
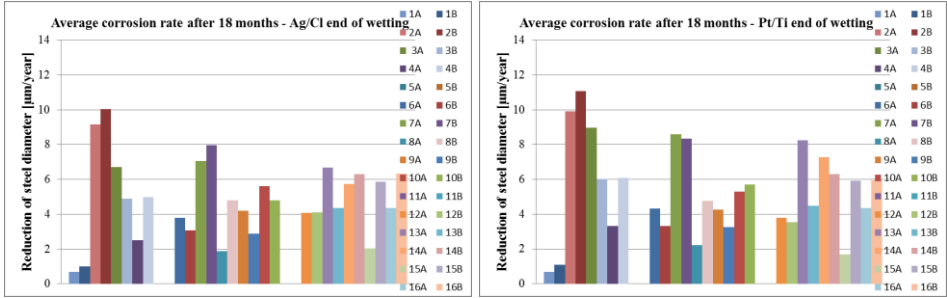
Figure 5-19: Average corrosion rate at the end of wet phases with external and internal electrode after 18 months of exposure
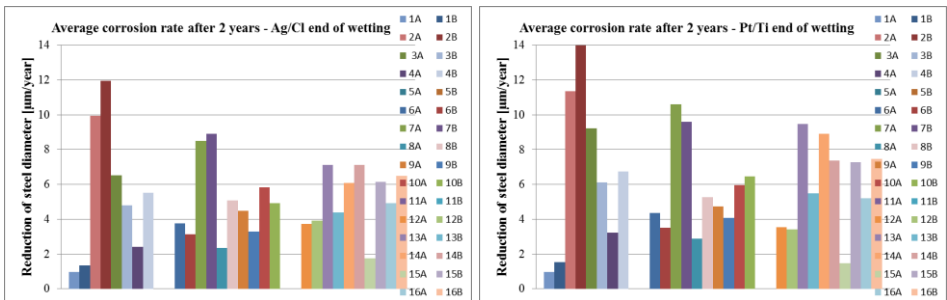
Figure 5-20: Average corrosion rate at the end of wet phases with external and internal electrode after two years of exposure

Taking into consideration that the instantaneous corrosion of steel reinforcement is stabilized after two years of exposure in case of sustained loading, it is expected that the average corrosion, for the specific period of time, will not increase much in future years for those beams. In contrast, steel corrosion of beams under variable loading and with longitudinal cracks, is still in progress. Therefore, it is difficult to estimate the average corrosion rate for long-term prediction.

The average corrosion rate, given in terms of the reduction of the steel diameter per year in Figs. 5-15, 5-16, 5-17, 5-18, 5-19 and 5-20, is the idealized situation where corrosion of the steel surface is assumed to be uniform. However, in case of cracked concrete local corrosion activity has to be distinguished from uniform corrosion and additional localized corrosion assessment should be carried out in order to get a better understanding and analysis of the results. In other words, the determination of the localized corrosion state is required for the concrete beams. Furthermore, it has to be emphasized that most of the work conducted by many authors, aforementioned in Chapter 3 in relation to steel corrosion of cracked

concrete, considered corrosion development as uniform corrosion which can lead to a misinterpretation of the results.

5.3.   Localized corrosion assessment

As already explained in Section 5.1 a HCP record can only qualitatively provide an indication of corrosion activity in concrete beams. Besides average (mixed) HCP values, recorded during wetting phases with external Ag/AgCl and internal Pt/Ti reference electrodes, HCP point measurements were recorded complementary. During two years of exposure, HCP point (spot) measurements were recorded by placing an external Ag/AgCl reference electrode on a wet sponge on the concrete cover at the end of wetting and drying cycles as was shown in Chapter 4 (Fig. 4-1a). The procedure of HCP point (local) measurements and the results for all cracked concrete beams during two years of exposure are given in Appendix A.

Altered electrochemical behavior, within the rebar itself, was recorded in most of the beams over a prolonged time interval of two years. While average HCP measurements indicate the instant that the passive film is broken somewhere along the steel rebar in a cracked beam, the crack position where it has locally occurred, is not known yet. For that purpose, point (local) HCP measurements can be relevant in order to give the indication where local corrosion occurs. Furthermore, it is expected that at the beginning of exposure, when depassivation of rebars occurred, steel corrosion occurred locally at the position of only one crack in the concrete beam, as seen from measurements, where a localized corrosion pit will be formed over time of exposure. At the instant of a localized disappearance of the passive film, the rest of the steel rebar is still passivated and cathodically protected. However, the passive layer was broken during the time of exposure in the region of many cracks, or sometimes even in the uncracked part of the beam between the cracks where, besides localized steel corrosion, uniform corrosion can take place. "Critical points" where the maximum localized steel corrosion occurs in time in each concrete beam, can be foreseen by using HCP point measurements. In most of the beams, the highest absolute HCP point value illustrates the highest probability of the highest localized corrosion activity which is expected to occur in that crack position. Furthermore, the crack at that position is, in most cases, the maximum crack width observed in the concrete beam, but this is not always the case as can be seen in the graphs given in Appendix A.

According to the HCP point measurements, crack positions below which the rebar suffers from substantial localized corrosion in each concrete beam can be clearly recognized. For instance, it can be seen that probably localized corrosion will occur in cracked concrete beams at the crack positions as is shown in Table 5.1. However, it does not necessarily mean that localized steel corrosion occurs below the mentioned crack positions only, because further corrosion activity at other parts of the steel rebar is also possible. On the other hand, if for instance all HCP values within one beam exceed a value of -250 mV vs Ag/AgCl (which can be converted to ~ -270 mV vs SCE based on ASTM C876-91, 1999), it does not mean necessarily that steel corrosion occurs along the whole steel rebar.

Table 5-1: Crack positions in concrete beams with high probability of localized steel corrosion

Beam	Concrete *cover* (mm)	Crack position
2A	C=20	1, 4, 7, 9
2B	C=20	2, 5, 6, 8
3A	C=20	1, 3, 7, 9
3B	C=20	3, 4
4A	C=20	3
4B	C=20	3
6A	C=30	3
6B	C=30	3
7A	C=30	3, 7
7B	C=30	3, 5, 7
8A	C=30	2
8B	C=30	3
9A	C=30	1, 5
9B	C=30	2, 4
10A	C=30	2, 3, 4
10B	C=30	2, 4
12A	C=40	1
12B	C=40	1, 3
13A	C=40	1, 3, 4, 5
13B	C=40	2, 3, 5
14A	C=40	2, 4, 5
14B	C=40	2, 6
15A	C=40	4
15B	C=40	2, 3, 5
16A	C=40	2, 5
16B	C=40	1, 2

It has to be emphasized that peak values among measurements given in Appendix A for each beam are more relevant than absolute values in order to recognize possible points (cracks) where localized steel corrosion could occur. In other words the gradient between active and passive area is more important than the values themselves.

Information on the localized corrosion rate is not available via HCP point measurements; only an indication of localized steel corrosion can be obtained. For estimation of the localized corrosion rate is required to use a relatively small counter electrode, in comparison with the embedded one (titanium mesh), in order to estimate local corrosion rates above cracks in each concrete beam. Based on that, a "measuring head" was employed at the end of each experiment, before the concrete beams were dismantled, as can be seen in Fig. 5-21a. A "measuring head" consists of an Ag/AgCl reference electrode, which is embedded in the middle of the head, and a counter zinc electrode with a diameter of 60 mm as is shown in Fig. 5-21b. The purpose of using zinc as an external counter electrode with a relatively small diameter, was to limit, as much as possible, the polarized surface area of the steel reinforcement. The LPR method is employed with the reinforcing bar as the working electrode, Ag/AgCl the reference external electrode and zinc the external counter electrode. The reinforcing bar and the "measuring head" were connected to the potentiostat and the same procedure of polarization is applied as is already explained for the polarization of the whole rebar with embedded counter electrode (titanium mesh) in Chapter 4.
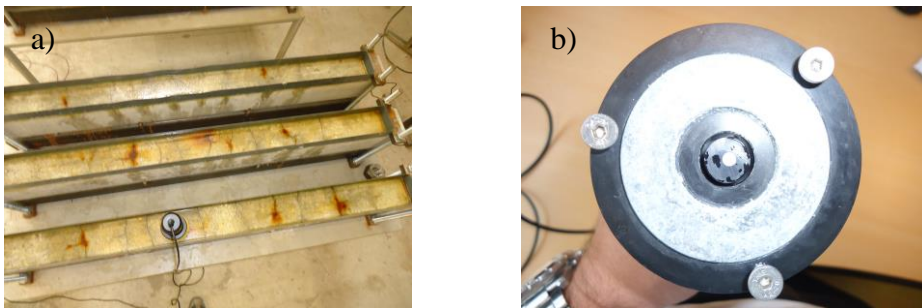
Figure 5-21: Localized corrosion measurements

After two years of exposure localized corrosion measurements were carried out on all cracked beam specimens where the "measuring head" was placed above each crack in a concrete beam. Results for all cracked beams are given in the following and the position of the crack where the maximum localized corrosion activity is recorded for every beam can be denoted as a "critical point".

After two years of exposure the reinforced concrete beams were taken out of the set-up. Furthermore, beams were dismantled in order to visualize chloride penetration and chloride-induced corrosion inside the beam in a way which is explained and shown in Appendix B. Based on that, the picture of steel corrosion for the crack position with the maximum localized corrosion damage (critical point) for each beam is shown as well in the sequel.

Beam 2A

Crack position $N^o 9$
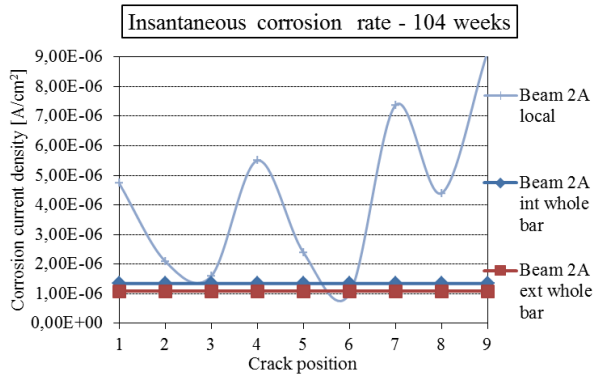
Beam 2B

Crack position $N^o 6$
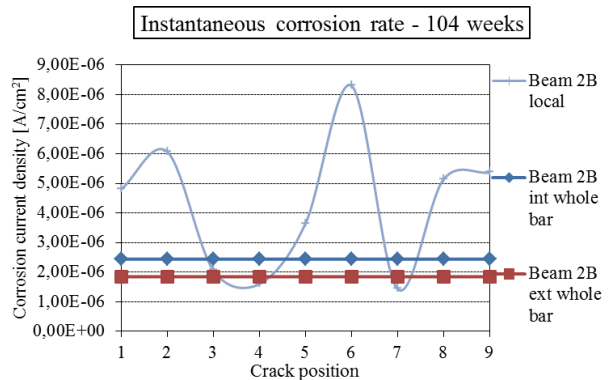
Beam 3A

Crack position N°4
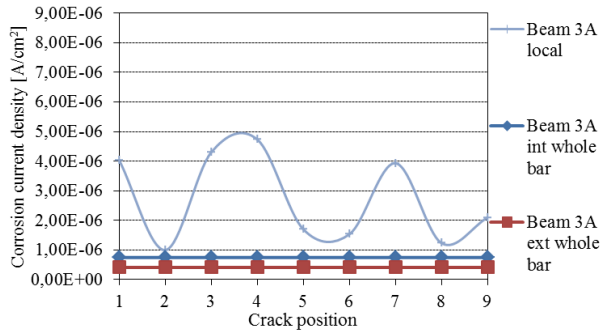
Beam 3B
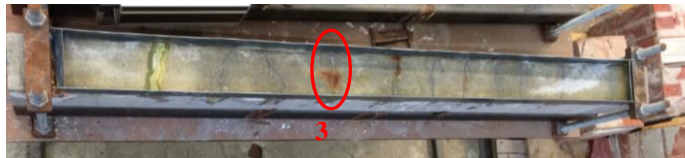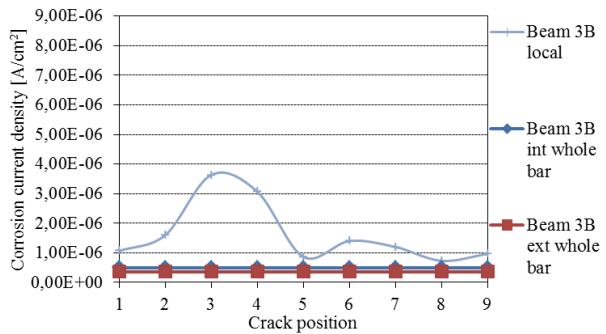
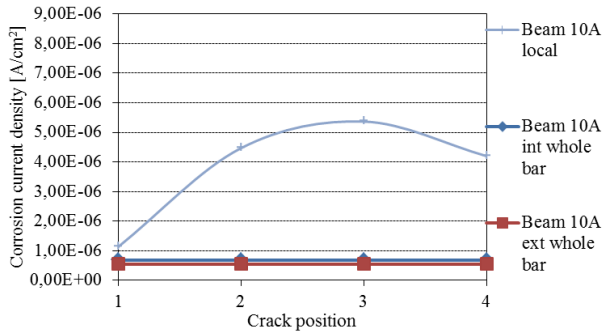**Crack position N°3**

Beam 4A

Crack position $N^o 3$

Instantaneous corrosion rate - 104 weeks
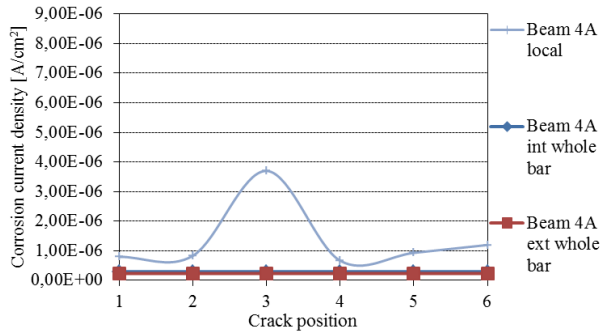
Beam 4B
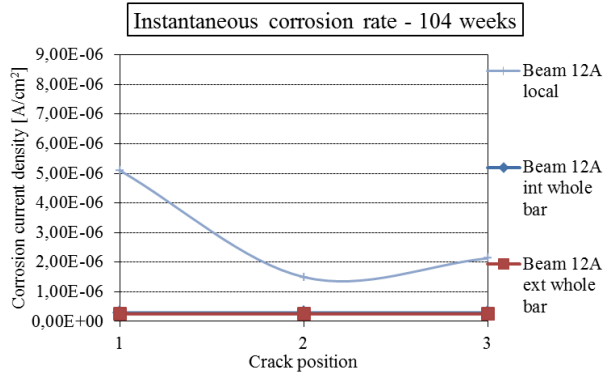

Crack position $N^o 3$

Instantaneous corrosion rate - 104 weeks
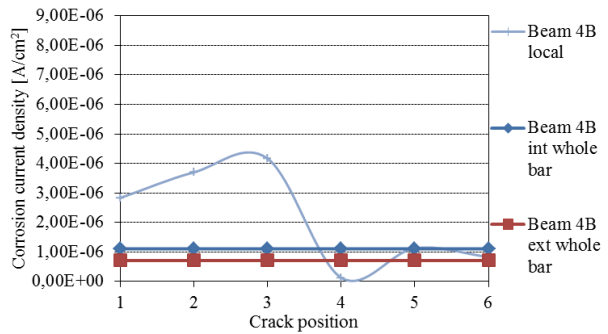
Beam 6A

Crack position N°3
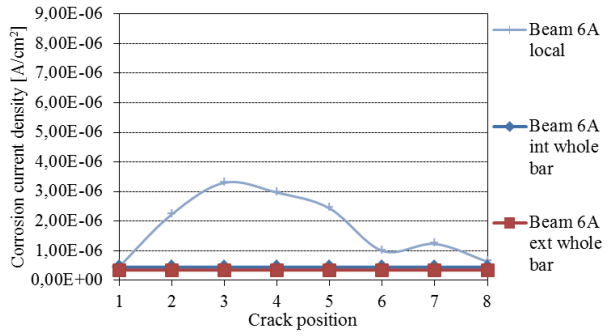
Beam 6B
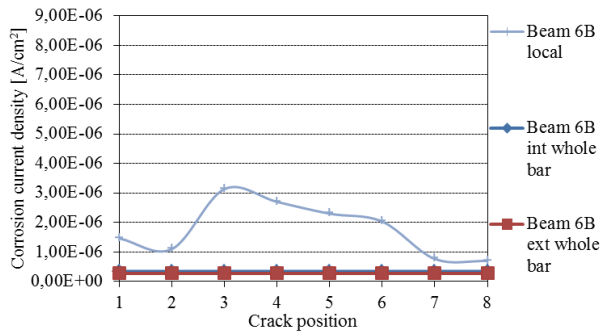
Crack position N°3

Beam 7A

Crack position N⁰ 3

Instantaneous corrosion rate - 104 weeks
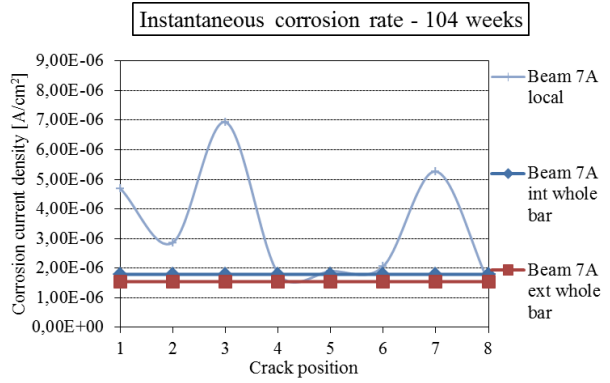
Beam 7B

Crack position N⁰ 3


Instantaneous corrosion rate - 104 weeks
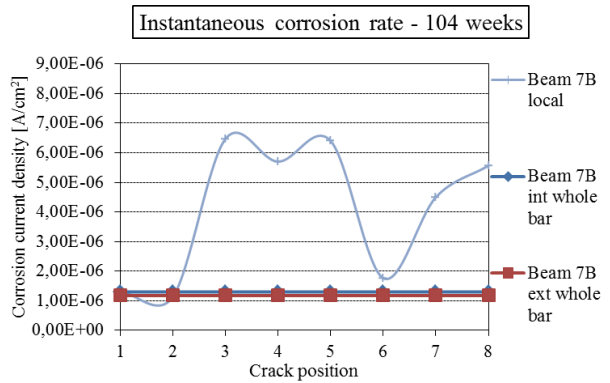
Beam 8A

Crack position N°2
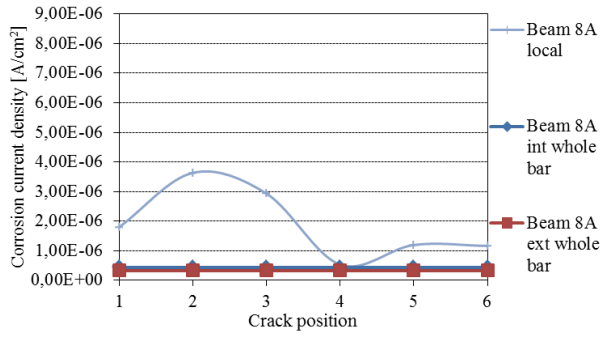
Beam 8B

Crack position N°3
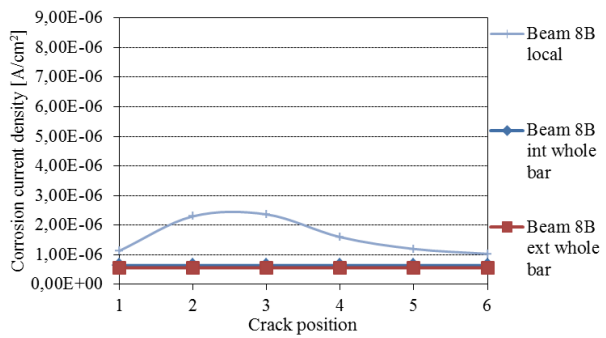
Beam 9A

Crack position $N^o 5$

Instantaneous corrosion rate - 104 weeks
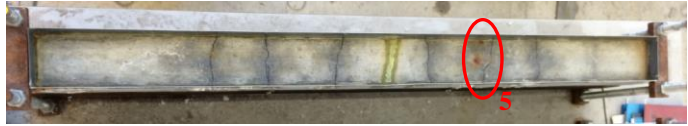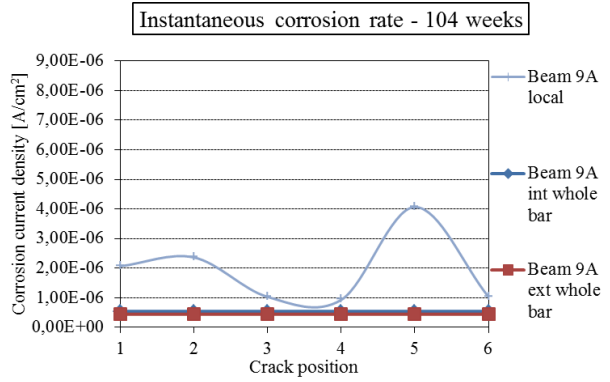
Beam 9B

Crack position $N^o 4$
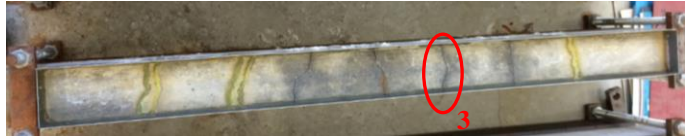
Instantaneous corrosion rate - 104 weeks

Beam 10A

Crack position N° 3

Beam 10B

Crack position N° 2
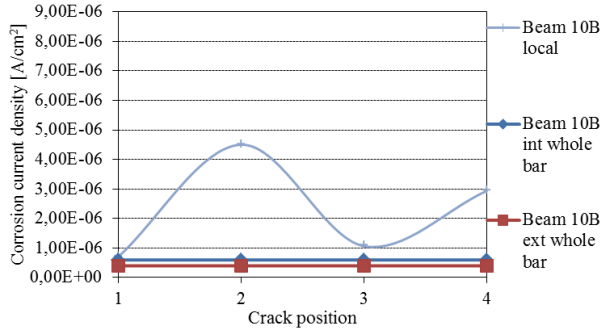
Beam 12A

Crack position Nº 1

Instantaneous corrosion rate - 104 weeks

Beam 12B

Crack position Nº 1

Instantaneous corrosion rate - 104 weeks

Beam 13A

Crack position N° 3

Instantaneous corrosion rate - 104 weeks

Beam 13B

Crack position N° 5

Instantaneous corrosion rate - 104 weeks
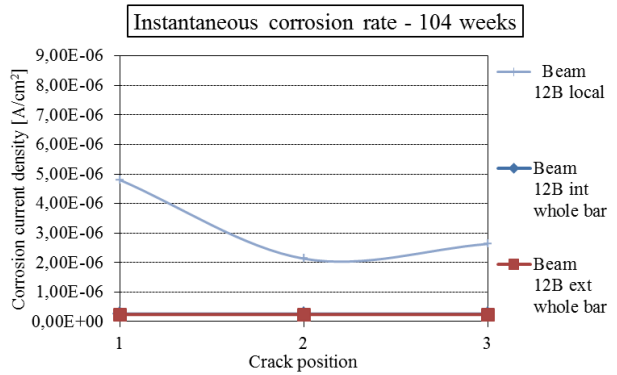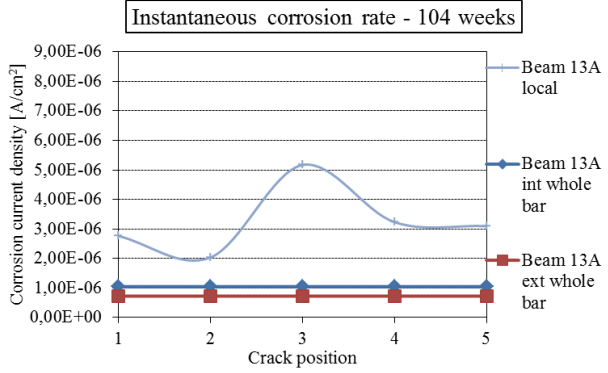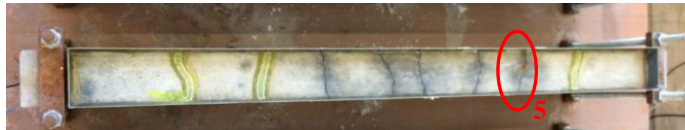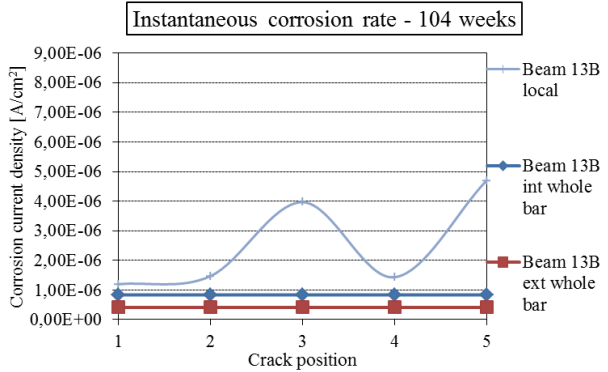
Beam 14A
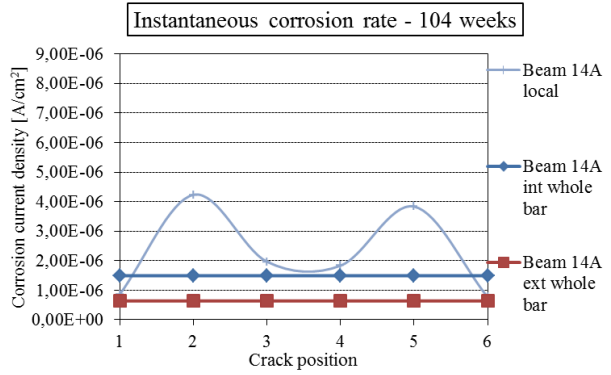
Crack position N°2

Beam 14B

Crack position N°2
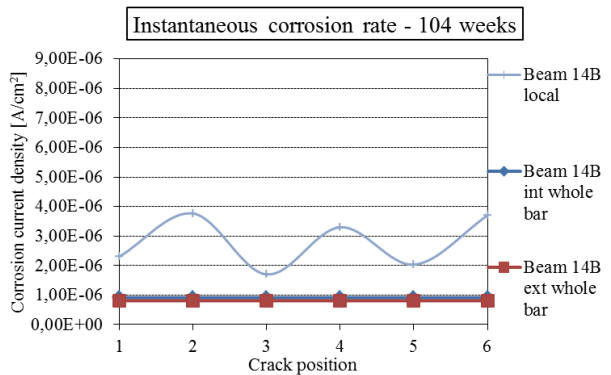
Beam 15A

Crack position N°4

Instantaneous corrosion rate - 104 weeks
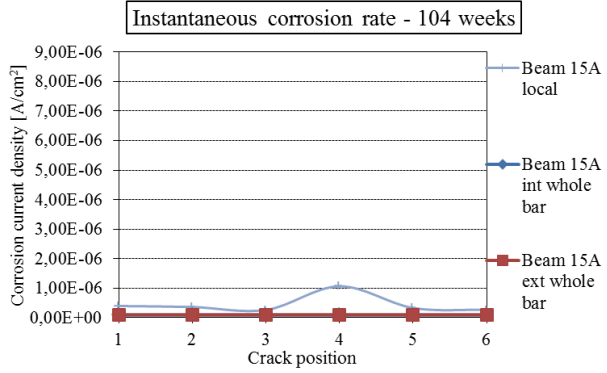
Beam 15B

Crack position N°3
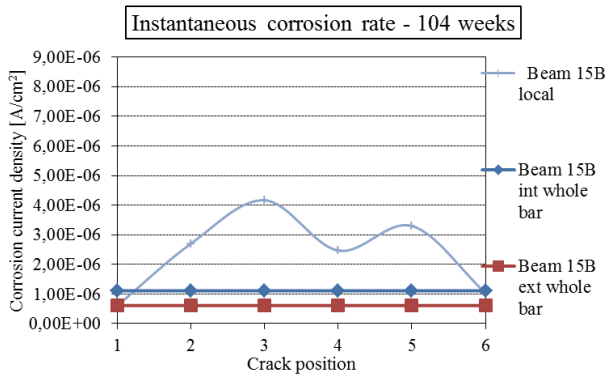
Instantaneous corrosion rate - 104 weeks

Beam 16A

Crack position Nº 2

Instantaneous corrosion rate - 104 weeks

Beam 16B

Crack position Nº 1

Instantaneous corrosion rate - 104 weeks
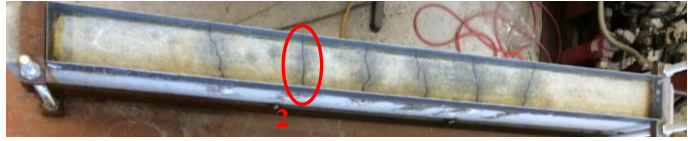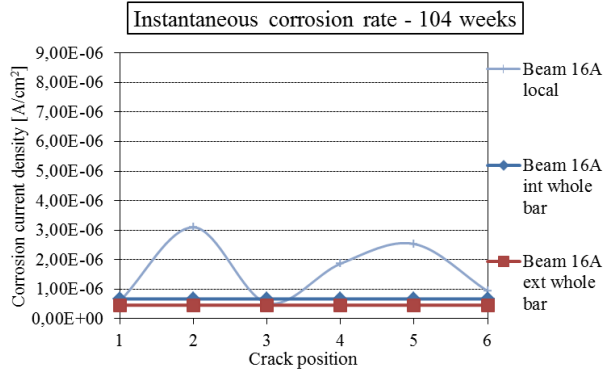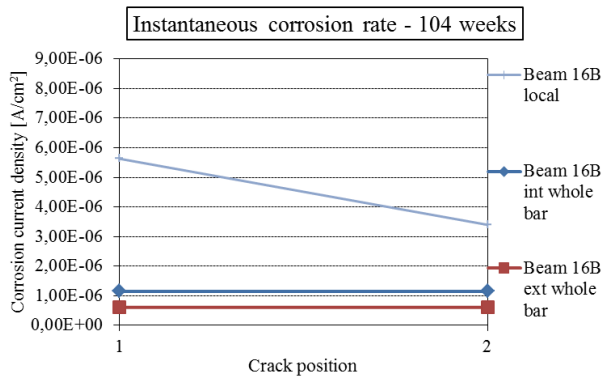
According to the experimental results for the localized corrosion assessment, no direct relationship can be deduced between crack width at the concrete surface and recorded value of localized corrosion rate along steel rebar of concrete beams after two years of exposure. Furthermore, the derived values of localized corrosion rates are affected by many factors (i.e. concrete cover, ohmic drop, crack geometry, real polarized steel area, shape of the developed corrosion pit within the crack etc.) which obviously play a role. It can be emphasized that the trend, in terms of the gradient between measured values at points within the concrete beam, is more important than the derived values of localized corrosion activity. On top of all that, the electrochemical mechanism of steel corrosion must not be neglected within measurements which are recorded for concrete beams. In relation to that, in many cases recorded localized corrosion currents are completely different for the same crack width at a different position in the concrete beam. Furthermore, below a larger crack width at the concrete surface sometimes even lower corrosion activity was detected in comparison with corrosion activity below a lower crack width. However, in most of the beams the highest localized corrosion current density, recorded by LPR at the crack positions which transversally intersect the steel rebar in the concrete, is observed at the position of the maximum surface crack width in the beam, but this is not necessarily the case. The constant moment region where the maximum bending moment applies, the region between supports, is the most endangered area in terms of concrete-steel interface in cracked beams as was expected. Furthermore, in all cracked beams in the experiments the critical point is in the constant moment region where the highest steel stress and the damage at the level of the rebar is expected to occur, with only one exception (Beam 2A).

In the graphs, besides the values of the localized corrosion current density, the average value of the steel corrosion in each concrete beam is shown as well, measured by both reference electrodes, internal and external. Taking into consideration that the localized rebar corrosion values are measured by using the external Ag/AgCl reference electrode, it can be relevant to relate the maximum localized corrosion where an Ag/AgCl electrode is used as well, with the measurements of the average corrosion value assumed to be uniform along the whole rebar. The ratio between the maximum localized rebar corrosion and the average value for the whole rebar after two years of exposure varied between 3 and 15 but mostly it was between 5 and 10. It depends on many factors, but the governing factor in the experiments is the number of pits and also how corrosion is really developed within a rebar. In other words, for the hypothetically same

maximum localized corrosion rate in some beams, the ratio is higher in the case of a smaller number of cracks which leads to a smaller number of pits and, therefore, a higher ratio between the derived values of average uniform and maximum localized corrosion. For instance, beams 12A and 12B are a clear example of that high ratio.

It can be concluded that values recorded by using HCP point (local) measurements provided a very good indication of steel corrosion. In addition, in most of the beams, the highest HCP point absolute value was confirmed to be the position of the highest localized corrosion current as well by LPR recording localized corrosion activity along the steel rebar in the concrete beams. Furthermore, many positions of corrosion pits were clearly foreseen, firstly by local HCP measurements and additionally confirmed by localized LPR measurements, and visualized at the end of testing when the concrete beams were sawn and opened in order to verify the predictions based on the non-destructive techniques. Before the concrete beams were dismantled and sawn, corrosion products had been mostly visible at the positions of the foreseen corrosion pits at the concrete surface. The position of the crack where the maximum localized corrosion current was observed in every beam, is marked in the given pictures for all cracked concrete beams. Later, when the concrete beams were dismantled and sawn, as is shown in Appendix B, the confirmation was obtained that it was really the area which suffers from substantial rebar corrosion more than the other areas of the rebar within the same concrete beam. In other words, the critical point or hot spot is highlighted for every cracked concrete beam in the experiments. In order to quantify steel corrosion damage at that position, an analytical analysis is carried out in Chapter 6, where in Section 6.3 a localized steel stress-surface crack width relation is established for the maximum localized corrosion in concrete beams.

5.4.   Chloride penetration in cracked and uncracked concrete

It is quite common to carry out an analysis of chloride penetration and chloride profiles in concrete which is exposed to a chloride solution during experimental testing. The chloride content at some distance from the exposed concrete surface can be predicted from the required information about the chloride diffusion coefficient using Fick's second law. The first step is the collection of powder concrete samples and after that the chloride content can be determined by a chemical analysis. The powder samples can be obtained by drilling perpendicular to the exposed surface, taken a few times for one depth to achieve an average

value. The other method which can be applied to take powder samples is slice drilling from a side core face. However, by using this method there is a risk to change the chloride content by cutting a core caused by cooling water. In this experiment grinding was applied where the diameter was 70 mm. The thickness of every layer was 1 mm and samples were grinded until a depth of 30 mm was reached as is shown in Fig. 5-22a.

After sampling, determination of the chloride content at different depths from the exposed concrete surface, was carried out by chemical analysis. Since free chlorides lead to corrosion of reinforcement, some techniques are available for chloride content determination (titration method, X-Ray fluorescence spectrometry, Quantab simplified method etc.). However, the titration method which was given by Nordtest (1996) is the most common method to determine the chloride content in the concrete. This is a simple method which requires the use of hot nitric acid to dissolve powder samples and extract all the chlorides. After filtering and cooling silver nitrate is added to the solution (Fig. 5-22b).

Figure 5-22: Chloride content determination by chemical analysis

The solution has been titrated with ammonium thiocyanate and the required data of chloride percentage by weight of concrete has been obtained. The analysis has been conducted for a few samples at different depths from the exposed surface (2.5 mm, 4.5 mm, 10 mm, 20 mm and 30 mm). In addition, chloride profiles have been determined in terms of chloride content as a function of the distance from the exposed concrete surface. Furthermore, the diffusion coefficient and surface chloride concentration have been predicted from the best fit curve after a specific period of exposure time. In order to monitor chloride profiles of uncracked concrete in function of time, the analysis has been conducted on concrete cubes after six months, after one year and two years of exposure. Chloride profiles for uncracked concrete cubes are shown in Fig. 5-23.
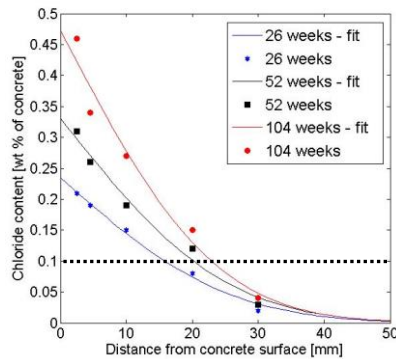
Figure 5-23: Chloride profiles for uncracked concrete

They can be transferred into chloride percentage by weight of cement as well. Based on the concrete mixture, it was estimated that approximately a factor 8 should be applied in order to transfer values from chloride percentage by weight of concrete into chloride percentage by weight of cement. At the instant that the steel reinforcement in the uncracked beams was depassivated, the chloride threshold level was around 0.1 chloride % by weight of concrete or 0.8 chloride % by weight of cement.

After two years of exposure the concrete cubes and all concrete beams were split into two parts in order to check the chloride penetration depth. A silver nitrate solution (0.1 M $AgNO_3$) was sprayed on the surfaces in both of them in order to visualize the chloride ingress. The chloride penetration in all (uncracked and cracked) concrete beams is shown in Appendix B. The chloride penetration depth in the concrete cubes and uncracked (unloaded) beams with various concrete cover are shown in Figs. 5-24 and 5-25. The average chloride penetration depth in cubes and uncracked (unloaded) reinforced concrete beams was around 30 mm after two years of exposure to aggressive environmental conditions.

It is of vital importance to highlight that chlorides in the uncracked parts of the concrete region, i.e. the region between the cracks in case of cracked beams, penetrate into the concrete much deeper than in the case of fully uncracked (unloaded) reinforced concrete beams as can be seen in Fig. 5-26. This phenomenon can be clearly observed in all uncracked sections for the constant moment region between the supports for cracked beams as is depicted in Appendix B.

 Chloride ions are not present in concrete

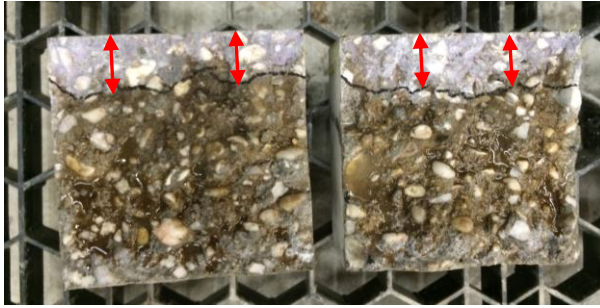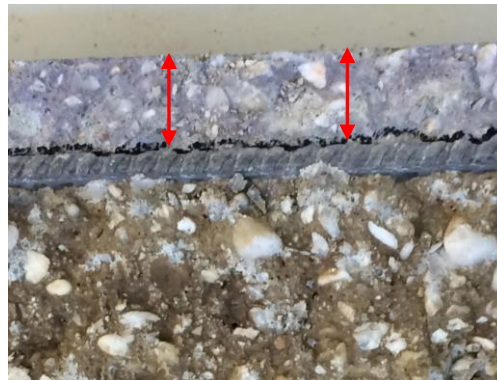 **Chloride ions are present in concrete**

Figure 5-24: Chloride penetration in concrete cube after two years of exposure
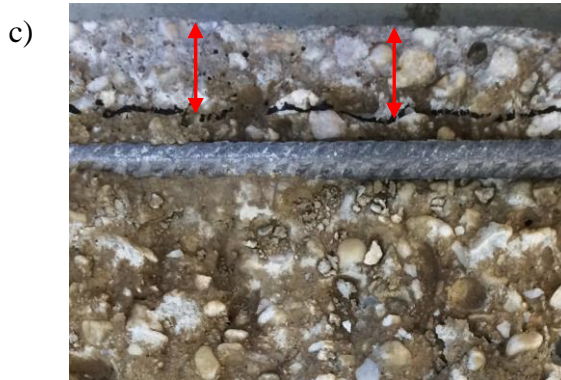
a)

b)

c)

Figure 5-25: Chloride penetration in uncracked (unloaded) concrete beam with a concrete cover of: a) 20 mm; b) 30 mm; c) 40 mm

Fig. 5-26 depicts that the chloride penetration depth in the uncracked region, for cracked concrete between the cracks, in many cases reaches almost the bottom of the beam. However, this is not always the case. The range of chloride penetration for that area in the constant moment region varied significantly, from 40 mm to even 140 mm which occurs for a number of reasons. First of all, chlorides can penetrate from two directions where one route is diffusion through uncracked concrete, between the cracks, and the other is orthogonally from the crack faces along the steel rebar. The microstructural alterations in terms of internal cracks and micromechanical changes must not be neglected as well. Furthermore, considerable micro-cracking occurs in the uncracked part, between the cracks, facilitating ingress of chlorides. Secondly, the distance between the cracks plays a role as well for this phenomenon. If the main cracks are closer to each other, there is a higher probability that close-by positioned principal cracks will extend to the next main crack and cause significant damage at the steel-concrete interface between them. However, the steel stress is the parameter which mostly affects the characteristics of crack and damage at the steel-concrete interface in general. A higher steel stress, for example, leads to wider and deeper cracks. Furthermore, a higher steel stress leads to a higher damage not only in the region of the crack itself, but at the steel-concrete interface in the region between the cracks as well. These microstructural and mechanical changes will contribute to a significant extent to chloride, water and oxygen penetration and it will affect the electrochemical phenomena at the steel surface. Therefore, the existence of internal microcracks cannot be ignored in relation to corrosion activity.
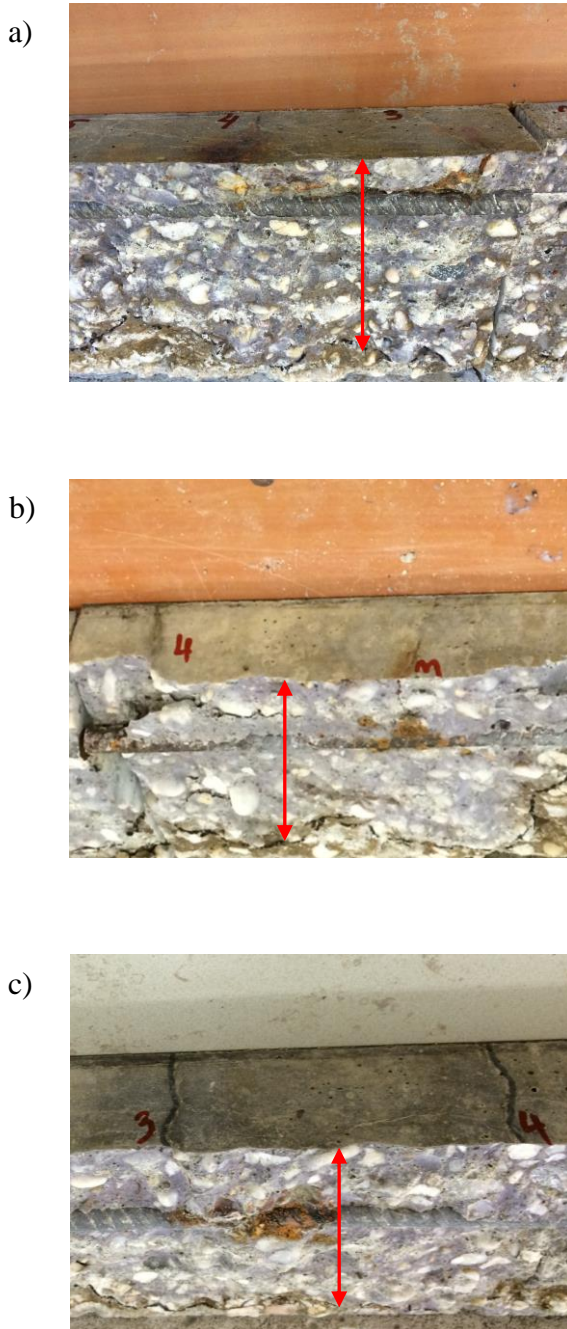
a)

b)

c)

Figure 5-26: Chloride penetration in cracked concrete, between the cracks for the constant moment region, with a concrete cover of: a) 20 mm; b) 30 mm; c) 40 mm

It can be concluded that the standard procedure for the determination of chloride profiles is not the appropriate measure for the prediction of the diffusion coefficient in case of uncracked concrete, between the cracks, for the maximum constant moment region. On top of that all, the transport mechanism of chlorides is completely different in uncracked unloaded concrete compared with uncracked concrete, between the cracks, in the loaded state. Furthermore, the steel stress is most probably a parameter which affects the surface crack width, crack depth and damage at the steel-concrete interface not just in the cracked region, but also in the uncracked region, between the main cracks, at the same time. Based on that, the experimental crack pattern and prediction of relation between crack width and steel stress is analyzed in Chapter 6.

5.5.   Conclusions

The following important conclusions can be drawn based on the experimental results:

- HCP measurements lead to a good indication of the passive or active state of the steel reinforcement in general, for both reference electrodes, internal and external. Variations between measurements are obviously present due to the role of ohmic drop. An accurate relation between measurements of the damage at the steel-concrete interface, micromechanics and microstructure within the concrete cover is not possible and only the probability of steel corrosion can be assessed. The LPR technique was applied in order to quantitatively assess the corrosion state of the steel reinforcement in the concrete beams.

- In the presence of longitudinal cracks the corrosion process progresses much faster than in the case of pure bending cracks. Therefore, longitudinal cracks can be much more dangerous than pure bending cracks for the service life of concrete structures. Load variation also leads to an increase of the corrosion rate even after two years of exposure. Furthermore, the maximum service load level governs the development of the corrosion, rather than the frequent service load level or the quasi-permanent service load level.

- For the same mean crack width a larger concrete cover leads to a smaller number of cracks and as such lower corrosion activity. However, crack

frequency is a secondary parameter while the dominating parameter is the damage at the steel-concrete interface which is determined implicitly by the employed level of steel stress. A higher steel stress can lead to a higher crack width and more secondary cracks at the level of the reinforcing bar, which is much more important than the surface crack width.

- In contrast to beams with longitudinal cracks and beams under alternating load conditions, in all beams under sustained loading conditions, stabilization of steel corrosion was observed after two years of exposure. However, this occurred due to the reduction of load and steel stress at constant deflection due to the effects of creep and shrinkage in time, which will be analysed in Chapter 6.

- No direct relationship was found between crack width at the concrete surface and recorded value of localized corrosion activity along the steel rebar embedded in the concrete beams after two years of exposure. However, the "critical point" which denotes the crack position of maximum localized steel corrosion in a concrete beam, is highlighted. In addition, the critical point is situated in the region of the maximum bending moment where the maximum concrete damage at the level of the bar occurs.

- The difference between chloride penetration in uncracked unloaded concrete and cracked concrete, between the cracks, in a loaded state has to be highlighted and emphasized. Furthermore, the effect of internal secondary cracks and microcracks cannot be ignored in relation to corrosion activity. According to the experimental observations in relation to chloride penetration in cracked concrete, it can be concluded that actual theoretical models for the probabilistic determination of service life for concrete structures should be revised. Basing service life prediction on the diffusion of chlorides without regarding the substantial effect of cracks leads to misinterpretation.

Chapter 6

Analytical verification of tests

6.1. Experimental crack pattern according to tests and prediction of relation between crack width and steel stress

The diameter of the reinforcing bar and the dimensions of the concrete cross section were as follows:

$\phi = 12 \ mm$

$b = 100 \ mm$

$h = 150 \ mm$

The tensile splitting and compressive cube strength were found to be:

$f_{ct,spm} = 2.8 \ MPa$

$f_{ccm,28} = 31 \ MPa$

The modulus of elasticity for this concrete (C20/25) is assumed to be:

$E_{cm} = 30000 \ MPa$

Concrete tensile and flexural tensile strength are:

$$f_{ct} = 1.0 \cdot f_{ct,spm} = 2.8 \ MPa$$

$$f_{ct,fl} = \frac{f_{ctm}}{\alpha_{fl}} = 4.18 \ MPa$$

$$\alpha_{fl} = \frac{0.06 \cdot h^{0.7}}{1 + 0.06 \cdot h^{0.7}} = 0.67$$

One reinforcing bar was tested to check the limit tensile stress in the region of linear-elastic behaviour, the yielding strength and the ultimate tensile strength:

$$f_{max,lin} = 529 MPa$$

$$f_{ys} = 561 MPa$$
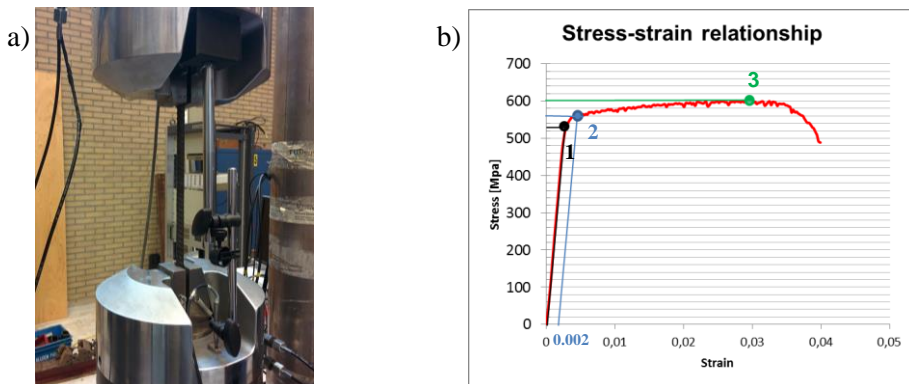
$$f_{uts} = 601 MPa$$

Figure 6-1: Determination of б-ε relation of the reinforcing bar

The strain at reaching the yield strength f_{ys} was $\varepsilon_s = 0.0038$ and the strain just before failure was 0.03.

The modulus of elasticity was determined in the region of linear-elastic behaviour as stress-strain ratio:

$$E_s = 200000 \ MPa$$

The steel cross-sectional area, the moment of inertia and the resisting moment are as follows:

$$A_s = \frac{\phi^2 \pi}{4} = 113.04\,mm^2$$

$$I = \frac{b \cdot h^3}{12} = 28125000\,mm^4$$

$$W = \frac{I}{0.5 \cdot h} = 375000\,mm^3$$

The ratio between modulus of elasticity of steel and concrete is:

$$\alpha_e = \frac{E_s}{E_{cm}} = 6.67$$

Taking into consideration the small size of the reinforced beam, the calculation based on the "tensile tie model" is not appropriate. Therefore, an alternative procedure is followed:
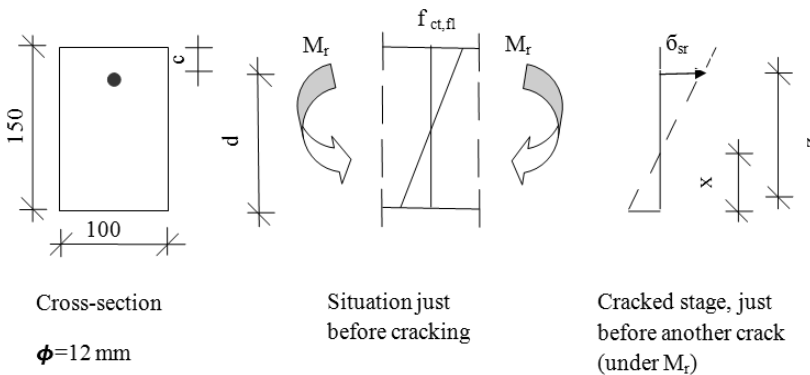

Cross-section

ϕ=12 mm

Situation just before cracking

Cracked stage, just before another crack (under M_r)

Figure 6-2: Cracking formation stage

Just after cracking the elastic state applies:

$$\frac{\varepsilon_c}{\varepsilon_s} = \frac{x}{d - x}$$

$$N_c = N_s$$

$$0.5 \cdot b \cdot x \cdot \varepsilon_c \cdot E_{cm} = A_s \cdot E_s \cdot \varepsilon_s$$

$$\frac{x}{d} = -\alpha_e \cdot \rho + \sqrt{(\alpha_e \cdot \rho)^2 + 2 \cdot \alpha_e \cdot \rho}$$

6.1.1. *Surface crack width-steel stress relation for a cover of 20 mm*

$d = 124mm$

The reinforcement ratio is:

$$\rho = \frac{A_s}{b \cdot d} = 0.009116$$

The height of the compressive zone:

$x = 36.35mm$

Internal lever arm:

$$z = d - \frac{1}{3}x = 111.88\,mm$$

The cracking moment follows from:

$$M_r = f_{ct,fl} \cdot W = 1.57 \cdot 10^6 \, Nmm$$

Under the action of this cracking moment the steel stress in the crack is:

$$\sigma_{sr} = \frac{M_r}{A_s \cdot z} = 123.91 MPa$$

The stress σ_{sr} in the crack becomes smaller with increasing distance from the crack. Just at the onset of the formation of the next bending crack the strain in the concrete can be calculated as follows:

$$\varepsilon_r = \frac{f_{ct,fl}}{E_c} = 0.1393 \cdot 10^{-3}$$

At the level of reinforcement the concrete strain can be calculated as:

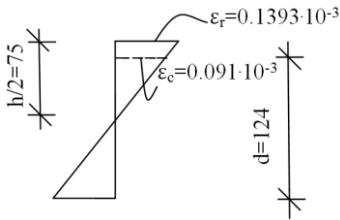$$\varepsilon_c = \frac{\dfrac{h}{2} - d}{\dfrac{h}{2}} \cdot \varepsilon_r = 0.091 \cdot 10^{-3}$$

Figure 6-3: Concrete strain at the surfuce and level of the reinforcement for a cover of 20 mm

Consequently, the stress in the steel at the end of the transmission length l_t is:

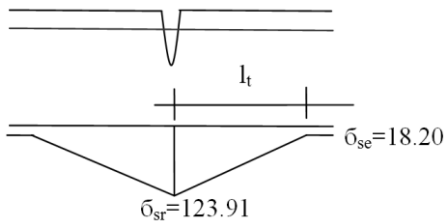$$\sigma_{se} = E_s \cdot \varepsilon_c = 18.20 MPa$$

Figure 6-4: Steel stress in the crack and at the end of the transmission length for a cover of 20mm

The force introduced into the concrete over the distance l_t is:

$$N_t = (\sigma_{sr} - \sigma_e) \cdot A_s = 11.95 \cdot 10^3 N$$

If the bond strength is assumed to be constant:

$$\tau_{bm} = 1.8 \cdot f_{ctm} = 5.04 \, N\!\!\diagup\!\! mm^2$$

Due to the contribution of the concrete cover, the transmission length can be calculated as follows:

$$l_t = 0.75c + \frac{N}{\phi \cdot \tau_{bm} \cdot \pi}$$

where the crack spacing can vary between l_t and $2l_t$:

$$s_{min} = 1.0 \cdot l_t = 77.92mm$$

$$s_{mean} = 1.5 \cdot l_t = 116.88mm$$

$$s_{max} = 2.0 \cdot l_t = 155.84mm$$

For the determination of the strain over s_{mean} the following expression is used:

$$\varepsilon_{sm} = \frac{\sigma_s}{E_s}\left[1 - \beta_1 \cdot \beta_2 \cdot \left(\frac{\sigma_{sr}}{\sigma_s}\right)^2\right]$$

$\beta_1 = 1.0$ - *bond factor for ribbed steel*

$\beta_2 = 0.5$ - *for long term loading*

The mean crack width can be calculated as follows:

$$w_{mean} = s_{mean} \cdot \varepsilon_{sm} = 114.38 \cdot \frac{\sigma_s}{200000} \cdot \left[1 - 0.5 \cdot \left(\frac{123.91}{\sigma_s}\right)^2\right]$$

where σ_s is the steel stress in the crack under the external load.

Therefore, the relation between mean surface crack width and steel stress is as follows:

$\sigma_s = 200\ MPa \implies w_{mean} = 0.09mm$

$\sigma_s = 300\ MPa \implies w_{mean} = 0.16mm$

$\sigma_s = 400\ MPa \implies w_{mean} = 0.22mm$

$\sigma_s = 500\ MPa \implies w_{mean} = 0.28mm$

However, surface crack width and crack space can vary in function of the specific steel stress. Therefore, the relation between surface crack width and the steel stress in the experiments depends on the crack spacing as follows:

$$\sigma_s = 200 \ MPa \implies 77.92mm \leq s \leq 155.84mm \implies 0.06mm \leq w \leq 0.12mm$$

$$\sigma_s = 300 \ MPa \implies 77.92mm \leq s \leq 155.84mm \implies 0.11mm \leq w \leq 0.22mm$$

$$\sigma_s = 400 \ MPa \implies 77.92mm \leq s \leq 155.84mm \implies 0.15mm \leq w \leq 0.30mm$$

$$\sigma_s = 500 \ MPa \implies 77.92mm \leq s \leq 155.84mm \implies 0.19mm \leq w \leq 0.38mm$$

The relation between surface crack width and steel stress for a concrete cover of 20 mm in the stabilized cracking stage is given in Fig. 6-5 for minimum, maximum and mean theoretical value of crack spacing.
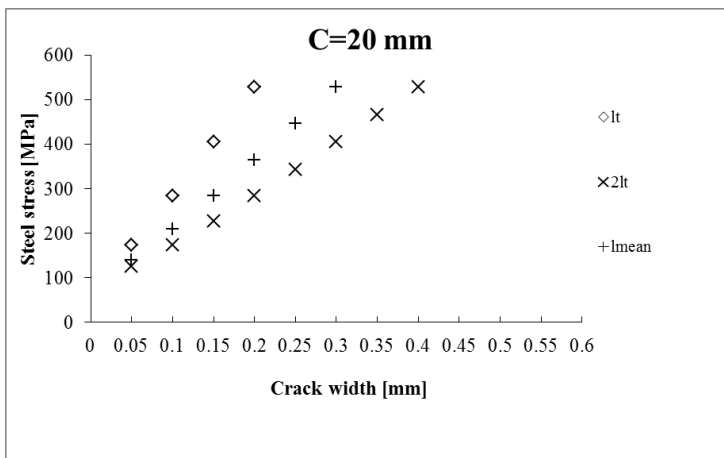

Figure 6-5: The relationship between surface crack width and steel stress for a cover of 20 mm

6.1.2. Surface crack width-steel stress relation for a cover of 30 mm

$$d = 114mm$$

The reinforcement ratio is:

$$\rho = \frac{A_s}{b \cdot d} = 0.009116$$

The height of the compressive zone:

$$x = 34.59 mm$$

Internal lever arm:

$$z = d - \frac{1}{3}x = 102.47\, mm$$

The cracking moment follows from:

$$M_r = f_{ct,fl} \cdot W = 1.57 \cdot 10^6\, Nmm$$

Under the action of the cracking moment the steel stress in the crack is:

$$\sigma_{sr} = \frac{M_r}{A_s \cdot z} = 135.30 MPa$$

The stress σ_{sr} in the crack becomes smaller with increasing distance from the crack. Just at the onset of the formation of the next bending crack the strain in the concrete can be calculated as follows:

$$\varepsilon_r = \frac{f_{ct,fl}}{E_c} = 0.1393 \cdot 10^{-3}$$

At the level of the reinforcement the concrete strain can be calculated as:

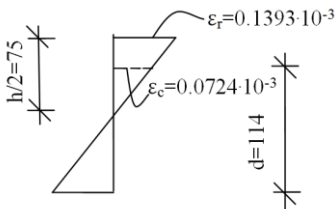$$\varepsilon_c = \frac{\frac{h}{2} - d}{\frac{h}{2}} \cdot \varepsilon_r = 0.0724 \cdot 10^{-3}$$

Figure 6-6: Concrete strain at the surface and level of the reinforcement for a cover of 30 mm

Consequently, the stress in the steel at the end of the transmission length l_t is:

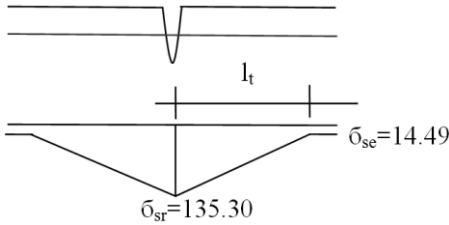$$\sigma_{se} = E_s \cdot \varepsilon_c = 14.49 MPa$$

Figure 6-7: Steel stress in the crack and at the end of the transmission length for a cover of 30mm

The force introduced into the concrete over the distance l_t is:

$$N_t = (\sigma_{sr} - \sigma_e) \cdot A_s = 13.66 \cdot 10^3 N$$

If the bond strength is assumed to be constant:

$$\tau_{bm} = 1.8 \cdot f_{ctm} = 5.04 \, N/mm^2$$

Due to the contribution of the concrete cover, the transmission length can be calculated as follows:

$$l_t = 0.75 \cdot c + \frac{N}{\phi \cdot \tau_{bm} \cdot \pi}$$

Where the crack spacing can vary between l_t and $2l_t$:

$$s_{min} = 1.0 \cdot l_t = 94.41 mm$$

$$s_{mean} = 1.5 \cdot l_t = 141.62 mm$$

$$s_{max} = 2.0 \cdot l_t = 188.82 mm$$

For the determination of the strain over s_{mean} the following expression is used:

$$\varepsilon_{sm} = \frac{\sigma_s}{E_s}\left[1 - \beta_1 \cdot \beta_2 \cdot \left(\frac{\sigma_{sr}}{\sigma_s}\right)^2\right]$$

$\beta_1 = 1.0$ - *bond factor for ribbed steel*

$\beta_2 = 0.5$ - *for long term loading*

The mean crack width can be calculated as follows:

$$w_{mean} = s_{mean} \cdot \varepsilon_{sm} = 137.87 \cdot \frac{\sigma_s}{200000} \cdot \left[1 - 0.5 \cdot \left(\frac{135.30}{\sigma_s} \right)^2 \right]$$

Where σ_s is a steel stress in crack under external load.

Therefore, the relation between mean surface crack width and steel stress is:

$\sigma_s = 200\ MPa \Rightarrow w_{mean} = 0.11mm$

$\sigma_s = 300\ MPa \Rightarrow w_{mean} = 0.19mm$

$\sigma_s = 400\ MPa \Rightarrow w_{mean} = 0.26mm$

$\sigma_s = 500\ MPa \Rightarrow w_{mean} = 0.33mm$

However, surface crack width and crack space can vary in function of the specific steel stress. Therefore, the relation between surface crack width and steel stress in the experiments depends on the crack spacing as follows:

$\sigma_s = 200\ MPa \Rightarrow 94.41mm \leq s \leq 188.82mm \Rightarrow 0.07mm \leq w \leq 0.15mm$

$\sigma_s = 300\ MPa \Rightarrow 94.41mm \leq s \leq 188.82mm \Rightarrow 0.13mm \leq w \leq 0.26mm$

$\sigma_s = 400\ MPa \Rightarrow 94.41mm \leq s \leq 188.82mm \Rightarrow 0.18mm \leq w \leq 0.36mm$

$\sigma_s = 500\ MPa \Rightarrow 94.41mm \leq s \leq 188.82mm \Rightarrow 0.23mm \leq w \leq 0.46mm$

The relation between surface crack width and steel stress for a concrete cover of 30 mm in the stabilized cracking stage is given in Fig. 6-8 for the minimum, maximum and theoretical mean value of crack spacing.
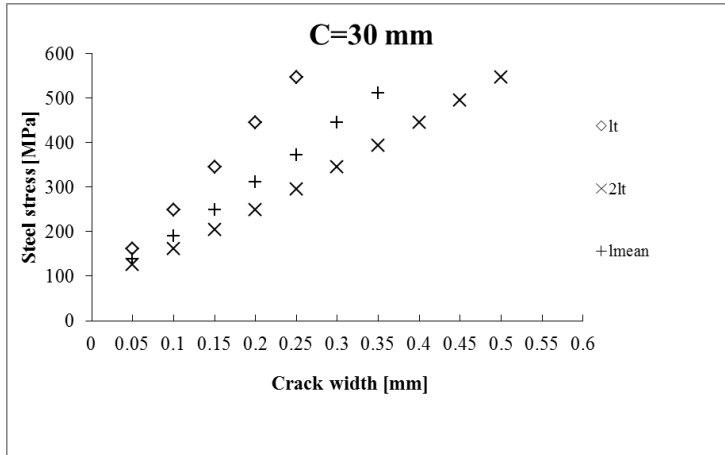
Figure 6-8: The relationship between surface crack width and steel stress for a cover of 30 mm

6.1.3. *Surface crack width-steel stress relation for a cover of 40 mm*

$d = 104mm$

The reinforcement ratio is:

$$\rho = \frac{A_s}{b \cdot d} = 0.009116$$

The height of the compressive zone:

$$x = 32.77mm$$

Internal lever arm:

$$z = d - \frac{1}{3}x = 93.08mm$$

The cracking moment follows from:

$$M_r = f_{ct,fl} \cdot W = 1.57 \cdot 10^6 Nmm$$

Under the action of this cracking moment the steel stress in the crack is:

$$\sigma_{sr} = \frac{M_r}{A_s \cdot z} = 148.95 MPa$$

The stress σ_{sr} in the crack becomes smaller with increasing distance from the crack. Just at the onset of the formation of the next bending crack the strain in the concrete can be calculated as follows:

$$\varepsilon_r = \frac{f_{ct,fl}}{E_c} = 0.1393 \cdot 10^{-3}$$

At the level of reinforcement the concrete strain can be calculated as:

$$\varepsilon_c = \frac{\dfrac{h}{2} - d}{\dfrac{h}{2}} \cdot \varepsilon_r = 0.0538 \cdot 10^{-3}$$
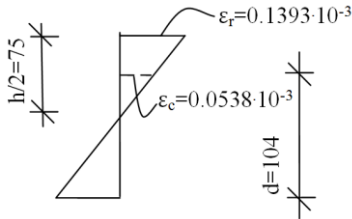
Figure 6-9: Concrete strain at the surface and level of the reinforcement for a cover of 40 mm

Consequently, the stress in the steel at the end of the transmission length l_t is:

$$\sigma_{se} = E_s \cdot \varepsilon_c = 10.77 MPa$$
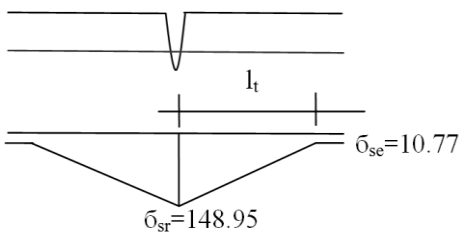
Figure 6-10: Steel stress in the crack and at the end of the transmission length for a cover of 40mm

The force introduced into the concrete over the distance l_t is:

$$N_t = (\sigma_{sr} - \sigma_e) \cdot A_s = 15.62 \cdot 10^3 N$$

If the bond strength is assumed to be constant:

$$\tau_{bm} = 1.8 \cdot f_{ctm} = 5.04 \, {N\!\!\big/\!\!mm^2}$$

Due to the contribution of the concrete cover, the transmission length can be calculated as follows:

$$l_t = 0.75 \cdot c + \frac{N}{\phi \cdot \tau_{bm} \cdot \pi}$$

Where the crack spacing can vary between l_t and $2l_t$:

$$s_{min} = 1.0 \cdot l_t = 112.25 mm$$

$$s_{mean} = 1.5 \cdot l_t = 168.37 mm$$

$$s_{max} = 2.0 \cdot l_t = 224.50 mm$$

For the determination of the strain over s_{mean} the following expression is used:

$$\varepsilon_{sm} = \frac{\sigma_s}{E_s}\left[1 - \beta_1 \cdot \beta_2 \cdot \left(\frac{\sigma_{sr}}{\sigma_s}\right)^2\right]$$

$\beta_1 = 1.0$ - *bond factor for ribbed steel*

$\beta_2 = 0.5$ - *for long term loading*

The mean crack width can be calculated as follows:

$$w_{mean} = s_{mean} \cdot \varepsilon_{sm} = 163.37 \cdot \frac{\sigma_s}{200000} \cdot \left[1 - 0.5 \cdot \left(\frac{148.95}{\sigma_s}\right)^2\right]$$

Where σ_s is the steel stress in the crack under the external load.

Therefore, the relation between mean surface crack width and steel stress is:

$$\sigma_s = 200 \, MPa \implies w_{mean} = 0.12 mm$$

$$\sigma_s = 300 \, MPa \implies w_{mean} = 0.22 mm$$

$$\sigma_s = 400 \ MPa \implies w_{mean} = 0.31 mm$$

$$\sigma_s = 500 \ MPa \implies w_{mean} = 0.40 mm$$

However, surface crack width and crack space can vary in function of the specific steel stress. Therefore, the relation between surface crack width and steel stress in the experiments depends on the crack spacing as follows:

$$\sigma_s = 200 \ MPa \implies 112.25mm \le s \le 224.50mm \implies 0.08mm \le w \le 0.16mm$$

$$\sigma_s = 300 \ MPa \implies 112.25mm \le s \le 224.50mm \implies 0.15 \le w \le 0.30mm$$

$$\sigma_s = 400 \ MPa \implies 112.25mm \le s \le 224.50mm \implies 0.21 \le w \le 0.42mm$$

$$\sigma_s = 500 \ MPa \implies 112.25mm \le s \le 224.50mm \implies 0.27mm \le w \le 0.54mm$$

The relation between surface crack width and steel stress for a concrete cover of 40 mm in the stabilized cracking stage is given in Fig. 6-11 for the minimum, maximum and theoretical mean value of crack spacing.
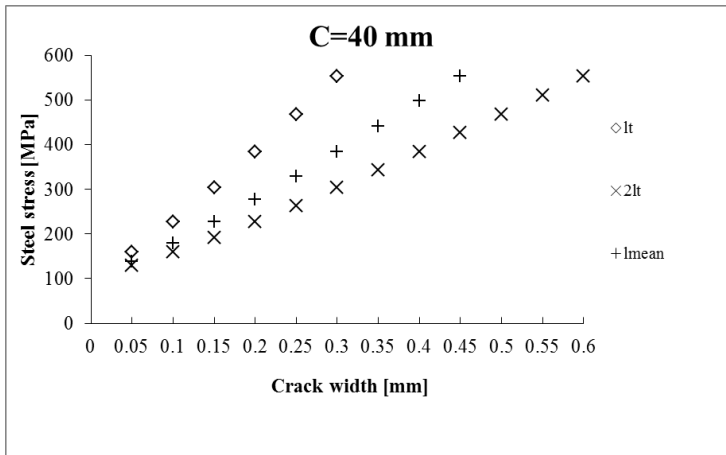
Figure 6-11: The relationship between surface crack width and steel stress for a cover of 40 mm

6.2. Reduction of load on beams at constant deflection due to the effects of creep and shrinkage

6.2.1. The influence of creep

Creep is a time-dependent deformation which has to be taken into account regarding the long-term behavior of concrete beams under a sustained loading.

The curvature κ is formulated as follows (Fig. 6-12):

$$\kappa = \frac{\varepsilon_s}{(d-x)} = \frac{\sigma_s / E_s}{(d-x)} \tag{6-1}$$

The steel stress σ_s follows from:

$$\sigma_s = \frac{P \cdot a}{z \cdot A_s} = \frac{P \cdot a}{(d - \frac{x}{3}) \cdot A_s} \tag{6-2}$$

Combining Eq. (6-1) and Eq. (6-2) the curvature can be expressed as:

$$\kappa = \frac{P \cdot a}{E_s A_s \cdot d^2 (1 - \frac{1}{3} \cdot \frac{x}{d})(1 - \frac{x}{d})} \tag{6-3}$$

Fig 6-12: Strains and forces in beam with constant deflection

Taking into consideration that stresses are in the elastic stage:

$$\frac{x}{d} = -\alpha_e \cdot \rho + \sqrt{\left(\alpha_e \cdot \rho\right)^2 + 2 \cdot \alpha_e \cdot \rho} \tag{6-4}$$

At first loading the modulus of elasticity of concrete C20/25 was about:

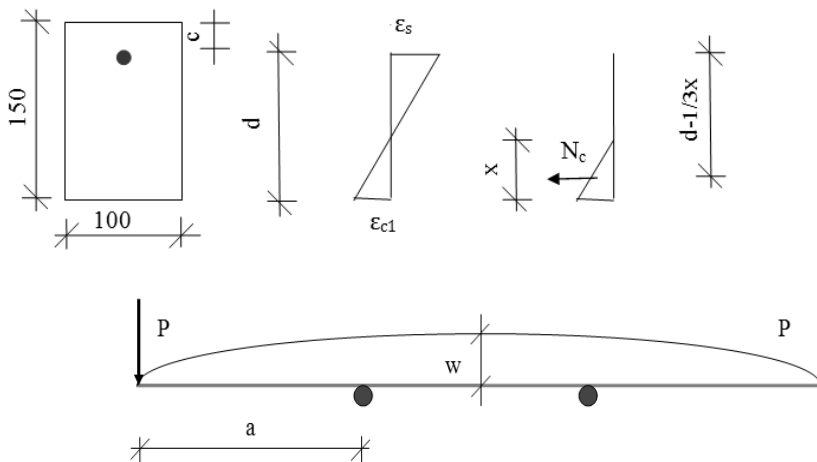$$E_{c0} = 30000 \; MPa$$

It means that at the beginning of the test:

$$\alpha_{e0} = \frac{E_s}{E_{c0}} = 6.67$$

Substituting values in Eq. (6-3), the curvature at the beginning of the test was:

$$k = 1.60 \frac{P_0 \cdot a}{E_s A_s d^2} \tag{6-5}$$

After 2 years under loading the value E_{c0} is reduced to an effective value of:

$$E_{ct} = \frac{E_{c0}}{1 + \phi(t, t_0)} \tag{6-6}$$

The creep coefficient φ(t,t₀) can be determined with equations found in building codes. In the Dutch Code VBC the following expression for φ(t,t₀) is found:

$$\phi(t, t_0) = k_c \cdot k_d \cdot k_b \cdot k_h \cdot k_t \le \phi_{max} \tag{6-7}$$

For the situation considered (beams in the laboratory) the coefficients in the previous equation are about:

$k_c = 2.6$; $k_d = 1.0$; $k_b = 1.3$; $k_h = 1.16$; $k_t = 0.97$; and $\phi_{max} = 3.8$

With those values a value for φ(t,t₀) = 3.8 is found. The effective E_{ct} – modulus after 2 years follows then from:

$$E_{ct} = \frac{E_{c0}}{(1 + \phi)} = \frac{E_{c0}}{1 + 3.8} = 0.21 E_{c0} = 6250 MPa \tag{6-8}$$

It means that after 2 years of testing under loading:

$$\alpha_{et} = \frac{E_s}{E_{ct}} = 32$$

Substituting these values in Eq. (6-3) and (6-4), the curvature at the end of the test was:

$$k = 2.65 \frac{P_t \cdot a}{E_s A_s d^2} \tag{6-9}$$

However, the curvature has not been changed since the beginning of the experiment. It means that the values found for curvature at the beginning of the test with Eq. (6-5) and at the end of the test with Eq. (6-9) should therefore be the same. From this condition it can be concluded that the load was reduced to about 60% from the initial value:

$$P_t = 0.6 \cdot P_0$$

6.2.2. *The influence of shrinkage*

The free shrinkage of the concrete, according to the VBC is equal to:

$$\varepsilon_{sh} = \varepsilon_{sh,0} \cdot k_b \cdot k_h \cdot k_p \cdot k_t \le \varepsilon_{max}$$

In the case considered the following values apply:

$\varepsilon_{sh,0} = 0.4 \cdot 10^{-3}$; $k_b = 1.3$; $k_h = 1.16$; $k_p = 1.0$; $k_t = 0.97$; and $\varepsilon_{max} = 0.50 \cdot 10^{-3}$

With these values it was found that $\varepsilon_{sh} = 0.50 \cdot 10^{-3}$

If the beam shrinks, the reinforcement at the tensile side resists the shortening. Therefore the curvature develops in time. In the following consideration a part between two neighbouring cracks is regarded.

At first the moment of inertia of the composite cross-section is determined.
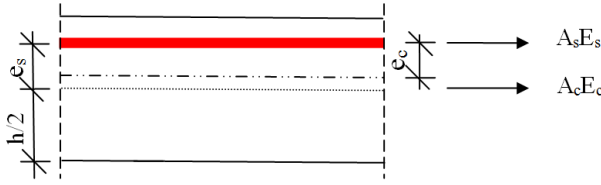
Figure 6-13: Determination of centre of gravity of composed (concrete-steel) cross section

For the determination of the centre of gravity the E-modulus of the composing materials is required. For the E-modulus of concrete the effect of time has to be regarded. Since the force in the concrete develops in time the E-modulus follows from:

$$E_{ct} = \frac{E_{c0}}{1 + 0.8\phi(t,t_0)} = 7425 MPa \qquad (6\text{-}10)$$

The distance e_c from the reinforcing steel to the centre of gravity of the (E-weighted) composed cross-section follows from:

$$e_c = \frac{e_s \cdot A_c E_{ct}}{A_s E_s + A_c E_{ct}} \qquad (6\text{-}11)$$

For the case of C=20 mm, with e_s = 75 - 26 = 49 mm, E_{ct} = 7.425 N/mm^2, A_s = 113 mm^2 and A_c = 15000 mm^2, it was found that e_c = 41 mm.

The further calculation is carried out in three steps (Fig. 6-14):

Figure 6-14: Steps in calculation of curvature beam due to shrinkage

a) The steel is uncoupled from the concrete and the shrinkage is supposed to occur freely, so without the restraining effect of the steel. The corresponding shrinkage strain is $\varepsilon_{sh} = 0.50 \cdot 10^{-3}$

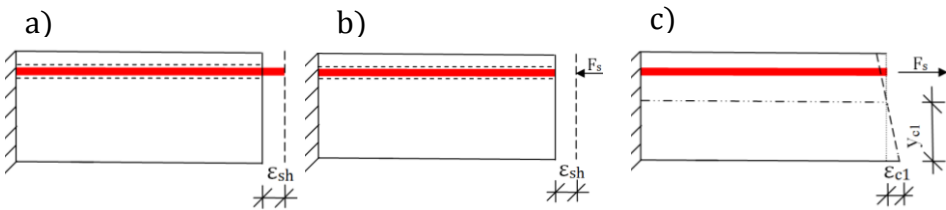b) The steel is subjected to a compressive force which is so large that the steel fits again to the concrete. That means that the steel strain is equal to $\varepsilon_{sh} = 0.50 \cdot 10^{-3}$. The force on the steel, necessary to achieve this situation is:

$$F_s = A_s E_s \varepsilon_{sh} = 11304 N \qquad (6-12)$$

c) After the steel has been coupled again with the concrete, the force F_s is applied with inverse sign to the composite member, at the level of the reinforcing steel. This results both in an elongation and a curvature.

In this case only the curvature κ_{sh} is relevant. The moment applied on the composite cross section is equal to:

$$M = F_s \cdot e_c = 463464 Nmm$$

where e_c - eccentricity of the steel to the neutral axis of the composite cross section (41mm)

The stress σ_{c1} at the top of the unreinforced outer face of the cross section follows from:

$$\sigma_{c1} = \frac{M \cdot y_{c1}}{I_c} \qquad (6-13)$$

where:

y_{c1} is the distance from the neutral axis to the unreinforced outer face of the cross section:

$$y_{c1} = 75 + 9 = 84 mm$$

I_c is the moment of inertia of the combined cross section, which is equal to:

$$I_c = \frac{1}{12} bh^3 + A_c (e_s - e_c)^2 + \alpha_e A_s \cdot e_c^2 = 34.17 \cdot 10^6 mm^4 \qquad (6-14)$$

Where:

$$\alpha_e = \frac{E_s}{E_{ct}} = \frac{200000}{7425} = 26.94$$

Using the values derived, with Eq. (6-13) it is found that the stress σ_{c1} caused by the bending moment M is equal to $\sigma_{c1} = 1.1$ N/mm^2.

The corresponding strain ε_{c1} follows from:

$$\varepsilon_{c1} = \frac{\sigma_{c1}}{E_{ct}} = 0.152 \cdot 10^{-3}$$

The corresponding curvature is (see also Fig. 6-13):

$$k_{sh} = \frac{\varepsilon_{c1}}{(\frac{h}{2} + e_s - e_c)} = 0.18 \cdot 10^{-5} \tag{6-15}$$

6.2.3.   *The influence of creep and shrinkage together*

In Section 6.2.1 the reduction of the load was calculated ignoring the effect of shrinkage. It was found that due to creep alone the loads P on the beam reduce to a value of about 60% of the initial value. However, as shown, also a relatively small curvature occurs due to shrinkage. This means that in reality the reduction of P is even larger. In Section 6.2.1 the reduction was calculated directly from the reduction of the E-modulus in time, without the need to calculate the curvature in detail. In Section 6.2.2, however, an absolute value for the curvature was derived, Eq. (6-15). In order to make a comparison also absolute values for the curvature have to be derived for the influence of creep. These, however, depend on the magnitude of P.

As an example it is assumed that the stress in the steel due to initial loading is equal to $\sigma_s = 350$ N/mm^2 and that the reinforcement ratio is 1%. In that case it was found from Eq. (6-4) that x/d = 0.305. The initial curvature is then calculated as follows:

$$k = \frac{\sigma_s / E_s}{d \cdot (1 - \frac{x}{d})} = 2.03 \cdot 10^{-5} \tag{6-16}$$

The relation between load P and the curvature at initial loading (solid line) is shown in Fig. 6-15.
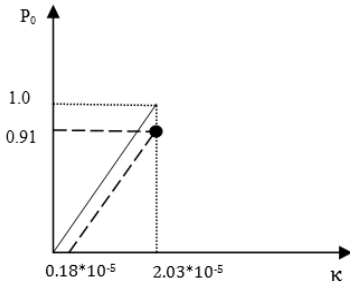
Figure 6-15: Load application and effect of shrinkage only on initial load P_0

The load application was stopped when the curvature $\kappa = 2.03 \cdot 10^{-5}$ [1/mm] was reached. In the hypothetical case that there would be no creep but only shrinkage, this would mean that the P-κ line moves over a distance $\kappa = 0.18 \cdot 10^{-5}$ from the origin (dotted line). Since the deflection of the beam was kept constant, this results in a decrease of the load with a factor $(2.03-0.18)/2.03 = 0.91$ due to shrinkage only. However, creep and shrinkage occur in parallel. Furthermore, creep occurs initially under a load $1.0P_0$ and finally under a load $0.91P_0$. In order to avoid a more complicated calculation it is assumed that the creep on average occurs under a constant value of the load equal to the mean value between $1.0P$ and $0.91P_0$, being $0.955P_0$. If the reduction of the load P_0 due to creep occurs under this mean value $0.955P_0$, the value of P_t after the 2 years would be $P_t = 0.60 \cdot 0.955P_0 = 0.57P_0$.

If the stress in the steel would be smaller, e.g. 250 N/mm^2, the initial curvature at load application would be smaller as well. As an example, for $\sigma_s = 250$ N/mm^2 the initial curvature would be $\kappa = 1.45 \cdot 10^{-5}$. Due to shrinkage only, the load then decreases to $(1.45-0.18)/1.45P_0 = 0.88P_0$. As a result of shrinkage and creep the load reduces to $0.6 \cdot 0.94P = 0.56P_0$. It can be concluded that the steel stress is not very influential on the reduction rate of the load in the experiments.

6.2.4. *The influence of time dependent effects on the steel stress and crack width*

In the previous calculations it was shown that the loads P_0 on the structure, at constant deflection, will decrease to 55-60% of their initial value. This holds as well true for the bending moment. In this section it will be analyzed which is the effect on steel stress and crack width. In Section 6.1 the relation was derived between surface crack width and stress in the reinforcing steel at the beginning of

the tests. For the case of gradually changing stresses in time the E-modulus of the concrete follows from Eq. (6-10). The value is $E_{ct} = 7425$ N/mm^2. For the proportionality ratio $\alpha_e = E_s/E_{ct}$ this leads to a value of $\alpha_e = 27$. For this value, in combination with $\rho = 0.01$ the value of x/d, found with Eq. (6-4) is x/d = 0.51 and the height of the compressive zone is then x=61.63 mm. The inner lever arm is:

$$z = d - \frac{1}{3}x = 103.46\,mm$$

The lever arm z_0 at initial loading was:

$$z_0 = d - \frac{1}{3}x_0 = 111.88\,mm$$

It can be concluded that in time the inner lever arm decreases with a factor 103.46/111.88 = 0.93. Hence, if the load on the structure would remain the same, the steel stress would increase with a factor 1/0.93 = 1.08. However, it was already shown in previous sections that the load decreases to about 0.57P_0 in the meantime. This means that the steel stress changes in the experiments with a factor:

$$f = 0.57 \cdot 1.08 = 0.61$$

As an example, according to Fig. 6-5 it is calculated that for a mean crack width 0.15 mm a steel stress of 284 N/mm^2 is required. This means that the steel stress reduces from $\sigma_{s0} = 284$ N/mm^2 to $\sigma_{st} = 0.61 \cdot 284 = 173$ N/mm^2 after 2 years. It can be read in the same figure that the crack width reduces from the initial value of $w_{m0} = 0.15$mm to $w_{mt} = 0.076$mm.

It can be concluded that steel stress was decreased to about 60% of the initial value in the reinforcing bars in case of beams under sustained curvature. Consequently, the mean crack widths decreased also to about 50% of the initial value. This can be one of the reasons why corrosion activity was stabilized after two years of exposure for beams under sustained loading. On the other hand, in beams with longitudinal cracks and under variable loading corrosion activity is still in progress.

6.3. Localized steel stress-surface crack width relation for the maximum localized corrosion in concrete beams

Based on the analytical verification of the steel stress-surface crack width ratio for different concrete covers, which is given in Section 6-1, the mean steel stress was calculated. Furthermore, it can be of vital importance to determine the steel stress in the "critical point" which is the crack position for the maximum localized corrosion activity in each beam by using the developed calculation procedure for the different concrete covers and by the known surface crack width at that crack position and the distance of the next crack at both sides. According to that, the localized steel stress-surface crack width relation, for the maximum localized corrosion in the critical point, at the beginning of exposure for each cracked concrete beam is calculated and the results are shown in Fig. 6-16.

The maximum localized steel corrosion in the "critical point" for each cracked concrete beam in the experiments is a point of major interest. Visualization and verification of maximum localized steel corrosion attack in that critical point for each cracked concrete beam after two years of exposure was already given in Section 5.3 and Appendix B. Therefore, limitations are required regarding localized corrosion activity of steel reinforcement in that "critical point" for each concrete beam.
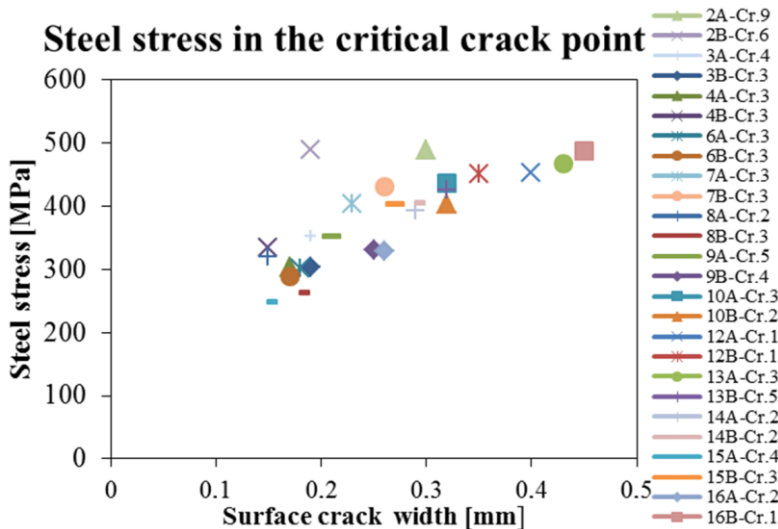

Figure 6-16: Localized steel stress-surface crack width relation for the maximum localized corrosion in the critical point for all cracked concrete beams in the experiments

It is already analytically verified in this chapter that the relation between the surface crack width and the steel stress depends on the concrete cover. Furthermore, in order to generate the specific target surface crack width a higher concrete cover led to a lower steel stress. In other words, for the same surface crack width at the level of the steel rebar a lower crack width will be obtained for the higher concrete cover.

The concrete cover affects the derived value of the maximum localized corrosion current density results for the localized measurements (Section 5.3) for each "critical point" in the experiments. For instance, for the same steel stress in the crack, the higher concrete cover led to slightly lower corrosion current density in the measurements. However, this occurred due to the fact that the higher concrete cover led to a higher real-assumed ratio of localized polarized steel area and therefore, higher real-derived corrosion damage for the same steel stress in the crack. In other words, the measured maximum localized corrosion current density is different for the different concrete covers. In order to avoid complex correlations between corrosion current densities, the calculated value is always sensitive to the real localized polarized steel area, and the visualization of localized corrosion activity for the different concrete covers is much more simple and reliable enough to correlate the steel stress at the positions of the "critical point" and localized corrosion activity in the experiments. Furthermore, steel stress determines the damage at the level of steel reinforcement rather than surface crack width, which is just a consequence of the steel stress and depends also on some other parameters, like bond strength, concrete cover etc.

According to the steel stress in the crack, for the maximum localized corrosion damage in the concrete beams in the experiments, the corrosion activity over prolonged time was assessed as is shown in Table 6-1.

Table 6-1: Corrosion progress in the crack for the maximum localized corrosion in beams

6_s in the crack	Localized corrosion activity
6_{sr} to 250 MPa	Negligible to Low
250 to 300 MPa	Low to Moderate
300 to 350 MPa	Moderate to High
350 to 500 MPa	High to Severe

6.4.   Conclusions

Crack patterns for the test conditions and the prediction of the relationship between surface crack width and steel stress for concrete covers of 20 mm, 30 mm and 40 mm, were analyzed. The relation between surface crack width and steel stress in the experiments in the stabilized cracking stage was given for the minimum, maximum and mean theoretical value of the crack spacing.

The reduction of the load and the steel stress in the beams at constant deflection due to the effects of creep and shrinkage were determined. It was calculated that the steel stress decreased to about 60% of the initial value in the reinforcing bars in case of beams under sustained curvature, which is one of the reasons why corrosion activity was stabilized after two years of exposure for beams under sustained loading. However, if the load on the concrete member had remained the same, the steel stress would have increased with 8% of the initial value, where the stabilization of corrosion activity would have been questionable.

The maximum localized steel corrosion in the "critical point" for each cracked concrete beam in the experiments was a point of major interest. The "critical point" was the crack position for the maximum localized corrosion in each beam, for which the localized steel stress-surface crack width relationship was derived. In order to limit corrosion activity in that "critical point" over a prolonged period of time, the steel stress limitations according to Table 6-1 were assumed for the case of the experimental conditions.

Chapter 7

Service life of cracked reinforced concrete structures in an aggressive environment

7.1. Service life modelling

The most general conceptual model, as proposed by Tuutti (1982), was taken as a basis for the derivation of many mathematical models. These models can be broadly divided into chloride penetration and corrosion propagation prediction models which are further divided into analytical models and numerical models. While analytical models are based on mathematical equations with an exact outcome, in numerical models approximate outcomes from the equations can be obtained by various techniques. Furthermore, both analytical models and numerical models are divided into deterministic models and stochastic models. A deterministic model is a mathematical model with a fixed input value for each variable in the mathematical equation. Contrary, stochastic models are based on a probability approach. The range of each variable may be wide and its value depends on many factors (like concrete composition, environmental conditions, loading etc.). Taking into consideration that concrete is a heterogeneous material which is exposed to variable environmental conditions, stochastic models are more logical than deterministic models.

Chloride penetration models which are officially recognized (DuraCrete, 2000; fib Model Code, 2013), have been developed based on diffusion only, which is considered as the governing transport mechanism of chlorides in concrete. These chloride penetration models define a specific initiation period during which the

steel reinforcement is protected by a passive layer. However, the concrete is implicitly assumed to be uncracked. First of all, modelling of chloride penetration in cracked and uncracked concrete has to be distinguished. Modelling of chloride penetration in cracked and uncracked concrete can also be subdivided, based on its moisture saturation, into modelling of saturated and unsaturated concrete. While in the case of models for saturated uncracked concrete diffusion is considered as the governing transport mechanism of chlorides, in models for uncracked unsaturated concrete this is not the case. Furthermore, capillary suction is considered as the governing mechanism of chloride transport in this kind of concrete.

The models (DuraCrete, 2000; fib Model Code, 2013) are based on diffusion as the governing mechanism in concrete which is exposed to chlorides, with the analytical outcome. However, an apparent chloride diffusion coefficient (D_{app}) was used in the model in order to compensate the role of cracking, capillary suction, chloride binding, the degree of hydration etc. In other words, D_{app} leaves the possibility open that other factors might play a role in relation to chloride penetration in concrete.

Measuring and monitoring chloride penetration and corrosion propagation of steel reinforcement in time in concrete, exposed to chloride attack, is necessary in order to model the behaviour. Based on these models reliable service life predictions should be established. However, observations in practice have shown so far that these models often lead to erroneous predictions in relation to the structure's service life. This is caused by the absence of some relevant factors which should be involved at least indirectly for a more reliable assessment of the structure's service life. The factors which should be involved, directly or indirectly, in reliable models are exposure conditions, concrete cover thickness, concrete cover quality, type of loading (history, sustained and alternating load), presence of cracks, binder type, concrete resistivity, temperature, moisture content, aging factor, chloride binding etc.

Service life models generally distinguish two subsequent stages, the initiation and the propagation stage. However, in the presence of cracks depassivation of steel reinforcement can occur locally within a very short period of time, which however does not necessarily mean that the target service life is reached. Based on that, service life models for cracked concrete structures, in comparison with uncracked concrete structures, should contain at least one more stage - the early propagation stage. In this respect, further logic questions can be raised like:

- How to quantify the influence of cracks in relation to durability and service life?

- Is the role of cracks only relevant in the early propagation stage?

- Or, is the role of cracks relevant for determination of the whole service life?

7.2. Treatment of the significance of cracks

As far as models for chloride penetration in cracked concrete are concerned, it should be emphasized that they are still under development due to difficulties to include cracks in the model. Furthermore, crack tortuosity and geometry must not be neglected in relation to chloride penetration in concrete. In recent years a growing number of studies was dedicated to the influence of cracks on the deterioration of steel reinforcement. However, in most of the cases the focus is actually on steel corrosion-induced cracks in, at the early beginning, uncracked concrete specimens. It has to be emphasized that load- or deformation-induced cracks and corrosion-induced cracks are two different issues. Steel corrosion-induced cracking represents a limit state criterion, in uncracked concrete in the propagation period, which can take place many years or even decades after a "structures' birth". However, load- or deformation-induced cracks can be present since the early beginning of structures' service life, especially when cracks intersect steel reinforcement. The theoretical target service life may have already been reached before a corrosion-induced crack has occurred in uncracked concrete members. Furthermore, corrosion-induced cracking has not been adopted directly as a parameter which is taken into account in modelling corrosion progress so far, due to the complexity of the phenomena involved. It is obvious that the influence of load- and deformation-induced cracks should be taken into account, explicitly or implicitly, in future service life models.

In order to reflect reality in a reliable way, many bending cracks were induced in the concrete beams as explained in Chapter 4 of the present study. An experimental set-up was developed where besides surface crack width, the role of crack distance (crack frequency), concrete cover thickness and type of load was recognized as well in relation to chloride-induced corrosion. In the present study, all bending cracks intersect the steel reinforcement. Furthermore, bending cracks intersect the steel rebar, even if the surface crack width was very small during the

loading procedure. According to the official approaches the results of the present study would lead to the erroneous conclusion that the design service life is reached from the early beginning of exposure for even hair line cracks. In the present study, the steel reinforcement was intersected by load-induced cracks and a different approach and limitations are required in order to control the role of cracks on chloride-induced corrosion and the corresponding service life of concrete members.

It has to be emphasized that the propagation period, according to research work carried out in relation to durability of cracked concrete in an aggressive environment, actually corresponds to the localized propagation period while the passive layer is quite often still present in the uncracked part at some distance from the main cracks. The difference between the propagation period in uncracked concrete and the localized propagation period in cracked concrete should be distinguished in future interpretations, especially when cracks intersect steel reinforcement. According to that, two different types of corrosion processes can be distinguished in cracked concrete structures as depicted in Fig. 7-1:

- Localized corrosion - by direct access of chlorides through cracks

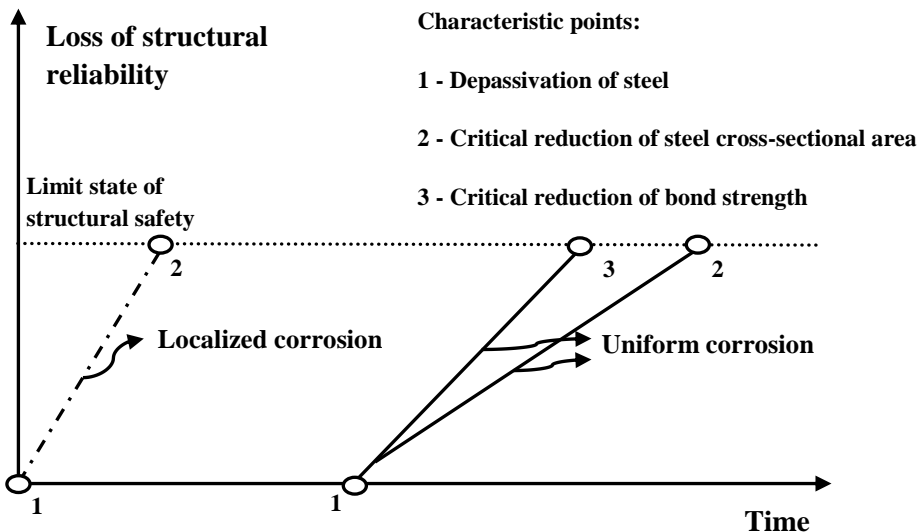- Uniform corrosion - by chloride transport through the concrete cover

Fig. 7-1: Corrosion processes and failure criteria in cracked reinforced concrete structures

Localized corrosion is characterized by the position of the main crack and the damage of the concrete at the bar level for a crack which intersects the steel reinforcement; loss of structural reliability can occur due to reduction of the steel diameter in that point. Local depassivation can occur within a few months, sometimes even a few days, but it does not necessarily mean that the specified service life of that concrete member is reached. This leads to the conclusion that limited localized loss of steel cross section should be allowed within the desired service life.

In case of uniform corrosion, which occurs in the uncracked part of the concrete member, except the reduction of steel diameter the loss of bond strength is a potential failure mechanism as well. In case of uniform corrosion, depassivation of steel reinforcement will occur when chloride ions, water and oxygen penetrate through the uncracked part of the concrete cover. Depassivation of steel reinforcement in the uncracked part between the main cracks, should be considered as a limit state which determines the end of the specified service life of a concrete member, due to fact that the chloride content at the bar level has reached a critical value.

It is relevant to distinguish between localized and uniform steel corrosion in cracked reinforced concrete structures. Fib Model Code (2013) focuses only on the diffusion of chlorides through the concrete cover and the calculation of the time necessary to reach depassivation of the steel. Although, the chloride penetration in uncracked concrete is uniform along the bar, the corrosion process is not uniform because the chloride threshold value will not anymore be the same along the rebar after the corrosion initiated at some local position. Taking into consideration that there is a high probability that the steel rebar is able to uniformly corrode in a short period of time after the corrosion initiated at some spot in the uncracked part of the concrete, the depassivation of steel reinforcement is considered as the theoretical end of service life. So fib Model Code (2013) only recognizes uniform chloride penetration along the rebars, but ignores the effect of local penetration through a major crack. This leads to reasonable results for the calculation of service life only if localized corrosion does not govern. This is only the case if access of chlorides to the bar is limited, but can be erroneous if access of chlorides is easy due to extensive micro-cracking in the region where the rebars intersect the main crack, especially if dynamic loading prevents crack healing.

Most codes of practice limit the surface crack width as well as prescribe a minimum concrete cover, without a clear concept behind it. So, without realizing, they address two goals: the limitation of both localized and uniform corrosion. The treatment of the surface crack width only is not adequate. The crack width is defined at the outer face, mostly under a load different from the load which creates the largest damage (the maximum service load). Moreover, they define the concrete cover as a value which is dependant on concrete strength. This is satisfactory since the effects are exchangeable (larger concrete strength – smaller concrete cover, or contrary). However, basically only the undamaged virgin situation is considered, which is correct in a laboratory specimen, but not in a structure subjected to loads.

Another aspect of cracks to be regarded in relation to steel corrosion, is the distinction between cracks due to external influences and due to internal load effects. Different types of cracks are induced due to loading and imposed deformations, not only on a macro-level but also on a meso-level and a micro-level where cracks are observed starting from the ribs of the rebar. The presence of the internal cracks, starting from the ribs of the rebar, might significantly reduce the transport distance between the rebar and concrete surface between the main cracks. Based on that, the influence of internal cracks on the effective undamaged (virgin) concrete cover must not be neglected. This effect should be at least indirectly quantified in relation to both localized and uniform steel corrosion. Cracks are also formed due to internal loads like restrained shrinkage of the concrete or swelling of the rebar due to rusting. The last mechanism can even lead to longitudinal cracks or loss of bond strength.

It is obvious that surface crack width should not be an isolated parameter which can be correlated to steel corrosion which was explained in Chapter 5 of the presented research work. Furthermore, it was already shown in Chapter 6 that damage of the concrete at the level of the bar is much more important than surface crack width in relation to steel deterioration. In some codes the surface crack width is corrected by a "cover factor". The argument is that the surface crack width increases with the thickness of the cover and that basically the crack width at the bar level matters. However, it is not only the crack width at the bar level that is important, but especially the microcrack zone adjacent to it that facilitates the local access of chlorides to the bar. Instead it is much more logic, useful and reliable enough to use the maximum steel stress as a possible limitation regarding the influence of load-induced cracks on the development of steel corrosion.

7.3.   Treatment of the significance of steel stress

In order to estimate the probability of localized corrosion damage in the crack, it is of vital importance to have a reliable prediction of the behaviour of the steel reinforcement exposed to aggressive agents (chlorides, water and oxygen) which penetrate through the crack. Taking into consideration that the surface crack width-effective crack width ratio depends on many parameters, where the concrete cover, bond strength, steel stress and formation of internal cracks may play an important role, the analysis sometimes goes along with oversimplifications. However, due to the aforementioned difficulties of effective crack width (crack width at the level of the bar) and damage estimation, it was shown in this research that it would be more logic and also more convenient to use the steel stress in the crack as a limitation of possible localized corrosion progress in time.

The position with the maximum localized steel corrosion can be notified as the "critical point" in each cracked reinforced concrete member in daily practice. Therefore, steel stress limitations are given regarding localized corrosion activity of steel reinforcement in that "critical point" , based on the experimental results, for cracked reinforced concrete members where transversal load- or deformation-induced cracks intersect the steel reinforcement under aggressive environmental conditions as is depicted in Fig. 7-2.
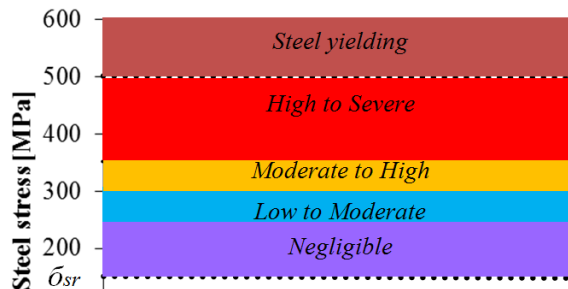

Figure 7-2: Localized corrosion progress in the critical point of concrete member

Uncracked reinforced concrete members, unloaded or subjected to a small load so that the cracking moment is not reached, after corrosion initiation mostly corrode uniformly. Cracked reinforced concrete members are able to corrode locally significantly before uniform corrosion in the uncracked part at the concrete surface, between the main cracks, even occurs. Furthermore, the length

of the localized steel corrosion area can be easily spread in time due to the presence of internal cracks next to the main crack in the case of a high steel stress which can lead to a significant debonded area at the level of the steel reinforcement and longitudinal cracking can occur with direct access of chlorides to the rebar, which is the most dangerous situation.

In the tests negligible localized corrosion was recorded in the "critical point" only if the steel stress in that crack was lower than 250 MPa. In that case corrosion started locally, but then re-passivation occurred and corrosion progress was interrupted over time. Localized corrosion progress in "critical points", where the steel stress is higher than 250 MPa in all cracked concrete beams, was observed to have a progress from low to moderate up to 300 MPa, moderate to high up to 350 MPa which is determined, for the test conditions, to be a limit of potential undesirable severe corrosion activity in aggressive environmental conditions.

A high steel stress affects the development of internal cracks, next to the main crack, which are not visible at the concrete surface. Furthermore, a high steel stress determines the development of internal cracks even in the uncracked part at the concrete surface, between the main cracks, and reduces the effective concrete cover of the uncracked part through which chloride penetration is facilitated towards the steel reinforcement. In other words, it is more logic and reliable to control the quality of the steel-concrete interface in general, which is more relevant for potentially localized and uniform corrosion activity than the surface crack width, by limiting the maximum steel stress rather than the maximum surface crack width in reinforced concrete members for a given bar diameter. In addition, maximum steel stress determines directly the damage at the level of steel reinforcement, whereas maximum surface crack width is a consequence where its width at the surface depends on the interaction of the maximum steel stress, bond strength, crack distance, development of internal cracks, cover depth etc.

As is depicted in Fig. 7-3, based on the experimental results in this research work, localized corrosion progress in time can be related to maximum steel stress for cracked reinforced concrete members in a severe environment and it has to be distinguished from uniformly distributed corrosion along the whole rebar which occurs mostly in uncracked concrete members.
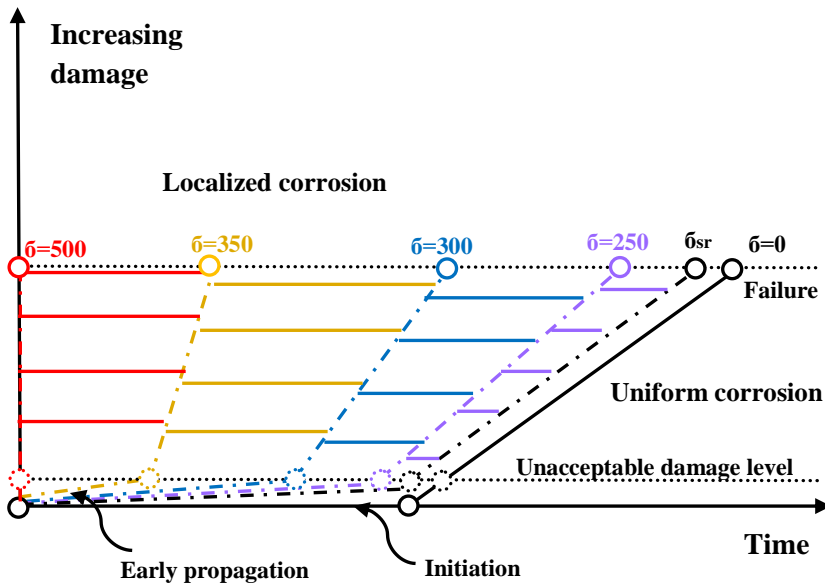
Figure 7-3: Corrosion progress in time is related to maximum steel stress for cracked reinforced concrete members

According to the experimental investigations in this research work, it was highlighted that even the presence of bending cracks which intersect steel reinforcement can locally lead to depassivation of steel reinforcement in a very short period of time, sometimes even a few days, for aggressive environmental conditions. That moment is denoted as the beginning of the early propagation period. However, taking into consideration that only localized depassivation of steel reinforcement does not lead to the end of service life of a concrete member, a negligible localized loss of steel cross section should be accepted in SLS. The determination of the exact level of unacceptable loss of steel cross section was not a goal of this research work, but in order to be at the safe side a low percentage of localized reduction of steel cross section of steel reinforcement should be allowed in the SLS.

The theoretical end of service life should be the instant in time when the aforementioned unacceptable loss of steel cross section is reached in any point of the concrete member. However, it is logic that this will occur where the maximum steel stress applies during service life. According to that, the progress of steel corrosion was assessed for a constant bar diameter (12 mm) in the present research. Localized progress of steel corrosion in that point is negligible in time

for a maximum steel stress which is lower than 250 MPa in a concrete member. Consequently, it leads to the conclusion that for that case the influence of cracking is important only in the early propagation stage and negligible localized corrosion damage would occur before uniform corrosion will occur in the uncracked part at the concrete surface, between the main cracks. However, if the maximum steel stress is in the region between 250 MPa and 300 MPa in a reinforced concrete element, the impact of cracking is not only relevant in the early propagation stage but also low to moderate impact should be noticed in relation to the determination of whole service life in the SLS. In addition, by increasing the maximum service load and steel stress from 300 MPa up to 350 MPa, it might lead to significant reduction of service life. Furthermore, the level of unacceptable loss of steel cross section or even bond strength reduction sometimes might be reached in a short period of time for a maximum steel stress which is higher than 350 MPa. However, the maximum steel stress in relation to durability and service life of reinforced cracked concrete members in an aggressive environment, should not be considered as an absolute value, but should be regarded in conjunction with the bar diameter, the concrete cover and the concrete strength.

7.4.   Service life design in an aggressive environment

According to the service life design concept, structural safety has to fulfill requirements for a specified period of time for which no, or limited, maintenance and repair are to be expected. However, it is of vital importance to realize that the service life concept, for a lot of concrete structures which were built in the last 50 years, was limited to a conservative traditional approach which can lead to erroneous predictions in relation to the structure's service life. Furthermore, daily practice has already shown the complexity involved in the appropriate determination of design parameters which affect durability and the intended service life of concrete structures. In the presence of bending cracks, which are mostly present in daily practice, steel corrosion damage has the ability to occur locally on a very small area. In order to keep it at an acceptably low level, limitations regarding the damage at the level of steel reinforcement are required to reach the desired service life.

The present research work demonstrated that the role of load- and deformation-induced cracks should not be neglected in relation to service life predictions, and

should be quantified by the limitation of maximum steel stress occurring for a concrete element during service life. In order to take a step forward towards direct incorporation of the influence of load- and deformation-induced cracks in a more reliable assessment of the structures' service life, an explanatory model for cracked reinforced concrete members/structures in an aggressive environment is proposed as illustrated in Fig. 7-4. According to the explanatory model, negligible localized corrosion of steel reinforcement should be allowed in SLS. Localized depassivation of steel reinforcement should not be considered as the moment when the target desired service life is finished. The target desired service life is reached at the moment at which a low percentage of the localized reduction of steel cross section is higher than the localized negligible loss. In other words, the negligible loss of steel cross section is an acceptable damage in the SLS.

In order to limit the influence of load- and deformation-induced cracks on the desired service life of cracked reinforced concrete elements in relation to chloride-induced corrosion, it was already emphasized that it would be much more logic, better and convenient to limit maximum steel stress rather than, as it is done in the current codes of practice, maximum surface crack width. Furthermore, by limiting maximum steel stress, not only surface crack width, but also crack width at the level of steel reinforcement, development of internal cracks and crack tortuosity would be implicitly limited as well.

According to the basic principle of structural design, the load which is expected to occur during the functional service life of structures, should be resisted with a certain safety margin. In addition, in this research work it was already illustrated that load variation leads to an increase of corrosion activity. Furthermore, it was highlighted that the maximum service load level governs the development of the corrosion, rather than the frequent or the quasi-permanent service load level. In relation to that, design of a specified service life for durable concrete structures should account for the maximum service load in the future. It would be more reliable to target the desired service life based on maximum service load, rather than is currently prescribed in Eurocode 2 (2005) where a maximum surface crack width limitation is defined for the quasi-permanent load combination. In other words, maximum service load determines the desired service life of concrete structures. Future investigations of steel corrosion behavior in concrete beams under a different number of re-loading and un-loading cycles per specific period of time in conjunction with the maximum service load, would be useful to determine the role of alternating load in relation to the damage at the steel-concrete interface and, therefore, corrosion development.
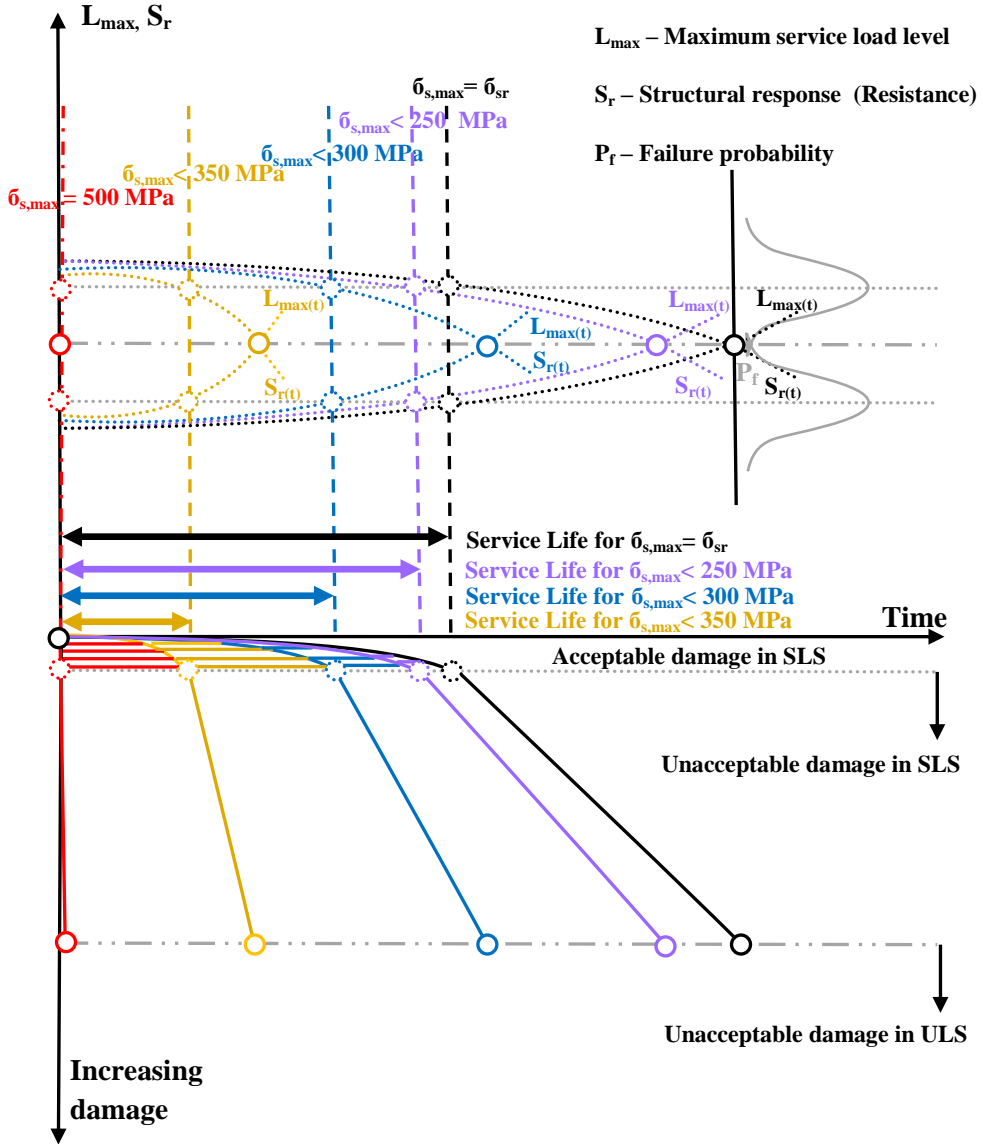
Figure 7-4: Service life explanatory model for cracked reinforced concrete members/structures in an aggressive environment

In order to obtain a certain structural safety level, design of durable concrete structures is a pre-requisite for having "through-life health performance" for a specified period of time which is denoted as specified service life. In addition, by choosing appropriate combinations of environmental classes, structural detailing and concrete compositions, safety factors are applied based on the maximum allowable steel stresses expected to occur in cracked reinforced concrete structures during the specified service life. In relation to that, three facts of vital importance are derived from the present research as illustrated by the explanatory model in Fig. 7-4, which gives an impulse towards recognition of the role of cracks in service life design. For practical situations, the following tendentious statements are made. Service life is:

- Hardly shortened, as long as the maximum steel stress is kept to be lower than 250 MPa under the maximum service load

- Shortened from a small to a considerable extent for maximum steel stresses between 250 MPa and 350 MPa under the maximum service load

- Endangered, if the maximum steel stress is higher than 350 MPa under the maximum service load

in comparison with uncracked concrete members exposed to aggressive environmental conditions.

However, giving an impulse to improved regulations for durability design by using this approach for cracked reinforced concrete members in aggressive environmental conditions, does not restrictively underestimate the influence of other parameters on the desired service life of concrete structures. Furthermore, in a future durability performance-based design approach, the role of maximum steel stress for the specific environmental class, should be judged in conjunction with, among others, bar diameter and cover depth at a certain concrete strength under the maximum service load, in order to ensure the desired service life of the concrete structure.

As far as the bar diameter is concerned, it has to be emphasized that it was not a variable in the conducted research. However, the bar diameter plays a role in service life in relation to corrosion. A larger bar diameter has a more unfavourable ratio of cross-sectional area to perimeter. So, larger diameter would lead to higher damage, meso- and micro-cracking around the bar at the same steel

stress and, therefore, a higher corrosion rate can be expected. On the other hand, reduction of steel cross-sectional area for a larger diameter is less affected by corrosion. For example, a 1 mm diameter loss corresponds to 10% and 5% reduction of the bar diameter of a 10 mm and a 20 mm bar, respectively. Furthermore, the reduction of the cross-sectional area in that case is around 19% and 10%, respectively. This has not been investigated but should not be forgotten in future design rules.

It can be highlighted that in future service life design a balance between maximum allowable steel stress and the bar diameter must be achieved. Taking into consideration the aforementioned advantages and disadvantages of using a larger bar diameter, a logic solution is to use lower maximum allowable steel stresses for the larger bar diameters. Furthermore, for each bar diameter a maximum allowable stress should be defined in the SLS. Consequently, the table for the maximum allowable steel stresses in conjunction with the bar diameters should not be based on the table with surface crack width limit control, as it is at the moment in Eurocode 2 (2005), but based on experimental results in relation to steel corrosion in an aggressive environment. For example, the present research work showed that for a bar diameter of 12 mm, the maximum allowable steel stress should not be higher than 250 MPa in an aggressive environment related to the test conditions. In the future investigations in relation to chloride-induced corrosion, for a constant total steel cross-sectional area different combinations of bar diameter and number of bars should be monitored in terms of both, localized and uniform corrosion, in order to define recommendations for the concrete members exposed to the aggressive environment.

The concrete cover is a parameter which plays a significant role in service life design as well. The concrete cover corresponds to the distance which chlorides, oxygen and water have to travel in order to reach the steel reinforcement. In other words, a larger cover at a certain concrete strength leads to a longer travel distance for aggressive agents and, therefore, a longer service life. Furthermore, a larger concrete cover gives a better confining action and as such a better resistance to internal cracking which plays a role in both, damaged area around the main crack (localized corrosion) and shortening effective undamaged (virgin) concrete cover (uniform corrosion along certain length). A larger concrete cover leads also to lower crack frequency and larger crack distance at the concrete surface, which enhances durability and service life of the concrete member.

7.5. Conclusions

An apparent chloride diffusion coefficient (D_{app}) is used in officially recognized models for service life assessment behind which the role of other factors which might affect service life of concrete members, is hidden. The service life models for cracked concrete, in comparison with uncracked concrete which consists of the initiation and propagation stage, should contain one stage more - the early propagation stage. The influence of load- and deformation-induced cracks should be taken into account in future concepts for service life design, by the limitation of maximum steel stress, rather than maximum surface crack width, for the given bar diameter in concrete member under maximum service load. The higher the maximum steel stress, the larger the damage around the bar and the facilitated access of chlorides.

Two different types of corrosion processes can be distinguished in cracked concrete structures, localized and uniform corrosion. The localized depassivation of steel reinforcement is not necessarily the theoretical end of service life of a concrete element where negligible localized loss of steel cross section should be allowed in the SLS. The uniform corrosion along a certain bar length occurs mainly by chloride transport through the "uncracked" part at the concrete surface, between the main cracks. The maximum steel stress affects both, localized and uniform corrosion along a certain bar length by the damage at the bar level and the reduction of the effective undamaged concrete cover, respectively.

In future service life design for an aggressive environment, the role of maximum steel stress should be judged in conjunction with the bar diameter and the concrete cover at a certain concrete strength under the maximum service load, in order to reach the desired service life of a concrete structure.

Chapter 8

Conclusions and recommendations for future research

8.1.   Summary

Chloride penetration and chloride-induced corrosion are substantially influenced by the presence of cracks. Bending cracks which intersect steel reinforcement, facilitate significantly the chloride penetration into concrete. Steel corrosion development is clearly influenced by the presence of bending cracks, crack distance (crack frequency) and damage of the concrete at the level of the rebars by internal cracks (meso- and micro-cracks). Consequently, the role of load- or deformation-induced cracks must not be neglected and should be revised in relation to durability and service life of concrete structures.

In order to generate new knowledge and contribute to the improvement of existing codes and engineering practice, an appropriate experimental set-up was developed. It was illustrated in the present research work that localized steel corrosion occurs mostly where cracks intersect the steel reinforcement. However, in some cases steel corrosion occurs at some distance from the crack or even between the cracks where chlorides penetrate through internal, meso- and micro-cracks. In order to limit the influence of load- and deformation-induced cracks on durability and service life of cracked reinforced concrete structures in relation to chloride-induced corrosion, it is highlighted that it would be much more logic and reliable to limit maximum steel stress for a given bar diameter rather than maximum surface crack width, as is prescribed in the current codes of practice. Furthermore, by limiting the maximum steel stress, not only the surface crack

width, but also the damage of the concrete at the level of the rebar and as such the accessibility of chlorides, oxygen and water to the reinforcing steel, would be limited as well. Based on the experimental observations, a service life explanatory model for cracked reinforced concrete members/structures exposed to an aggressive environment was proposed. For the sake of daily practice, in the future a durability performance-based design approach is proposed, where the maximum steel stress for the specific environmental class, should be used as a criterion in conjunction with bar diameter, cover depth and concrete strength under the maximum service load, in order to ensure the desired service life of a concrete structure.

8.2.   Conclusions

The aim of this research work was to shed more light on the role of load-induced cracks on the durability and service life of reinforced concrete structures in relation to chloride-induced corrosion. The interrelated influence of surface crack width, concrete cover, crack distance (crack frequency) and type of loading on the corrosion of steel reinforcement in concrete beams exposed to aggressive environmental conditions has been monitored for two years. The following conclusions can be drawn based on the experimental results:

- The maximum service load level governs the development of steel corrosion, rather than the frequent service load level or the quasi-permanent service load level. In order to design durable concrete structures, certain limitations are required at the maximum service load level during service life.

- Chloride penetration in uncracked unloaded concrete should be distinguished from the uncracked concrete at the surface, between the main cracks, in the loaded state. Furthermore, the presence of internal meso- and micro-cracks, starting from the ribs of the rebar, facilitate chloride penetration and must not be ignored in relation to the development of steel corrosion. According to the experimental results for chloride penetration in the cracked concrete, reconsideration of theoretical models is required for the probabilistic determination of service life.

- The development of chloride-induced steel corrosion occurs much faster in the presence of cracks which are parallel to the steel reinforcement than in the presence of pure bending cracks which intersect the steel reinforcement.

Consequently, longitudinal cracks have the potential to extremely reduce the service life of concrete structures, much more than pure bending cracks.

- The steel-concrete interface must be taken into consideration in relation to the development of steel corrosion in concrete where localized steel corrosion must be distinguished from uniform steel corrosion.

- Surface crack width limits should not be judged as an isolated criterion. In order to avoid complex surface crack width limitations in codes based on cover depth, maximum steel stress, bond strength, crack distance, development of internal cracks, crack tortuosity etc. , it would be much more logic, convenient and reliable enough to limit the maximum steel stress which determines directly the damage of the concrete at the level of the bar in the bending crack. Furthermore, the maximum steel stress also affects the development of internal cracks in the uncracked part at the surface, between the main cracks, reducing the effective undamaged concrete cover.

- Localized depassivation of steel reinforcement should not be considered as the moment in time that the desired service life is reached. Negligible corrosion of the steel reinforcement should be allowed in SLS. In other words, the early propagation period should be incorporated as a part of the desired service life for cracked reinforced concrete members/structures.

- According to the explanatory model, if it is ensured that the maximum steel stress in a cracked reinforced concrete member exposed to an aggressive environment is kept below 250 MPa under maximum service load during the service life, the role of cracks is important only in the early propagation stage and the desired service life might be only negligibly shortened in comparison with an uncracked concrete member. However, if the maximum steel stress is higher than 350 MPa under maximum service load, the desired service life may be significantly reduced in an aggressive environment.

- The traditional prescriptive approach should be replaced by a performance-based design approach in the future. The role of the maximum steel stress should be treated in conjunction with the bar diameter, the concrete cover and the concrete strength under the maximum service load for the specific exposure class, in order to reach the optimal solution for the desired service life of a concrete structure.

8.3.   Recommendations for future research

In the course of the present study, the future approach to the most challenging practical issue in relation to the direct incorporation of the role of load- and deformation-induced cracks in service life of concrete structures was established. However, this approach should be further transformed and developed from the laboratory research level to official acceptance in practice by existing design codes. In order to encourage engineers in daily practice to employ the performance-based approach where the maximum steel stress, in conjunction with the other relevant durability-related parameters, is limited in concrete members/structures under maximum service load, recommendations for future research work can be outlined as follows:

- Investigation of steel corrosion behavior in concrete beams for the same steel cross-sectional area and load, but with different combinations of bar diameters and number of bars. By testing that, corrosion damage in time should be properly monitored and its long term development in terms of both, localized and uniform steel corrosion, should be determined in order to obtain practical solutions for concrete members exposed to the aggressive environment.

- Numerical analysis of the influence of the maximum steel stress on the behaviour at the steel-concrete interface i.e. free-bond length, bond-slip relationship and the level of spreading of internal cracks. A possible scan analysis of the steel-concrete interface would be of vital importance in order to verify a sophisticated numerical analysis.

- Testing the influence of the maximum steel stress for a specific bar diameter in collaboration with other durability-related parameters i.e. concrete cover, concrete quality, loading history, exposure class etc. , on the development of the localized and uniform steel corrosion in concrete will be of crucial importance in future research work. In order to employ a performance-based approach to ensure the desired service life of future concrete structures, the coupled effect of degradation mechanisms i.e. steel corrosion induced by chlorides and carbonation, could be adopted as the worst possible scenario in aggressive environmental conditions.

- Investigation of the impact of steel stresses, under the same maximum variable load with a different number of re-loading and relaxing cycles per

specific period of time, on steel corrosion development. By testing, the role of the number of re-loading cycles could be identified as a potentially relevant parameter which contributes to the damage at the steel-concrete interface and additional development of internal, meso- and micro-cracks.

- Testing of the structural performance of concrete beams under the same load in time, where the influence of time dependent effects might play a significant role in relation to the increase of the maximum steel stress which would affect the potential acceleration of deterioration of the steel reinforcement.

References

Adiyastuti, S.M., 2005. *Influence of cracks on chloride induced corrosion in reinforced concrete structural members.* Doctoral Thesis, The University of New South Wales, Sydney, Australia, 186 pp.

Aldea, C.M., Shah, S.P., Karr, A., 1999a. *Permeability of cracked concrete.* Materials and Structures, 32: 370-376.

Aldea, C.M., Shah, S.P., Karr, A., 1999b. *Effect of cracking on water and chloride permeability of concrete.* Journal of Materials in Civil Engineering, 11(3): 181-187.

Aldea, C.M., Young, F., Wang, K. and Shah, S.P., 2000. *Effects of curing conditions on properties of concrete using slag replacement.* Cement and Concrete Research, 30(3): 465-472.

Alonso, C., Andrade, C., Rodriguez, J. and Diez, J., 1998. *Factors controlling cracking of concrete affected by reinforcement corrosion.* Materials and Structures, 31(7): 435-441.

Andrade, C., Alonso, C., Molina, F. J., 1993. *Cover cracking as a function of bar corrosion: Part I-Experimental test.* Materials and structures, 26(8): 453-464.

Andrade, C., Alonso, C., 1996. *Corrosion rate monitoring in the laboratory and on-site.* Construction and Building Materials, 10(5): 315-328.

Andrade, C., Alonso, C., 2001. *On-site measurements of corrosion rate of reinforcements.* Construction and building materials, 15(2): 141-145.

Antoni, T.H., Saeki, N., 2005. *Chloride penetration into fiber reinforced concrete under static and cyclic compressive loading.* International Conference on Durability of Building Materials and Components, Lyon, France, pp. 52-59.

Arya, C., Buenfeld, N.R., Newman, J.B., 1990. *Factors influencing chloride-binding in concrete.* Cement and Concrete Research, 20: 291-300.

Arya, C. and Ofori-Darko, F., 1996. *Influence of crack frequency on reinforcement corrosion in concrete.* Cement and Concrete Research, 26(3): 345-353.

Arya, W., 1995. *The relevance of cracking in concrete to reinforcement corrosion.* The Concrete Society, Technical Report No. 44

Audenaert, K., Marsavina, L., De Schutter, G., 2009. *Influence of cracks on the service life of concrete structures in a marine environment.* Key Engineering Materials, 399: 153-160.

Bamforth, P., 1999. *The derivation of input data for modelling chloride ingress from eight-year UK coastal exposure trials.* Magazine of Concrete Research, 51: 87-96.

Bamforth, P.B., 1996. *"Definition of Exposure Classes for Chloride Contaminated Environments".* Fourth International Symposium on 'Corrosion of Reinforcement in Concrete Construction', Cambridge, UK.

Bentur, A., Diamond, S., Berke, N.S., 1997. "Steel Corrosion in Concrete: Fundamentals and Civil Engineering Practise", Taylor & Francis

Bertolini, L., Elsener, B., Pedeferri, P., Polder, R.B., 2004. *Corrosion of steel in concrete: prevention, diagnosis, repair.* Wiley-VCH Verlag GMBH & Co., Weinheim, Germany, 392 pp.

Broomfield J.P., 1996. *Techniques to assess the corrosion activity of steel reinforced concrete structures.* ASTM STP 1276, 91–106

Brühwiler, E., Wittman, F.H., 1990. *The wedge splitting test, a new method for performing stable fracture mechanics tests.* Engineering Fracture Mechanics, 35(1/2/3): 117-125.

Build NT492, 1999. Concrete, Mortar and Cement-Based Repair Materials: *Chloride Migration Coefficient from Non-Steady-State Migration Experiments.* Nordtest method.

C876-91, A., 1991. *Standard test method for half-cell potential of reinforcing steel in concrete.* American society for testing and materials.

Castel, A., Vidal, T., François, R. and Arliguie, G., 2003. *Influence of steel-concrete interface quality on reinforcement corrosion induced by chlorides.* Magazine of Concrete Research, 55(2): 151-159.

CEB Bulletin 182, 1987. *Durable concrete structures.* CEB-RILEM International workshop - Final report

CEB, C.E.-I.d.B.T.T., 1992. *Durable concrete structures* - Design guide.

Committee, ACI, 1994. 224 Report *"Control of Cracking in Concrete Structures".*

Costa, A., Appleton, J., 1999a. *Chloride penetration into concrete in marine environment- part 1: Main parameters affecting chloride penetration.* Materials and Structures, 32: 252-259.

Costa, A., Appleton, J., 1999b. *Chloride penetration into concrete in marine environment- part 2: Prediction of long term chloride penetration.* Materials and Structures, 32: 354-359.

Crank, J., 1983. *The mathematics of diffusion.* Oxford University Press.

de Schutter, G., 1999. *Quantification of the influence of cracks in concrete structures on carbonation and chloride penetration.* Magazine of Concrete Research, 51(6): 427-235.

Djerbi, A., Bonnet, S., Khelidj, A., Baroghel-Bouny, V., 2008. *Influence of traversing crack on chloride diffusion into concrete.* Cement and Concrete Research, 38: 877-883.

DuraCrete, E.U.B., 2000. DuraCrete Final Technical Report. *Probabilistic Performance Based Durability Design of Concrete Structures.* Document BE95-1347/ R17.

Edvardsen, C., 1999. *Water permeability and autogenous healing of cracks in concrete.* ACI Materials Journal, 96(4): 448-454.

EN 1992-1-1, 2005. *Eurocode 2; Design of Concrete Structures, Part 1-1: General Rules and Rules for Buildings.* Committee of European Normalisation (CEN), Brussels.

Fedrizzi, L., Azzolini, F., Bonora, P.L., 2005. *The use of migrating corrosion inhibitors to repair motorways concrete structures contaminated by chlorides*. Cement and Concrete Research, 35: 551-561.

Feliú, V., González, J.A., Feliú, S., 2004. *Algorithm for extracting corrosion parameters from the response of the steel–concrete system to a current pulse*. Electrochemical Society, 151, 134-140.

fib, 2006. fib Bulletin 34, *Model code for service life design.* International Federation for Structural Concrete (fib), Lausanne, Switzerland, pp. 126.

fib, 2013. *Model Code for Concrete Structures 2010*

Francois, R. and Arliguie, G., 1999. *Effect of microcracking and cracking on the development of corrosion in reinforced concrete members.* Magazine of Concrete Research, 51(2): 143-150.

Francois, R., Arliguie, G., 1998. *Influence of service cracking on reinforcement corrosion*. Journal of Materials in Civil Engineering, 10(1): 14-20.

Francois, R., Castel, A., Vidal, T., Vu, N.-A., 2006. *Long term corrosion behaviour of reinforced concrete structures in chloride environment.* Journal de Physique IV France, 136: 285-293.

Garces Rodriguez, O., Hooton, R.D., 2003. *Influence of cracks on chloride ingress into concrete.* ACI Materials Journal, 100(2): 120-126.

Glass, G.K., Buenfeld, N.R., 2000. *The influence of chloride binding on chloride induced corrosion risk in reinforced concrete.* Corrosion Science, 24: 329-344.

Goto, Y., 1970. *Cracks formed in concrete around deformed tension bars.* ACI Journal, Proceeedings 68(4): 35-47.

Gowripalan, N., Sirivivatnanon, A., Lim, C.C., 2000. *Chloride diffusivity of concrete cracked in flexure.* Cement and Concrete Research, 30: 725-730.

Granju, J.-L., Ullah Balouch, S., 2005. *Corrosion of steel fibre reinforced concrete from the cracks.* Cement and concrete research, 35: 572-577.

Hu, J., Koleva D.A., Petrov P., van Breugel, K., 2012. *Polymeric vesicles for corrosion control in reinforced mortar: Electrochemical behaviour, steel surface analysis and bulk matrix properties.* Corrosion Science, 65: 414-430.

Ismail, M., Toumi, A., Francois, R., Gagne, R., 2008. *Effect of crack opening on the local diffusion of chloride in cracked mortar samples.* Cement and Concrete Research, 38: 1106-1111.

Ismail, M., Toumi, A., Francois, R., Gagne, R. , 2004. *Effect of crack opening on the local diffusion of chloride in inert materials.* Cement and Concrete Research 34: 711-716.

Jaffer, S.J., Hansson, C.M., 2009. *Chloride-induced corrosion products of steel in cracked-concrete subjected to different loading conditions.* Cement and Concrete Research, 39: 116-125.

Jang, S.Y., Kim, B.S., Oh, B.H., 2011. *Effect of crack width on chloride diffusion coefficients of concrete by steady-state migration tests.* Cement and Concrete Research, 41: 9-19.

Keddam, M., Takenouti, H., Nóvoa, X.R., Andrade, C., Alonso C., 1997. *Impedance measurements on cement paste*. Cement and Concrete Research, 27 (8): 1191-1201.

Koleva D.A., 2007. *Corrosion and protection in reinforced concrete - Pulse cathodic protection: an improved cost-effective alternative.* Doctoral Thesis, Delft University of Technology, the Netherlands

Koleva, D.A., de Wit, J.H.W., van Breugel, K., Veleva, L., van Westing, E.P.M., Copuroglu, O., Fraaij, A.L.A., 2007. *Correlation of microstructrure, electrical properties and electrochemical phenomena in reinforced mortar. Breakdown to multi-phase interface structures. Part II: pore network, electrical properties and electrochemical response.* Materials Characterization, 59(6): 801-815.

Koleva, D.A., de Wit, J.H.W., van Breugel, K., van Westing, E. J., 2007. *Investigation of Corrosion and Cathodic Protection in Reinforced Concrete I. Application of Electrochemical Techniques.* Electrochemical Society, 154(4): 52-61.

Koleva D.A., Guo, Z., van Breugel, K., de Wit, J.H.W., 2009. *Microstructural properties of the bulk matrix and the steel cement paste interface in reinforced concrete, maintained in conditions of corrosion and cathodic protection.* Materials and Corrosion, 60: 561-567.

Koleva D.A., Guo, Z., van Breugel, K., de Wit, J.H.W., 2009. *Conventional and pulse cathodic protection of reinforced concrete: Electrochemical behavior of the steel reinforcement after corrosion and protection.* Materials and Corrosion, 60: 344-354.

Koleva D.A., van Breugel, K., 2011. *The integration of EIS parameters and bulk matrix characteristics in studying reinforced cement-based materials.* Impedance Contributions Online, 9(3): 1-14.

Konin, A., Francois, R., Arliguie, G., 1998. *Penetration of chlorides in relation to the microcracking state into reinforced ordinary and high strength concrete.* Materials and Structures, 31: 310-316.

Küter, A., Geiker, M.R., Olesen, J.F., Stang, H., Dauberschmidt, C., Raupach, M., 2005. *Chloride ingress in concrete cracks under cyclic loading.* Proceedings of ConMat '05, Vancouver, BC, Canada.

Li, C., 2003. *Life-cycle modeling of corrosion-affected concrete structures: Propagation.* Journal of Structural Engineering, 129: 753.

Lim, C.C., Gowripalan, N., Sirivivatnanon, V., 2000. *Microcracking and chloride permeability of concrete under uniaxial compression.* Cement and Concrete Composites, 22: 353-360.

Linsbauer, H. and Tschegg, E., 1986. *Fracture energy determination of concrete with cube shaped specimens.* Zement und Beton, 31: 38-40.

Lorentz, T. and French, C., 1995. *Corrosion of reinforcing steel in concrete: effects of materials, mix composition, and cracking.* ACI Materials Journal, 92(2).

Maage, M., Helland, S., Poulsen, E., Vennesland, O., Carlsen, E., 1996. *Service Life Prediction of Existing Concrete Structures Exposed to Marine Environment.* ACI Materials Journal, 93: 602-607.

Mangat, P.S., Molloy, B.T., 1994. *Prediction of long term chloride concentration in concrete.* Materials and Structures, 27: 338-346.

Marcotte, T.D., Hansson, C.M., 2003. *The influence of silica fume on the corrosion resistance of steel in high performance concrete exposed to simulated sea water.* Journal of Materials Science, 38(4765-4776).

Marsavina, L., Audenaert, K., de Schutter, G., Faur, N., Marsavina, D., 2009. *Experimental and numerical determination of the chloride penetration in cracked concrete.* Construction and Building Materials, 23: 264-274.

Maruyama, I, Tanaka, K., Sato, P., 2006. *Distribution of chloride ion in cracked reinforced concrete prism transported by cyclic rain with chloride ion.* Seminar on Durability and Lifecycle Evaluation of Concrete Structures, Higashi Hiroshima, pp. 61-68.

Meijers, S.J.H., 2003. *Computational modelling of chloride ingress in concrete.* Doctoral Thesis, Delft University of Technology, the Netherlands

Miyazato, S. and Hiraishi, Y., 2005. *Transport properties and steel corrosion in ductile fibre reinforced cement composites,* pp. 20–25.

Mohammed, T.U., Otsuki, N., Hisada, M., Shibata, T., 2001. *Effect of crack width and bar types on corrosion of steel in concrete.* Journal of Materials in Civil Engineering, 13(3): 194-201.

NEN 6720, 1995. *Regulations for concrete TGB 1990 – Structural requirements and calculation methods.* NEN Institute, Delft

Neville, A., 1995. *Chloride attack of reinforced concrete: an overview.* Materials and Structures, 28: 63-70.

Nordtest, N., 1996. Build 208: *Concrete, Hardened: Chloride Content by Volhard Titration.* Nordtest.

Oh, B.H., Jang, S.Y., 2007. *Effects of material and environmental parameters on chloride penetration profiles in concrete structures.* Cement and Concrete Research, 37: 47-53.

Otieno, M., Alexander, M. and Beushausen, H., 2008. *Corrosion propagation in cracked and uncracked concrete.* CRC, pp. 157.

Otieno, M., Beushausen, H. and Alexander, M., 2012. *Towards incorporating the influence of cover cracking on steel corrosion in RC design codes: the concept of performance - based crack width limits.* Materials and Structures: 1-12.

Otieno, M.B., Alexander, M.G., Beushausen, H.-D., 2010. *Corrosion in cracked and uncracked concrete - influence of crack width, concrete quality and crack reopening.* Magazine of Concrete Research, 62(6): 393-404.

Otsuki, N., Miyazato, S.I., Diola, N.B., Suzuki, H., 2000. *Influences of bending crack and water-cement ratio on chloride-induced corrosion of main reinforcing bars and stirrups.* ACI Materials Journal, 97(4): 454-464.

Pacheco, J., 2015. *Corrosion of steel in cracked concrete: Chloride microanalysis and service life predictions.* Doctoral Thesis, Delft University of Technology, the Netherlands

Pease, B.J., 2010. *Influence of concrete cracking on ingress and reinforcement corrosion.* Technical University of Denmark, Lyngby, Denmark, 169 pp.

Ramm, W., Biscoping, M., 1998. *Autogenous healing and reinforcement corrosion of water-penetrated separation cracks in reinforced concrete.* Nuclear Engineering and Design, 179: 191-200.

Raupach, M., 2006. *Models for the propagation phase of reinforcement corrosion–an overview.* Materials and Corrosion, 57(8): 605-613.

Rostam, S., 2003. *Reinforced concrete structures–shall concrete remain the dominating means of corrosion prevention?.* Materials and Corrosion, 54(6): 369-378.

Sagüés, A.A., Pech-Canul, M.A., Al-Mansur, A.K.M.S., 2003. *Corrosion macrocell behavior of reinforcing steel in partially submerged concrete columns.* Corrosion Science, 45: 7-32.

Sahmaran, M., 2007a. *Effect of flexure induced transverse crack and self-healing on chloride diffusivity of reinforced mortar.* J Mater Sci, 42: 9131-9136.

Sahmaran, M., Li, M., Li, V.C., 2007b. *Transport properties of Engineered Cementitious Composites under chloride exposure.* ACI Materials Journal, 104(6): 303-310.

Sahmaran, M., Yaman, I.O., 2008. *Influence of transverse crack width on reinforcement corrosion initiation and propagation in mortar beams.* Canadian Journal of Civil Engineering, 35: 236-245.

Schießl, P., Raupach, M., 1997. *Laboratory studies and calculations on the influence of crack width on chloride-induced corrosion of steel in concrete.* ACI Materials Journal, 94(1): 56-61.

Scott, A., 2004. *The influence of binder type and cracking on reinforcing steel corrosion in concrete.* PhD Thesis.

Scott, A. and Alexander, M., 2007. *The influence of binder type, cracking and cover on corrosion rates of steel in chloride-contaminated concrete.* Magazine of Concrete Research, 59(7): 495-505.

Spiesz, P. and Brouwers, H.J.H., 2013. *The apparent and effective chloride migration coefficients obtained in migration tests.* Cement and Concrete Research, 48: 116-127.

Stern, M. and Geary, A.L., 1957. *Electrochemical polarization.* J. Electrochem. Soc. 104(1): 56-63.

Suryavanshi, A.K., Scantlebury, J.D., Lyon S.B., 1995. *The binding of chloride ions by sulphate resistant Portland cement.* Cement and Concrete Research, 26: 717-727.

Šavija, B., Pacheco, J., & Schlangen, E., 2013. *Lattice modelling of chloride diffusion in sound and cracked concrete.* Cement and Concrete Composites, 42, 30-40.

Šavija, B., Schlangen, E., Pacheco, J., Millar, S., Eichler, T., & Wilsch, G., 2014. *Chloride ingress in cracked concrete: a laser induced breakdown spectroscopy (LIBS) study.* Journal of Advanced Concrete Technology, 12(10), 425-442.

Šavija, B., 2014. *Experimental and numerical investigation of chloride ingress in cracked concrete.* Doctoral Thesis, Delft University of Technology, the Netherlands

Tammo, K., Thelandersson, T., 2009. *Crack behaviour near reinforcing bars in concrete structures.* ACI Structural Journal, 106(3): 259-267.

Tang, L., 1996. *Chloride transport in concrete- measurement and prediction.* Chalmers University of Technology, Göteborg, Sweden, 88 pp.

Tottori, S., Tsuchida, S. and Miyagawa, T., 1999. Deterioration prediction of concrete structures based in the exposure test results concerning cracking and rebar corrosion. Concrete Research and Technology, 10(3): 1-16.

Tuutti, K., 1982. *Corrosion of steel in concrete.* Swedish Cement and Concrete Research Institute, Stockholm, 1982, 469.

Walraven, J., C. 2015. *Damage of Concrete Structures due to aging.* XXVII Scientific and Technical Conference "Building Failures", Poland, 131-140 pp.

Wang, C., Jiang, J., Sun, G., Han, J., Qiao, Y., 2011. *The research of the effect of dynamic load and temperature on the diffusion performance of chloride ion in concrete.* Advanced Materials Research, 163-167: 3167-3173.

Wang, K., Jansen, D.C., Shah, S.P., 1997. *Permeability study of cracked concrete.* Cement and Concrete Research, 27(3): 381-393.

Win, P.P., Watanabe, M., Machida, A., 2004. *Penetration profile of chloride ion in cracked reinforced concrete.* Cement and Concrete Research, 34: 1073-1079.

Yi, S.-T., Hyun, T.-Y., Kim, J.-K., 2011. *The effects of hydraulic pressure and crack width on water permeability of penetration crack-induced concrete.* Construction and Building Materials, 25: 2576-2583.

Yoon, I.S., Schlangen, E., 2010. *Long/short term experimental study on chloride penetration in cracked concrete.* Key Engineering Materials, 417-418: 765-768.

Yoon, I.S., Schlangen, E., de Rooij, M.R., van Breugel, K., 2007. *The effect of cracks on chloride penetration into concrete.* Key Engineering Materials, 348-349: 769-772.

Appendix A

HCP point measurements using an Ag/AgCl electrode for cracked concrete beams during 2 years of exposure

During two years of HCP point measurements where the tip of the electrode was pressed on a wet sponge on the concrete cover along the rebar position (in the middle of cross-section), values were recorded as depicted in Fig. A-1. The first point was always at 100 mm distance from the edge of the container, the second one at the position of the first crack, the third one between the first and the second crack, the next one at the position of the second crack, the next one between the second and the third crack, until the last crack was reached. Finally, the point before the last one is the last crack and the last point is, as well as the first point, at 100 mm from the container edge on the opposite side as can be seen in Fig. A-1. In order to reach a stable value every point measurement lasted at least five seconds.
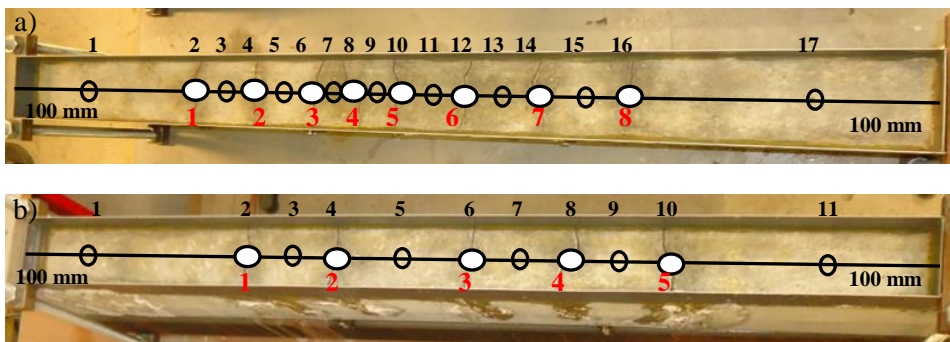
Figure A-1: HCP point measurements – schedule for beam with: a) 8 cracks b) 5 cracks

The results of HCP "point" measurements for all cracked beams using an Ag/AgCl external electrode at the end of wet and dry phases during two years of exposure are shown as follows:

Beam 14A-dry phases

Beam 14B-dry phases

Beam 14A-wet phases

Beam 14B-wet phases

Beam 15A-dry phases

Beam 15B-dry phases

Beam 15A-wet phases

Beam 15B-wet phases

Beam 16A-dry phases

Beam 16B-dry phases

Beam 16A-wet phases

Beam 16B-wet phases
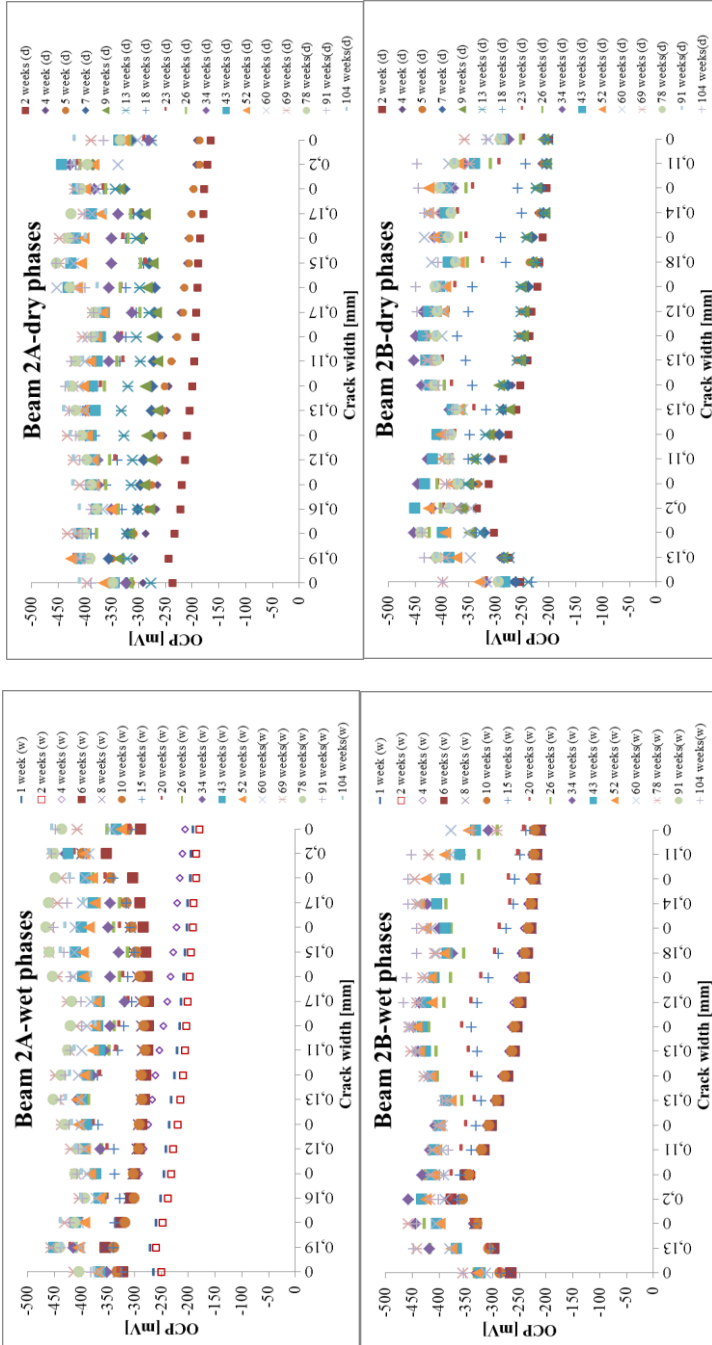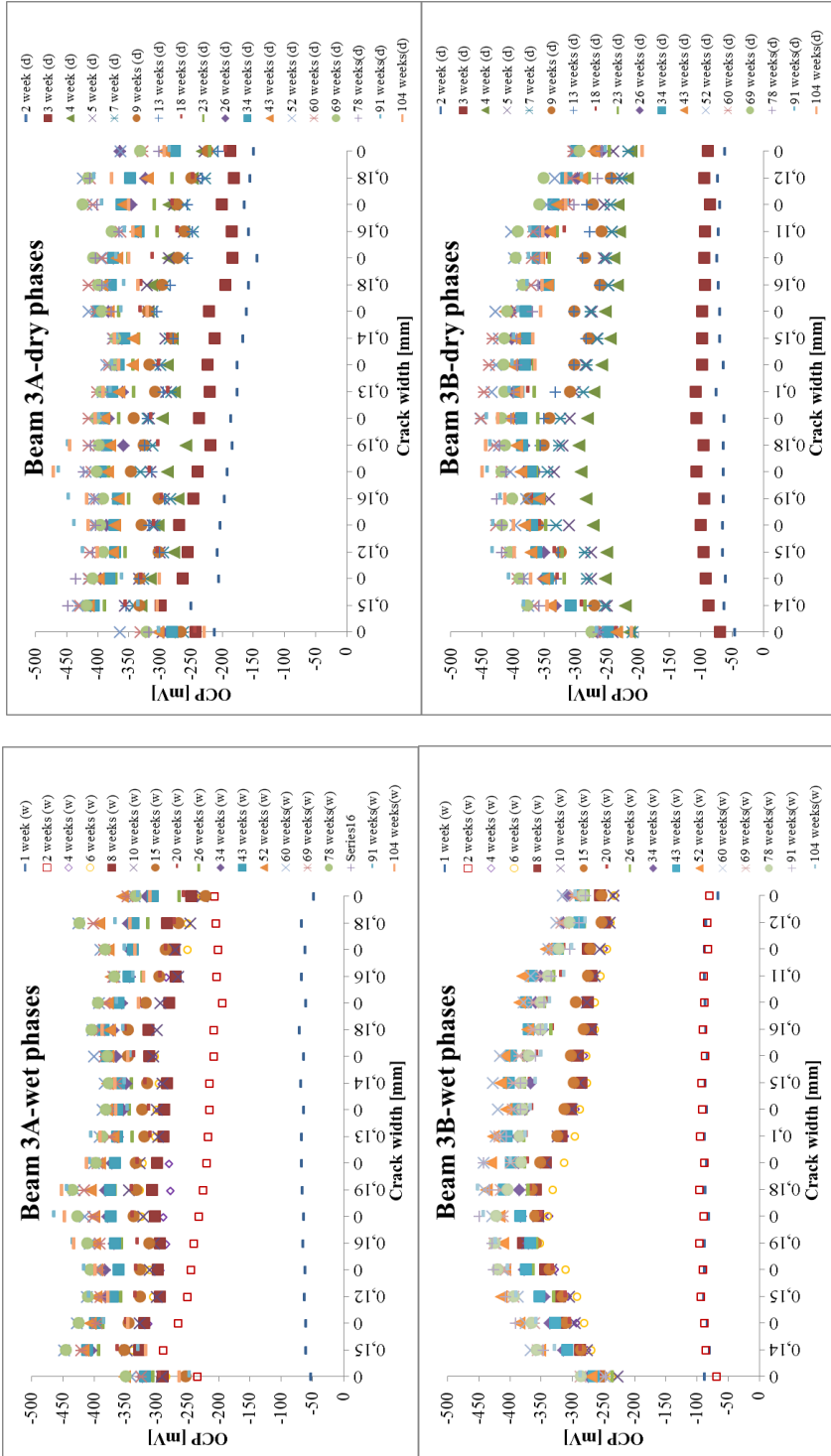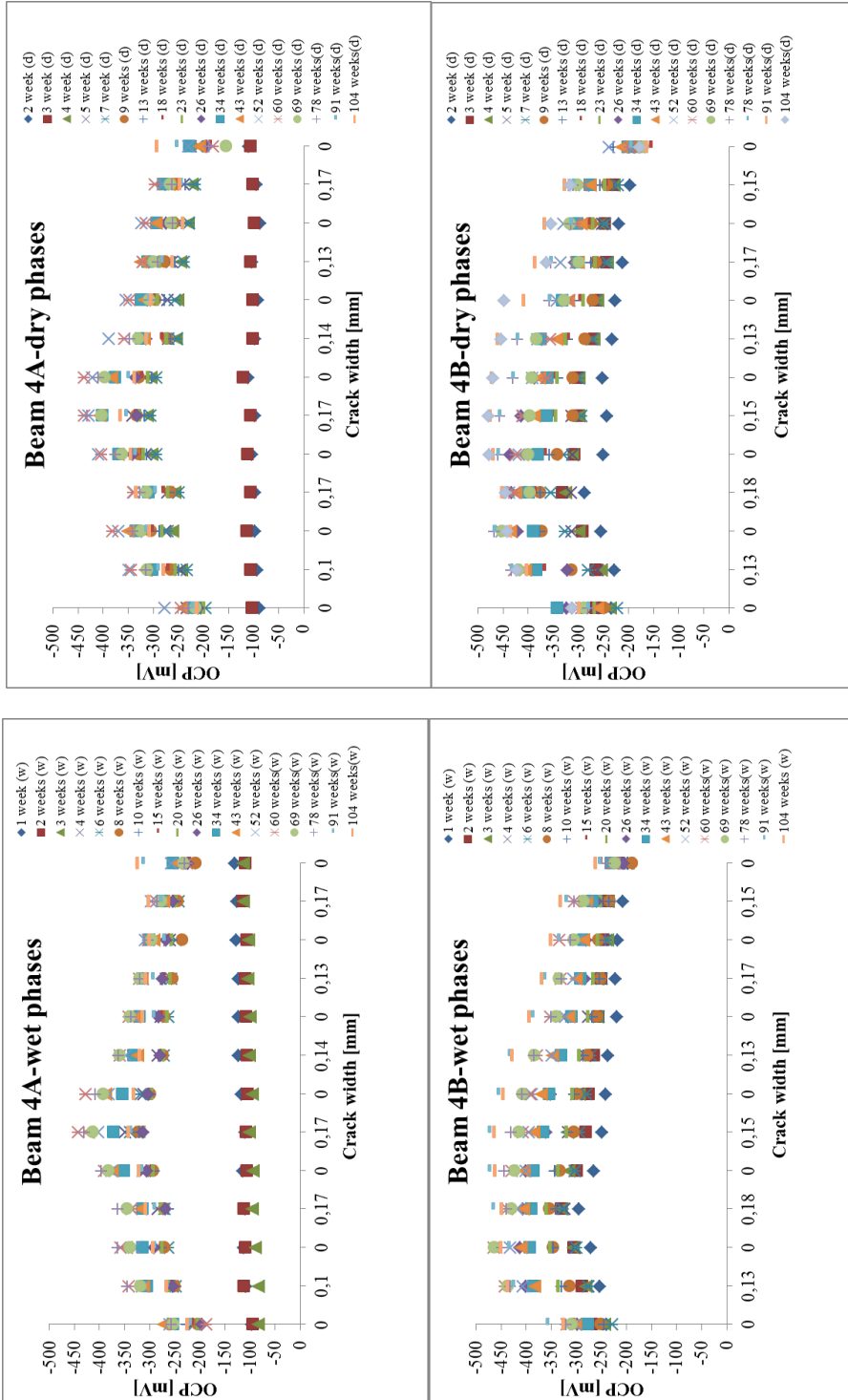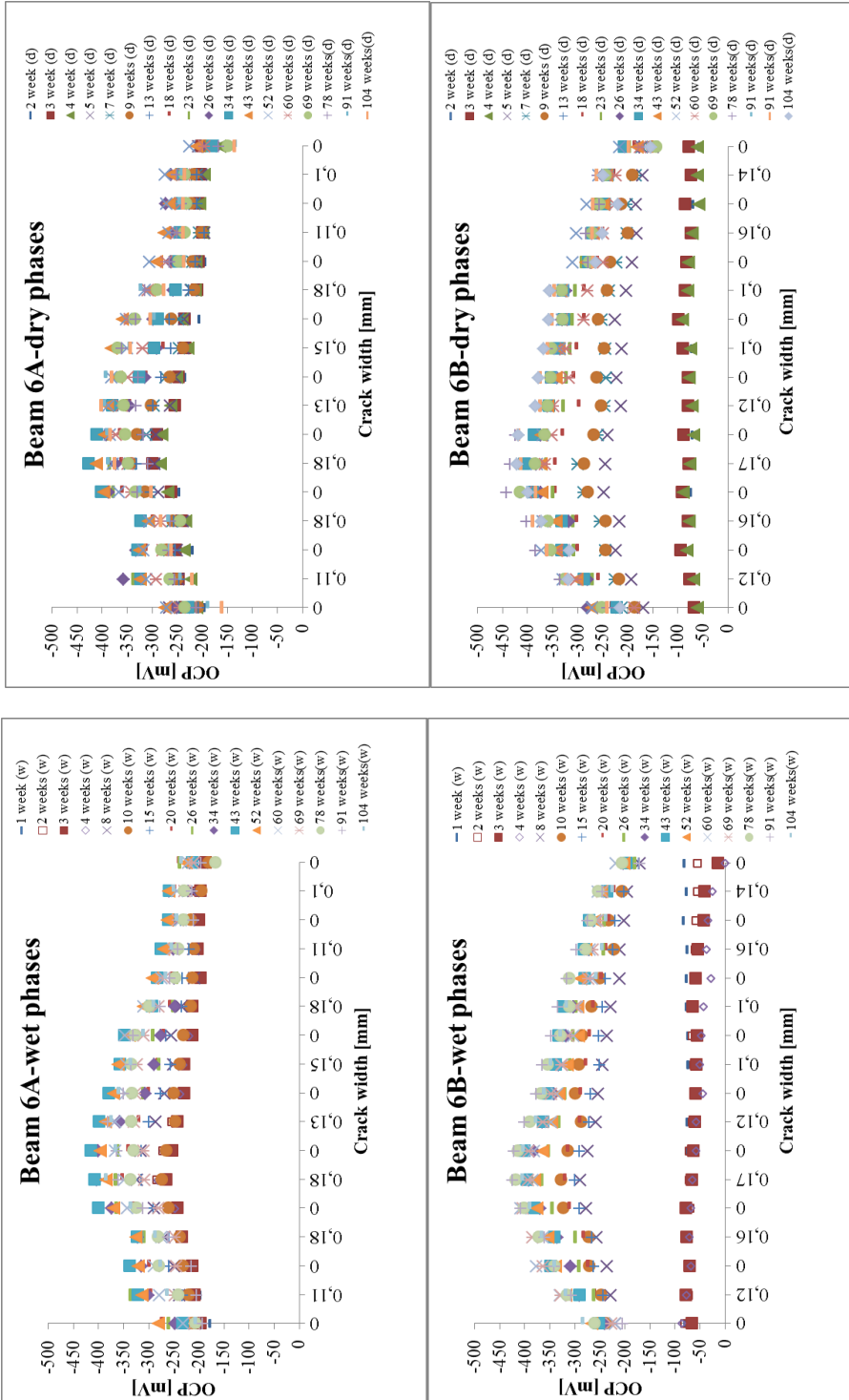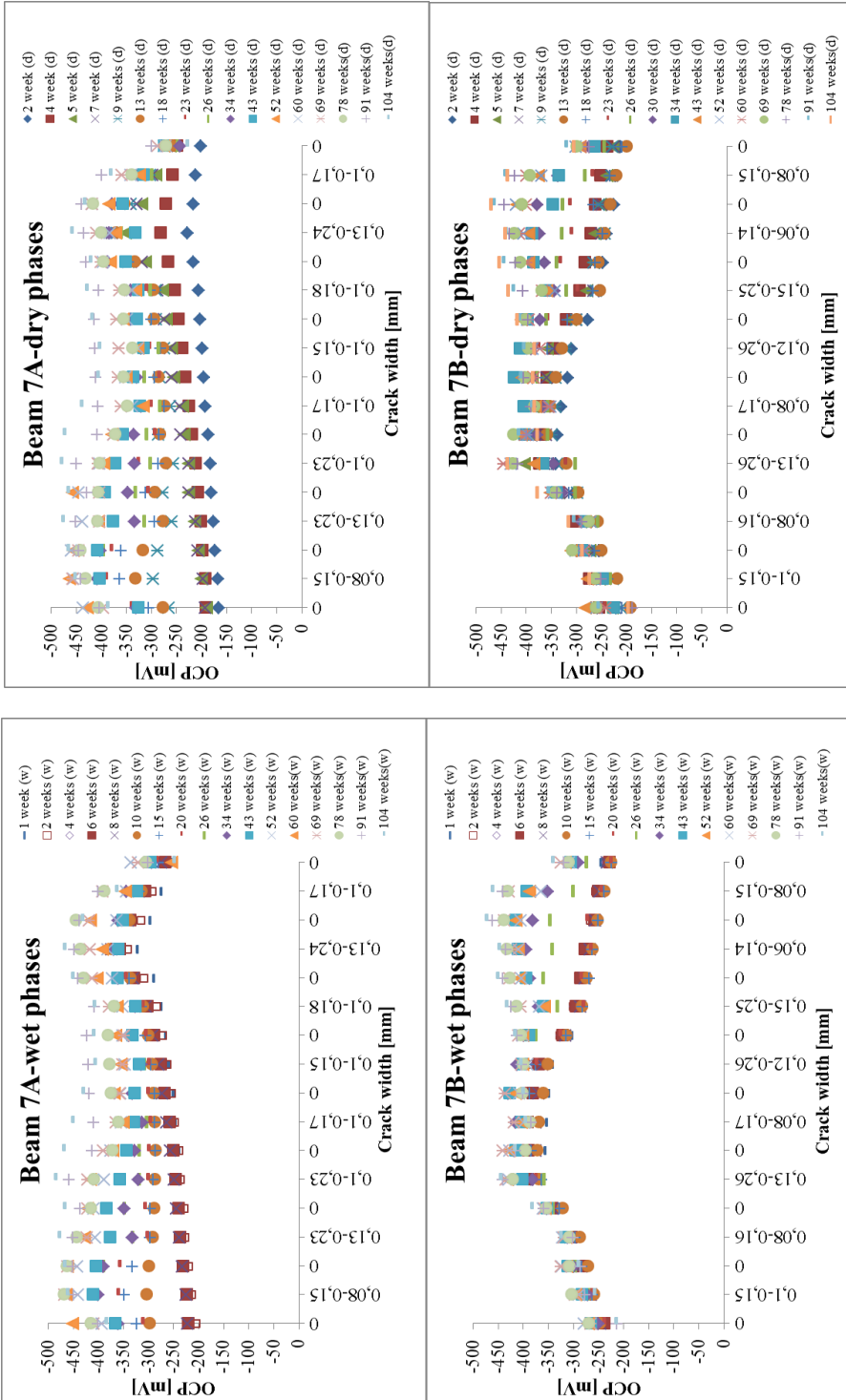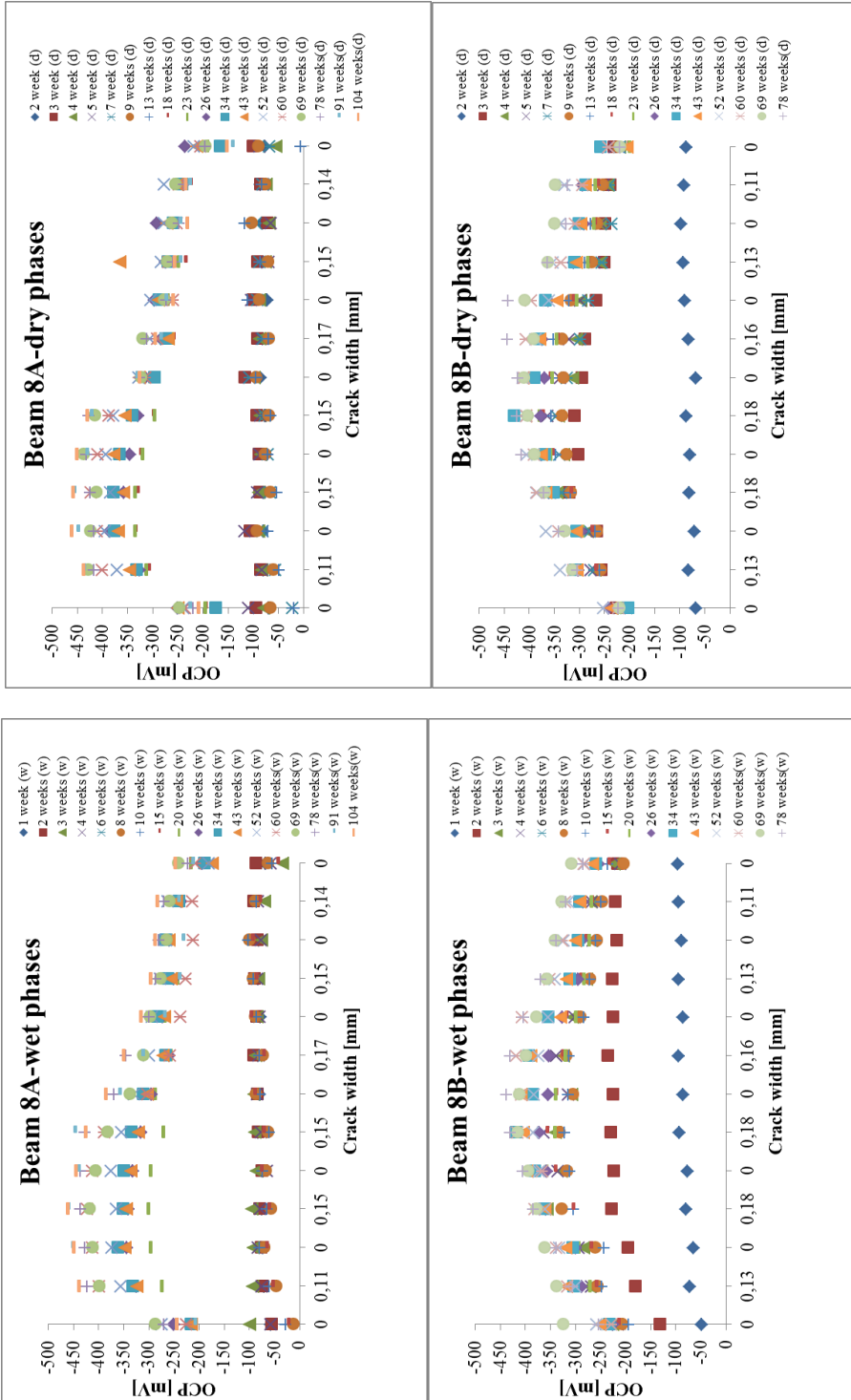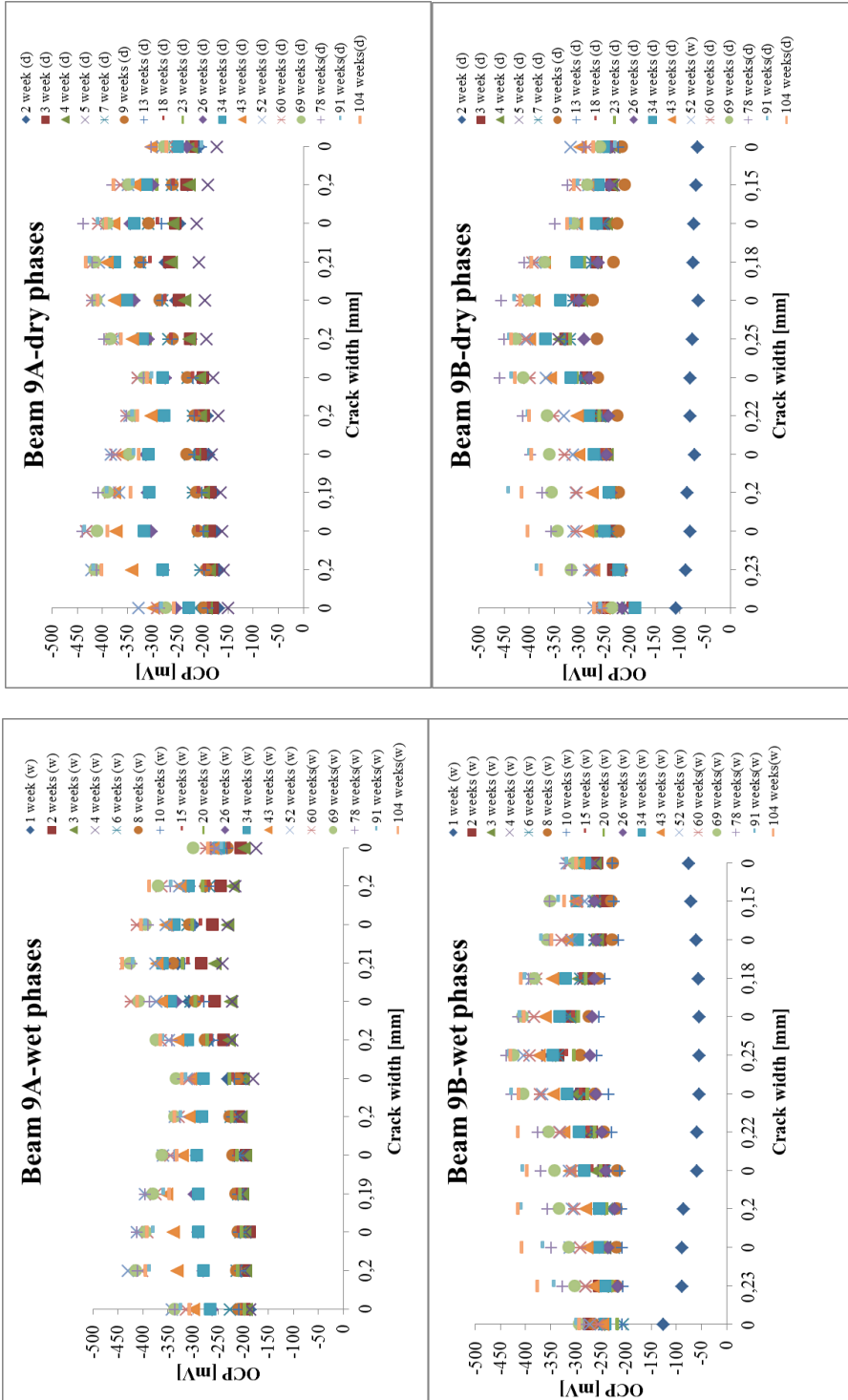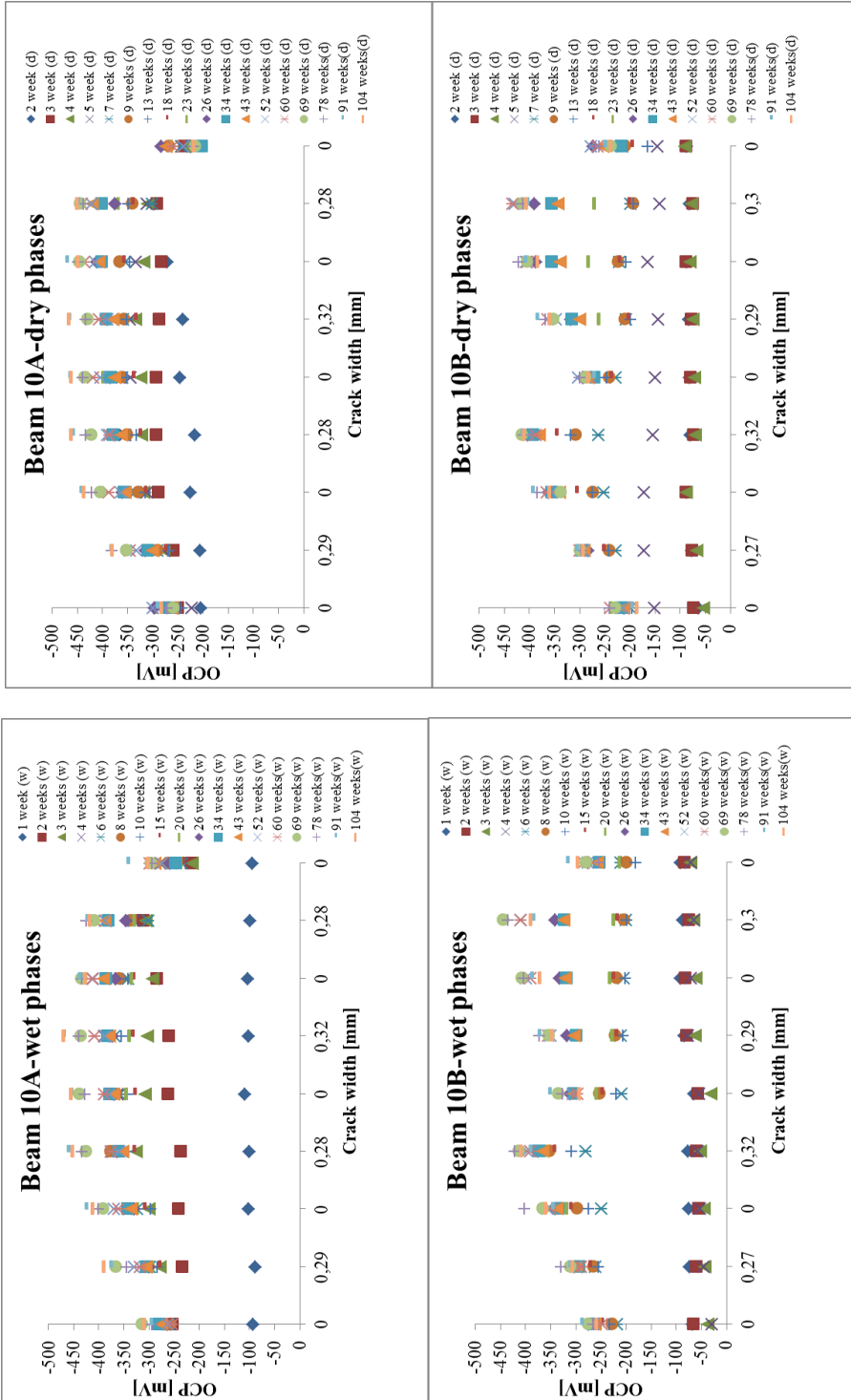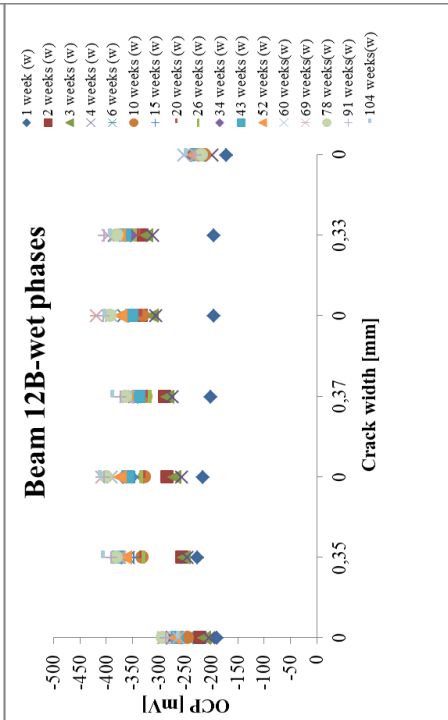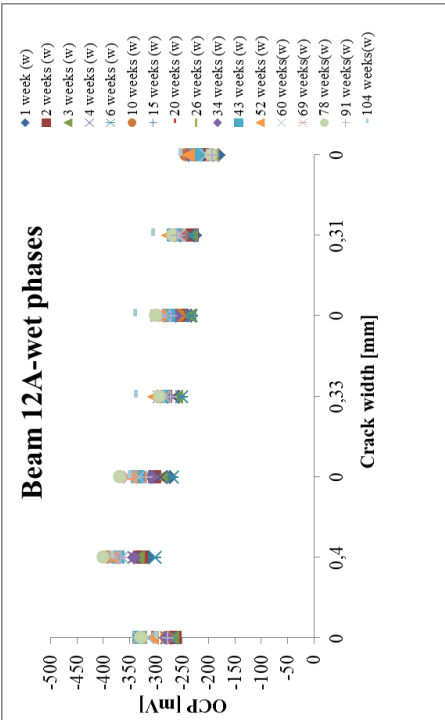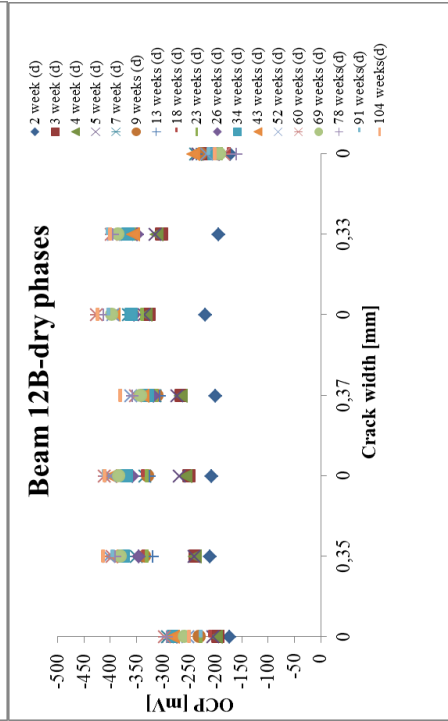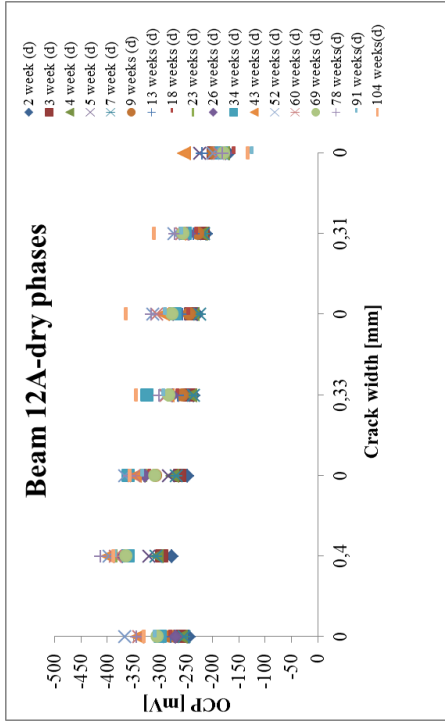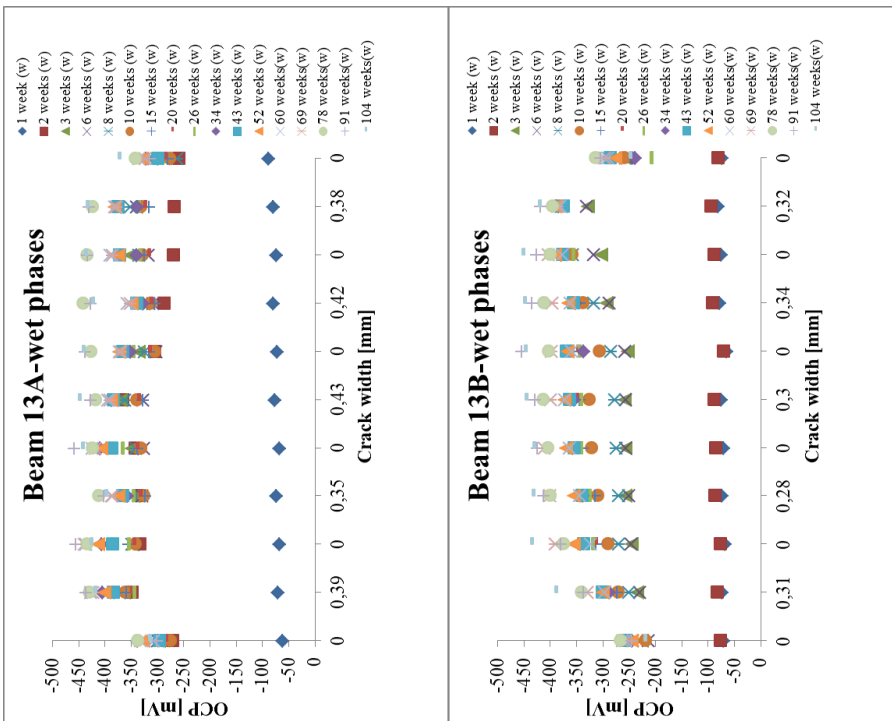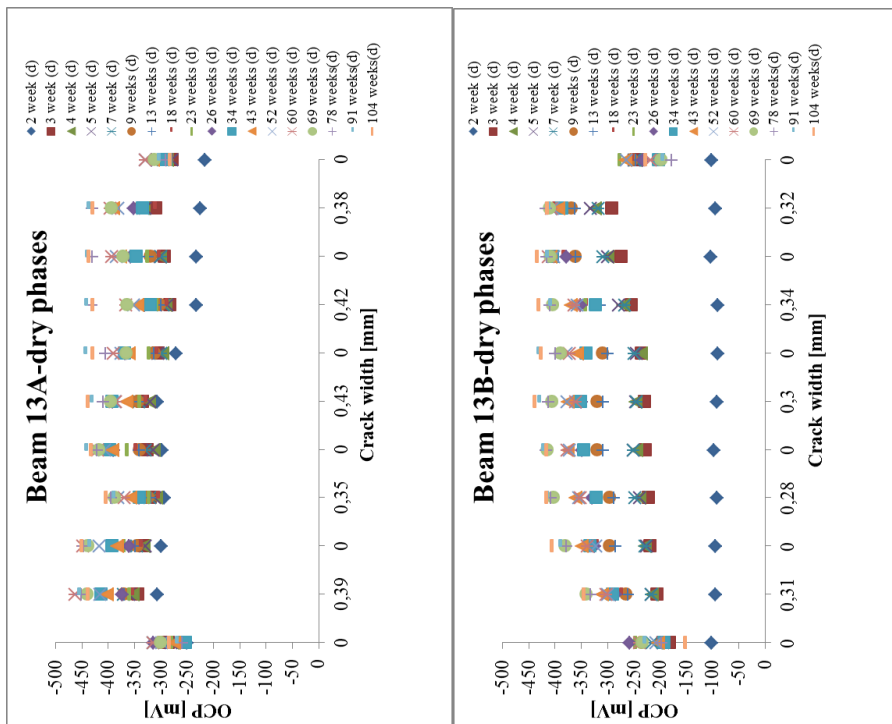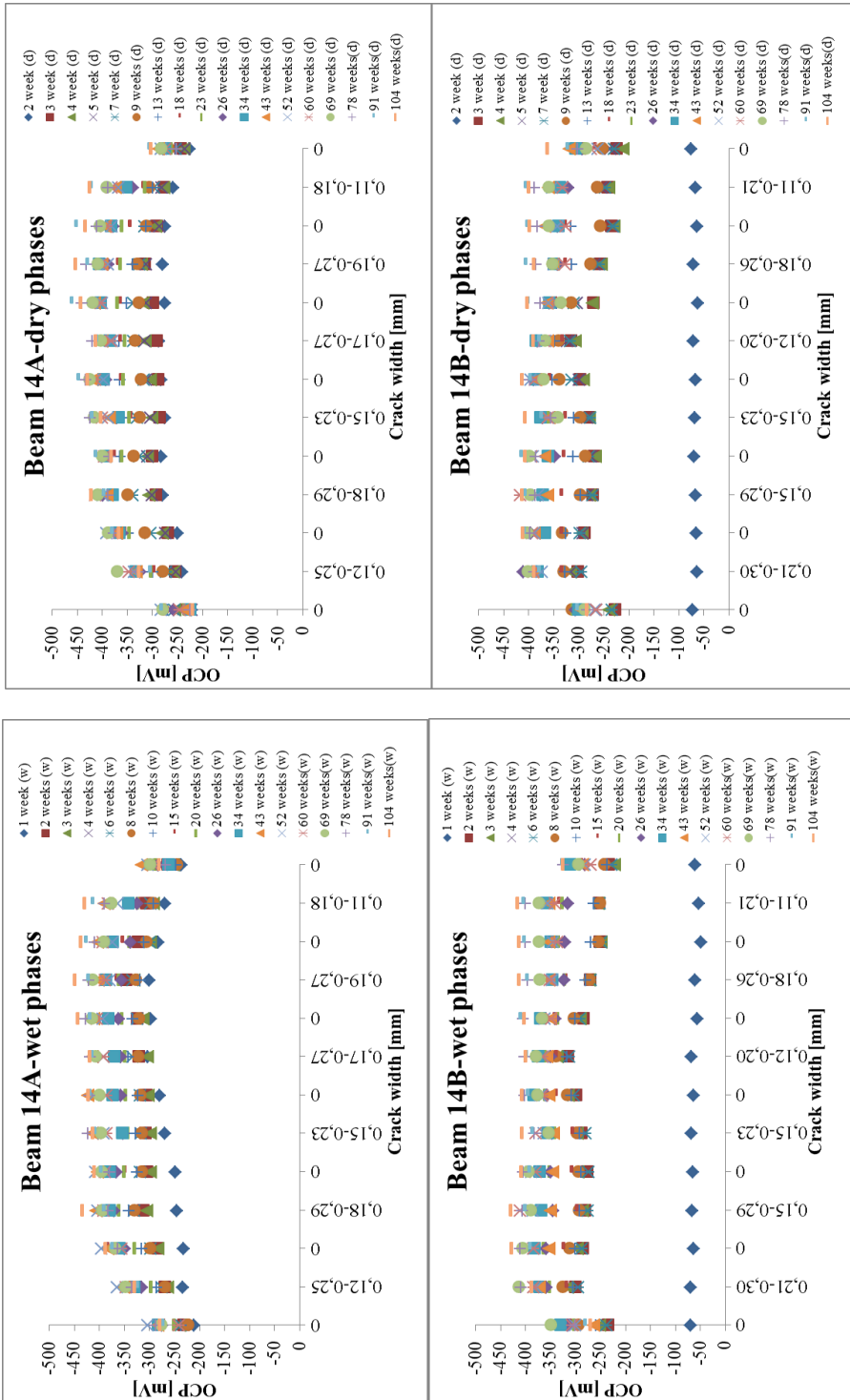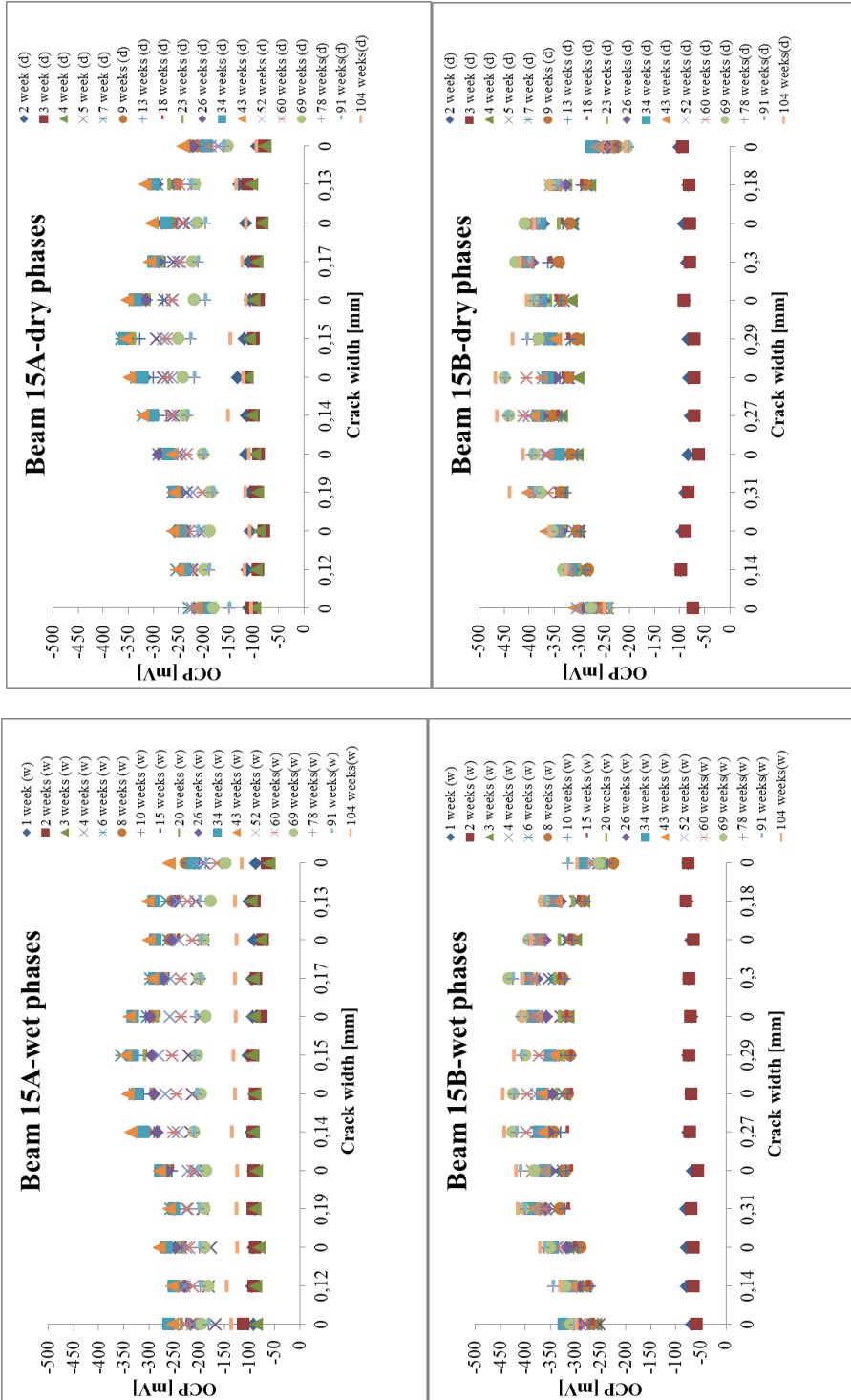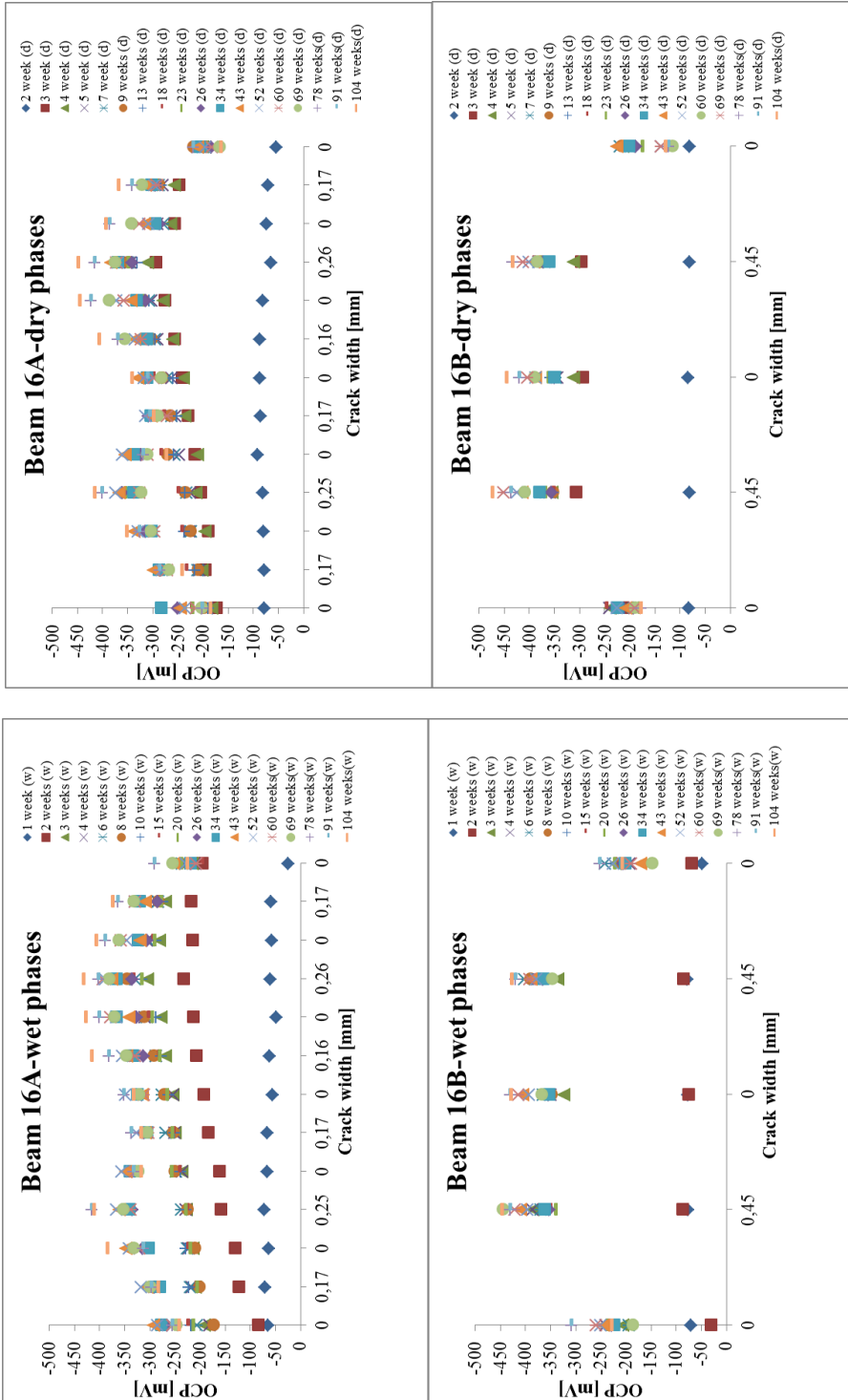
Appendix B

Visualization of chloride penetration and chloride-induced corrosion in reinforced concrete beams after 2 years of exposure

After two years of exposure the reinforced concrete beams were taken out from the set-up and the containers were removed from the top of the beams as can be seen in Fig. B-1.

Figure B-1: Reinforced concrete beams were taken out from the set-up

The beams were cut by a diamond saw in three pieces where the length of each piece was around 50 cm (Fig. B-2a). Furthermore, a splitting test was carried out for each piece which was split in the middle of the cross-section so that a clear view was provided of the area around the reinforcing bar (Fig. B-2b).
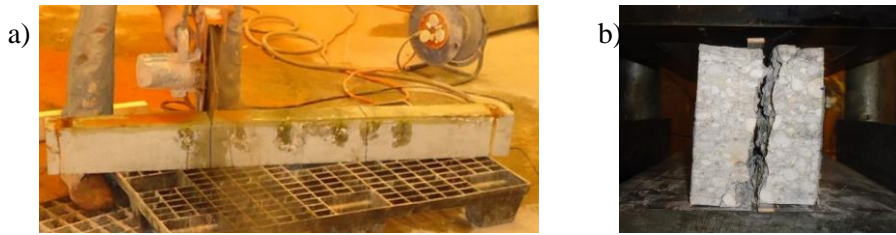
Figure B-2: a) Beams are cut by a diamond saw in thirds;   b)Splitting test

After splitting (Fig. B-3a), the pieces were composed on the table back into one whole beam (Fig. B-3b) which looks like it was open in the middle as can be seen in the photos of all beams given later in this appendix.
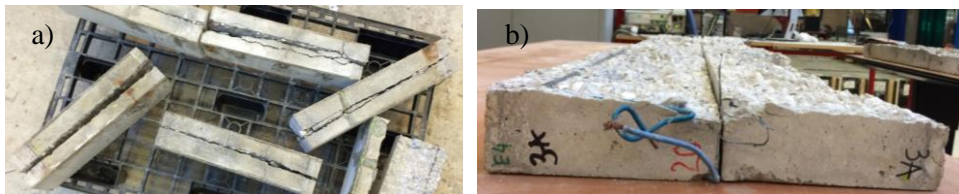
Figure B-3: a) Splitted pieces of beams;   b) Beams open in the middle

Furthermore, a silver nitrate solution (0.1 M $AgNO_3$) was sprayed on the faces of both parts in order to see the presence of chloride ions inside the beams. Consequently, after spraying silver chloride precipitation was visible after 15 minutes and photos were taken again of all beams in order to see the chloride penetration in each of them.

The beams before and after spraying silver nitrate looks as follows:

 Concrete before $AgNO_3$ was sprayed

 Chloride ions are not present in concrete

 Chloride ions are present in concrete

Beam 1A
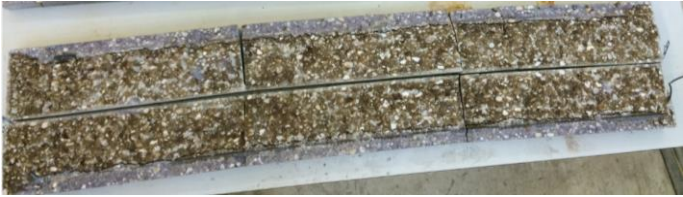
Beam 1B

Beam 2A

Beam 2B
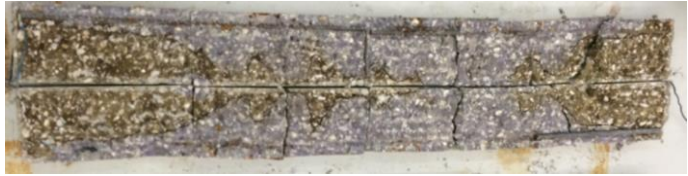
Beam 3A
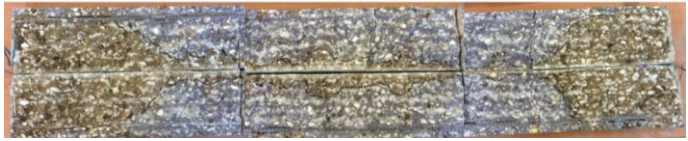
Beam 3B

Beam 4A
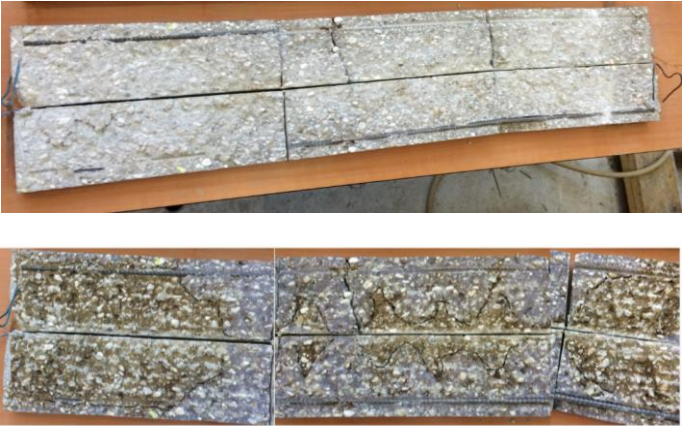
Beam 4B
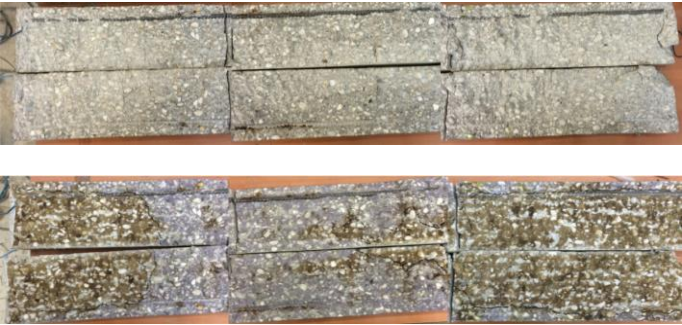
Beam 5A

Beam 5B
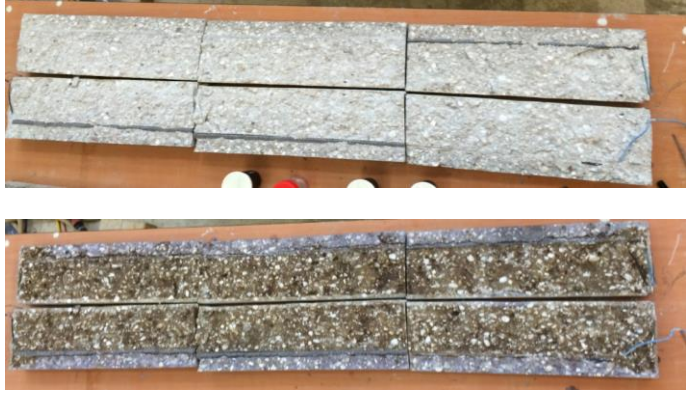
Beam 6A
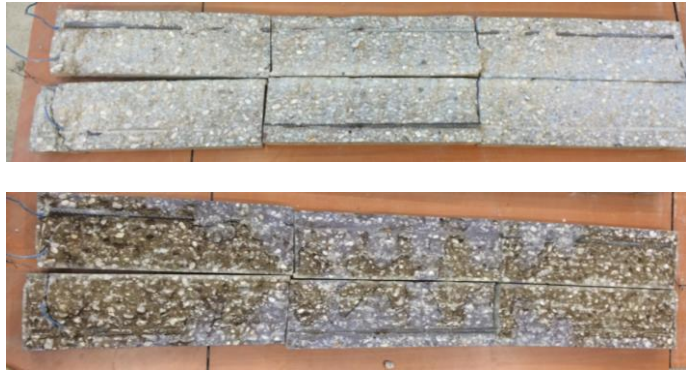
Beam 6B
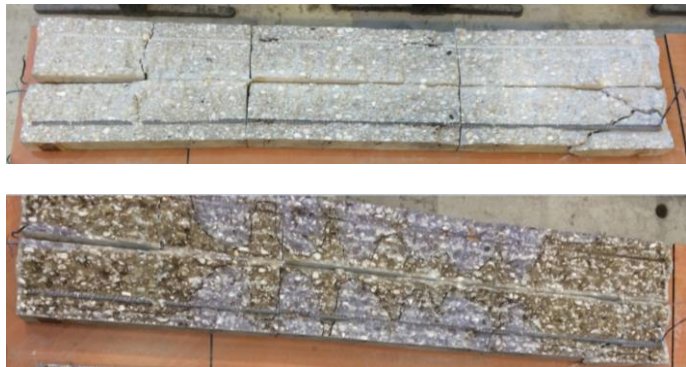
Beam 7A

Beam 7B

Beam 8A

Beam 9A
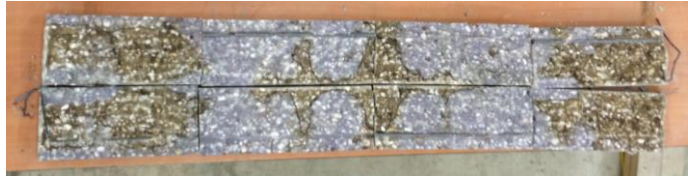
Beam 9B

Beam10A

Beam 10B
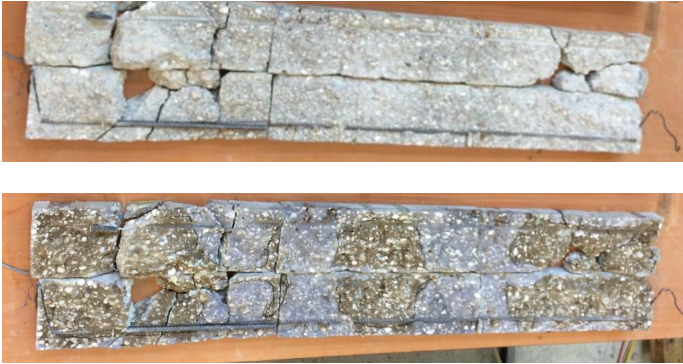
Beam 11A
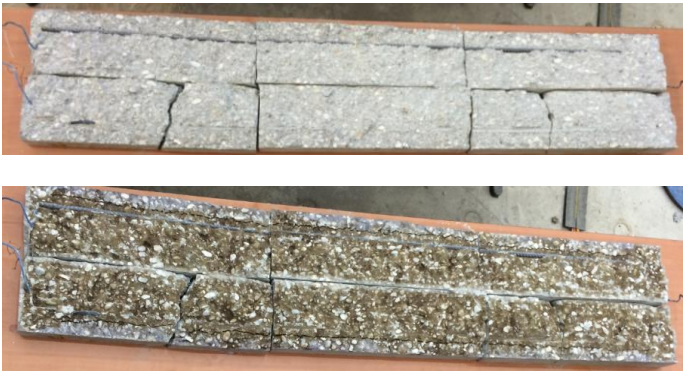
Beam 12A
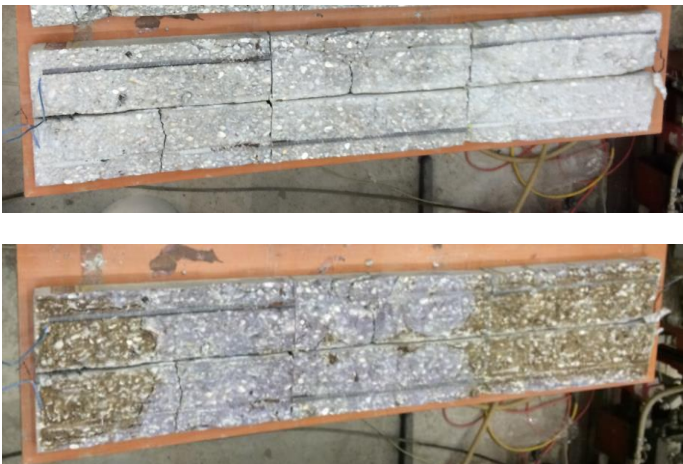
Beam 12B

Beam 13A
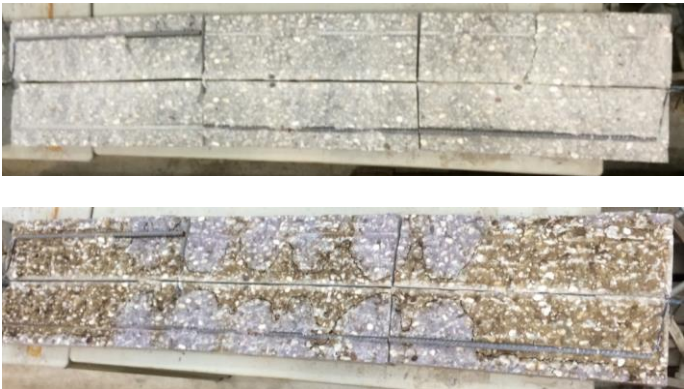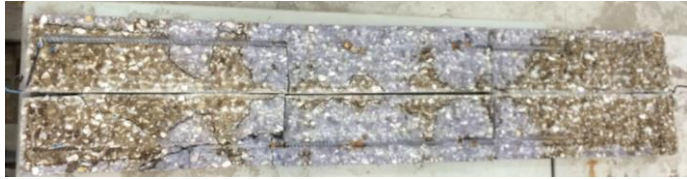

Beam 13B

Beam 14A

Beam 14B

Beam 15A

Beam 15B

Beam 16A

Beam 16B

Acknowledgements

This PhD has presented the biggest challenge and the most exciting adventure in my life at the same time. Without the help of many people, reaching my final destination would have been an impossible mission during this long journey. In 2011 a one way ticket was given to me by TU Delft with an expected arrival at a PhD thesis in 2015. My journey was under the umbrella of the IS2C (Integral Solutions for Sustainable Construction) program, funded by STW (Dutch Science Foundation). I gratefully acknowledge the support of STW and many thanks also to the head of IS2C, Prof. Eddie Koenders.

The person who arranged my ticket for this journey to explore "the World of Durable and Sustainable Concrete Structures", is my promotor Prof. Joost Walraven. Without his guidance this thesis would have never seen the light of day. I would like to express my sincere gratitude to him for giving me a chance to be a part of the expedition, guiding me along the road, believing in me during the trip's ups and downs and bringing me to the final destination. During the trip he exposed me to *a New World of Looking from a Different Perspective*. Through many discussions, he taught me how to be an independent researcher. I was incredibly lucky to work with him and I have learned a lot from him. Joost, I will be always indebted to you for everything you have done for me. With your support and encouragement any mission is possible!

I also owe a big gratitude to Dr. Dessi Koleva for many constructive discussions and invaluable advices during the entire journey. She has helped me a lot to deal with corrosion in concrete and to develop an experimental set-up and program. I have been very fortunate to meet her. Dessi, coffee breaks with you were work, fun and pleasure at the same time for me. I would like to say a very big thank you!

My gratitude also goes to Prof. Dick Hordijk for the great support, especially during the last year of my journey, when I was finishing this thesis.

I would like to thank all the members of my doctoral committee for taking the time to review the draft thesis and giving me their suggestions and comments.

Special thanks go to Reza Sarkhosh, my officemate, who became my good friend throughout this long journey. Reza, thanks a lot for all your support, the design of thesis cover and the many nice moments in and out of University!

I am very thankful to the technicians of Stevin Laboratory II for their assistance in overcoming all obstacles along the road. Special thanks goes to Ton Blom, Kees van Beek and Fred Schilperoort for their contribution to this body of work.

I would like also to thank my fellow PhD candidates, Yuguang Yang, Sana Amir, Kassahun Minalu, Patrick van Hemert, Eva Lantsoght, Toan Nguyen, the other colleagues within the Concrete Structures section, Cor van der Veen, Steffen Grunewald, Rene Braam, Sonja Fennis, Albert Reitsema, Sebastiaan Ensink, Paul Lagendijk, Marco Roosen, Kees Blom, Henk Spiewakowski, Albert Bosman and Marjo van der Schaaf, other colleagues from the whole department of Structural Engineering, Nynke Verhulst, Natalie Carr, Jose Pacheco, Damian Palin, Arthur Slobbe, Alexander Schmets, Somi Lotfi, Sjors van Es, Renee Mors, Farhad Pargar, Agus Susanto, Rita Esposito and many other colleagues for all your support and sharing a lot of memorable moments. I'd also like to thank my fellow Structural Synergy organizing committee and many other colleagues from the TU Delft for the great time we have spent together.

Within the Structural Engineering department I want to specially thank my dear Serbians, Marija, Branko (paranymph) and Mladena, who made me Delft feel like Serbia. We were not in the same section, but we all played for the same team.

I was extremely lucky to meet Dimitrije (paranymph) at the beginning of this journey in Delft. As a student in the Faculty Aerospace Engineering, he continuously refuelled the plane which I used for this journey. Furthermore, he has been motivating me in every aspect of my life and we became like a brothers. Dimitrije, lets continue to fly! Thanks for everything! Thanks go also to his family and his girlfriend, Zvezdana, who has shared many nice moments with us.

I am also very grateful to Yasmina Bennani, all my friends from the group "Delfćani" (Marko, Violeta, Jovic, Steva, Ljilja, Darko, Jasmina, Laza, Sonja, Maja...), Thijs, Yaredo, Vahid, Stevan and many other friends for a wonderful PhD life in Delft. Many thanks also to Frank for the Dutch conversation lessons.

In the second half of this journey, I moved to Rotterdam. A lot of people there made me feel at home. I want to thank Dragana, Mira, Milan, Nena, Tanja, Aca, Nastasja, Valerija, Marko, Maja, Nele, Dick and many, many others for memorable precious moments which you shared with me.

I 'd also like to thank all my friends and cousins in Niš for giving me constant support before and during this journey. A list would be very long if I write all of them down, but some of them which come on my mind at this moment are Sandra, Deki, Pavke, Goran, Andrea, Mladen, Marjan, Žarko, Marko, Andrija, Sanja, Vlada, Marta, families Blagojević and Simić and many, many others…

I would like to thank my brother, Danijel, and his wife, Milica, for all their generous support during this journey. Special thanks go to their children, my nephews, Danilo (Titi) and Darija for all their love and inspiration. Many thanks also to my grandparents, those who are with us and those who are not with us anymore. Thank you for believing in me and supporting me following pursuit of my dreams.

Finally, the most important acknowledgement goes to my parents to whom this mission is dedicated. With their unreserved support, extensive encouragement and unconditional love (even from far away) it has not been difficult to cope with any of the challenges along the way to the goal. Mama, Tata, hvala na svemu!!!

The mission is completed. I am ready for a new challenge which is going to be…

Andrija

November 2015

Delft, the Netherlands

Curriculum Vitae

Andrija BLAGOJEVIĆ

September 2, 1983   Born in Niš, Serbia

1998 – 2002   Graduated with distinction from Gymnasium „Stevan Sremac", Niš, Serbia

2002 – 2010   Dipl. Ing. / MSc in Civil Engineering with distinction at Department of Structural Engineering, Faculty of Civil Engineering and Architecture, University of Niš, Serbia

2011 – 2015   PhD Researcher at Concrete Structures, Faculty of Civil Engineering and Geosciences, Delft University of Technology, the Netherlands

2016 –   R&D and Consultant at B|A|S Research & Technology

Email: adiaki83@yahoo.com